Ex vivo human pancreatic cancer avatars; an in-line personalised therapeutic response assessment platform.



A thesis submitted for the degree Doctor of Philosophy
by

Daniel Llwyd Hughes
MBBCh, MSc, MRCS

St Cross College
University of Oxford
Trinity 2022

Supervisors:
Professor Eric O'Neill (University of Oxford)

Professor Somnath Mukherjee (Department of Oncology , Oxford University Hospitals NHS Foundation Trust)

Mr Zahir Soonawalla (Department of HPB surgery , Oxford University Hospitals NHS Foundation Trust)



The work presented in this thesis was performed at the Old Road Campus Research Building (ORCRB), Department of Oncology, University of Oxford. This study was funded by a Cancer Research UK Clinical Research Training Fellowship

Acknowledgements

I would like to thank my supervisor Professor Eric O'Neill for his support over the last three years. I am grateful for your guidance and for allowing me to have this opportunity to gain further experience within clinical academia. You taught me how to address clinical questions within a scientific context. I would also like to thank my clinical supervisors Professor Mukherjee and Mr Soonawalla for your support and for providing me with opportunities to discuss my clinical hypotheses.

I must also thank the wider team within the O'Neill group for welcoming me to the lab and for your kindness and friendship over the years. Simone, Fiona, Daniela, Maria T, Maria C, Michael, Luana, Asmita and Sophie, you all made my time in Old Road Campus such a positive experience. I particularly want to express my sincere gratitude to Frances who has been an invaluable mentor and friend. Your outstanding support and guidance has made such a difference.

I must also thank my family who have been a constant source of encouragement and support during this time. To my wife Samantha, thank you for your continuous support over the years. I could not have finished this without you. Finally to little Tomos, thank you for keeping me company in the night whilst I was writing the thesis. I enjoyed our conversations.

Ronald Gray
12-07-1929 to 23-09-2011

Publications

Hughes DL, Hughes A, Soonawalla Z, Mukherjee S, O'Neill E. Dynamic Physiological Culture of Ex Vivo Human Tissue: A Systematic Review. Cancers (Basel). 2021 Jun 8;13(12):2870. doi: 10.3390/cancers13122870. PMID: 34201273; PMCID: PMC8229413.

Hughes DL, Willenbrock F, Soonawalla Z, Mukherjee S, O'Neill E. Predicting Early Disease Recurrence of Pancreatic Cancer following Surgery: Determining the Role of NUDT15 as a Prognostic Biomarker. Curr Oncol. 2022 Apr 6;29(4):2516-2529. doi: 10.3390/curroncol29040206. PMID: 35448180; PMCID: PMC9032287.

Abstract

A paradigm shift in long-term survival rates for patients with Pancreatic Ductal Adenocarcinoma (PDAC) has yet to be witnessed. Long-term survival is only achieved in a small minority of patients. Systemic control of the disease can be secured with chemotherapy, however PDAC harbours high rates of chemotherapeutic resistance. Within current clinical practice, chemotherapeutic treatment strategies for PDAC are dictated by the patients' level of fitness. There is no assessment of the individual's tumour biology or acknowledgement of the significant heterogeneity that exists across tumours. Precision therapy incorporates individual tumour phenotype and biological characteristics and utilises this information to guide future management. Such an approach may improve the outcome for patients with PDAC. Whilst several different models for precision therapies have been reported, they all possess weaknesses that limit their use within a clinical setting. Within this thesis, I present the creation of patient derived cancer avatars as a method for delivering precision therapy for patients with PDAC. This approach allows for the creation of individual and miniature versions of a patient's tumour for detailed cellular profiling in addition to an opportunity to perform a therapeutic drug screen. This approach overcomes several of the limitations of other models of precision therapy notably the preservation of the cellular diversity of the primary tumour and can be implemented within a clinically meaningful time frame. I further investigated as to whether long-term ex vivo culture of patient avatars can be achieved through utilising novel perfusion culture. To date, we are the first group to describe the use of perfusion culture of PDAC tissue slices. We demonstrated that perfusion culture is associated with a physiological benefit as we were able to maintain both glucose and lactate levels at a constant level during 12 days of ex vivo culture ($p < 0.001$ and $p<0.0001$ respectively). Native functional biological processes within the avatars were preserved ex vivo through the use of perfusion culture. Avatars that were cultured with perfusion culture ex vivo maintained a significantly higher proliferation rate ($p < 0.01$) and demonstrated reduced rates of cell death as per cleaved caspase 3 activation ($p < 0.01$). The metabolic activity of the avatars (mTOR) was preserved with perfusion culture ($p < 0.01$). Our model system also preserved native immune cells present within the tumour during ex vivo culture. Our initial experience with ex vivo chemotherapy treatment of avatars demonstrated a correlation with the patients' clinical response to adjuvant therapy. Therefore, the avatar response to treatment may provide a unique opportunity and a window of insight into the future response of the patient to systemic treatment. This information can be harnessed and utilised to create individual, personalised treatment regimes for each patient. This in turn would change the historic approach to systemic therapy for PDAC, evolving from a generic, standardised treatment approach for all patients to establishing an individual, customisable regime for an individual tumour for each patient. Such an approach may finally translate into prolonging survival for patients with this lethal disease.

Table of Contents

Chapter 1

Introduction 1
1.1 Pancreatic Ductal Adenocarcinoma 1
1.1.1 Epidemiology and prognosis of PDAC 7
1.1.2 Disease presentation, diagnosis and molecular subtyping of PDAC 9
1.1.3 Current standard of care for patients with PDAC 13
1.1.4 The role of Adjuvant Chemotherapy 17
1.1.5 The role of Neo-Adjuvant Chemotherapy 19
1.1.6 The role of Immunotherapy 22
1.2 Current challenges in clinical practice with PDAC management 24
1.3 Precision therapy 29
1.3.1 Models for therapeutic drug screens on primary tumours 33
1.3.2 Patient derived cell lines 33
1.3.3 Patient derived organoids and bioprinted tumours 34
1.3.4 Patient derived Xenografts 37
1.3.5 Primary tissue slice culture 41
1.3.6 The optimal system for precision therapy 43
1.4 Aims 44

Chapter 2

Materials and methods 45
2.1 Overview of methods 45
2.2 Creation of patient derived cancer avatars from resected primary tumours 45
2.2.1 Tissue transport, acquisition and preparation 46
2.2.2 Avatar creation with the vibratome 47
2.2.3 Perfusion plate set up 49
2.2.4 Mathematical modelling of shear stress and determining the Geospatial distribution of the perfusate 51
2.3 In vitro experiments 53
2.3.1 Cell Culture 53
2.3.2 Cellular protein extraction and quantification, SDS-PAGE electrophoresis and Western Blotting technique 53
2.3.3 Profiling of Metabolic substrates 56
2.4 Ex vivo avatar culture, treatment and analysis 57
2.4.1 Ex vivo culture 57
2.4.2 Tissue Processing and Embedding 57
2.4.3 Histological analysis 58
2.4.3.1 Analysis strategy 59

2.4.3.2 Immunohistochemistry (IHC) 61
2.4.3.3 Masson's Trichrome Staining 63
2.4.3.4 Multiplex IF staining 64
2.4.3.5 Spatial transcriptomics 66
2.4.4 Ex vivo avatar treatment 67
2.4.5 RNA extraction from avatars and qPCR 68
2.5 Bioinformatics analysis 70
2.5.1 Clinical datasets 70
2.5.2 Differential gene expression 71
2.5.3 Gene set enrichment analysis of pathways 72
2.5.4 Survival analysis 72
2.5.5 Biomarker validation 72
2.6 Statistical analysis 73
2.7 General laboratory reagents 73

Chapter 3

Patient derived Pancreatic Cancer Avatars 77
3.1 Establishing a protocol for the creation of patient derived pancreatic cancer avatars 77
3.2 Aims 77
3.3 Implementing precision therapy for PDAC 78
3.4 Patient identification and recruitment 79
3.5 Diagnostic work-up and management algorithm for PDAC 80
3.6 Tissue acquisition and transport 82
3.7 Avatar creation 84
3.7.1 Determining the optimal culture media for patient derived cancer avatars 91
3.7.2 Embedding and Microtome optimisation 94
3.8 Established pancreatic cancer avatars 96
3.9 Discussion 98

Chapter 4

Ex vivo perfusion culture of cancer avatars 106
4.1 Perfusion culture 106
4.1.1 Aims 108
4.2 Results 108
4.2.1 Establishing the perfusion system 108
4.2.2 Monolayer cell culture under perfusion conditions 115
4.2.2.1 Metabolic profiling of nutrient availability during static culture 116
4.2.2.2 Physiological benefits associated with perfusion culture. 119
4.2.3 Perfusion culture of patient derived cancer avatars 122
4.2.3.1 Avatar proliferation index during ex vivo culture 127
4.2.3.2 Avatar cell death trends during ex vivo culture 129
4.2.4 Spatial transcriptomic changes within the avatars during ex vivo culture 135

4.2.5 Mathematical modelling of shear stress exerted on to the avatars during perfusion culture 140
4.3 Discussion 142

Chapter 5

Profiling the cellular composition of avatars during ex vivo culture 149
5.1 Cellular diversity of PDAC tumours 149
5.1.1 Aims 152
5.2 Results 152
5.2.1 Extra Cellular Matrix composition 152
5.2.2 Tumoural compartment within the avatars 155
5.2.3 Immune infiltrate within avatars 157
5.2.3.1 Creation of a Mulitiplex Immunofluorescence Immune Panel 158
5.2.3.2 Avatar immune infiltrate at baseline 162
5.2.3.3 Spatial analysis of immune infiltrate within the avatars 163
5.2.3.4 Determining the stability of the immune infiltrate within avatars during ex vivo culture 169
5.3 Discussion 174

Chapter 6

Evaluating patient derived pancreatic cancer avatars as a model for precision therapy 182
6.1 Systemic therapy for PDAC 182
6.1.1 Aims 185
6.2 Results 185
6.2.1 Drug delivery 185
6.2.2 Ex vivo treatment of patient derived cancer avatars 187
6.2.3 Comparing therapeutic response between patient derived cancer avatars following ex vivo treatment 194
6.2.4 Molecular profiling pancreatic avatars into transcriptomic subtypes 195
6.2.5 Correlating the avatar and patient response to chemotherapy 197
6.3 Discussion 209

Chapter 7

Identifying a biomarker for localised disease 215
7.1 Aims 218
7.2 Results 218
7.2.1 TCGA analysis 218
7.2.1.1 Impact of early recurrence on overall survival 220
7.2.1.2 Demographics of patients with an early recurrence 220
7.2.2 Differential gene expression of tumours with an early recurrence 222
7.2.3 Alteration in signalling pathways associated with early recurrence 225
7.2.4 Identification of biomarkers for early recurrence 228

7.2.4.1 Determining the accuracy of biomarkers at identifying early recurrence 230
7.3 Discussion 237

Chapter 8

Discussion 241
8.1 Key advantages of using avatars for precision therapy 242
8.2 Incorporating patient derived cancer avatars into clinical practice 246
8.2.1 Neo-Adjuvant therapy dictated by cancer avatar response. 246
8.2.2 Determining the standard of care for patients with metastatic disease. 248
8.3 Critical analysis of patient derived cancer avatars as a model for precision therapy. 248
8.4 Impact of the Covid-19 pandemic 251
8.5 Future work 253
8.6 Conclusion 257

A Appendix 259

Bibliography 261

List of figures

Figure 1. 1– Hallmarks of PDAC. 4

Figure 2. 1– Perfusion plate 51

Figure 2. 2– IHC analysis strategy 60

Figure 3. 1 – Implementation of precision therapy within a clinically meaningful time frame 79

Figure 3. 2 - Transport route and logistic planning for tissue acquisition. 84

Figure 3. 3 – The use of a temporary tissue scaffold increases the avatar creation yield. 87

Figure 3. 4 – Optimisation of the clearance angle for vibratome tissue slice creation. 89

Figure 3. 5 - Determining the optimal vibratome settings for avatar creation. 90

Figure 3. 6 – Optimising avatar culture media. 92

Figure 3. 7– Association between biliary drainage and avatar contamination 94

Figure 3. 8– Optimisation of the microtoming technique for PDAC avatars. 95

Figure 3. 9– Successful creation of patient derived avatars. 97

Figure 3 .10 – Implementation of precision therapy within the current NHS infrastructure. 104

Figure 4. 1– Dynamic physiological culture techniques that have been utilised for ex vivo culture of primary human tissue. 109

Figure 4. 2– Perfusion plate layout. 112

Figure 4. 3– Geospatial distribution of the perfusate. 115

Figure 4. 4 – Metabolic profiling of nutrient availability during static culture. 117

Figure 4. 5 - Physiological benefits associated with perfusion culture. 121

Figure 4. 6 – Macroscopic images of patient derived PDAC avatars and their surface area during ex vivo culture. 123

Figure 4. 7– Perfusion culture preserves microscopic viability of PDAC avatars during ex vivo culture. 126

Figure 4. 8 - Proliferation index trend during ex vivo culture of PDAC avatars. 128

Figure 4. 9 - Apoptosis rates of PDAC avatars on day 5 of ex vivo culture. 130

Figure 4. 10 - Metabolic activity of PDAC avatars during ex vivo culture. 132

Figure 4. 11 - GeoMx segmentation of PDAC avatars. 134

Figure 4. 12 - Spatial transcriptomic changes of the tumour compartment of PDAC avatars during ex vivo culture. 136

Figure 4. 13 - Spatial transcriptomic changes of the stromal compartment of PDAC avatars during ex vivo culture. 137

Figure 4. 14 - Quantification of epithelial tumour cells during ex vivo culture. 138

Figure 4. 15 - Quantification of activated fibroblasts during ex vivo culture. 139

Figure 4. 16– Virtual simulation and mathematical modeling of shear stress experienced during perfusion culture. 141

Figure 5. 1– Determining the stability of the Extra Cellular Matrix during ex vivo perfusion culture. 154

Figure 5. 2 – Profiling the stability of the tumour compartment during ex vivo culture. 156

Figure 5. 3 – Creation of a Multiplex IF panel for immune profiling of patient derived cancer avatars during ex vivo culture. 160

Figure 5. 4 – Machine based learning enables the identification of distinct cell phenotypes. 161

Figure 5. 5- Immune profiling of patient derived pancreatic cancer avatars. 163

Figure 5. 6- Evaluating the spatial relationship between immune cell phenotypes and the tumour cells within patient derived cancer avatars. 165

Figure 5. 7 – Mapping immune cell infiltrate within pancreatic cancer avatars. 168

Figure 5. 8 – Stability of immune cell infiltrate during perfusion culture. 172

Figure 6. 1 - Illustration of ex vivo treatment of cancer avatars experiment design 187

Figure 6. 2 – Proliferation index of PDAC avatars following ex vivo drug treatment. 189

Figure 6. 3 – Apoptosis rates of PDAC avatars following ex vivo drug treatment. ... 191

Figure 6. 4– γ- H2AX positivity rates of PDAC avatars following ex vivo drug treatment. 193

Figure 6. 5 - Profiling three different avatar responses to ex vivo Gemcitabine treatment. 195

Figure 6. 6 – Determining whether tumour subtypes correlate with Gemcitabine response 197

Figure 6. 7 – Correlating avatar and patient response for PDCA14. 198

Figure 6. 8 – Correlating avatar and patient response for PDCA16.. 203

Figure 6. 9 – Correlating avatar and patient response for PDCA17. 207

Figure 7. 1 – Overview of patient selection process from the TCGA dataset..... 219

Figure 7. 2– Impact of early recurrence on overall survival.. 220

Figure 7. 3 – Identification of DE genes in patients with an early disease recurrence using edgeR. 223

Figure 7. 4– Pathway enrichment analysis of the normalised enrichment scores (NES) of the 50 hallmark cancer pathways presented in a stacked bar chart ordered by FDR. 226

Figure 7. 5– KEGG pathways enrichment analysis. 228

Figure 7. 6 – Comparative analysis of DE genes between DESeq2 and edgeR 229

Figure 7. 7 - Receiver operating characteristic curve analysis to determine biomarker sensitivity. 231

Figure 7. 8 – NUDT15 expression within avatars. 234

Figure 7. 9 – Evaluating NUDT15 as a biomarker. 234

Figure A. 1– Selection process for qPCR primers. 259

Figure A. 2 - Modifications performed on the μ-Slide III 3D Perfusion (Ibidi) to optimise for avatar culture..... 259

Figure A. 3- Representative H&E images of the tissue viability scoring criteria..... 260

List of Tables

Table 2. 1 qPCR primers 70

Table 2. 2 Chemical reagents used..... 74

Table 2. 3 Primary and Secondary antibodies used for IHC 75

Table 2. 4 Primary and Secondary antibodies used for Western Blot..... 75

Table 2. 5 Primary and Secondary antibodies used for Multiplex IF 75

Table 3. 1 – Demographics of patient derived cancer avatars 98

Table 5.1 - Determining the stability of the avatar immune component during ex vivo culture.....169

Table 5.2 - Monitoring the spatial relationship between immune cell phenotypes and the tumour cells during ex vivo perfusion culture 173

Table 6. 1– RNA extraction methods trialled 196

Table 7. 1 –Demographics of the TCGA patient cohort..... 221

Table 7. 2- Top 20 DE genes between patient with and without an early recurrence following resection for PDAC 224

Table 7. 3– Survival outcomes of recruited patients..... 232

Abbreviations

5FU:	5-Fluorouracil
α –SMA:	alpha-Smooth Muscle Actin
ADP:	Adenosine Diphosphate
ATP:	Adenosine Triphosphate
CA19-9:	Carbohydrate Antigen 19-9
CAFs:	Cancer Associated Fibroblasts
C-C3:	Cleaved Caspase 3
CDKN2A:	Cyclin Dependent Kinase Inhibitor 2A
CA:	Carbohydrate Antigen
CAP:	Chest Abdomen Pelvis
CK19:	Cytokeratin-19
CT:	Computerised Tomography
CXCR2:	C-X-C Motif Chemokine Receptor 2
DAPI:	4’,6-Diamidino-2-Phenylindole
DE:	Differentially expressed
DMEM:	Dulbecco's Modified Eagle Medium
DMSO:	Dimethyl Sulfoxide
DNA:	Deoxyribonucleic acid
DPX:	Di-N-Butyl Phthalate in Xylene
ECM:	Extra Cellular Matrix
EGF:	Epidermal Growth Factor
ESPAC:	European Study Group for Pancreatic Cancer
EUS:	Endoscopic Ultrasonography
EUS:	Endoscopic Ultrasound
FCS:	Foetal Calf Serum
FDR:	False Discovery Rate
FFPE:	Formalin-Fixed Paraffin-Embedded
FOLFIRINOX:	Fluorouracil, Folinic acid, Irinotecan and Oxaliplatin
FU:	Fluorouracil
GEM:	Genetically Engineered Mouse
GSEA:	Gene Set Enrichment Analysis
H&E:	Hematoxylin and Eosin
hENT1:	Human equilibrative nucleoside transporter 1
HPB:	Hepato-Pancreato-Biliary
HRP:	Horseradish Peroxidase

iCAFs:	Inflammatory fibroblasts
IF:	Immunofluorescence
IHC:	Immunohistochemistry
IPMNs:	Intraductal Papillary Mucinous Neoplasms
KRAS:	Kirsten Rat Sarcoma
LAPC:	Locally Advanced Pancreatic Cancer
LG-DMEM:	Low Glucoses - Dulbecco's Modified Eagle Medium
LMA:	Low Melting Agarose
MAPK:	Mitogen-activated protein kinase
MCNs:	Mucinous Cystic Neoplasms
MDSCs:	Myeloid-derived suppressor cells
MDT:	Multidisciplinary Team
Mg:	Milligram
Ml:	Millilitre
Mm:	Millimetre
MMP:	Matrix Metalloproteinases
mTOR:	Mammalian Target of Rapamycin
myCAFS:	Myofibroblasts
OUH:	Oxford University Hospitals
NICE:	National Institute for Health and Care Excellence
PAAD:	Pancreatic Adenocarcinoma
PanCK:	Pan-Cytokeratin
PanIN:	Pancreatic Intraepithelial Neoplasia
PARP**:**	Poly (ADP-ribose) polymerase
PBMC:	Peripheral Blood Mononuclear Cells
PCR:	Polymerase Chain Reaction
PD-1:	Programmed cell-death receptor
PD-L1:	Programmed death-ligand 1
PDAC:	Pancreatic Ductal Adenocarcinoma
PDCA:	Patient Derived Cancer Avatar
PDGF:	Platelet Derived Growth Factor
PDX:	Patient Derived Xenograft
PET:	Positive Emission Tomography
pNET:	pancreatic Neuro-Endocrine tumour
RCT:	Randomised Clinical Trial
RIPA:	Radioimmunoprecipitation Assay Buffer
RNA:	Ribonucleic acid
RNA-Seq:	RNA Sequencing
ROI:	Region of Interest
SC:	Static Culture
TAM:	Tumour associated macrophages

TCGA:	The Cancer Genome Atlas
TGF-β1:	Transforming Growth Factor Beta 1
TME:	Tumour Microenvironment
TP53:	Tumour protein p53
Tregs:	Regulatory T cells
TSG:	Tumour Supressor Genes
µg:	Microgram
µl:	Microlitre
µm:	Micrometre

Chapter 1

Introduction

1.1 Pancreatic Ductal Adenocarcinoma

Pancreatic Ductal Adenocarcinoma (PDAC) remains as one of the most fatal gastrointestinal tract (GIT) malignancies. Globally, it is recorded as the 7th highest cause of cancer mortality (Rawla et al., 2019). Epidemiological studies have confirmed an annual increased incidence rate of PDAC (A. P. Klein, 2019). Based on population level data, the age-standardised incidence rate has increased to 1.03% per year, which translates to PDAC rising to be the second cause of cancer mortality in the western world by 2030 (McGuigan et al., 2018; Saad et al., 2018)

The term 'Pancreatic Cancer' is an umbrella term that incorporates all malignancies that originate from within the pancreas. PDAC is the predominant tumour type of the exocrine pancreas and actually accounts for 90% of all recorded pancreatic cancers (McGuigan et al., 2018). It predominantly arises within the pancreatic head (~ 70% of cases), followed by an equal distribution in the pancreatic body and tail (15% each) (Luchini et al., 2016).This harbours clinical significance with regard to disease presentation (Porta et al., 2005). Whilst some pancreatic cancers can originate from within the endocrine pancreas (pancreatic Neuro-Endocrine tumour (pNET)), these should not be considered comparable to PDAC ((Young et al., 2015). pNETs are associated with a greater overall survival and they also possess a unique

hormone producing capacity which can be pharmacologically targeted with somatostatin analogue therapy (Oberg, 2018).

De novo PDAC tumour development occurs from pre-existing precursor lesions within the pancreatic parenchyma. Two distinct precursor lesion phenotypes have been described in the tumorigenesis of PDAC: Pancreatic Intraepithelial Neoplasia (PanIN) and cystic lesions of the pancreas. PanINs are microscopic lesions within the pancreatic ductal system that are defined by cytological and architectural atypia (Riva et al., 2018). Hruban et al (2001), proposed a classification system that consisted of a hierarchical grouping that quantified the extent of dysplasia present. PanIN 1,2 and 3 correlate with low-grade, intermediate and high-grade dysplasia respectively (Hruban et al., 2001). However, ambiguity of the proposed nomenclature was observed across the literature with variation in the quantification of the histological features for each lesion subtype. As a direct consequence, the classification system was revised in 2015 to a binary, two-tiered low-grade (encompassing PanIN 1 and 2) and high-grade PanIN (replacing PanIN 3) system in an attempt to improve the homogeneity of the diagnosis and the wider medical literature (Basturk et al., 2015). It is proposed that PanINs progress from low to high grade, to eventually carcinoma in situ prior to invasive disease as these lesions accumulate additional genetic mutations and progressive telomerase shortening (Bardeesy et al., 2002).Whilst the concept of a pre-malignant, precursor lesion is exciting for a potential identification target of early disease, it must be emphasised that PanINs are a microscopic phenomenon and thus are undetectable by current cross-sectional imaging modalities. Cystic lesions of the pancreas represent the other

precursor lesions for PDAC. Contrary to PanINs, these cystic lesions are visible on cross-sectional imaging. Of all of the cystic lesions of the pancreas, both Intraductal Papillary Mucinous Neoplasms (IPMNs) and Mucinous Cystic Neoplasms (MCNs) harbour malignant potential and are therefore considered as precursor lesions (Hruban et al., 2007).The rates of malignancy progression vary between both precursor lesions (Riva et al., 2018). The fact that these cysts can be detected by cross-sectional imaging is clearly advantageous in the attempt to identify early non-invasive disease. Unfortunately, population-based studies have illustrated that the prevalence of pancreatic cysts (both precursor lesions and benign lesions with no malignancy risk) increases with age (Kromrey et al., 2018). Therefore, the identification of a cystic lesion itself is not an indication for intervention, especially given the significant morbidity and mortality risk associated with pancreatic surgery. Current diagnostic strategies focus upon identifying high-risk stigmata within these cysts in order to determine which cysts have a greater potential to progress to invasive disease. Within this cohort of patients, if there are no significant comorbidities, surgical intervention is advocated.

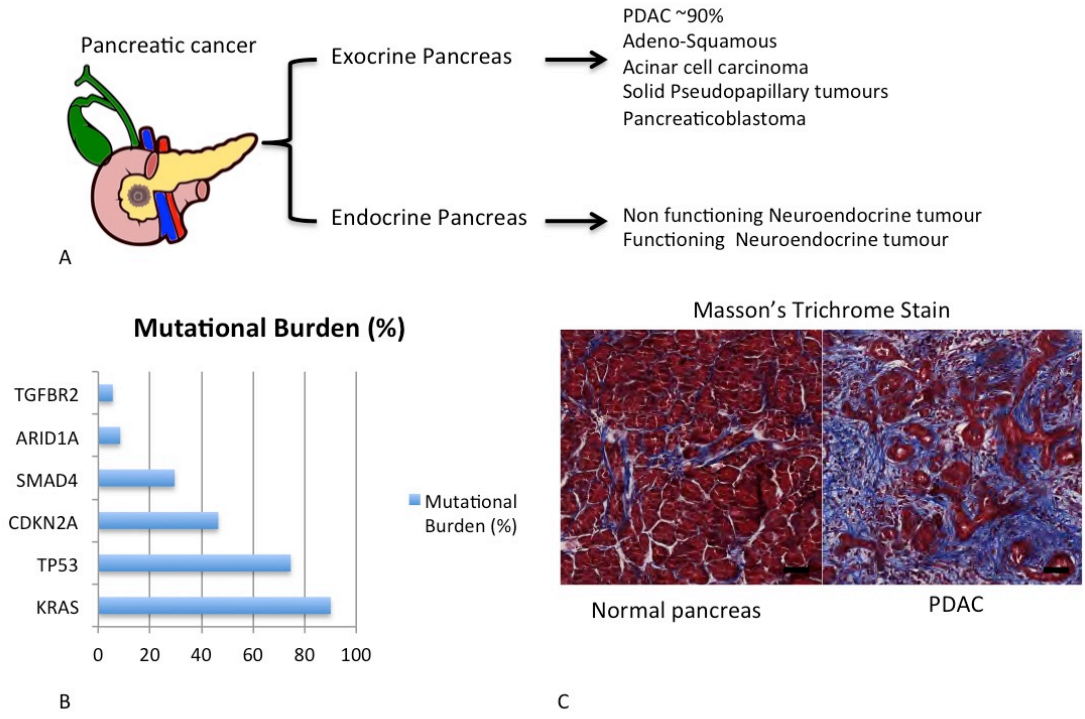

Figure 1. 1– Hallmarks of PDAC. (A) Visual illustration of the different types of endocrine and exocrine pancreatic cancer. (B) Mutational burden of PDAC tumours (Aguirre et al, 2018). (C) Desmoplastic stroma associated with PDAC tumours. Representative Masson's Trichrome stain for collagen deposition in both normal pancreatic tissue and PDAC, scale bar 100 um.

PDAC development is underpinned by driving genetic mutations. The cardinal mutation is a mutation in the KRAS gene (Bryant et al., 2014). This is present in approximately 90% of all PDAC tumours (Aguirre et al., 2018). Of the described mechanisms, by far the most frequent is a missense mutation affecting the guanine nucleotide at position 12 (G12) within the KRAS protein (Bryant et al., 2014). As a result, KRAS is permanently bound to Guanosine-5'-triphosphate (GTP) and as a direct consequence there is unopposed activation and signalling of the Mitogen-activated protein kinase (MAPK) pathway resulting in uncontrolled pro-tumorigenic

cellular function such as cell proliferation and migration (di Magliano et al., 2013). Through utilising whole exome and RNA sequencing of PDAC tumours, Aguirre et al (2018) demonstrated additional key driver mutations in PDAC, albeit at a lower incidence when compared to KRAS mutations. These mutations are present in the following tumour suppressor genes: Tumour protein p53 (TP53), Cyclin Dependent Kinase Inhibitor 2A (CDKN2A) and SMAD family member 4 (SMAD4) (at rates of approximately 74.6%, 46.5% and 29.6% respectively) (Aguirre et al., 2018).

PDAC tumours possess several unique characteristics that make them distinctively different to other solid GIT malignancies. All tumours possess underlying genetic mutations that drive uncontrolled proliferation. There is a failure in local regulatory mechanisms, notably the loss of function in Tumour Supressor Genes (TSG) either through mutational inactivation or deletion , or as a result of specific DNA methylation with subsequent epigenetic silencing of the gene. Most tumours possess a mutational burden involving several genes. Historically both malignant melanoma and lung cancer have a high mutational burden (Galuppini et al., 2019; Willis et al., 2019). However PDAC has a significantly lower mutational burden, with the aforementioned genes noted in the previous paragraph. This genetic characteristic of PDAC tumours carries clinical implications. Firstly, it has been reported that tumours with a lower mutational burden have a significantly reduced response rate to check-point blockade immunotherapy (Yarchoan et al., 2017). Secondly, and of greater clinical significance, the cardinal driving mutation of PDAC (specifically $Kras^{G12D}$) has yet to be successfully targeted by pharmacological agents in a human context. Therefore, the direct oncogenic pathway involved with PDAC

tumorigenesis has yet to be manipulated. The main pathognomonic histological feature of PDAC is the florid desmoplastic reaction associated with the tumour. As a consequence, a dense stroma centres around the tumour (Xie et al., 2015). In actual fact, the vast majority of the tumour mass is not formed of the tumour cells themselves (less than 20% of the tumour is composed of tumour cells), rather, it is the desmoplastic stroma (H. Huang et al., 2019). The stromal compartment is certainly not a barren wasteland. It is a thriving ecosystem that is multicellular in origin. It is composed of stromal cells (such as Cancer Associated Fibroblasts (CAFs), immune cell populations, endothelial cells and an abundance of Extra Cellular Matrix (ECM) proteins. The ECM domain includes several different forms of collagen (with a predominance of type 1 collagen), fibronectin, laminin and glycosaminoglycans such as hyaluronic acid (Mollenhauer et al., 1987; Weniger et al., 2018). A symbiotic relationship exists between the tumour cells and the stromal compartment. The tumour cells can directly influence the surrounding microenvironment. An example of such an influence is through the secretion of mitogenic stimuli, such as growth factors (epidermal growth factor (EGF) and platelet derived growth factor (PDGF)) or by cytokine release (notably Transforming Growth Factor Beta 1 (TGF-β1)) which in turn can activate pancreatic stellate cells that are in a quiescent state (Phillips, 2012; Rasheed et al., 2012). Once activated (denoted by alpha-Smooth Muscle Actin (α - SMA) expression), the stellate cells undertake synthesis and deposition of further ECM proteins into the tumour microenvironment (TME) (Phillips, 2012). Reciprocally, the ECM can release both cytokines and growth factors that directly effect tumour cells by inducing proliferation and invasion (Phillips, 2012). The TME also serves as a nutritional reservoir that can be utilised by tumour cells during periods of nutrient

deprivation to fuel metabolic processes (Olivares et al., 2017). The desmoplastic stroma possesses physical properties due to its tensile strength. These include compression of the vasculature that renders the tumour more hypoxic to creating an impenetrable barrier that limits drug delivery to the tumour cells (Liang et al., 2017; Neesse et al., 2015). As a consequence, a significant effort has been made to develop novel stromal-targeted therapies in an attempt to alter and produce a less hostile TME in PDAC.

Despite all the advances in treatment strategies, no significant impact has been made on prolonging the overall survival rate for this malignancy. An alarming report published in 2019 illustrated a minimal improvement in 5 year survival trends for PDAC when compared to other gastrointestinal tract malignancies across 7 countries (Rawla et al., 2019). The specific reasons for the lack of progress are vast; they range from the unique biological characteristics that PDAC tumours possess, the diagnostic challenge of identifying early localised disease to the organisational structure of healthcare delivery and the availability of effective chemotherapeutic treatment strategies. What is clear is the need to consider alternative approaches to managing this disease in order to produce a paradigm shift and create a favourable outcome.

1.1.1 Epidemiology and prognosis of PDAC

The incidence for this lethal malignancy is increasing. In 2018, the global cancer statistics consortium published that there were 458,918 new cases of pancreatic

cancer globally (Bray et al., 2018). As a sequel, this surge in new diagnoses resulted in 432,242 deaths (which is accountable for 4.5% of all cancer mortality) (Bray et al., 2018). Higher rates of new diagnoses were observed in Europe and North America when compared to Africa (Rawla et al., 2019). Two possible explanations exist for this geographical variation observed in PDAC incidence; firstly, this may be attributable to social practices, specifically alcohol consumption and smoking (two well-known carcinogenic risk factors for PDAC), in addition to the obesity pandemic present in the western world. Secondly, lower rates may be observed in developing countries as a consequence of a lack of access to appropriate cross-sectional imaging or resources for biopsy acquisition for the confirmation of the diagnosis or the completeness of their national cancer registries. A male predominance was noted in new PDAC cases in 2018, which is likely to be attributable to a higher exposure risk to carcinogenic agents (Bray et al., 2018).

The prognosis for patients with PDAC is guarded. Long-term survival is dependent on the disease burden present at the initial diagnosis. For patients with tumour confined to the pancreas, with no regional lymph node involvement (stage I), who undergo surgical resection and complete adjuvant chemotherapy, the 5 year survival is 36%. However, as the disease progresses a rapid fall in the 5 year survival trend is observed; 12% for stage III disease (tumour involvement of the peri-pancreatic vasculature with or without local lymph node involvement) and unfortunately only 3% for patients with metastatic disease (stage IV) (NCI, 2018).This clearly highlights the need to improve diagnostic pathways for patients in order to ensure that an earlier diagnosis is achieved. Interestingly, Huang et al (2018) demonstrated that

age negatively impacted longer survival irrespective of the tumour stage (3 year survival in resected stage 1 disease in patients <60 was 23-39% vs in patients>70 was 17-30%) (L. Huang et al., 2018). This reinforces the need for a careful preoperative work up and robust evaluation of the risk benefit ratio in the elderly patient.

1.1.2 Disease presentation, diagnosis and molecular subtyping of PDAC

Despite the inherent aggressive tumour biology that PDAC possesses, its presentation is often insidious. The presenting symptom is often disproportionate to the underlying disease burden present. Symptoms arise secondary to local tumour mass effect, local invasion or distant metastasis. Symptoms are also dependent on the anatomical origin of the tumour (Porta et al., 2005). The most common hospital presentation is with painless jaundice, an ominous sign of the potential devastating underlying diagnosis without any prior investigations (Porta et al., 2005). Jaundice occurs secondary to extrinsic compression of the bile duct by the tumour, an example of local mass effect. Additionally the tumour may grow and obstruct the duodenum, resulting in gastric outlet obstruction. An important symptom to note is new onset diabetes or a sudden worsening in glycemic control in a known diabetic (Pannala et al., 2009). These symptoms could potentially be used as a novel initial screening tool. The aforementioned symptoms are all drastic, concerning in nature and suggest pancreatic pathology. Unfortunately, the vast majority of PDAC initially presents with vague and non-specific symptoms, ranging from nausea, anorexia, weight loss, vague abdominal pain, asthenia and back pain (Porta et al., 2005). The

non-specific nature of these symptoms and the high prevalence of these symptoms in benign conditions drives the diagnostic uncertainty. To highlight this issue further, the yearly prevalence of lower back pain is 20%, and of all the consultations within primary care for back pain, less than 1% would be due to an underlying malignant disease process (Atlas et al., 2001; Deyo et al., 1992). Therefore the key step is successfully differentiating between these patients, as referring every patient to secondary care would be inappropriate and would significantly overburden the diagnostic services. The diagnostic challenge associated with pancreatic cancer is clearly highlighted in the work of Lyratzopoulos et al., 2015 (Lyratzopoulos et al., 2015). They conducted a review of the National Audit of Cancer Diagnosis in Primary Care 2009-2010 database, a database that holds electronic primary care records for 14,931 patients. They devised 3 time metrics to assess the patient's diagnostic journey: patient interval – time period between the development of the symptoms and the initial consultation with a General Practitioner, primary care interval – the time interval between first consultation in primary care and referral to a specialist in secondary care and finally the pre-referral interval – a combination of the previous parameters. Their data demonstrates that for all cancers, the patient interval is prolonged (Lyratzopoulos et al., 2015). This is an issue that can only be improved by increasing the general public's awareness of cancer specific symptoms. For cancers with specific, classic symptoms (for example a breast lump in breast cancer or a skin mole that is changing in malignant melanoma) a short primary care interval was observed (mean of 6 days and 17 days respectively). However for cancers with non-specific symptoms (notably pancreatic cancer) the primary care interval was significantly longer (33 days) (Lyratzopoulos et al., 2015).

PDAC is diagnosed on radiological imaging (by a Computerised Tomography (CT) scan). Historically, if a lesion was suspicious on a CT, then this was enough of a justification for surgical intervention if the patient was physiologically fit. There often was no histological confirmation of the disease preoperatively. However, advances in medical technology (notably the development of Endoscopic Ultrasound (EUS)) have permitted a reliable method of tissue acquisition. Not only does this permit histological confirmation of PDAC preoperatively, but it also has enabled molecular profiling of the disease and an opportunity to attempt precision therapy.

One of the most exciting advances in our understanding of PDAC behaviour over recent years has been the identification of PDAC subtypes based on molecular profiling. This has only been possible as a consequence of advances in gene sequencing technology that can now be reported in a clinically meaningful time frame and is of a reasonable cost. PDAC may have a common tissue of origin, however it is clear from the pre-existing literature on the molecular subtypes that this is a very heterogenous tumour with each subtype having a distinct clinical disease course. Three landmark papers were originally published on the molecular subtyping of PDAC, each with their own method and reported outcome (Bailey et al., 2016; Collisson et al., 2011; Moffitt et al., 2015). The first paper by Collisson et al (2011) concluded with the identification of 3 different subtypes; Classical, Exocrine like and Quasimesenchymal. The Quasimesenchymal subtype had a significantly worse overall survival (Collisson et al., 2011). The authors observed a high expression of GATA6 within the classical subtype of tumours (Collisson et al., 2011). Moffitt et al

(2015) performed subtyping not only on the tumour, but also the adjacent stroma (Moffitt et al., 2015). Their final report noted three different tumour subtypes (Epithelial, Basal and Classical) and they were able to distinguish between two very different stromal characteristics (activated and normal) (Moffitt et al., 2015). Not only was a survival difference observed amongst the tumour subtypes, but also within the stromal compartment (with Basal and activated stroma harbouring the worse prognosis respectively) (Moffitt et al., 2015). Bailey et al (2016), utilised the pre-existing subtype signatures proposed by Collisson et al (2011) and (Moffitt et al (2015) for the foundation of their analysis and concluded that four different tumour subtypes were identifiable; Squamous, Immunogenic, Pancreatic Progenitor and ADEX (Bailey et al., 2016). When survival trends were compared, the Squamous subtype displayed a significantly worse survival (Bailey et al., 2016). Despite the authors reporting and naming different subtypes, there is clearly a recurring theme amongst all classifications proposed. This theme is the presence of one subtype that has a significantly worse survival outcome when compared to its counterparts. Collectively, the general consensus now is that there are two main subtypes; Classical-Pancreatic (which possesses a more favourable prognosis) and a Squamous subtype (Collisson et al., 2011). The underlying question is what drives the aggressive phenotype of the Squamous subgroup. The answer is likely the fact that this cohort of PDAC tumours represents tumours with greater stemness-like characteristics, particularly the loss of endodermal differentiation and significant downregulation of key driver genes for pancreaticogenesis and development, notably GATA6 expression (Collisson et al., 2011). Further sequencing analysis has confirmed that within squamous tumours there is hypermethylation and subsequent

downregulation with a loss of genetic machinery responsible for endodermal cell differentiation (PDX1, HNF1B) (Bailey et al., 2016). This results in a loss of endodermal characteristics. Higher expression of mesenchymal genes is also noted in this subgroup. Bailey et al, demonstrated that the squamous subgroup of PDAC tumours have significantly higher levels of TP63ΔN gene expression (Bailey et al., 2016). Concordant TP53 mutation and TP63ΔN promotes epithelial to mesenchymal transition (Bailey et al., 2016). When compared to the other PDAC subtypes, squamous tumours are driven by gene programwes such as TGF-β signalling , hypoxia, alteration in metabolic pathways/autophagy and inflammation (Bailey et al., 2016).

Through interrogating PDAC tumours on a multi-omic platform, it is clear that the biology of these tumours is different across subtypes and as a consequence treatment regimes should vary accordingly. Whilst the potential benefits of molecularly profiling PDAC tumours are very clear, it is worth highlighting the fact that as of yet this is not currently implemented in clinical practice. Genetic sequencing does not form part of the standard histopathology report of resected tumours.

1.1.3 Current standard of care for patients with PDAC

Only one treatment strategy has been proven to prolong overall survival for patients with PDAC. Surgical resection of the tumour with loco-regional lymphadenectomy is

the only chance of cure. Surgery significantly extends life expectancy when compared to observation alone (Chakraborty et al., 2013). This finding is consistent across several studies and is irrespective of the underlying age of the patient (Park et al., 2019). The anatomical location of the tumour dictates the nature of the surgery, of which there are three possibilities. For tumour arising within the pancreatic head (the majority of PDAC tumours), a pancreaticoduodenectomy is indicated. For tumours within the pancreatic body or tail, a distal pancreatectomy is the oncological procedure of choice. Finally, for individuals with PDAC and concurrent multifocal precursor lesions (widespread IPMN) or for patients who are at significant risk of pancreatic anastamotic failure, a total pancreatectomy should be considered. The first pancreaticoduodenectomy was performed in 1898 by an Italian Surgeon called Alessandro Codivilla (Are et al., 2011). However, the procedure gained its eponymous name the Whipple procedure after the significant contribution to pancreatic surgery by an American surgeon called Allen Oldfather Whipple in the late 1940s (Are et al., 2011). Notably he converted the procedure from a two-staged to a single-staged operation. Since then, the nature of the operation and surgical principles have remained the same with only some minor modifications as a result of evolving surgical technology. Briefly, the procedure consists of the removal of the whole duodenum, the head of the pancreas, the distal (lower third) of the bile duct, the distal stomach and the regional lymph nodes. A modification to this procedure is the pylorus preserving approach, where the pylorus of the stomach is preserved. After resection of the specimen, the reconstruction phase can commence. A loop of small bowel is used to re-establish GIT continuity by joining it to the residual pancreatic remnant, stomach and bile duct for biliary drainage. Some variation

exists with regard to the nature of the reconstruction. For patients with locally advanced or metastatic disease, palliative procedures should be considered depending on their underlying symptoms (stent insertion or palliative bypass).
It is important to emphasise that pancreatic surgery is burdened with a significant complication rate. The nature of the surgery is high risk and despite advances in surgical care, there remains a 30-40% risk of any complications (La Torre et al., 2012). The post procedure mortality rate has reduced, but remains at 5% even for low risk patients (Balcom et al., 2001). This is an important factor when discussing treatment strategies for PDAC. For each patient a careful assessment of their functional capacity is mandatory. The clinical decision-making process must not only determine if the disease is resectable, but also whether the patient would survive such an operation.

Currently, disease resectability is defined by the presence and the extent of tumour involvement with the peri-pancreatic vasculature on cross-sectional imaging. Several different clinical practice guidelines exist on the topic, however there are some subtle differences amongst them (Tempero et al., 2017; Vauthey et al., 2009).Up front resectable disease constitutes tumours localised to the pancreas with no radiological evidence of vascular involvement. Locally advanced disease may be borderline resectable or unresectable. The differentiating factor is the extent of vascular invasion and whether resection and vascular reconstruction can be undertaken. A large body of evidence exists that demonstrates that venous resection can be performed safely (Tseng et al., 2004). However, the evidence for concomitant arterial resection is much weaker. Not only is arterial reconstruction

technically much more challenging but higher rates of post-operative morbidity and mortality are observed (Adham et al., 2006). At the time of writing this thesis, surgery for oligometastatic disease was not considered a routine standard of care (Voss et al., 2019). However, within the current literature there are a few published case series from very high volume centres documenting their experience and outcomes following multi-visceral pancreatic surgery (notably concomitant liver resection for PDAC liver metastases) (Hackert et al., 2017). This may reflect the natural evolution of the surgical management of PDAC

Despite the clear survival benefit that surgery provides (when compared to observation alone), it is essential that when surgery is performed, the tumour is excised in its entirety and that there is no residual disease. The oncological aim is to remove all the disease locoregionally en bloc in order to achieve a R0 resection (R0 denotes the descriptive terminology that pathologist use to describe whether complete excision has been achieved). The R0 status of a patient is an independent prognostication predictor of overall survival (Strobel et al., 2017). Achieving an R0 resection status is paramount during surgery and this is the principal argument for extended pancreatic resections (vascular or multi-visceral resection). A positive resection margin (R1 – residual microscopic disease at the transection margin) significantly reduces long-term survival (Demir et al., 2018). Currently within the United Kingdom, the governing body the National Institute for Health and Care Excellence (NICE) suggests that all patients with a good performance status who have local disease should undergo curative surgery (NICE, 2018).

1.1.4 The role of Adjuvant Chemotherapy

There is no doubt that Chemotherapy plays an integral part in the management of PDAC. It provides an opportunity to gain systemic control over the disease. The seminal randomised clinical trial (RCT) published by the Gastrointestinal Tumor Study Group in 1985 demonstrated a clear survival advantage when Fluorouracil was given as part of a chemoradiotherapy regime followed by maintenance chemotherapy after curative surgery when compared to surgery alone (median survival 20 vs 11 months) (Demir et al., 2018). The result of this trial influenced clinical practice for over a decade and provided the foundations for the role of adjuvant therapy. The EORTC trial published in 1999 failed to demonstrate a statistically significant survival advantage when adjuvant chemoradiotherapy was used alone without maintenance chemotherapy (Klinkenbijl et al., 1999). This finding was reproduced in the European Study Group for Pancreatic Cancer (ESPAC)-1 trial in 2001, which showed survival following curative resection of PDAC was prolonged with adjuvant Fluorouracil (FU) and folinic acid when compared to observation alone and that chemoradiotherapy negatively impacted survival (Neoptolemos et al., 2004). The role of Gemcitabine as adjuvant therapy for PDAC gained significant attention following the publication of the CONKO-01 trial in 2007 (Oettle et al., 2007). The CONKO-01 trial demonstrated a significantly longer disease-free survival in the Gemcitabine group when compared to the control arm (13.4 vs 6.0 months) (Oettle et al., 2007). Naturally, the next question in the saga of identifying the optimal adjuvant chemotherapy regime for PDAC was whether FU or Gemcitabine should be first line treatment. The ESPAC-3 trial attempted to answer

this question in 2010, however no significant differences were noted in median survival or progression free survival (Neoptolemos et al., 2010). An important finding from the trial was a significantly lower rate of drug induced serious adverse events in the Gemcitabine arm (Neoptolemos et al., 2010). Current clinical practice in the United Kingdom is dictated by the results of the ESPAC-4 trial. ESPAC-4 demonstrated a survival benefit of combination chemotherapy (comprising Gemcitabine and Capecitabine) when compared to monotherapy with Gemcitabine alone (Neoptolemos et al., 2017). A breakthrough trial was published in 2018 by the Canadian Cancer Trials and PRODIGE Group (Conroy et al., 2018). The PRODIGE-24 trial compared survival following adjuvant Gemcitabine or a modified FOLFIRINOX regime (comprising fluorouracil, folinic acid, irinotecan and oxaliplatin) (Conroy et al., 2018). The study reported a remarkable overall survival of 54 months in the arm that received the modified FOLFIRINOX regime (Conroy et al., 2018). Such an overall survival has never been reported before in the context of PDAC. However this survival benefit did come at a cost, as a much higher rate of grade 3 or 4 adverse drug events were noted in the modified FOLFIRINOX regime (Conroy et al., 2018). Therefore, potentially this regime would be reserved for a selective sub-cohort of patients (younger patients with limited comorbidities and a good performance status). It is likely that this regime will be first line therapy in the near future. Therefore, NICE advocates that patients with a good performance status should receive combination therapy, whereas for frailer patients, monotherapy with Gemcitabine is indicated (NICE, 2018).

1.1.5 The role of Neo-Adjuvant Chemotherapy

The role of Neo-Adjuvant Chemotherapy for PDAC remains a debatable topic. Another layer of complexity is inserted into the debate as one should also consider the two distinct biological features of PDAC upon diagnosis; resectable disease and locally advanced disease. As a consequence, several arguments have been made advocating the role of Neo-Adjuvant therapy. Firstly, from our experience with adjuvant chemotherapy for PDAC, what is clear is that the full chemotherapy regime must be completed in order for the individual patient to gain a survival benefit (Neoptolemos et al., 2010). Unfortunately, from real world data, we are aware that only a minority of our patients (approximately 30%) complete adjuvant therapy (Oettle et al., 2007). The reasons for incomplete treatment range from post-operative complications following pancreatic surgery with a subsequent prolonged hospital stay to a delayed recovery with the development of frailty (thus rendering the patient unsuitable for chemotherapy). Therefore by providing up-front chemotherapy, the compliance rates increase and we can be sure that the full regime is completed. Another key argument for the role of Neo-Adjuvant chemotherapy is that it may treat the micrometastatic disease associated with PDAC. From clinical experience, patients with small tumours on imaging who undergo resection may still succumb to recurrent disease with early relapse (Haeno et al., 2012). This reinforces the theory of early dissemination in PDAC. Therefore Neo-Adjuvant chemotherapy may provide the opportunity to gain systemic control over the disease prior to local control with tumour resection. Another critical consideration is that whilst the patient is on Neo-Adjuvant treatment, this time

frame provides a unique insight into the tumour's biological behaviour. It is estimated that 20% of patients will have disease progression whilst on Neo-Adjuvant treatment, which serves as a proxy measure for an aggressive disease phenotype (Gillen et al., 2010). These individuals would not have been cured by surgery; therefore this proxy measure can be used as a selection tool in order to select appropriate patients for surgery and to ensure that no patient suffers the morbidity of pancreatic surgery with no overall survival benefit. The final argument for Neo-Adjuvant treatment is its ability to potentially downstage the disease. This is especially the case for locally advanced pancreatic cancer (He et al., 2014). Neo-Adjuvant treatment can shrink the tumour size, increase the R0 rate, decrease the positive nodal burden and potentially convert unresectable to resectable disease (Seufferlein et al., 2019).

Despite the proposed benefits of Neo-Adjuvant chemotherapy, it is important to evaluate the current published data on the topic. To date, several systematic reviews with meta-analyses have been published on the role of Neo-Adjuvant chemotherapy (Assifi et al., 2011; Gillen et al., 2010). These are limited by their retrospective nature, ambiguity of disease terminology and limitations with the methodology. However, prospective RCT are being conducted on the topic. Two current RCT to note are the Prep-02/JSAP05 and PREOPANC-1 trial (Motoi et al., 2019; Versteijne et al., 2020). The Prep-02/JSAP05 was a Japanese trial that compared Neo-Adjuvant chemotherapy with Gemcitabine and S1 (a combination of tegafur, gimeracil and oteracil) followed by surgery and adjuvant S1 against upfront surgery and adjuvant S1 (Motoi et al., 2019). The Neo-Adjuvant arm had a higher resection rate (93% vs

82%), a significantly higher median overall survival (36.72 vs 26.65 months, p-0.015) and a lower rate of positive lymph node involvement (59.6% vs 81.5%) (Motoi et al., 2019). However caution is required when interpreting these results as such a response to S1 chemotherapy has yet to be seen in a western population of patients. The PREOPANC-1 trial was a European trial that assessed Neo-Adjuvant chemoradiotherapy with Gemcitabine followed by surgery and adjuvant Gemcitabine against up-front surgery and adjuvant Gemcitabine(Versteijne et al., 2020). Whilst no difference was noted in the primary endpoint of the trial – median overall survival (13.7 vs 17.1 months, p=0.074), a subgroup analysis of individual patients who completed all 3 treatments (Neo-Adjuvant, surgery and adjuvant chemotherapy) displayed a significant survival benefit (29.9 months vs 16.8 months, p=0.001) (Versteijne et al., 2020). At the beginning of 2022, the long-term results of the PREOPANC trial were published. The authors demonstrated that Neo-Adjuvant chemotherapy was associated with an improved overall survival when compared to upfront surgery (hazard ratio, 0.73; 95% CI, 0.56 to 0.96; *P* = .025) (Versteijne et al ., 2022). The 5 year overall survival with Neo-Adjuvant therapy was 20.5% whereas with upfront surgery it was only 6.5% (Versteijne et al ., 2022). A recently published European survey that assessed the opinions of pancreatic surgeons and medical oncologists regarding Neo-Adjuvant chemotherapy, illustrated that in the context of borderline resectable or locally advanced disease, the majority consensus (48%) would advocate Neo-Adjuvant treatment (Heinrich et al., 2019). However, for resectable disease, only a minority 9% would recommend Neo-Adjuvant chemotherapy (Heinrich et al., 2019). Further research is required to determine the

role of Neo-Adjuvant chemotherapy in patients with localised diseased that would be amenable for up front resection.

1.1.6 The role of Immunotherapy

Over the last decade, we have witnessed the revolution of immunotherapy within oncology. The complex interface between the immune system and cancer is being interrogated. What is clear from the wider literature is that cancer cells can manipulate the host's immune system to promote immune evasion of tumours, metastases and an overall aggressive disease phenotype. Through understanding which mechanisms are altered, this serves as a reference for pharmacological targeting in order to overcome the immune resistance and to utilise the host's immune system for effective cancer cell killing and immune surveillance.

Immunotherapy utilises a variety of strategies in order to achieve a positive clinical effect. These include promoting immune cell infiltration into tumours, reducing the presence of regulatory/immunosuppressive cell types to overcoming and breaking checkpoint blockage signalling. For several solid organ malignancies we have observed the clear clinical benefit of immunotherapy. This is notably the case with malignant melanoma. Even in the context of unresectable stage 3 or 4 disease, immunotherapy can significantly improve prognosis and overall survival (Robert et al., 2014).

Unfortunately for PDAC, immunotherapy has not yet been widely implemented into clinical practice. There are several proposed mechanisms for the immune resistance within PDAC tumours. This ranges from the predominantly immunosuppressive immune cell infiltrate, low mutational burden with subsequent low neoantigenicity and immunosuppressant properties of the stroma. To date only one immunotherapy regime has been licenced for PDAC. The United States Food and Drug Administration granted approval for the use of anti-PD-1 therapy for PDAC however this is only in a very specific patient cohort (microsatellite unstable tumours) (Yoon et al., 2021).

Current research efforts have been focussing on manipulating a variety of immune mechanisms within PDAC tumours. Immune checkpoint blockage serves as a desirable target for immunotherapy. To date there have been 15 clinical trials utilising check point inhibitors for PDAC (Timmer et al., 2021). The median overall survival reported varies from 3.1 – 15 months, however it is worth highlighting that this is in the context of patients with metastatic or locally advanced tumours (Timmer et al., 2021). Advances in technology have allowed for novel immunotherapy techniques to be trialled, an example of which has been oncolytic viral therapy. Preliminary results from murine model experiments have demonstrated that oncolytic virus use can increase overall survival, increase infiltration of CD8+ cells into the tumour and downregulate immunosuppressive function of macrophages (Zhang et al., 2020). Such an approach has subsequently been implemented into phase 1 clinical trials with varying results (Hirooka et al., 2018). What is clear is the need to develop physiologically representative models

which can be utilised to further assess immunotherapy treatment strategies for PDAC.

1.2 Current challenges in clinical practice with PDAC management

Despite all the advances over the last decade, several barriers still exist that continue to impede our efforts to prolong survival for our patients with PDAC. One of the core elements of this problem is our ability to detect patients with early disease. Early disease is localised to the pancreas and localised disease can be resected and thus there is a chance of cure. The harsh reality we face in clinical practice is that the vast majority of our patients (50-60%) are diagnosed with metastatic disease at their initial diagnosis (Hidalgo et al., 2015). A further 30 % are diagnosed with locally advanced disease (Hidalgo et al., 2015). Therefore, our pool of patients that would be eligible for curative treatment – surgery, is immediately reduced to a very small number. There are several reasons for this ranging from disease biology to the organisational delivery of health care services. As highlighted previously, the symptoms of PDAC in most cases are vague and nonspecific (Porta et al., 2005). Definitive, hard red flag symptoms only arise secondary to local mass effect or local invasion. A substantial effort has been made to increase the general public's awareness of PDAC symptoms through general campaigning and media advertisement by pancreatic cancer charities in an attempt to reduce diagnostic delays.

A consequence of the centralisation of pancreatic surgery services in the United Kingdoms to supra-regional specialist centres is that the time to diagnosis/management may be prolonged, as patients are referred from primary to secondary to tertiary level care. Another very important consideration of this organisational set up is the possibility of inappropriate investigations and interventions prior to a review by the surgical team. This includes routine placement of biliary tract stents (Lee et al., 2018). Not only does this predisposes to infective complications and can potentially delay both surgery and Neo-Adjuvant therapy, but may also complicate surgery.

As there is a need to identify early disease, significant research efforts have been made to identify novel biomarkers for PDAC. Despite several potential biomarkers showing optimistic results for early disease recognition, none as of yet have been validated for routine clinical use (Iwanicki-Caron et al., 2013; Melo et al., 2015). In fact, only one biomarker, a tumour marker is routinely used in clinical practice, Carbohydrate antigen 19-9 (CA19-9). CA19-9 is a tetrasaccharide epitope to the sialylated Lewis antigen (Vestergaard et al., 1999). It is used both as an adjunct to diagnose PDAC and to monitor tumour responsiveness to treatment (Takahashi et al., 2010). However, CA19-9 can be raised in benign conditions and in other malignancies (Goonetilleke et al., 2007). In addition, approximately 10% of Caucasians are unable to produce the CA19-9 epitope, thus causing a falsely negative result (Scara et al., 2015). These factors limit the usefulness of this biomarker.

The cardinal issue in clinical practice is the high rates of chemotherapeutic resistance observed in PDAC tumours. The mechanisms of resistance may be intrinsic to the tumour or may be as a consequence of chemotherapy induced adaptation strategies by the tumour cells (Long et al., 2011). Despite Gemcitabine being the principal chemotherapy regime for PDAC for several decades, the individual patient response rate to the drug is predicted to be approximately 25% (Sheikh et al., 2010). Even with combination therapy there is no uniform response. Through utilising the molecular subtypes of pancreatic cancer, it appears that even the different subtypes may benefit from different chemotherapy regimes (Aguirre et al., 2018; Tiriac et al., 2018).

As suggested previously, PDAC tumours possess several biological characteristics that may contribute to pharmacodynamic resistance to chemotherapy observed in clinical practice. The abundance of the desmoplastic stroma not only disrupts normal pancreatic architecture but also causes significant compression on the vasculature leading to a reduction of the blood vessel diameter, and thus in turn blood flow to the tumour (Feig et al., 2012). This has served as a proposed mechanism for drug resistance as a consequence of the lack of a delivery of the drug to the tumour - the stroma provides a physical barrier that impedes delivery (Olive et al., 2009). Naturally, targeting the stromal barrier would appear as a logical decision when creating novel treatment strategies for PDAC. Certainly in the context of a Genetically Engineered Mouse (GEM) model that recapitulates human PDAC tumours with an abundance of stroma, depleting the stroma through hedgehog signaling pathway inhibition resulted in an increase in tumour vascularity, higher

concentration of Gemcitabine within the tumour and a greater overall survival with fewer liver metastases (Olive et al., 2009). Unfortunately, this finding has yet to be replicated in a human patient cohort. To date, two clinical trials combining Gemcitabine and a sonic hedgehog pathway inhibitor have displayed no survival benefit (Catenacci et al., 2015; E. J. Kim et al., 2014). It would appear that global depletion of PDAC stroma may be detrimental to long-term survival. Emerging evidence from the wider literature demonstrated that stroma depletion through sonic hedgehog inhibition resulted in more aggressive tumours (Rhim et al., 2014). Through utilising a genetic engineered mouse model with sonic hedgehog deletion, Rhim et al, demonstrated that the tumours that developed had much less stroma present however an aggressive disease phenotype was identified with higher proliferation rates and undifferentiated histology (Rhim et al., 2014). This suggests that within the stromal compartment there are some anti-tumorigenic properties. Therefore future attempts at stromal manipulation should identify and target specific components that drive disease progression instead of a non-specific , generalised, pan-stroma inhibition.

Intrinsic cell mechanisms in PDAC that contribute to drug resistance are vast. After delivering the drug to the tumour in a sufficient concentration, the next paramount step is ensuring cellular uptake. This can be manipulated by the tumour through two mechanisms – increasing extracellular export of the drug and inhibiting drug uptake. Upregulation and overexpression of drug efflux pumps, notably the ATPbinding cassette transporter proteins by cancer cells, promotes active expulsion of the drugs

from within the cells, thus contributing to lower intracellular drug concentration and a subsequent lower therapeutic effect (Konig et al., 2005). In the context of Gemcitabine treatment, significant progress has been made in our understanding of drug resistance. The crucial step is ensuring drug uptake. This is regulated by Human equilibrative nucleoside transporter 1 (hENT1). hENT1 encodes for a glycoprotein with a transmembrane domain that enables cellular uptake of pyrimidine nucleoside therapies (notably Gemcitabine) (Greenhalf et al., 2014). Therefore cancer cells can manipulate this mechanism (conversely to the function of the ATPbinding cassette transporter proteins) and downregulate hENT1, resulting in less drug uptake (Greenhalf et al., 2014). It has been demonstrated that patients with PDAC tumours that have a low hENT1 expression, who are treated with Gemcitabine have a worse overall survival (Greenhalf et al., 2014). After cellular uptake of Gemcitabine, it requires conversion to its active metabolite form (Andersson et al., 2009). This cascade of events is initiated by the phosphorylation of Gemcitabine by deoxycytidine kinase (Andersson et al., 2009). Therefore PDAC tumours with lower levels of deoxycytidine kinase that are treated with Gemcitabine have a worse prognosis (Sebastiani et al., 2006). There is some conflicting evidence within the wider literature regarding the therapeutic benefits of hENT1 expression as a biomarker to guide chemotherapeutic treatment strategies with Gemcitabine. In 2013, a published randomised control trial compared Gemcitabine and CO-101 (Poplin et al., 2013). CO-101 consists of a Gemcitabine molecule that is covalently bound to an elaidic acid molecule (Poplin et al., 2013). The presence of the elaidic acid molecule permits the entry of the drug into cells irrespective and independently of nucleoside transporters (Poplin et al., 2013). The rationale for the trial was to

assess whether C0-101 use in patients with low hENT1 expression improved survival. Unfortunately overall survival did not differ between both treatment arms (Poplin et al., 2013). The trial concluded that Gemcitabine response could not be predicted by hENT1 expression (Poplin et al., 2013).

It is clear that PDAC tumours are heterogenous and vary significantly between patients. It is essential that we understand the mutations, dysregulated signaling pathways and cellular resistance mechanisms in each tumour prior to starting treatment. Unfortunately, in the United Kingdom, chemotherapy for PDAC is defined by the individual patient's performance status. This rigid and binary approach to chemotherapy prescribing neglects all of the individual's unique tumour biology. Adopting the approach of a one treatment strategy for all patients in PDAC is both incorrect and ineffective. It will not translate to better patient outcomes. What is required is an intelligent and multimodal approach that is driven by disease biology and treatment that is personalised and precise.

1.3 Precision therapy

Several different definitions exist for precision therapy within the wider literature (Vogenberg et al., 2010). However, the key underlying message is that it is the selection of the correct treatment regime for each individual patient. The premise of this approach is acknowledging that a universal treatment strategy for all patients is inappropriate, that patients will respond differently to the same therapy and that

there is a need to prescribe therapy based on previously acquired evidence that is both confirmatory and predictive of a therapeutic response. Clearly in the context of PDAC this is required as significant variation in treatment response rates is observed across all patients and there is an evident need to gain systemic control over the disease.

Precision therapy has yet to be implemented as a routine treatment strategy for PDAC. However, it is a standard of care for several cancers within different medical disciplines. Within the field of haematology, patients with suspected/confirmed leukaemia undergo early and extensive multi-omic profiling. One of the earliest discoveries was that of the stratification of patients based on a genetic driver of the disease, notably the presence of a fusion gene (Breakpoint Cluster Region – ABL1 gene also referred to as Philadelphia Chromosome Translocation) (Quintas-Cardama et al., 2009). These patients would be commenced on a Tyrosine kinase inhibitor and gain a significant therapeutic benefit in light of the drug inhibition of the deregulated and over activated protein signaling cascade that was driven by their mutation (Quintas-Cardama et al., 2009). The same approach has been observed in other solid tumour types. In the context of breast cancer, after diagnosis the tumours are profiled to detect whether amplification of HER2 is present (Gutierrez et al., 2011). This phenomenon is present within 20% of all breast cancers and is synonymous with an aggressive disease phenotype and poor survival (Gajria et al., 2011). This selective patient cohort is a candidate for Trastuzumab therapy (Herceptin) (Gajria et al., 2011). A significant survival advantage was observed in the context of both metastatic and localised disease when HER2 +ve breast cancer

patients where commenced on Herceptin (Gutierrez et al., 2011). Within the GIT, colorectal cancer patients can be stratified based upon tumour over expression of Epidermal growth factor receptor (EGFR) (Pabla et al., 2015). Cetuximab therapy enables inhibition of the overactive EGFR pathway (Pabla et al., 2015). In 2007, Jonker et al, demonstrated in a RCT in a cohort of treatment resistant colorectal cancer patients that combining cetuximab with supportive care was associated with a significantly longer overall survival when compared to supportive care alone ($p=0.005$) (Jonker et al., 2007). The scenarios described above are examples of when specific signaling pathways are dysregulated within a select patient cohort and subsequently targeted with pharmacological inhibition. This does serve as one form of precision therapy. However in the context of PDAC, single aberrant pathway inhibition is unsuccessful (due to the relative low numbers of patients with druggable mutations). The question therefore remains as to how do we assess therapeutic response to numerous therapies in our patients with PDAC without exposing them to potential therapeutic harm. The answer consists in approaching precision therapy from a different perspective, notably by using some aspect/form of the individuals' tumour as a foundation for a drug screen.

Recent advances in sequencing technology have the potential to lead future developments in precision therapy. The Know Your Tumour (KYT) initiative, based in North America, illustrated the organisational requirements and infrastructure needed to deliver a national programme for tumour sequencing (Pishvaian et al., 2018). A landmark initiative was commenced in 2017 in an attempt to improve outcomes for patients with PDAC in the UK. The PRECISION-Panc platform was

established in order to deliver a national, multi centre network where patients with suspected or confirmed PDAC could be entered into a dynamic prospective study (Dreyer et al., 2020). The infrastructure allows for vast collection of both tissue and serum samples for mass analysis. The focus is to ensure rapid translation of scientific discoveries into clinical practice. Once a patient is recruited, a high throughput multiomic sequencing process is undertaken in order to create a comprehensive molecular report on the individual's tumour (Dreyer et al., 2020). Not only does this create a data rich archive (which exponentially increases in depth with each patient recruited) that will help consolidate our understanding of PDAC biology but it also ensures continuous direct feedback into clinical practice. The infrastructure overcomes the historic problems encountered within PDAC research, notably the lack of access to or volume of tissue, low tissue yields upon biopsy with hypocellularity and the logistical challenges associated with research (Froeling et al., 2021). A unique aspect of the platform is that it allows for synchronous biomarker discovery/validation in parallel with patient stratification for prospective clinical trials. The sequencing output from the initial recruitment allows for molecular profiling of patients, which can subsequently be used for trial inclusion. The pancreatic cancer individualised multi-arm studies or "PRIMUS" are prospective clinical trials managed by the PRECISION-Panc consortium that allow for the assessment of survival outcomes in a unique subset of PDAC patients (Dreyer et al., 2020). The trials are designed to assess timing of therapies, optimal combinations of treatment, patient stratification and novel therapeutic targets /strategies.

1.3.1 Models for therapeutic drug screens on primary tumours

Different models for precision therapy have been described that utilise a tissue sample from the patient (either from the primary or from an accessible metastasis) to conduct a drug screen and to determine a therapeutic response. These models vary significantly in complexity, ranging from patient derived cell lines to patient derived xenograft models, all of which have the ability to assess for a drug response in the patient's native tumour. This information can inform and dictate future treatment strategies. As the models become more complex this in turn will create a more physiologically representative system and thus will likely produce more robust and valid results. However as the precision therapy model further develops it will have additional financial implications and other practical considerations. Therefore equilibrium is required between the complexity of the system, overhead costs and the ability to conduct a high throughput drug screen.

1.3.2 Patient derived cell lines

Patient derived cell lines are representative of a precision therapy model of relative low complexity for establishment. After the acquisition of the tumour, tissue dissociation is performed (using a combination of manual dissection and enzymatic digestion) until a single monolayer cell solution is created (Kodack et al., 2017). The cell line can be subsequently passaged over time to increase the overall yield/availability of the cells for performing a drug screen. Kodack et al, 2017

published their extensive experience with creating patient derived cancer cell lines from 568 patient specimens (ranging from resectional material , biopsies and malignant effusions) (Kodack et al., 2017). They successfully created a number of cancer cell lines from a broad range of tumours. The highest success rate for cancer cell line creation was from colorectal, pancreatic and lung cancer tumours (Kodack et al., 2017). Kim et al published their series of 23 patient derived cell lines from patients with lung cancer which they were able to use for a drug screen (S. Y. Kim et al., 2019). Of interest was that the in vitro response to tyrosine kinase inhibition mimicked that of the patient's response in the clinic, thus validating their model (S. Y. Kim et al., 2019). The clear benefits of using patient derived cell lines for precision therapy is the relative inexpensive cost for establishing and maintaining the cells, the speed of creation and the relatively large yield of samples with the subsequent ability to conduct a broad and extensive drug screen. However, the model is associated with several limitations, notably the cellular diversity of the tumour is lost. The full TME is missing and as a consequence may directly impact on the validity of the drug screen. During prolonged ex vivo culture, genetic drift may occur and the cell population may alter. As a consequence of the dissociation process, there is a selective outgrowth of one clonal cell type and as such a uni-dimensional view of therapeutic response is obtained.

1.3.3 Patient derived organoids and bioprinted tumours

Patient derived organoids are representative of a precision therapy system that has transitioned from 2D to 3D. This transition is accompanied by another layer of

complexity with regard to establishing the system, however it possesses several advantages over its 2D patient derived cell lines counterpart system. Organoids are derived from primary human tissue (both normal and pathological state) and represent a 3D cellular cluster (Fatehullah et al., 2016). Organoids have been successfully cultured from several different human tumours, ranging from colon to prostate cancer (Fatehullah et al., 2016). The initial protocol for organoid creation is very similar to that of patient derived cell lines (Driehuis et al., 2020). The native tissue is dissociated as per the previously described physical and mechanical methods, however what is different is that the organoids are cultured within a matrigel solution (Driehuis et al., 2020). This matrigel provides a structural support scaffold for the organoids during ex vivo culture (Kaur et al., 2021). Another important difference is that the organoid culture media is heavily supplemented with additional growth factors, nutrients and inhibitors (Georgakopoulos et al., 2020). This is in order to control and promote differentiation of the organoids towards their intended final form (mimicking their tissue of origin). Organoids are an appealing system for precision therapy as the initial creation yield is high. From a small amount of primary tissue, numerous organoids can be created (Fatehullah et al., 2016). As such several different analyses / drug screens can be performed. Long-term storage and multiple passages are also possible (Fatehullah et al., 2016). Organoids can be manipulated ex vivo with genetic manipulation (using CRISPR technology), a technique that can be used to study disease pathogenesis. As organoids are a 3D multi cellular structure, they also recapitulate cell-cell interaction (J. Kim et al., 2020). Calvo, et al 2019 established patient organoids from resected PDAC tumours (Romero-Calvo et al., 2019). They demonstrated that the organoids

retained the morphological histology features of the primary tumour (Romero-Calvo et al., 2019). Interestingly they also illustrated that the gene expression profile was similar between primary tumour and organoid (Romero-Calvo et al., 2019). However this model does have limitations that should be discussed. Organoids are predominantly unicellular entities. They do no successfully capture the diversity of the primary tumour. The TME is not recapitulated. Whilst novel techniques of multicellular 3D printing of organoids has been described, this technology is expensive and not readily accessible to all (Velasco et al., 2020). Organoids are also devoid of an immune component. The presence of the matrigel scaffold may impede drug delivery and penetration to the organoid and may influence biological processes (Fatehullah et al., 2016). There are also practical considerations associated with this technique. Successful culture and maturation rates are variable, not all organoids will have successful establishment within the media. This may result in an outgrowth of a selective sub clonal cellular population, which results in the organoids not being truly representative of the entire primary tumour. Heterogeneity may therefore exist between organoids, which may confound the results of a drug screen. The model fails to replicate the biomechanical forces experienced in vivo by the tumour (Fatehullah et al., 2016).

Tissue acquisition may serve as a rate-limiting step for some precision therapy platforms. Recent advances in bioengineering technology coupled with our understanding of the multicellular nature of cancer have permitted the development of novel tissue engineering techniques. An example of this would be 3D bioprinting. This method utilises the principle of multicellular deposition in a serial layer

construct in order to establish a 3D model (Datta et al, 2020). Several different techniques of 3D bioprinting have been described (Ozbolat et al 2016, Gudapati et al, 2016). This technique has been applied to establish 3D cancer constructs. Langer et al, published their experience of bioprinting replica PDAC tumours (Langer et al, 2019). Their construct consisted of PDX tissue, fibroblasts and human umbilical vein endothelial cells (Langer et al, 2019). They noted that a cancer-stroma interface was established (Langer et al, 2019). The tumour cells remained functionally active with preserved ki67 activity (Langer et al, 2019). They were also able to use their model for therapeutic testing with Gemcitabine (Langer et al, 2019). An interesting comparison that the authors noted was that the bioprinted tumour had the same morphology as that of the primary patient tumour (Langer et al, 2019). This highlights the benefit of using 3D bioprinting technology as it creates a construct that replicates the spatial characteristics of the in situ tumour and as such can be subsequently utilised for precision therapy.

1.3.4 Patient derived Xenografts

Patient derived Xenograft (PDX) is an example of one of the more complex models for precision therapy. The approach entails obtaining a sample of the patient's primary tumour, with subsequent manual dissection of the tumour into smaller tumour fragments prior to implantation into the mouse. Implantation sites may very but generally there are 2 main approaches: subcutaneous and orthotopic.

Subcutaneous implantation is by far the most common approach, predominantly due to the relatively easy access to the anatomical site. There are other advantages for subcutaneous implantation, notably the ability to readily detect and palpate the tumour. This permits easy monitoring for engraftment and tumour growth, where tumour volume can be calculated with caliper measurements without the need for formal imaging techniques. However, subcutaneous implantation is not without its limitations. Notably, the approach creates tumours that do not fully recapitulate the clinical phenotype of the primary tumour. This is clearly illustrated in the case of flank implantation of pancreatic tumours within a xenograft model (S. M. Jiang et al., 2012). One of the cardinal clinical features of PDAC is a high rate of metastatic dissemination and a global cachexia syndrome, both of which are not features present within the orthotopic flank model (Go et al., 2017; S. M. Jiang et al., 2012) . This has subsequently prompted further efforts to develop orthotopic models. Go et al, 2017 published their experience of creating an orthotopic PDX model for PDAC (Go et al., 2017). After a subcostal incision, the tumour fragment was secured to the native mouse pancreas via a continuous suture prior to being returned into the abdominal cavity, which was subsequently closed (Go et al., 2017). They noted all 13 mice had histological evidence of metastatic dissemination (Go et al., 2017). However, the metastasis was exclusively to the lung, with only 1 mouse with a detectable liver metastasis(Go et al., 2017). This is contrary to our experience with managing patients with PDAC, where the liver is the most frequent anatomical site for metastasis (Peixoto et al., 2015). The authors also demonstrated evidence of cancer cachexia, with measureable differences in muscle wasting within the mice

(Go et al., 2017). It is therefore clear that an orthotopic implantation PDX model has additional advantages over the conventional flank model.

Historically, the main challenge of using PDX as a model for precision therapy was the high rates of xenograft rejection (C. Xu et al., 2019). As a consequence, research efforts have been focussed on establishing immunodeficient mice. Currently several different mouse models have been created that are sufficiently immunodeficient so that rejection does not occur. These include nude mice (which congenitally lack a thymus and are therefore unable to produce T cells), severely compromised immune deficient (SCID) mice (where there are no functional B and T cells) and non-obese diabetic (NOD) SCID mice (which share the same properties as SCID mice with an additional impairment to NK function) (Jung et al., 2018). The most recent mouse model, NOD-SCID IL2RGamma null (NSG), represents a severely immunocompromised mouse (C. Xu et al., 2019). NSG have a genetically engineered defect in the interleukin 2 receptor γ-chain and as a direct consequence are defective in T , B and NK cells (C. Xu et al., 2019). Higher rates of tumour implantation and successful engraftment rates are reported within mouse models with more severe immunodeficiency (Pompili et al., 2016). The natural limitation of using immunocompromised PDX models is that they provide no information regarding the interaction between tumour and immune system or immune cell infiltrate into the tumours. These are key components to understand, especially within the context of PDAC where a lack of immune cell engagement may be responsible for the poor survival outcome. Efforts have been focussed on developing humanised mice for PDX models, whereby immunocompromised mice receive a

transplantation of human hematopoietic stem cells. After maturation, these models are able to produce functional human immune cells (Okada et al., 2019).

Precision therapy administered through PDX models has several advantages. Given the complexity of the system, a comprehensive overview of the tumour is obtained. The model produces 3D tumours that are multicellular in origin and also creates a functional TME that is representative of an in vivo tumour. This allows the assessment of cell-cell interaction and biomechanical forces. It allows researchers to study disease dissemination and metastatic patterns, thereby providing a more comprehensive evaluation of the tumour behaviour. After successful growth, the PDX tumours can be split and subsequently re-implanted in further mice in order to increase the number of samples per patient. Of greatest importance is the fact that the PDX models retain the original sensitivity of the tumour to treatment (Pompili et al., 2016). Several studies have published high levels of concordance between patient and PDX response to therapy (Bertotti et al., 2011; Topp et al., 2014). However, PDX themselves are not flawless models. One of the fundamental limitations is that there is no intact functional immune component (C. Xu et al., 2019). This therefore precludes the system from evaluating immunomodulatory drugs. This is a clear disadvantage, especially given the rapid development of the field of immuno-oncology and the need to be able to screen novel immunotherapies in vivo. Over time, the tumoural stroma is gradually replaced by murine stroma and murine fibroblasts which are functionally different to human fibroblasts (C. Xu et al., 2019) . Therefore the PDX loses representation of the primary tumour. Successful engraftment rates vary between tumours, with tumours possessing an aggressive

disease phenotype typically associated with higher rates of engraftment (Okada et al., 2019). There are of course practical aspects to consider, the optimal implantation site, the technically challenging protocol and of course the time lag delay for tumour growth. Some studies reported a tumour growth phase ranging from 2- 8 months prior to commencing a pre-clinical study (Jung et al., 2018). This time lag delay is clearly going to negatively impact the versatility of the system and the ability to implement this model within a clinically meaningful time frame, especially for aggressive malignancies (notably PDAC) where time is of the essence and systemic therapy should be commenced promptly. Finally, there are significant financial costs associated with this model of precision therapy, both in terms of cost of establishing a PDX model initially, but also for long term maintenance. This is an important consideration, especially in the context of our current health care infrastructure. If precision therapy is to be implemented as a routine standard of care for patients with PDAC then it would have to be a cost effective service.

1.3.5 Primary tissue slice culture

Primary human tissue culture serves as an alternative technique for precision therapy. This technique consists of creating multiple tissue slices from a core of tissue. This approach overcomes several of the limitations associated with organoid or cell line creation as it does not require significant processing of the tissue following acquisition. When compared to xenograft models, it can be established

within a quicker time frame and there is no maturation phase required. Its use has been described in a variety of tumour types.

There was initial concern that the technique would not be viable for ex vivo pancreas tissue culture. Davies et al, initially described a comprehensive overview and optimisation process for tissue slice culture (Davies et al., 2015). They concluded that culturing tissue slices on a filter support significantly improved viability when compared to when tissue was cultured in a 'free floating' state (Davies et al., 2015). However they noted that culture under hypoxic conditions was detrimental to successful long-term culture (Davies et al., 2015). The tumour types used initially by Davies et al, (breast and prostate cancer) do not possess an excessively hypoxic core. This contrasts with PDAC tumours where tumour hypoxia is a cardinal feature secondary to the desmoplastic stroma present. Therefore, the practicality of using tissue slice culture for PDAC was questioned. Misra et al, compared culture oxygen conditions (hypoxia, normoxia and hyperoxia) when culturing PDC slices (Misra et al, 2019). Their approach to tissue slice creation constituted of using the vibratome to cut the tissue, however they did not use an agarose scaffold for stability during cutting and created thicker tissue slices of 350 µm thickness. They concluded that none of oxygen culture conditions were detrimental to long term culture. Successful culture of PDAC tissue slices to 96 hours ex vivo was reported (Misra et al, 2019). They characterised biological processes (ki67 and mTOR activity) and cell populations present within the tissue slices however there was no drug treatment assessment (Misra et al, 2019). Kokkinos et al, published their experience of ex vivo PDAC culture in 2021 (Kokkinos et al, 2021). Their tissue processing technique

differed from the previously described method; instead of using a vibratome, manual dissection with a scalpel was performed (Kokkinos et al, 2021). Instead of using a filter support, they described using a gelatin sponge as a scaffold for support (Kokkinos et al, 2021). This also ensured that the tissue slice was kept above the level of the media. They successfully cultured PDAC tumour tissue to 12 days ex vivo. In addition to quantifying biological processes, they also performed drug treatment (with Abraxane) and were able to assess for a therapeutic response (Kokkinos et al, 2021). The limitations highlighted within the organotypic tissue slice model include a lack of circulation (a physiological force), accumulation of metabolic waste products / secretions from the exocrine pancreas and variation in nutrient availability. Incorporating perfusion culture technology within the organotypic tissue slice model could theoretically overcome these limitations.

1.3.6 The optimal system for precision therapy

The use of precision therapy for PDAC management may finally allow a paradigm shift in the long-term survival rates for our patients. The optimal system should meet four desired criteria. Firstly, for it to be utilised as a clinical tool, it must be delivered within a clinically meaningful time frame, in parallel with the patients journey. Therefore there should be a minimal delay between the acquisition of tumour and the establishment of the model. Secondly, the cost to establish and to run the system should be affordable. This is especially important given the increase in disease incidence observed and the potential number of patients that would require

this service. Thirdly, the system must accurately mimic the primary tumour. This should include the cellular diversity of the tumour, an intact TME and a functionally intact immune compartment. Finally the system should allow a broad, high throughput therapeutic drug screen.

1.4 Aims

The aim of this thesis is to establish an individual treatment algorithm for patients with pancreatic cancer that utilises tumour biology to select chemotherapeutic treatment strategies. This will be achieved through the following objectives:

1) Establish a protocol for creating patient derived cancer avatars

2) Evaluate the role of perfusion culture for ex vivo culture of patient avatars

3) Determine the feasibility of ex vivo drug delivery

4) Correlate avatar and patient response to systemic chemotherapy

5) Identify biomarkers that may guide timing of systemic chemotherapy

Chapter 2

Materials and methods

2.1 Overview of methods

Within this thesis, experiments are broadly divided into 4 separate domains: creation of patient derived cancer avatars from resected tumours and perfusion system establishment, in vitro experiments, ex vivo avatar culture and histological analysis and finally bioinformatics analysis. A description of the methodologies utilised will be described in each corresponding section. The author of this thesis performed all experiments unless specified otherwise.

2.2 Creation of patient derived cancer avatars from resected primary tumours

This research project was approved by the Oxford Radcliffe Biobank. Ethical approval was obtained for the acquisition of human tumour tissue samples (Biobank reference 19/A056). All patients recruited to the study provided written consent confirming voluntary participation and permission for tissue donation for research. Patients were identified from the weekly Hepato-Pancreato-Biliary (HPB)

Multidisciplinary Team (MDT) meeting. Over the time period of three years (2018 – 2021) a total of 13 patients were recruited to this study.

2.2.1 Tissue transport, acquisition and preparation

Following surgical resection of the primary tumour, the specimen was transported on ice to the Pathology department. After the painting of the surgical margins by the pathologist was completed, a 5mm punch biopsy of the tumour centre was performed. A further punch biopsy of adjacent normal pancreatic tissue was also performed if there was sufficient tissue present. The specimens were subsequently transported in a 50ml falcon tube with chilled transport media (Low Glucose Dulbecco's Modified Eagle Medium LG-DMEM) on ice to the O'Neill laboratory.

Sample preparation was performed on ice throughout. The initial step consisted of a washing stage, where the sample was placed in a fresh 50 ml Falcon tube with LG-DMEM for 2 minutes prior to the media being aspirated and replenished. A further 2 minute incubation wash stage followed. During this incubation period, a 6% Low Melting Agarose (LMA) solution was prepared. The solidified solution was warmed in a microwave until it was transparent and in liquid form. A plastic embedding cassette was used to form the scaffold structure. An initial small amount (500 ul) of the LMA was decanted into the cassette in order to cover the base. After solidification, the core biopsy was placed in the cassette with a vertical lie (a green needle used to assist with positioning). The LMA was subsequently decanted slowly

so that the core biopsy was entirely covered by the LMA. Once the cassette was full, it was placed in the fridge at 4 °C for 15 minutes incubation in order to allow solidification of the entire scaffold.

2.2.2 Avatar creation with the vibratome

The Leica V1200 vibratome was used to create individual patient avatars from the core biopsy. As a first step, the buffer tray and specimen plate are detached and removed from the vibratome. The embedded core biopsy is superglued to the specimen plate and within 2 minutes it is fully adhered. The specimen plate is then reinserted into the buffer tray and is secured in place by a magnetic mechanism. A 100mls of sterile, chilled PBS is then poured into the buffer tray, which creates a reservoir into which the avatars are released following the cutting of the scaffold. A double-ended blade (Astra Superior platinum double edge) is then inserted into the vibratome and locked in place. Using the inbuilt computer control panel of the vibratome, the buffer tray can be raised or lowered in order for the best position to be achieved. The vibratome subsequently requires programming, where the positioning and the boundaries of the LMA scaffold are identified and defined. This is in order to allow fully automated and continuous cutting of the scaffold without the need for any manual input. The desired vibratome settings (in terms of cutting speed, blade amplitude and step thickness) are subsequently inputted via the console panel and saved. The programme can then be run and continuous passes of the blade through the scaffold will then occur. Once a tissue slice has been created

and released into the buffer tray, this is subsequently fished out with a small spatula and placed in a 12 well plate (pre filled with 1 ml LG-DMEM per well) on ice. Each tissue slice ("avatar") is placed in separate wells and the chronological order of the slices is recorded. Once all the tissue slices have been created, the blade is discarded and the buffer tray is emptied and subsequently sterilised.

The avatars are subsequently transported on ice to the tissue hood within the human tissue room for further modifications prior to culturing. Each avatar is removed and then using a scalpel, the excess LMA scaffold present circumferentially around the avatar is dissected away. Once the avatar has been fully isolated from the LMA scaffold, it is placed in another 12 well plate prior to ex vivo culture.

Where possible, the vibratome technique and system settings were optimised on human tissue samples. However, mouse pancreata was initially used as a surrogate in order to gain some initial experience and confidence with the vibratome technique without wasting precious human tissue samples. Mouse pancreata of *Kras*$^{LSL.G12D+-;}$ *Pdx-1-Cre* (KC) mice were kindly donated by other members of the O'Neill group (Simone Lanfredini, Asmita Thapa and Sophie Hughes).

2.2.3 Perfusion plate set up

The initial step consists of activating the Alvetex strata membrane in order to ensure it has hydrophilic properties. This is achieved by incubating the membrane in 70 % ethanol for 2 minutes followed by a media wash. Once activated, the membranes are kept in LG-DMEM prior to their use. The Alvetex Perfusion Plate (REPROCELL) is set up within the tissue culture hood and once the avatars have been loaded into it, it is subsequently transported into the incubator. The perfusion circuit comprises inflow and outflow tubing, which is constructed for each perfusion plate. Two different plastic tubings were purchased from Thermo Fisher Scientific (FB50855 and FB50857), one of which has an internal diameter of 2mm, whereas the other has an internal diameter of 3mm. One metre of both tubing is measured and cut, the two separate tubes is subsequently connected via a elbow luer connector. The tubing with the 3mm diameter is connected to a syringe, whereas the other end (which is the tubing with 2mm diameter) is connected to the perfusion plate at the inflow and outflow ports. The perfusion circuit is sterilised with 100% ethanol prior to its use. To prime the perfusion circuit, the syringes are filled with culture media prior to flushing through the tubing. Each syringe (Henke-Ject® 50 ml syringe) is connected and secured to individual pumps in order to achieve both an active inflow and outflow of media into the perfusion plate. An Alvetex membrane is inserted into each individual well within the perfusion plate. Patient avatars are subsequently placed on the Alvetex membranes and once all avatars have been positioned, the lid is applied to the perfusion plate so that its contents are sealed from the external environment (Figure 2.1). The perfusion plate is subsequently placed in an

humidified incubator at 37°C and 5% CO_2 for ex vivo culture. Daily checks are performed of the perfusion circuit to ensure that there is no evidence of pump malfunction or contamination of the system. Checks consisted of ensuring that the inflow/outflow tubing had not been displaced or detached, that the syringes attached to the mechanical pumps remained secure and that the correct volume of media had been infused and removed.

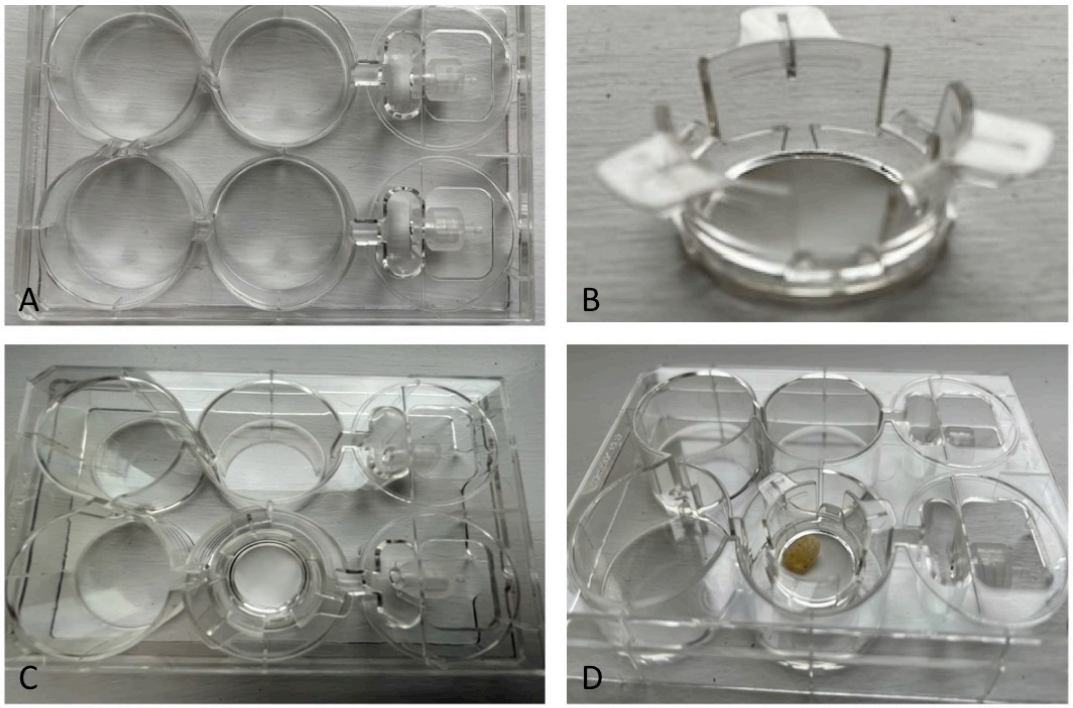

Figure 2.1 – Perfusion plate. (A) Photograph of an empty perfusion plate. The perfusion plate has 4 culture wells. The wells are all interconnected with communicating flow channels. The plate has both an inflow and outflow reservoir that can be connected to a perfusion circuit. (B) Photograph of the culturing basket that includes the alvetex strata membrane at its base. This is a hanging insert that is inserted within each culture well. (C + D) Photograph of both the perfusion plate and culturing basket in situ. Representative tissue placed to demonstrate how avatars are housed on the membrane.

2.2.4 Mathematical modelling of shear stress and determining the Geospatial distribution of the perfusate

In order to determine the extent of shear tension stress exerted on the avatars, mathematical simulation modelling was performed of liquid flow using the COMSOL Multiphysics software (COMSOL Inc, Sweden). The initial step comprises creating a

3D replicate of the perfusion well. The dimensions of the well are inputted into the software and a digital model is subsequently created. The 'laminar flow' software package is loaded. Within this package several different liquids and gasses can be selected to emulate flow, as there is no module for 'culture media' I used water as a proxy measure for 'culture media'. Within the model, I defined both the inflow inlet and outflow outlet prior to inputting the flow rate generated by the pump. The simulation is subsequently run and the visual output of the mathematical modelling of shear stress is produced with a heatmap displaying the corresponding values.

To assess the geospatial distribution of the perfusate, blue dye was loaded into the inflow reservoir. Active perfusion of 60 mls of water was subsequently delivered to the perfusion plate. Aerial images of the perfusion plate at predefined time points were taken with the LEICA S9i microscope. The images were subsequently imported into imageJ for analysis (Schneider et al., 2012). A spherical region of interest (ROI) was created in the centre of the first culture well. The mean grey value of the pixel brightness within the ROI was subsequently measured. Image pixels with a high bright intensity have a high grey value, whereas darker/saturated pixels have a low grey value. Determining the changes in the pixel brightness was used as a proxy measure for blue dye mixing within the well. The measurements were recorded and graphed in prism (v8).

2.3 In vitro experiments

2.3.1 Cell Culture

For all 2D cellular monolayer experiments, commercially available human derived pancreatic adenocarcinoma cell line was used (PSN1). Cells were cultured in Dulbecco's Modified Eagle Low Glucose Medium (LG-DMEM) (1000mg/L) with 10% Foetal Calf Serum (FCS) (Gibco). The media was supplemented with Penicillin/Streptomycin (P/S) (100 U/ml) (Gibco) antibiotics. All cells were maintained in an humidified incubator at 37°C and 5% CO_2 at all times. Cells were cultured using a 6 well plate with or without perfusion using the Alvetex Perfusion Plate (REPROCELL). Cells were closely monitored for confluency and when they reached 90-100% confluency they were subsequently split using 0.25% Trypsin-EDTA solution (Life Technologies). When indicated cells were frozen in freezing medium including 90% (v/v) FCS and 10% (v/v) Dimethyl sulfox-ide (DMSO). Following the trypsinisation of cells, they were subsequently pelleted after centrifugation and resuspended in freezing media in 2ml cryovials (Thermo Scientifc). All cryovials were stored for 24 hours in -80°C in a Nalgene Mr Frosty containing 200mL isopropanol, followed by long-term storage in liquid nitrogen.

2.3.2 Cellular protein extraction and quantification, SDS-PAGE electrophoresis and Western Blotting technique

Cell lysis was performed using a radioimmunoprecipitation (RIPA) buffer (50mM Tris-HCL pH7.5, 150mM NaCl, 0.5M EDTA, 1% NP40) with a PhosSTOP™ phosphatase inhibitor (Roche) and a cOmplete™ protease inhibitor (Roche). After the administration of the RIPA buffer, a cell scraper was used to increase the lysis yield of the cultured cells. A 23 gauge syringe needle was used to homogenise all cell lysates. The lysates were placed on the test tube rotator (LABINCO LD79 Digital Test-Tube Rotator) for 10 minutes followed by centrifugation at 10,000 rpm for 10 minutes. To determine the protein concentration of the lysed cells, the Thermo Scientific™ Pierce™ BCA Protein Assay Kit was used as per the manufacturer's protocol. In summary, the Albumin standard (1 ml ampule of 2 mg/ml) was diluted into 9 different concentrations (ranging from 0 to 2000 BSA final concentration μ/mL). The working reagent (WR) was subsequently prepared by adding 50 mL of reagent A to 1 mL of reagent B. A total of 25 μL of each standard and unknown sample was pipetted into a 96 well plate. Subsequently 200 μL of the WR was added to each well prior to placing the microplate on a plate shaker for a total duration of 30 seconds. The microplate was covered and incubated for 30 minutes at 37 °C. After cooling the microplate, the absorbance of each well was measured on the POLARstar OMEGA at a wavelength of 562 nm. The PRISM (version 9) software was used to plot a standard curve and to calculate the protein concentration of each unknown sample. Normalisation of the samples was performed with SDS-PAGE sample buffer added to all samples in addition to 20 μL of Dithiothreitol (DTT) prior to boiling the samples on Techne® Dri-Block®for 10 minutes at 95°C.

Protein extracts were loaded with equal amounts to NuPAGE™ 4-12% Bis-Tris Gel (Invitrogen) in Novex mini gel tanks that were filled with MOPS loading buffer. The PageRuler™ Plus prestained protein ladder marker was used. A PowerPac HC High-current power supply (Bio-Rad) was used to run the gel at 150V for 1.5 hours. Once the gel electrophoresis was completed, the protein samples were subsequently transferred on to a PVDF membrane Immobilon-P (Millipore). Prior to its use, the membrane was activated by submerging it in methanol for 2 minutes. A Bio-Rad mini gel blotting system was used for the process of gel-membrane transfer. Both the membrane and gel were placed between two sheets of Whatman paper and sandwiched by two sponges. The transfer process was conducted at a 100 V for 90 minutes using a transfer buffer (190mM glycine, 25mM Tris-HCL, 20% v/v methanol) and a PowerPac HC High-current power supply (BioRad). Once the transfer process was completed, a blocking step was performed which consisted of a 1 hour incubation in a blocking solution (5% w/v milk and PBS/0.01% Tween-20 (PBST)) on a SSL4 See saw rocker (Stuart) at room temperature. All membranes were incubated overnight at 4°C with the primary antibody in 5% skimmed milk PBS-T.

After the overnight incubation in the primary antibodies, the membranes were washed three times for five minutes in PBST on a Seesaw rocker. The membranes were subsequently re-incubated in appropriate secondary antibodies (depending on the species in which the first antibody was raised) in 5% skimmed milk PBS-T for 1 hour. Visualisation was performed using the LICOR Odyssey® Imaging System.

2.3.3 Profiling of Metabolic substrates

Profiling of metabolic nutrients was performed using a commercially available kit from Promega (Glucose-Glo ™ assay and Lactate-Glo ™ assay). These bioluminescent-based assays allowed quantification of glucose and lactate levels within the culture media. The assays were performed according to the specified protocol by the manufacturer. In summary, daily media extraction from the culture plate was obtained and diluted in PBS prior to storage in the -20°C freezer until the experiment was completed. The dilution volumes were dictated by plotting concentration curves. Once the experiment was completed, all samples were thawed and analysed en masse. A volume of 25 ul was loaded in triplicate of the daily media sample from both culture plates (one of which was maintained under perfusion and the other under static culture conditions) into a 96-well non-transparent plate. This was followed by adding 25 ul of the respective detection reagent (glucose or lactate) into each well. In the presence of the target metabolic substrate (glucose or lactate respectively), the detection reagent mix catalyses the reduction of NAD+ to NADH. Reductase enzyme utilises NADH and pro-luciferin reductase substrate to form luciferin. This is used by Ultra-GloTM Recombinant Luciferase to generate measurable and quantifiable light. Samples were incubated for 1 hour at room temperature prior to obtaining the luminescent measurement reading via the POLARstar Omega Microplate Readers (BMG LABTECH).

2.4 Ex vivo avatar culture, treatment and analysis

2.4.1 Ex vivo culture

Avatars were either cultured in an Alvetex Perfusion Plate (REPROCELL) if subjected to perfusion culture conditions, or within a conventional 6 well plastic culture plate (Corning) for static culture during the entire time course of ex vivo culture. All avatars were maintained in an incubator (Binder) at 37°C and 5% CO_2 for ex vivo culture. Avatar culture media was made in batch; per 500 ml of LG-DMEM this was supplemented with 0.1% FCS, Dexamethasone (50 ul), Soybean Tripsin Inhibitor (1 ml), Penicillin/Streptomycin/Neomycin cocktail (5 mls) and Amphotericin B (2 mls). Culture media was either delivered via continuous pump infusion or by manual renewal.

2.4.2 Tissue Processing and Embedding

All Human derived PDAC avatars were removed from their respective culture system (static or perfusion culture) and were placed in 5 mL of 10% neutral buffered formalin (NBF) for 12 hours. The avatars were then stored in 70% ethanol for 24 hours. Due to the small size of the avatars, in order to decrease the risk of losing the avatars during processing and embedding, the avatars were placed in individual Cellsafe Biopsy Insert (Electron Microscopy Science) and then placed in a Tissue Processing/Embedding Cassette (Histosette). Avatars were processed using a STP 120 Spin Tissue Processor (Thermo). Embedding in paraffin wax was performed

using a HistoStar tissue embedder (Thermo). The embedded PDAC avatars were stored in the 4°C fridge in the EON lab human tissue room. Mouse pancreata were processed and embedded using the same method. A microtome (Leica RM 212S) was used to cut and create 4 μm sections, which were mounted on to positively charged glass slides.

2.4.3 Histological analysis

In order to undertake histological analysis of the FFPE sections of the PDAC avatars, all slides were initially de-waxed in 2 separate Citroclear washes for 2 minutes each. The FFPE slides were then gradually rehydrated in a decreasing concentration of ethanol (a total of 5 concentrations were used – 100%, 100%, 90%, 70% and 50%) for 3 minutes each. The slides were subsequently washed in running tap water for 5 minutes. Selective staining of the slides was performed with either Immunohistochemistry (IHC), Immunofluorescence (IF), Hematoxylin and Eosin (H&E) or Masson's Trichrome stain. After staining, all slides were gradually dehydrated in ethanol (the ethanol concentrations used were 50%, 70%, 90%, 100% and 100%) for 30 seconds each. Excess ethanol was removed by performing 2 washes for 1 minute in Xylene. In a specific chemical fume hood, the slides were mounted with coverslips using Di-N-Butyl Phthalate in Xylene (DPX). Slides were left to dry overnight in the chemical fume hood. On the following day, all slides were inspected; trapped air bubbles under the cover slip were removed by applying sustained graded pressure, excess DPX was removed with a razor blade and the

slides were cleaned using 70% ethanol. The Aperio Scanscope slide scanner was used to scan slides and to create digitalised pathology images. All histological slides were scanned using the inbuilt x 40 magnification of the Aperio Scanscope

2.4.3.1 Analysis strategy

As the majority of the analysis of the avatars following ex vivo culture was going to be based upon staining of FFPE slides for proteins of interest, a reproducible analysis strategy was required for the quantification of the staining patterns observed. An initial method trialled was only assessing the tumoural areas within the avatars. However, this approach only provided a narrow view on a single compartment of the avatar. The avatar model was selected for this project as it retained the cellular diversity and heterogeneity of the primary tumour and as such this should be incorporated within the analysis. In order to obtain a global view of the avatar, numerous ROIs from across the entirety of the avatar were taken for quantification and analysis. It was felt that this provided a better representation of the functional state of the avatar in general. In order to remove selection bias for selective area quantification, a randomised ROI selection process was implemented. In summary, for each digital pathology image, a superimposed matrix of multiple squares (measuring 500 by 500 microns) was overlaid over the avatar. Each square (serving as a ROI) was annotated and numerically defined (Figure 2.2) . An online randomised number generator was subsequently used (https://www.randomizer.org/). The number generator would randomly select a sequence of numbers. These numbers were successively identified on the superimposed matrix squares on the digital

image. These individual annotated squares would then serve as ROIs to be formally quantified.

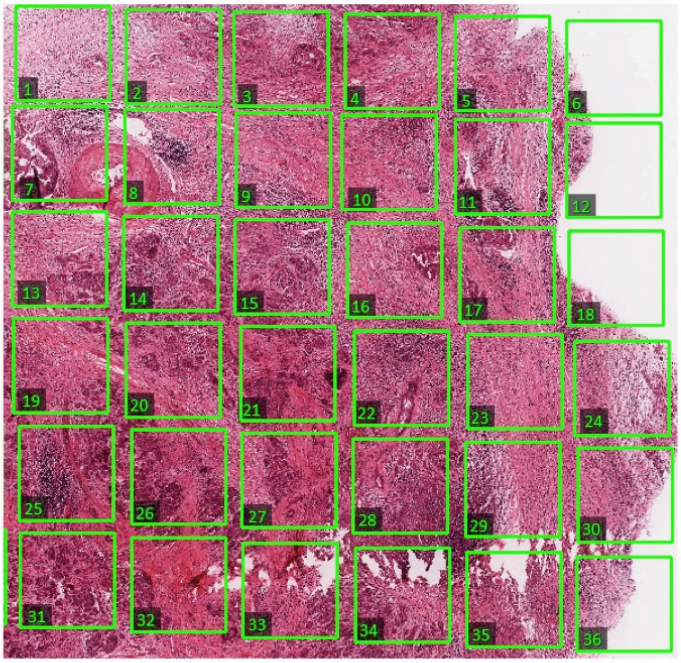

A

Random number generator	26	13	22
Corresponding area of annotated matrix	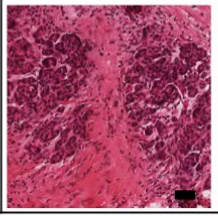	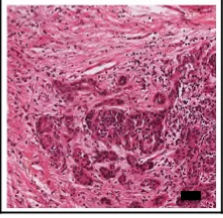	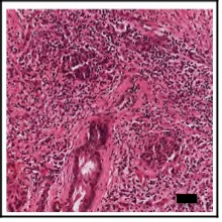

B

Figure 2. 2– Histological analysis strategy. (A) Representative image of an avatar with H&E staining. A superimposed matrix composed of multiple and numbered annotated squares (500 by 500 microns) is overlaid over the entire avatar. Image takes at x1 magnification. (B) Representative output from the random number generator. A number is selected at random from within the software. That number is correlated and matched with the annotated square of the same number. This annotated area is subsequently extracted, analysed and quantified. This is subsequently repeated (x10) in order to analyse the avatar, scale bar 50 um.

2.4.3.2 Immunohistochemistry (IHC)

Immunohistochemistry staining was performed for specific proteins. The conditions for each antibody was optimised (antigen retrieval method, retrieval buffer and antibody dilution). A number of different antigen retrieval methods were trialled, ranging from heat-induced antigen retrieval to enzymatic antigen retrieval (using proteinase k). Heat-induced antigen retrieval produced consistent, clean images with less nonspecific background staining when compared to other methods. Three different heat-induced antigen retrieval methods were trialled; pressure cooker, microwave and a portable pressure cooker (Nordic ware) that was inserted into a microwave. The latter was used for all antigen retrieval. The retrieval buffer used for all antigen retrievals was a Citrate Buffer (pH6) with 0.05 % Tween20.

After the FFPE slides were de-waxed and rehydrated, they were placed vertically in an IHC staining bin and 110mls of the retrieval buffer was added. The slides were incubated at room temperature for 5 minutes. A total of 700 mL of dH_20 was added to the portable pressure cooker, the IHC staining bin was subsequently inserted and the pressure cooker lid was closed. The portable pressure cooker was transported, inserted into a microwave and was heated at full power for 13 minutes. The portable pressure cooker lid was subsequently removed and the slides were left to cool at room temperature for 30 minutes. All slides were washed three times in dH_20 for 5 minutes whilst in a horizontal position on a Seesaw rocker.

A hydrophobic pap pen was used to circle each specimen on the slide. Blocking was performed using the Dako envision + Dual Endogenous Enzyme block for 1 hour. A humidified chamber was created and the primary antibody was diluted to its desired concentration using an antibody diluent (Abcam). All slides were incubated overnight in a humid chamber in 4°C with the respected primary antibody (table 2.3).

The following day, all slides were washed with dH_20 three times for 5 minutes prior to a 30 minute incubation with the secondary rabbit-HRP (Dako) antibody at room temperature. The secondary antibody was washed off with three washes of dH_20 for 5 minutes. The slides were developed by 3,3'-Diaminobenzidine (DAB) solution (Dako). The DAB solution was applied under direct vision using a Zeiss primo star microscope. A positive reaction was defined as when there was a development of brown pigmentation on the tissue slice. The DAB reaction was terminated by submerging the slides in water. All slides were washed for 5 minutes under running tap water prior to counterstaining with haematoxylin for 30 seconds. The slides were washed again under running tap water for 1 minute followed by a brief, 10 seconds submersion in Scott's tap water in order to 'blue' the nuclei. This was followed by a final wash under running tap water for 1 minute. All slides were then dehydrated through the passage of graded ethanol containers, followed by two xylene washes. Coverslips were mounted using DPX in the chemical fume hood. Digital images were obtained on the Aperio Slide scanner Software (Leica Biosystems).

The quantification of IHC staining was dependent on the nature of the target protein. For proteins with a nuclear localisation (Ki67 or Cleaved-Caspase 3) the

inbuilt nuclear detection algorithm within imagescope was used. The algorithm was initially trained by manually defining the threshold for a positive and negative DAB reaction; the minimum and maximum nuclear size required and the background stain levels within the tissue. The algorithm was saved as a macro so that it could be used repeatedly. The algorithm would subsequently be run on each selected annotated area. The algorithm would calculate the % positive nuclei present within the ROI. For IHC targets that were cytoplasmic in nature (pS6), the ROI was exported as a JPEG image, which was imported into imageJ. The image was converted into an 8 bit image prior to selecting a threshold that created a mask over the positive DAB reaction. This mask was subsequently measured and was used to calculate the % positive area within the ROI.

2.4.3.3 Masson's Trichrome Staining

In order to assess the collagen content of the avatars, the Masson's Trichrome Staining kit (abcam) was used to visualise the collagen. Initially, all slides were de-paraffinised and rehydrated in adherence to the previously described IHC protocol. During this time, the Bouin's fluid was pre-heated to 60°C in a water bath. FFPE slides were inserted into the Bouin's fluid and the temperature was maintained at 60 °C for one hour. A 10 minute incubation at room tempreture was performed in order to allow cooling of the slides. Excess Bouin's fluid was removed by rinsing the slides under running tap water for 5 minutes. Once washed, Weigert's Iron Hematoxylin

solution was applied to all slides for 5 minutes followed by a 2 minute wash under running tap water. The slides were covered with Biebrich Scarlet Acid Fuchsin Solution for 15 minutes. All slides were washed in dH_20 prior to the application of the Phomolybdic/Phosphotungstic Acid Solution for 10 minutes. The Phomolybdic/Phosphotungstic Acid Solution was tapped off each slide and the Aniline Blue Solution was applied for 10 minutes. This was followed by a wash in dH_20 and the application of Acetic Acid Solution (1%) for 5 minutes. The slides were subsequently dehydrated in 2 washes of 95% ethanol followed by 2 washes in 100% ethanol. The slides were cleared using a Xylene incubation for 1 minute, prior to mounting the coverslip with DPX in the chemical fume hood. In order to quantify the amount of collagen present, ROI's were randomly selected through the previously described method. Each selected ROI was exported as a JPEG image and opened in imageJ. The colour deconvolution plugin for imageJ was used to deconvolute the image (Chen et al. 2017). The blue channel was selected and the % positive area within the ROI was calculated.

2.4.3.4 Multiplex IF staining

The multiplex IF staining of avatars was performed in collaboration with the Oxford Translational Histopathology Lab. Leticia Campo kindly performed multiplex immunofluorescence staining on the avatars FFPE slides. In summary the slides were stained using the Leica BOND RXm autostainer machine (Leica, Microsystems) whilst following the OPAL™ protocol 28 (AKOYA Biosciences). A total of 6 staining cycles

were subsequently performed. The following primary antibody-opal fluorophore pairing was used: CD4 – Opal 520, CD8 – Opal 570, CD20 – Opal 480, Foxp3 – Opal 620, CD68 – Opal 690, pan Cytokerratin – Opal 780. In adherence to the manufacture's instructions, the primary antibodies were incubated for one hour and subsequently detected with the BOND™ 4 Polymer Refine Detection System (DS9800, Leica Biosystems). The DAB step was replaced by the opal fluorophores which consisted of a 10 minute incubation with no haematoxylin step. The antigen retrieval step was performed with Epitope Retrieval (ER) Solution 2 (AR9640, Leica 8 Biosystems) for 20 minutes at 100 °C. This was performed prior to the application of each primary antibody. VECTASHIELD® Vibrance™ Antifade Mounting Medium with DAPI 10 (H-1800-10, Vector Laboratories.) was used to mount each slide. The AKOYA Biosciences Vectra® Polaris™ was used in order to obtain whole slide scans and multispectral images (MSI). A batch analysis of every MSIs was performed using the inForm 2.4.8 software. The final step consisted of fusing the multiple batched analysed MSIs on the HALO (Indica Labs) software. This resulted in the creation of a spectrally unmixed reconstructed whole image of the avatar.

The analysis of the multiplex IF was performed on the Indica Labs HALO® (version 3.0.311.407). This software allows for deconvolution of the image by selecting individual flurophores for analysis. The initial step was teaching the software a Random Forest Classifier module in which the images were segmented into tumour and stromal regions. Manual annotation of the slides was performed to exclude areas with staining artefacts. Cell detection and subsequent phenotyping was performed using the Indica Labs - HighPlex FL v3.1.0 (fluorescent images). Individual

cells were defined by their expression of the specific markers: Tumour (DAPI+ panCytokeratin+), CD4 helper (DAPI+CD4+), CD8 cytotoxic (DAPI+CD8+), regulatory T-cell (DAPI+CD4+Foxp3+), B cells (DAPI+CD20+) and Macrophages (DAPI+CD68+). Proximity and spatial analysis was performed using the relevant software packages within the Indica Labs HALO® software.

2.4.3.5 Spatial transcriptomics

Spatial transcriptomic analysis of the avatars during ex vivo culture was performed using the GeoMx Digital Spatial Profiler (nanostring). This experiment was done in collaboration with the Medicines Discovery Catapult (Manchester, United Kingdom). The GeoMx experiment was conducted by Dr M Eyres (Medicines Discovery Catapult). After creating FFPE slides of the avatars as previously described, the GeoMx protocol was followed. Slides were incubated with primary antibodies attached to oligonucleotides with an ultra violet (UV) photocleavable linker. Through targeted delivery of UV illumination at specific target sites, the links are selectively broken and the corresponding oligonucleotide barcode is released, captured and quantified through sequencing. Regions of interest (ROIs) were selected within the avatars through using immunofluorescent markers for Pan-Cytokeratin (PanCK, tumour), CD45 (immune) and DAPi. ROIs were segmented into tumour (PanCK +) or stroma (PanCK-) areas of illumination (AOIs). A total of 96 AOIs were selected across the analysed avatars. Within each AOI, the whole cancer genome atlas module was applied. Raw reads per ROIs were collected and subsequently matched to target

genes using NanoString's custom oligonucleotide barcode-to-gene matching algorithm. Sequencing library size was assessed with a High Sensitivity D1000 Screen Tape assay for TapeStation systems (Agilent Technologies) and the expected library size of ~150bp was observed. QC steps were carried out to assess raw read threshold, percent-aligned reads and sequencing saturation. The limit of quantification (LOQ) was determined as the negative probe geomean + 2X the geometric standard deviations of the negative probes. Any probes that could not be detected in at least 5% of ROIs were filtered. Raw counts were then normalised by Q3 normalisation. Normalised counts were exported and processed further using R. Formal analysis and visualisation of the sequencing data was performed by Dr F Willenbrock (Postdoc within the O'Neill group).

2.4.4 Ex vivo avatar treatment

All ex vivo treatment of avatars was commenced on day 0 (day of tumour acquisition). Systemic chemotherapy was prepared in DMSO. After the avatars had been created and subsequently placed in the perfusion plate, preparation for drug delivery would commence. A new inflow circuit (comprising a syringe and tubing) would be established prior to being loaded with the intended treatment regime. This would be attached to the perfusion plate and connected to the perfusion pump. After the intended time period for drug delivery, the infusion would be stopped and the perfusion plate removed from the incubator and placed within a tissue culture

hood. The inflow circuit would be removed and the inflow channel on the perfusion plate would be temporarily occluded using a 2ml syringe. A brand new inflow circuit would then be created and the syringe filled with culturing media. The inflow circuit was primed with media (from the attached syringe) in order to remove any air bubbles present in the tubing prior to attachment to the perfusion plate. Priming ensured that there was a constant column of media from the syringe and the tubing to the perfusion plate.

2.4.5 RNA extraction from avatars and qPCR

RNA extraction and isolation from the avatars was performed using Monarch® Total RNA Miniprep Kit. After trialling different methods of tissue dissociation to increase the RNA yield , the following protocol was used for all RNA extraction. The avatar was initially suspended in 300 uL of DNA/RNA protection reagent from the Monarch® Total RNA Miniprep Kit. This was followed by manual dissociation using a pestle and mortar (TaKaRa BioMasher Standard). Manual dissociation was performed for 5 minutes; the sample was subsequently transferred to a qiashredder spin column and spun for 2 minutes at maximum speed. Enzymatic dissociation was performed with proteinase K as per the Monarch® Total RNA Miniprep. All subsequent steps were performed exactly as specified by the Monarch® Total RNA Miniprep Kit protocol. Residual gDNA was removed using on-column DNase I treatment. All RNA was eluted in 30 ul nuclease free water.

RNA was converted into cDNA using the LunaScript RT SuperMix kit (by New England Biolabs) as per the manufacturer's protocol. Each reaction yielded 20 ul of cDNA. Luna® Universal qPCR Master Mix was used in order to measure expression of individual genes of interest. Primers were designed online using PrimerBank (Zaidi et al., 2010b). Each gene primer was selected following the assessment of the melt curve (appendix A3) The reactions were performed in duplicate and were run for the full 45 cycles on a StepOnePlus™ Real-Time PCR machine. In order to determine the change in mRNA expression, normalisation to B2M was performed followed by the cycle threshold (CT) calculation method.

qPCR was used in order to subtype the avatars into classical and basal tumours. Beta-2 microglobulin (B2M) was used as a housekeeping gene for reference and for internal control. It was selected as it would not be affected by the metabolic conditions of the experiments. GATA6 was selected as a readout for basal tumours. It has been described at length within the literature. GATA6 expression is associated with organogenesis. Classical tumours have high GATA6 expression. Basal/Squamous tumours are characterised by a de-differentiated state. Therefore low GATA6 expression can be used as a proxy measure for a basal tumour (which has a relatively de-differentiated state). KRT81 has been demonstrated to be associated with basal tumours with increased expression when compared to classical tumours. It has been described within the literature as a specific gene that is highly expressed within basal tumours. Through using both genes, it is possible to profile the avatars and to determine their molecular subtype. Using two genes improves the accuracy

of the molecular subtyping. Due to the small RNA yield, further PCR on additional genes was not possible.

Table 2. 1 qPCR primers

Target	Forward sequence	Reverse sequence
B2M	CTCCGTGGCCTTAGCTGTG	TTTGGAGTACGCTGGATAGCCT
GATA6	CTCAGTTCCTACGCTTCGCAT	GTCGAGGTCAGTGAACAGCA
KRT81	AATTGAACACCACCTGCGGA	AGTGGGGGATCACACAGAGA

2.5 Bioinformatics analysis

All analysis of RNA sequencing data was performed in R version 3.6.3 (R Core Team 2014).

2.5.1 Clinical datasets

Bioinformatics analysis was performed on the Pancreatic Adenocarcinoma (PAAD) dataset. This dataset was constructed by The Cancer Genome Atlas (TCGA) and is hosted online on their server. The RNA sequencing data and the corresponding patient clinical information (version 2016 1 28) was downloaded through the firebrowse portal (http://firebrowse.org/). The 'dplyr' package was used for data 'cleaning' and filtering (Wickham et al., 2021). In summary, clinical variables of interest were converted into a binary 'correct' or 'incorrect' vector. The filter (),

select () and mutate () functions were used to select individual patients with the correct clinical information defined by the 'correct' vector and subsequently extracted and implanted into a new data frame. The process was repeated with the following clinical variables of interest: histology, site of sequencing and R status. This facilitated the creation of a uniform and homogenous desired patient cohort.

2.5.2 Differential gene expression

No standardised approach to differential gene expression analysis has been approved by consensus. The differential gene expression was calculated using two separate packages (edgeR and DESeq2) in order to improve the robustness of the results (Love et al., 2014; Robinson et al., 2010). Data generated from the edgeR analysis was used for creating graphical plots. The patient cohort with early recurrence was defined as the population of interest for the purpose of differential gene expression analysis, whereas the remaining cohort (no early recurrence) served as the control population. After visualisation of expression data, genes with a read count < 1 count per million (CPM) in at least 9 samples were set as the threshold for inclusion. The trimmed mean method (TMM) was used within edgeR to determine the normalisation factors for the sizes of the respective gene library. Differences in gene expressions were calculated and incorporated into a negative binomial model. A False Discovery Rate (FDR) of <= 0.01 was used as a threshold for gene identification. A Venn diagram was used to overlap results from both packages in order to assess the agreement and correlation of the individual results.

2.5.3 Gene set enrichment analysis of pathways

Gene set enrichment analysis (GSEA) was performed using the 'fgsea' package (Sergushichev, 2016). Predefined gene sets of the 'hallmarks of cancer' were downloaded from https://www.gsea-msigdb.org/gsea/index.jsp. KEGG pathways were downloaded from the Kyoto Encyclopedia of Genes and Genomes online https://www.genome.jp/kegg/. The edgeR results were compared to the ranked gene list. Significant pathway enrichment was defined by a FDR <0.01. GSEA pathway analysis results were presented as a stacked barchart.

2.5.4 Survival analysis

Survival analysis was calculated using the Survival package in R (Therneau, 2021). Cox Proportional Hazard Regressions were calculated and visualised with Kaplan-Meier curves.

2.5.5 Biomarker validation

Validation of biomarkers for their diagnostic ability to identify early recurrence was performed by computing generalised linear models. Receiver Operating Characteristic (ROC) curves were calculated and visualised with the 'pROC" package

(Robin et al., 2011). The area under the ROC curve (AUC) was calculated for each biomarker. An AUC value <0.5 was considered as a diagnostic failure with an inability to differentiate between the two desired patient cohorts.

2.6 Statistical analysis

All statistical analysis of experimental data was performed in GraphPad prism version 9 unless otherwise specified. Data analysis consisted of initially assessing the distribution of the data. In order to determine whether the data was normally distributed, Shapiro–Wilk test was performed. Numerical data that was normally distributed (parametric) was assessed with an unpaired Student T test, whereas non-normally distributed data (non parametric) was assessed with a Mann-Whitney U test. Comparing means across multiple independent groups was performed with a one-way ANOVA with Tukey's *post hoc* adjustment. For the analysis of categorical variables, a Chi-squared independence test was performed, unless a sample size of <10 was present whereby a Fischer's exact test was performed. Data from IHC staining was presented as mean ± SEM (error bars). All statistical results <0.05 were deemed statistically significant. In all figures: *p < 0.05; **p < 0.01; ***p < 0.001, *** P <0.001, **** P < 0.0001, ns = non significant.

2.7 General laboratory reagents

Chemicals were purchased directly from Sigma-Aldrich or from Thermo Fisher. They were used with adherence to the manufacture's guidelines, unless specified otherwise. Tissue culture plastic was obtained from Corning or from Sarstedt respectively. Perfusion plates and Alvetex membranes were purchased from REPROCELL. Fisher and VWR were the main suppliers for glassware used.

Table 2. 2 Chemical reagents used

List of chemical reagents
Fisher Scientific
2-Propanol
Ethanol (EtOH)
Glycine
Methanol (MeOH)
Sodium chloride
Tris base
Sigma-Aldrich UK
Low Melting Agarose
Dimethyl sulfoxide (DMSO)
Dithiothreitol (DTT)
Ethylenediaminetetraacetic acid (EDTA)
NP40
Sodium dodecyl sulphate (SDS)
Tween-20
Thermo Fisher
Bovine serum albumin (BSA)
Formaldehyde (PFA)
NuPAGE MOPS SDS Running Buffer (20X)
PageRuler™ Prestained Protein Ladder
Marvel
Milk powder
Roche
Protease inhibitors
Phosphatase inhibitors
Oxoid
Phosphate buffered saline (PBS) tablets

Table 2. 3 Primary and Secondary antibodies used for IHC

Antibody	Source (Catalogue number)	Dilution	Antigen Retrieval Buffer	Antigen Retrieval
Ki 67	Millipore (BA9260)	1:500	Citrate Buffer pH6	Heat-induced Epitope Retrieval
Cleaved-Caspase 3	CST (#9661)	1:200	Citrate Buffer pH6	Heat-induced Epitope Retrieval
pS6	CST (#4858)	1:50	Citrate Buffer pH6	Heat-induced Epitope Retrieval
γ – H2AX	CST (#9718)	1:50	Citrate Buffer pH6	Heat-induced Epitope Retrieval
NUDT15	Atlas (HPA038969)		Citrate Buffer pH6	Heat-induced Epitope Retrieval
Alpha-Smooth Muscle Actin		1:1000	Citrate Buffer pH6	Heat-induced Epitope Retrieval
Secondary Antibody	**Source (Catalogue number)**			
HRP labelled Polymer anti-Rabbit	Dako EnVision+ System (K4003)			

Table 2. 4 Primary and Secondary antibodies used for Western Blot

Antibody	Host	Isotype	Conjugate	Dilution	Source
pS6 (CST #4858)	Rabbit	IgG	Unconjugated	1/1000	CST
Cyclin D1 (Abcam, ab134175)	Rabbit	IgG	Unconjugated	1/10,000	abcam
Alpha-Tubulin (Abcam, ab7291)	Mouse	IgG	Unconjugated	1/10,000	abcam
Secondary antibodies					
Rabbit IgG	Goat	IgG	IRDye®800CW	1/5000	Licor
Mouse IgG	Goat	IgG	IRDye®680RD	1/5000	Licor

Table 2. 5 Primary and Secondary antibodies used for Multiplex IF

Primary Antibody	Source (Catalogue number)	Dilution	Antigen Retrieval	Assigned Opal	Opal Dilution
CD4	Leica Biosystems, (NCL-L-CD4-368)	1/100	20min ER2	520	1/150

CD8	Dako (M7103)	1/400	20min ER2	570	1/150
CD20	Dako (M0755)	1/400	20min ER1	480	1/150
FoxP3	Abcam (ab20034)	1/100	20min ER2	620	1/150
CD68	Dako (M0876)	1/400	20min ER2	690	1/150
Cytokeratin	Dako (M3515)	1/500	20min ER2	780	1/25

Chapter 3

Patient derived Pancreatic Cancer Avatars

3.1 Establishing a protocol for the creation of patient derived pancreatic cancer avatars

Cancer avatars provide a unique opportunity to deliver precision therapy. They are individual to each patient and can be created in a clinically meaningful time frame. They overcome the limitations associated with other methodologies to deliver precision therapy, notably the fact that the diversity of the tumour microenvironment is preserved (Powley et al., 2020). To date, no such protocol existed within our laboratory group.

3.2 Aims

Within this chapter, I aim to describe the establishment and optimisation process of our protocol for the creation of patient derived pancreatic cancer avatars. I will explore the key components that enable reproducible homogenous avatar creation. Precision therapy must run in parallel to the clinical journey of the patient. I therefore will describe the key infrastructure required to deliver precision therapy

within a health care setting. This will include an overview of the patient identification and recruitment process, in addition to our current standard diagnostic work up and management for patients with suspected pancreatic cancer within the Oxford University Hospitals (OUH) NHS trust. I will identify the organisational requirements and specific specialty input required in order to secure a streamlined process of tissue acquisition, high throughput drug screening and direct translational feedback into the clinic.

3.3 Implementing precision therapy for PDAC

We selected cancer avatar creation as our main method for precision therapy for PDAC. This technique can be implemented within a clinically meaningful time frame. From the patient's perspective, after their surgery they will be discharged home to continue with their general recovery. Historically, it was felt that patients should undergo adjuvant therapy as soon as possible in the postoperative period. However, evidence from the ESPAC-3 trial would suggest the contrary. No survival difference was noted between patients commencing their adjuvant chemotherapy within or after 8 weeks following their surgery (Valle et al., 2014). It transpires that completing the full chemotherapy regime (6 cycles) was the main prognostic variable that impacts overall survival (Valle et al., 2014). No difference was noted in survival if patients completed their chemotherapy (all cycles) within or after 8 weeks, however survival was significantly limited with an uncompleted chemotherapy regime both in the setting of before or after the 8 week time point (Valle et al., 2014). Therefore, as

a consequence, delaying adjuvant chemotherapy provides greater time for the patient to recover both mentally and physically and undergo pre-habilitation prior to commencing the most important component of PDAC management: systemic therapy. We aim to capitalise and utilise this time window to perform our drug screen (Figure 3.1).

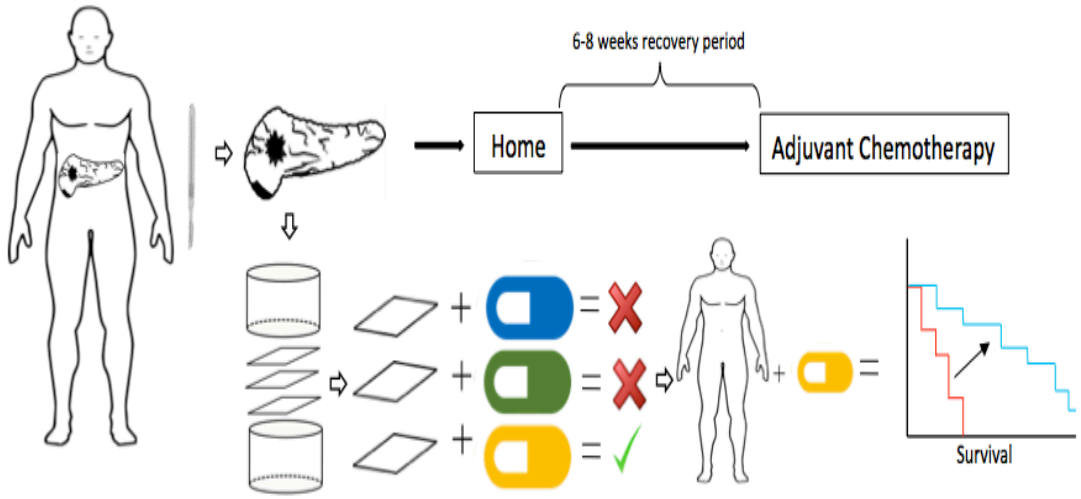

Figure 3. 1 – Implementation of precision therapy within a clinically meaningful time frame. Schematic illustration of how cancer avatar creation and subsequent drug screen can be undertaken in parallel to clinical practice. Avatars are created immediately at the point of surgery. Our approach incorporates the patient recovery phase as a time period for chemotherapeutic testing. Through a broad drug screen we aim to identify the optimal treatment strategy for each individual patient

3.4 Patient identification and recruitment

Patients were identified at the Hepato-Pancreato-Biliary (HPB) Multidisciplinary Team (MDT) meeting. This meeting occurs on a weekly basis. Patients with

suspected Pancreatic Ductal Adenocarcinoma (PDAC) are referred to the MDT for an evaluation that includes an appropriate diagnostic workup and a definitive management plan. Referrals may be received directly from Primary Care or from District General Hospitals within the geographical catchment area of OUH NHS trust. The MDT is diverse and is composed of numerous specialties including HPB Surgeons, Oncologists, Radiologists, Gastroenterologists and Specialist nurses. A case-by-case discussion of each patient is undertaken, where pre-existing imaging and previous results are reviewed. Further investigations are arranged prior to bringing the patient to the surgical clinic in order to discuss treatment options. Patients undergoing pancreatectomy for PDAC who were 18 years old or older who could consent were approached by Oxford Radcliffe Biobank (ORB). Written consent was obtained from all patients pre-operatively by ORB. Ethical approval was acquired for this study.

3.5 Diagnostic work-up and management algorithm for PDAC

All patients undergo a comprehensive and detailed diagnostic work up in order to determine whether they have localised disease. Patients with malignancy confined to the pancreas can be considered for surgical resection, the only curative treatment strategy for PDAC. Therefore all patients receive a full body (Chest, Abdomen and Pelvis) computerised tomography (CT) scan to assess for oligometastatic disease. Currently, the presence of oligometastatic disease is a contraindication to surgical resection. Pancreatectomy in the context of oligometastatic disease is associated

with very poor survival (Damanakis et al., 2019; F. Klein et al., 2012). Damanakis et al, demonstrated that the median overall survival was significantly shorter (4.5 months vs 12.2 months, p = < 0.001) for patients with multi organ metastatic disease when compared to patients with single organ metastasis (Damanakis et al., 2019). This suggests that tumour burden adversely impacts survival. With adherence to NICE guidelines, all patients with suspected PDAC receive a fluorodeoxyglucose-positron emission tomography (FDG-PET) to rule out occult metastatic disease (NICE, 2018). Our approach in OUH with regard to noeadjuvant chemotherapy is that it is reserved for patients with borderline or locally advanced pancreatic cancer.

After excluding metastatic disease through staging, the next key decision within surgical planning is defining whether there is resectable disease present. Several different guidelines have been published on the topic, each of which describes their own definition of resectable disease (NCCN, 2019; Varadhachary et al., 2006). Within OUH, the NCCN criteria are adopted to define resectable disease (NCCN, 2019). The relationship between the tumour and the peri-pancreatic vasculature ultimately dictates whether resection is possible. For isolated venous involvement, resection may be performed only if reconstruction is possible. Arterial resection remains controversial as substantial morbidity and mortality is observed following pancreatectomy with concomitant arterial resection, with no significant increase in long-term survival rates (Mollberg et al., 2011). The location of the tumour within the pancreatic parenchyma defines the surgical approach.

3.6 Tissue acquisition and transport

On the scheduled day of surgery, communication and coordination between the surgeons, pathologists, and biobank team is paramount in order to ensure successful tissue acquisition and a streamlined process of tissue transport. It is essential that there is no delay and that the time interval between tissue acquisition and tissue culture is kept to a minimum in order to maintain tissue viability. Every resected PDAC must undergo a thorough histopathological assessment in order to determine whether the tumour has been completely excised (RCPath, 2019). Residual malignant disease at the surgical transection margin (R1 status) is a well-known independent prognostic measure for poor survival in resected PDAC (Strobel et al., 2017). Due to the anatomical location of the pancreas and its local anatomical relationships, a standardised approach to pathology reporting is required (RCPath, 2019). The pathologist will define and paint each margin prior to determining whether invasive disease is present. A total of 7 margins require an assessment (RCPath, 2019). Therefore blind attempts of tumour biopsy within theatre will threaten the integrity of the margins and thus compromise patient care. The significance here is the need to involve the pathology team in order to obtain a biopsy of the tumour. This naturally introduces a time lag delay within the experimental design.

The situation is further complicated by the organisational structure of pancreatic cancer services within Oxford. Whilst all elective cancer surgery is performed at the Churchill Hospital, the histopathology department is sited at the John Radcliffe

Hospital (Figure 3.2) . Therefore the specimen in its entirety is immediately transferred to the John Radcliffe following resection. Prolonging the time interval between tissue acquisition and subsequent culture results in tissue degradation and reduces the likelihood of successful long-term culture (Annaratone et al., 2013). As a consequence we decided to transport all specimens on ice in an insulated cooler. After arriving in the pathology department, the surgical margins are painted and subsequently the specimen is opened longitudinally, at which point the pathologist takes a core biopsy (using a 5mm punch biopsy) of the centre of the tumour. The size of the tumour dictates the number of biopsies possible. The biopsy is then transported on its final journey, back to the O'Neill laboratory where the process of avatar creation can commence. As Figure 3.2 highlights, the total distance travelled (hospital to hospital to laboratory) is only 3.2 Km which normally takes approximately 30 minutes. Whilst this may appear as a quick turnaround, there are several barriers one should be aware of as these will introduce substantial time delay in the tissue acquisition process.

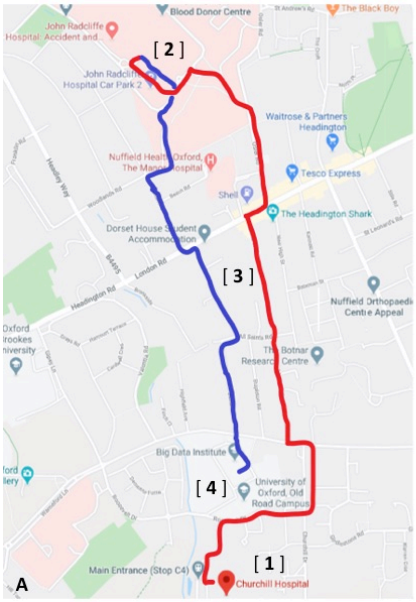

Organisational structure of pancreatic cancer surgery in Oxford

Churchill Hospital (CH) [**1**] – Main centre for elective pancreatic cancer surgery in Oxford

John Radcliffe Hospital (JR) [**2**] - Location of the department of Histopathology

Geographical logistics of tissue acquisition

Distance: 3.2 km *

Duration: 30 minutes *

Transport conditions of tissue ex vivo

CH → JR	JR → O'Neill Lab
Whole specimen transported on Ice	Punch biopsy of tumour transported in 50mls of culturing medium (4 °C) on Ice

Transport barriers and sources of prolonged tissue injury

[1] Intra-operatively, arterial isolation and ligation will render the tumour hypoxic. Vascular control is undertaken prior to parenchymal transection therefore there is a time lag before the specimen is resected. In addition there is a potential delay in collecting the specimen

[2] Any delay whilst waiting for the Pathologist to process the tumour, stain the surgical margins and undertake a punch biopsy of the centre of the tumour

B [3] Any delay in the transport of the tissue between sites

Figure 3. 2 - Transport route and logistic planning for tissue acquisition. (A) Map of the transport route undertaken for tissue transport. (B) Description of transport route and of the transport conditions * distance and duration values are reported for a completed round trip i.e. CH → JR→ O'Neill laboratory. 1 – Churchill Hospital, 2 - John Radcliffe Hospital, 3 – Transport route, 4 – O'Neill laboratory

3.7 Avatar creation

I constructed, optimised and established a protocol for the creation of patient derived cancer avatars. Initial attempts at converting the core biopsy to individual tissue slices consisted of manual dissection of the biopsy with a scalpel. Whilst this technique has been described as a method for tissue slice creation, I questioned its role in the context of creating avatars from a core biopsy.

The Leica V1200 Vibratome creates tissue slices by cutting tissue using a vibrating blade. It is an automated process and the desired tissue thickness can be programmed into the machine, thus consecutive tissue slices consistently have the

same thickness. Historical literature that describes the use of the vibratome for tissue slice creation advocates that the tissue can be glued on to the cutting platform and that it is sufficient to provide enough stability to withhold serial cuts (Nagaraj et al., 2018). However, such an approach can only be adopted if you have a large mass of tissue initially, gluing a greater surface area to the cutting platform translates to more surface tension and greater stability. Our method of tissue acquisition via core biopsy results in a much smaller sample size and volume (tissue cores varied between 0.5 cm – 1cm in height with a diameter of 5 mm, thus giving an overall volume of the biopsy between 98 and 196 mm^3) therefore gluing the biopsy directly to the cutting platform provided inadequate stability to withhold the cutting process. When creating tissue slices from hollow viscera such as the lung, it is possible to inflate the lung with agarose gel in order to maintain airway patency and provide stability for cutting (Akram et al., 2019). Clearly such an approach is not compatible with a core biopsy.

I therefore investigated the potential benefit of utilising a temporary support scaffold to determine whether it provided further stability to the core biopsy prior to vibratoming (Figure 3.3). Low Melting Agarose (LMA) was used as a scaffold as it can be dissected free from the tissue slice prior to culture. In addition, its low melting point properties negate the risk of thermal injury to the tissue. I observed that the use of a LMA scaffold increased the stability of the core biopsy on the cutting platform, which resulted in a decrease in detachment rates and a greater number of avatars created per biopsy. Serial increments in the concentration of the LMA scaffold resulted in greater stability (Figure 3.3. C). This was optimised in both mouse

pancreas and human pancreas (normal tissue and PDAC). Incubating the scaffold at 4 degrees for 15 minutes and placing the biopsy between two scaffolds (double embedding technique) provided the optimal condition for structural support. This became the standardised approach to all future avatar creation. The use of a LMA scaffold significantly increased our yield of avatars created per core biopsy when compared to no scaffold ($p = <0.01$) (Figure 3.3. E). This optimising step is crucial as it is imperative to ensure thickness consistency across all avatars in addition to maximising the number of avatars that can be created from a single biopsy.

A

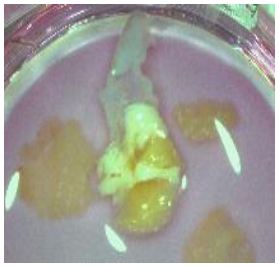

B

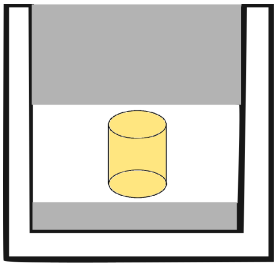

Technique	Sample	Outcome
No embedding	MT (n=4)	No stability in sample. Superglue use reduced overall quantity of tissue for slicing. Inconsistent thickness and overall low yield of tissue slices created
1% LMA	MT (n=3)	No stability in sample. Early displacement of tissue from agarose scaffold
3% LMA	MT (n=1) HT (n=2)	Mild improvement in stability of sample. Delayed displacement of tissue from agarose block
6% LMA $^{\$}$ with double embedding	MT (n=1) HT (n=3)	Significant improvement in stability of sample. No displacement of tissue from agarose scaffold. Thickness remained consistent over consecutive slices and overall yield significantly improved (>10 slices per biopsy)

C

D



E

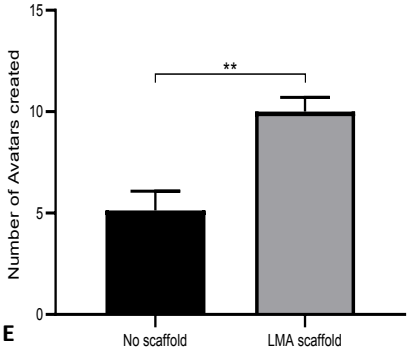

Figure 3. 3 – The use of a temporary tissue scaffold increases the avatar creation yield. (A) Photographic images demonstrating the initial variability in tissue slice size and thickness. (B) Illustration of the double embedding technique. Grey component represents the agarose scaffold. (C) Summary of embedding techniques trialled. (D) *Left* - Typical size of PDAC biopsy acquired, *Right* – size of avatars created with modified technique. (E) Number of avatars created with each technique. Data presented as mean ± SEM, statistical analysis performed by unpaired Student T test. Data information: **p < 0.01. LMA = Low melting Agarose, MT= Mouse Tissue, HT = Tissue, $^{\$}$ = Cooling period in fridge for 15 minutes

Early experience using the vibratome to create tissue slices highlighted that excess pressure across the specimen caused inconsistent detachment from the core biopsy and resulted in tissue folding and subsequent tissue loss. I therefore assessed whether altering the clearance angle of the vibratome blade impacted on avatar slice creation. The clearance angle is defined as the angle between the direction of forward motion and the most inferior aspect of the blade holder (Figure 3.4). The acuteness of the angle dictates how the slices detach from the tissue block. The optimal angle should be determined for each tissue type. I noted that using the most acute clearance angle (21°) resulted in smooth detachment of the tissue slices. No tissue folding occurred and there was minimal tissue loss. Consecutive tissue slices were created with 250 micron thickness. Tissue slices that are particularly thick are at higher risk of degradation as the thickness impedes nutrient delivery in the context of no blood supply (Naipal et al., 2016).

A

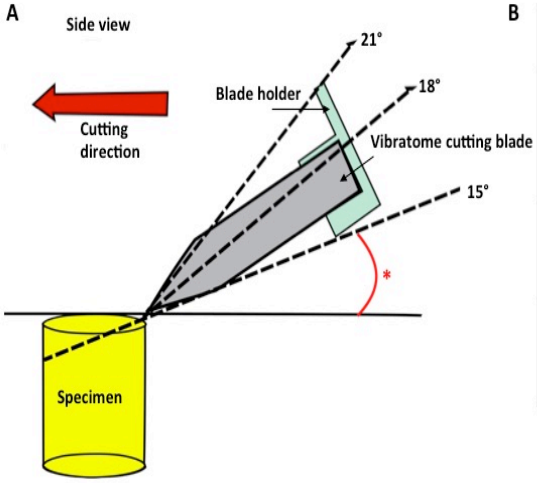

B

Clearance angle	Tissue used for optimisation	Outcome
15°	Mouse liver Mouse pancreas Human pancreas (n=2)	High pressure distribution across the specimen resulting in deformation of the slice with inconsistent detachment from the core biopsy and tissue folding
18°	Mouse pancreas Human pancreas Human PDAC (n=3)	Reduced tissue distortion, graded detachment from the core biopsy with some tissue folding
21°	Mouse pancreas Human pancreas Human PDAC (n=3)	Clean cut through specimen with smooth detachment and collection of tissue slice on the blade holder. No tissue folding

Figure 3. 4 – Optimisation of the clearance angle for vibratome tissue slice creation. (A) An illustration of tissue slice creation using the vibratome. The clearance angle (denoted by * on the schematic) is defined as the precise angle between the most inferior aspect of the blade holder and the direction of forward motion. The Leica VT1200 S has three defined clearance angles as described by the manufacture's manual; 15,18 and 21° respectively. (B) A summary of the clearance angles trialled. Both normal and tumour tissue were used in the optimisation steps in order to ensure the consistency of the tissue slices created was maintained. After testing, the 21° clearance angle allowed consistent and reproducible tissue slices. The pressure distribution was reduced over the surface area of the tissue. This was subsequently selected as the optimal clearance angle to use for the creation of human derived PDAC avatars

The final aspect of tissue slicing that required modification was the identification of the optimal settings of the vibratome (Figure 3.5). Two different settings are modifiable on the vibratome. These are the cutting speed and the blade amplitude. As per the manufacture's protocol, the vibratome settings should be adjusted to different tissue types. Whilst creating individual avatars from the core biopsy, the

passage of the blade should be smooth and uninterrupted. Slower speeds will result in excess pressure across the tissue from the blade. Higher blade amplitude may facilitate better cutting however tissue destruction may occur. The identification of the optimal settings (blade amplitude of 2mm and sectioning speed of 1.5 mm/s) allowed consistent avatar creation with minimal tissue loss.

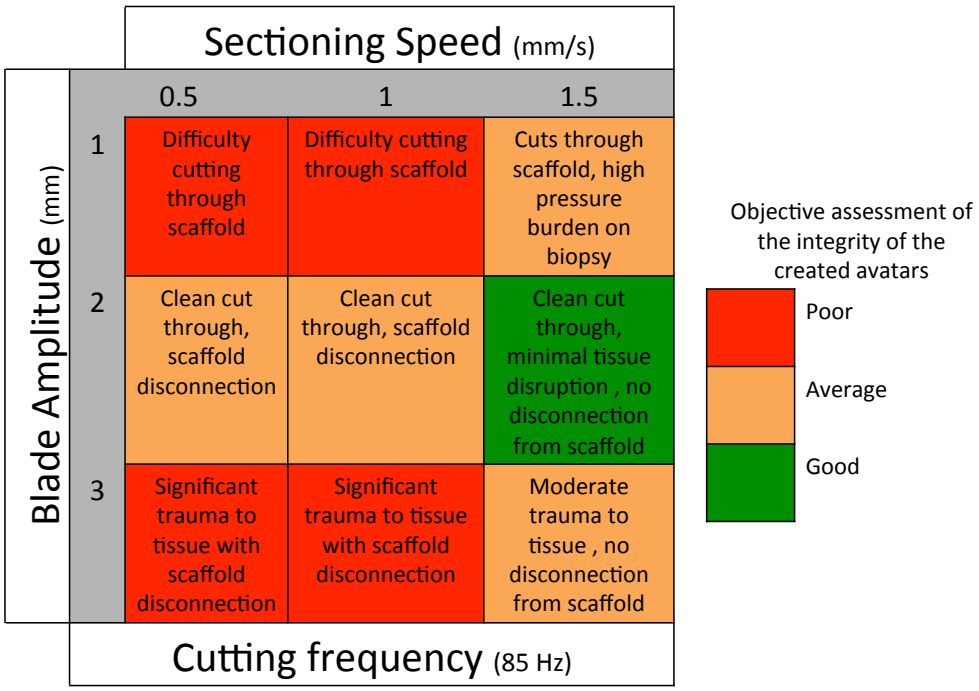

Figure 3. 5 - Determining the optimal vibratome settings for avatar creation. (A) Visual illustration of the different vibratome settings trialled. Two different variables can be altered; sectioning speed (defined as the speed of the blade through the tissue) and blade amplitude (extent of oscillation by the blade). An equilibrium between speed of tissue transection and degree of tissue disruption is required. Technical success is defined as the smooth detachment of an intact avatar from the tissue block with no tissue disruption. Conditions optimised on mouse pancreata and

human PDAC

3.7.1 Determining the optimal culture media for patient derived cancer avatars

One of the key components to successful long-term culture of ex vivo tissue is ensuring that the media is optimised according to the tissue being cultured (Georgakopoulos et al., 2020). This is evident in the case of long-term culture of organoids, where growth factor supplementation to the media is required to maintain the organoid state (Urbischek et al., 2019). As noted in our systematic review, media composition and supplementation vary significantly for different human tissues during ex vivo culture (Hughes et al., 2021). I selected to use Dulbecco's Modified Eagle Medium (DMEM) with low glucose concentration (1g/L) as a baseline media composition. My rationale for such an approach was that I wanted to create a culture media that was physiologically representative. High glucose DMEM (4.5g/L) is frequently used within experiments to establish hyperglycaemia, thus replicating the physiological conditions of Diabetes Mellitus (Pavlou et al., 2018). My concern was that excessive levels of glucose could contribute to cellular metabolic stress and as a consequence limit long-term culture rates.

Due to the native exocrine function of the pancreas with its proteolytic enzyme production capacity, auto-digestion may occur during ex vivo culture (Paoli et al.,

2020). Our initial experiences with culturing resected pancreas demonstrated early auto-digestion of the tissue. Our length of successful culture was limited to 24 – 48 hours, clear loss of surface area and large regions with necrotic changes were noted upon H&E staining. The supplementation of the base media with a soybean trypsin inhibitor and dexamethasone resulted in a decrease in auto-digestion rates and permitted longer culture ex vivo (Figure 3.6).

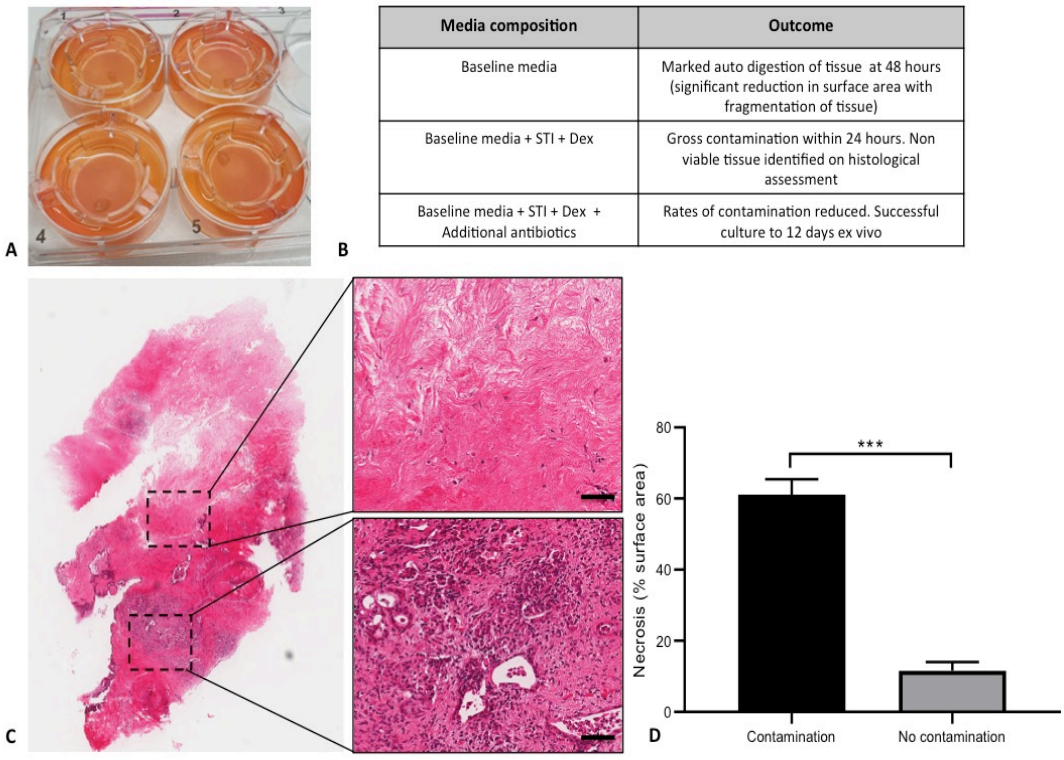

Figure 3. 6 – Optimising avatar culture media. (A) Photographic image of contamination of avatars during ex vivo culture. Contamination determined by marked change in media colour and offensive aroma. Contamination present within all four wells. (B) Chronological evolution of avatar culture media over time with subsequent results of maximal successful ex vivo culture duration. (C) Histological assessment of the effect of contamination on the integrity of the avatar. *Left* image

taken of the entire avatar*, top* image demonstrated the detrimental effect of contamination on the avatar - acellular region , necrotic with no preservation of native tissue architecture, *bottom* image representative of an area of the avatar where PDAC histology is preserved , scale bar 50 um. (D) Quantification of the extent of necrosis (as a percentage of the total surface area) of the avatar at 24 hours ex vivo. Data presented as mean ± SEM, statistical analysis performed by unpaired Student T test. Data information: *** $P \leq 0.001$.

One of the fundamental challenges with ex vivo culture of primary tissue is preventing contamination. Unfortunately, a total of 4 different patient avatars were lost to contamination despite our baseline media including Penicillin and Streptomycin for anti-microbial prophylaxis (Figure 3.7). All contamination occurred within 24 hours of culture and was identified by visible debris within the culture vessel, change in media colour and offensive aroma. An interesting observation was that all four of these patients had undergone preoperative biliary stenting and had a common bile duct stent in situ at the time of surgery. Upon reviewing the intraoperative bile duct swab culture, all 4 patients had a positive culture with gram-negative coliform bacteria present. As a consequence the media composition was revised and additional antimicrobial coverage (Amphotericin B and Neomycin) was added. Following the addition of the broader spectrum antimicrobial agents there were no further episodes of contamination of the avatars during ex vivo culture.

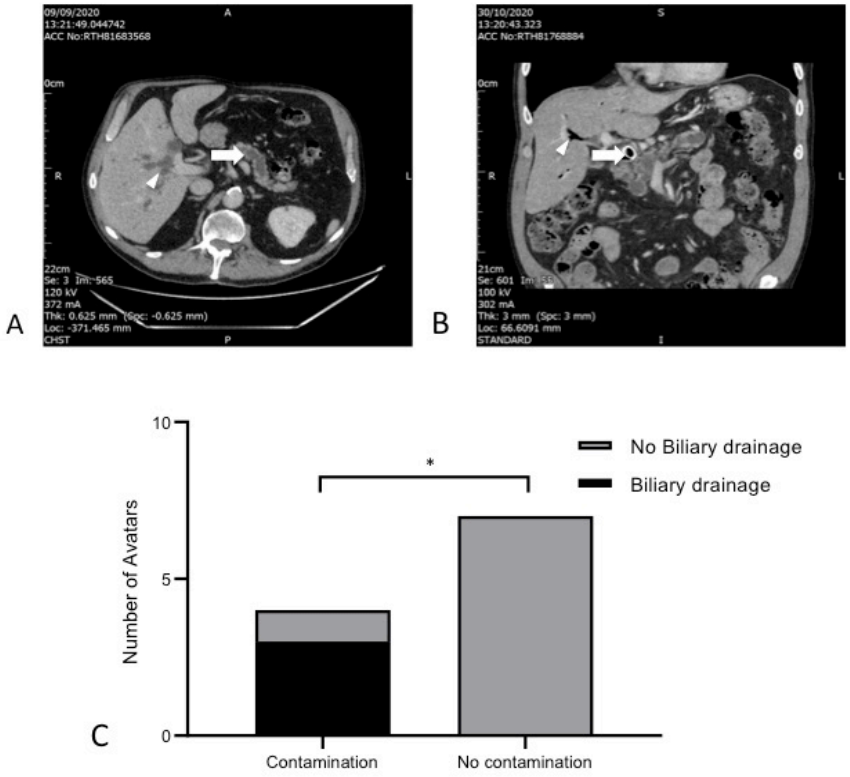

Figure 3. 7– Association between Biliary drainage and Avatar contamination. (A) 76 year old patient recruited to this study persented with obstuctive jaundice. Axial image of their Computerised Tomography (CT) scan demonstrating a pancreatic mass, dilated pancreatic duct (white arrow) and dilated intrahepatic bile ducts (white arrowhead). The patient subsequently underwent biliary drainage with stent insertion prior to surgery. (B) A axial CT scan image of the same patient following stent placement. White arrow demonstrates the stent, white arrow head illustrates the presence of pneumobilia indicative of stent patency. (C) Quantification of the total number of patient avatars lost to contamination in relation to the presence of peri operative biliary drainage. Statistical analysis performed Fischer's exact test. Data information: * $P \leq 0.05$.

3.7.2 Embedding and Microtome optimisation

The final aspect of the protocol that required optimisation was the microtoming technique required to create multiple FFPE tissue slides. Due to the very small

nature of the avatars (250 um thickness and 5mm diameter), any slight error processing the avatars would result in a significant loss of tissue. Any angulation of the specimen when being cut would result in only parts of the avatar being captured in the FFPE section, thus not representative of the full avatar. Through the optimisation process I noted that embedding whilst under sustained pressure resulted in the horizontal lie of the avatar within the FFPE block (Figure 3.8). When preparing FFPE slides, this translated into consistent FFPE slide creation with minimal wastage of tissue.

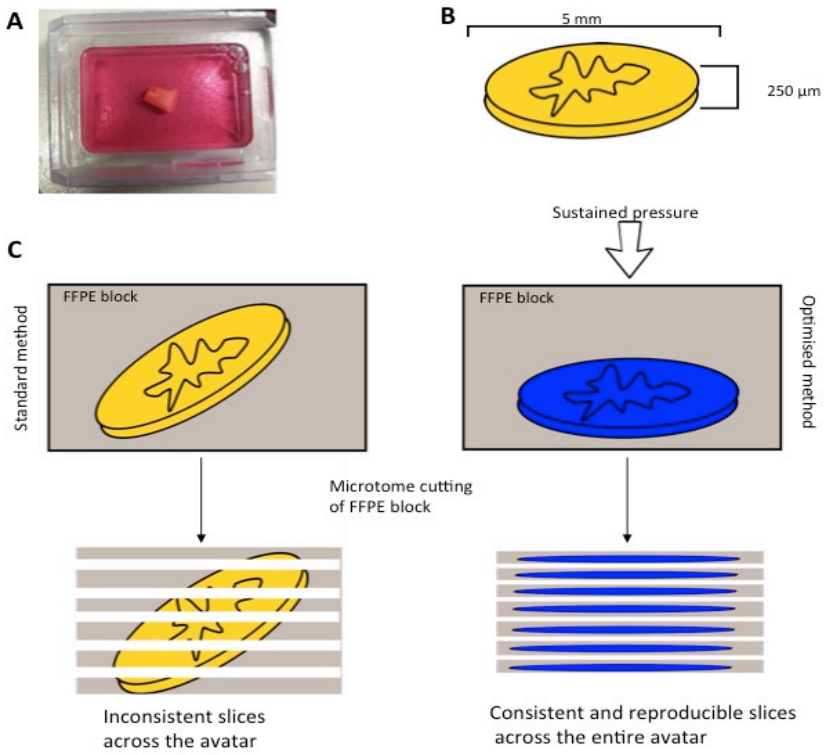

Figure 3. 8– Optimisation of the microtoming technique for PDAC avatars. (A) Macroscopic image of the punch biopsy acquired from the surgical specimen. (B) Dimensions of the PDAC avatar after vibratome slicing of the punch biopsy. (C)

Modification to the embedding technique prior to microtoming the FFPE block containing the PDAC avatar. Due to the limited amount of tissue available, it is essential that the avatar was embedded in an absolute horizontal plane. Any angulation to the embedded tissue would result in inconsistent tissue slice creation across the avatar and thus greatly reduce the overall tissue yield acquisition. Embedding whilst under sustained pressure resulted in a horizontal lie of the avatar which yielded consistent avatars

3.8 Established pancreatic cancer avatars

The proposed protocol describes the key procedural aspects required for avatar creation. From tissue acquisition, we were able to create multiple avatars within three hours. An important question that needed addressing was whether the process of avatar creation (the effect of the scaffold, the invasive process of slicing and the time interval for creation) produced an overwhelming stress on the tissue and resulted in significant necrosis and a loss of histological features. To investigate, I performed H&E staining on avatars at the baseline time point (within 6 hours of acquisition) (Figure 3.9). Histological architecture was preserved with identifiable components of the tumour microenvironment and of the normal pancreas (both exocrine and endocrine components). This demonstrates that our approach allowed avatar creation without compromising the integrity of the native tissue.

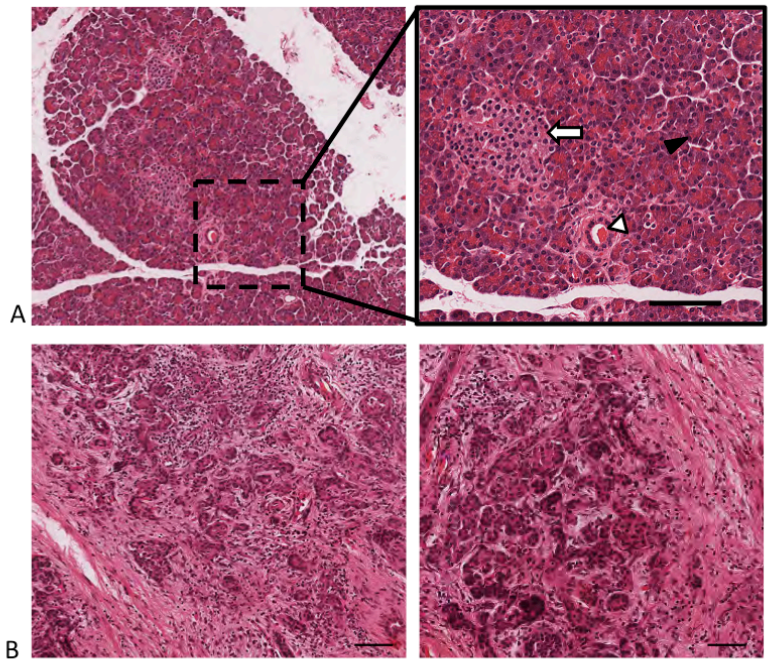

Figure 3. 9– Successful creation of patient derived avatars. (A) Histological image of a normal pancreas avatar. *Left* image taken at x5 magnification, *Right* image taken at x10 magnification, scale bar 50 um. Arrow identifies pancreatic islet, white arrowhead identifies a duct and black arrowhead identifies acinar cells. (B) Histological image of a pancreatic cancer avatar from two different patients. Tumour morphology and differentiation preserved after tissue slicing and avatar creation. Scale bar 50 um.

To date I have created 13 avatars from patients' primary tumour. The demographics of these patients are highlighted in Table 3.1. The gender split M:F was 10:3 respectively. The median age of the cohort was 69. The vast majority of the cohort (11/13) had evidence of nodal disease involvement. A positive surgical margin was present in 6 cases (46%).

Table 3. 1 – Demographics of patient derived cancer avatars

Patient	Gender (Age at diagnosis)	Tumour differentiation	T stage	N stage	Lymphatic invasion	Vascular invasion	R Status	Surgical procedure
1	M (76)	Poor	T2	N0	L0	V0	R0	Whipple
2	M (67)	Moderate	T2	N1 (1/19)	L0	V1	R1	Whipple
3	M (81)	Moderate	T1	N0	L0	V0	R0	TP
4	M (69)	Poor	T2	N2 (9/18)	L1	V1	R0	Whipple
5	F (65)	Moderate	T2	N1 (3/49)	L1	V1	R1	Whipple + PV resection
6	M (68)	Moderate	T3	N2 (5/24)	L1	V1	R1	Whipple
7	M (78)	Moderate	T1	N1 (2/32)	L1	V0	R0	TP
8	F (77)	Moderate	T1	N2 (4/19)	L1	V1	R1	TP
9	M (68)	Moderate	T2	N1 (3/38)	L1	V1	R1	Whipple
10	F (63)	Moderate	T2	N2 (5/18)	L1	V0	R0	Whipple
11	M (69)	Well	T2	N2 (4/52)	L1	V1	R1	Whipple
12	M (81)	Moderate	T2	N0	L0	V0	R0	Whipple
13	M (74)	Moderate	T2	N1 (2/44)	L1	V1	R0	Whipple

L1 – Lymphatic invasion, V1 – Vascular invasion, R1 – positive surgical margin, TP – Total Pancreatectomy, PV – Portal Vein

3.9 Discussion

Within this chapter I have demonstrated the creation, evolution and optimisation of the protocol for patient derived pancreatic cancer avatar establishment. This chapter also highlights the tissue acquisition pipeline that has been established here in Oxford. Clear communication, organisation and close team working between the surgical team and pathology department have resulted in a streamlined process of patient avatar creation, all within a clinically meaningful timeframe. As the patient leaves theatre for recovery, multiple homogenous and patient specific avatars have already been created and are ready for a high throughput drug screen.

This chapter highlights the frequent challenges that occur during avatar creation. Nagaraj et al emphasised that the amount of tissue acquired following resection dictates the possible number of avatars that can be created (Nagaraj et al., 2018). One of the limitations of using such an approach to deliver precision therapy is the relative low yield of tissue slices that can be created (Holliday et al., 2013; Naipal et al., 2016). As highlighted within our data (Figure 3.3) , the use of a temporary support scaffold significantly increases the total amount of tissue slices that can be created per biopsy. Reinforcement of the biopsy with the scaffold provides greater stability and as a consequence the biopsy can withhold several passes of the vibratome through the tissue.

Establishing physiologically representative culture media may serve as the final challenge to successful long-term tissue culture ex vivo. McKee et al, performed metabolic profiling of human plasma in order to determine the concentration of several key metabolites (McKee et al., 2017). What is interesting is that when

compared to commercially available culture media, the electrolytes and metabolites concentrations were outside the physiological limits of human plasma (McKee et al., 2017). Of the four commercially available media assessed (DMEM, MEM, M199, RPMI 1650) none of them matched the composition of human plasma with 100% accuracy. The electrolytes/metabolites that were most frequently present in concentrations outside the normal physiological range were sodium, calcium, chloride, glucose and sulfate (McKee et al., 2017). Metabolite excess or deprivation will adversely impact cell biology. Buras et al, demonstrated that hypercalcemia inhibited proliferation of differentiated cells (Buras et al., 1995), whereas hyperphosphatemia affects cellular differentiation rates (Mozar et al., 2008). Glucose concentration (notably hyperglycemia) within the media has been shown to impact on protein synthesis rates and modifies gene expression (Li et al., 2016). Through utilising a low glucose concentration media for the maintenance of the avatars, we attempted to minimise the possible impact of excess glucose on the native function within the tissue. The creation of novel physiologically representative culture media has been reported in the literature, where one of the marked benefits was noted within cell metabolism trends (Cantor et al., 2017; Vande Voorde et al., 2019). Cantor et al, illustrated that the difference in cell metabolism noted between conventional culture media and physiologically representative culture media resulted in different rates of uric acid production, which eventually dictated the chemotherapeutic sensitivity of the cells to 5-FU via the inhibition of uridine monophosphate synthase (Cantor et al., 2017). This reinforces the need to optimise the media composition for each tissue type. A further experiment that could be performed in the context of our pancreatic cancer avatars to further validate our

media, would be tissue dissociation and mass spectrometry to determine the native concentrations of electrolytes and metabolites within the tumours. This information could subsequently be used to adjust the media composition accordingly. However one should be mindful of the difficulty accessing fresh tissue and such an experiment would utilise a lot of limited resources.

Whilst routine supplementation of the culture media with antimicrobials for prophylaxis is a well-accepted technique, one should question the potential effects that long-term exposure to antibiotics induces within the tissue/cells. Emerging evidence from the literature suggests that cumulative exposure to antibiotics induces diverse alteration to gene expression (Ryu et al., 2017). Ryu et al, cultured a human liver cell line (HepG2 cells) with (penicillin and streptomycin) or without antibiotic supplementation of the media prior to performing RNA sequencing (Ryu et al., 2017). They noted a significant change in gene expression across 209 different genes predominantly involving the following pathways: polyamine regulation, fatty acid activation and xenobiotic metabolism signalling (Ryu et al., 2017). One could therefore question whether treating avatars with a short course of antibiotics (1-2 days) in order to eliminate any bacterial presence followed by culture in media devoid of antimicrobials would provide a physiologically representative system (Ierano et al., 2017).

An interesting observation from our early experience culturing pancreatic cancer avatars was that early contamination occurred exclusively in patients that had undergone preoperative biliary drainage. Biliary obstruction is a common occurrence

during pancreatic cancer tumorigenesis (Boulay et al., 2014). Biliary decompression can be achieved through stent placement via an endoscopic or percutaneous route (Boulay et al., 2014). The native biliary tract is considered sterile and it would appear that instrumentation of the biliary tree carries the risk of bacterial colonisation. An interesting study performed by Ruan et al, investigated 956 patients who had undergone endoscopic drainage of the biliary tree (Ruan et al., 2019). A total of 363 patients (38%) had positive bile cultures, of which the majority (96.7%) had a monomicrobial infection and the remaining 3.3% a polymicrobial infection (Ruan et al., 2019). The two most frequent microbes cultured were *Escherichia coli* and *Klebsiella pneumonia* (Ruan et al., 2019). It was noted that previous biliary tract instrumentation was an independent risk factor for a positive bile culture (Ruan et al., 2019). Whilst we are unable to definitively prove that the source of the contamination was the contaminated biliary tree in vivo, it would appear that a contamination rate occurred with greater frequency when pre-operatively biliary tract instrumentation was undertaken. This raises an interesting question as to whether the media antimicrobial composition should be altered in accordance to whether there is a stent in situ.

It appears that the dynamic relationship between the human microbiome and the pancreas is important not only for PDAC development but it may also dictate the responsiveness to treatment. Since the publication of the seminal ESPAC trials, Gemcitabine has been a cornerstone in the management of PDAC as an adjuvant chemotherapeutic strategy (Neoptolemos et al., 2010). However, the response rates to Gemcitabine differ across patients and the microbiome has been proposed as a

possible reason for this heterogeneity. Geller et al, demonstrated that Gammaproteobacteria could metabolise Gemcitabine from its active form to its inactive form (2',2'-difluorodeoxyuridine) through excess production of the enzyme cytidine deaminase (CDA) (Geller et al., 2017). Whilst their initial work was based on a mouse model of colon cancer, they further validated their finding within the context of PDAC. They performed PCR for 16S bacterial rDNA on 113 resected PDAC tumours and noted that Gammaproteobacteria was the most abundant bacteria present (51.7%) (Geller et al., 2017). Co-culturing the bacteria from the resected PDAC tumours with two different Gemcitabine sensitive colon cancer cell lines resulted in complete resistance and a lack of therapeutic affect (Geller et al., 2017). The efficacy of nucleoside analogues based chemotherapy is significantly reduced in the presence of Mycoplasma (Bronckaers et al., 2008). Therefore it is essential that we are conscious of this symbiotic relationship between PDAC and the host's microbiome. The significance of this within our proposed model for delivering precision therapy is clear. Complete ablation of the microbiome within the avatars through broad spectrum antibiotic use could potentially alter the treatment response.

Within this chapter, I have presented our novel protocol for patient derived pancreatic cancer avatar creation. The protocol is reproducible and allows consistent and homogenous avatar creation. This method can be implemented within clinical practice without significantly interrupting the normal timings of patients' scheduled treatment. Its use would assist clinicians with selecting the optimal treatment for each individual patient, where the decision is made upon documented evidence of

tumour response rather than an assumed response. In order to further improve our system, one should question whether it is possible to recapitulate the in vivo physiological conditions of the tumour during ex vivo culture.

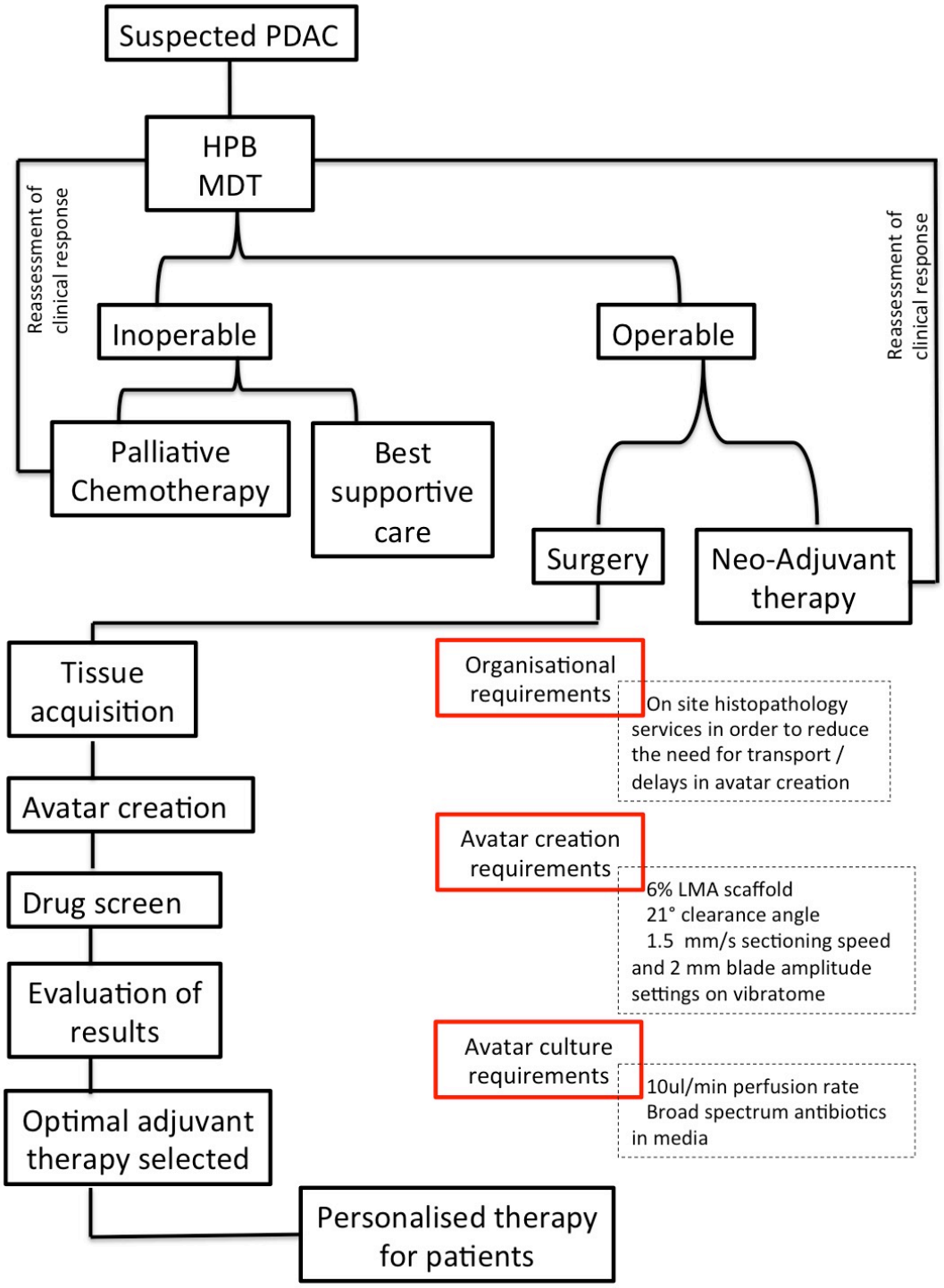

Figure 3. 10 – Implementation of precision therapy within the current NHS infrastructure. A visual overview of how precision therapy through avatar creation can be implemented within current clinical practice. The entire avatar creation process runs in parallel with the patient's treatment and as such does not interfere with current cancer treatment algorithms or introduce a time lag delay.

Chapter 4

Ex vivo perfusion culture of cancer avatars

4.1 Perfusion culture

Conventional static culture does not truly represent the physiological conditions in vivo. Several limitations exist with the technique, all of which may adversely affect the cultured specimen. These include the continuous need for media exchange in order to replenish nutrients, which results in an abrupt change in the culture environment and the possibility that oxygen levels may be outside the normal physiological range whilst under static culture (Pavlacky et al., 2020). Another issue is that the use of animal serum supplementation of the media for culture longevity remains as standard cell culture practice. For the aforementioned reasons, significant research efforts have been directed towards establishing culture systems that are more representative of human physiology. As such, much interest has been generated about the use of perfusion culture.

Much of the published evidence base regarding the benefit of perfusion culture has originated from within the field of transplantation. In transplant surgery, one of the most important aspects is organ preservation between the organ donor and recipient. Organ preservation is intrinsically intertwined with patient clinical

outcomes (Jochmans et al., 2020). Historically, ex vivo cooling of the donor organ was one of the first trialled methods to preserve the integrity of the organ (Bickford et al., 1937). This technique has served as the cornerstone method for organ transport and tissue preservation for several decades. However, recent advances in bioengineering technology have facilitated the ability to conduct ex vivo perfusion of organs intended for transplantation for prolonged duration. A commercially available ex vivo organ perfusion machine is now available (OrganOx) and has been licensed for routine use in the UK (NICE, 2019). Nasralla et al, 2018 demonstrated in their published randomised control trial that the use of normothermic machine perfusion of livers ex vivo resulted in a significant reduction in graft injury (denoted by the presence of transaminitis) and organ discard rate (Nasralla et al., 2018). Further research has illustrated that the use of normothermic machine perfusion can be used to evaluate high risk organs for physiological function prior to implantation in addition to being able to recondition the organs into an improved functioning state (Parente et al., 2020).

Given the clear advantages of organ perfusion ex vivo, it is unsurprising that perfusion technologies have been implemented in cell culture systems in order to determine whether the same physiological advantage is observed. Certainly the field of microfluidic technologies has significantly advanced over recent years (Terrell et al., 2020). However, the majority of the published literature predominantly focuses on microfluidic culture use combined with monolayer cell culture (Choi HJ, 2020; Sugihara et al., 2020). In order to evaluate its use for primary tissue culture, we conducted a systematic review of the concurrent literature regarding the use of

dynamic physiological culture techniques for ex vivo human tissue culture. Of 2078 articles identified, only 22 were included in the qualitative synthesis. Perfusion culture was described in 50% of the included articles. It was interesting to observe that the vast majority of articles (73%) were using dynamic physiological culture techniques for healthy human tissue in an attempt to re-establish normal physiological conditions ex vivo for prolonged culture. It is clear that the role of perfusion culture for diseased ("pathological") human tissue has yet to be determined.

4.1.1 Aims

Within this chapter, I aim to establish a perfusion culture platform that can be utilised to culture both cancer cell lines and patient derived cancer avatars ex vivo.

4.2 Results

4.2.1 Establishing the perfusion system

Three different methodologies could be implemented within our experimental design (Hughes et al., 2021) These included a rotational bioreactor (where cultured tissue was suspended in a "free falling" state), a rocking culture platform and a dynamic perfusion culture system that utilised a mechanical pump (Figure 4.1).

Following a critical review of each method, it was felt that using the dynamic culture system approach would be the most representative of the in vivo physiological conditions of the tumour vasculature, specifically its ability to deliver continuous fresh media to the avatars instead of redistributing the pre-existing culture media.

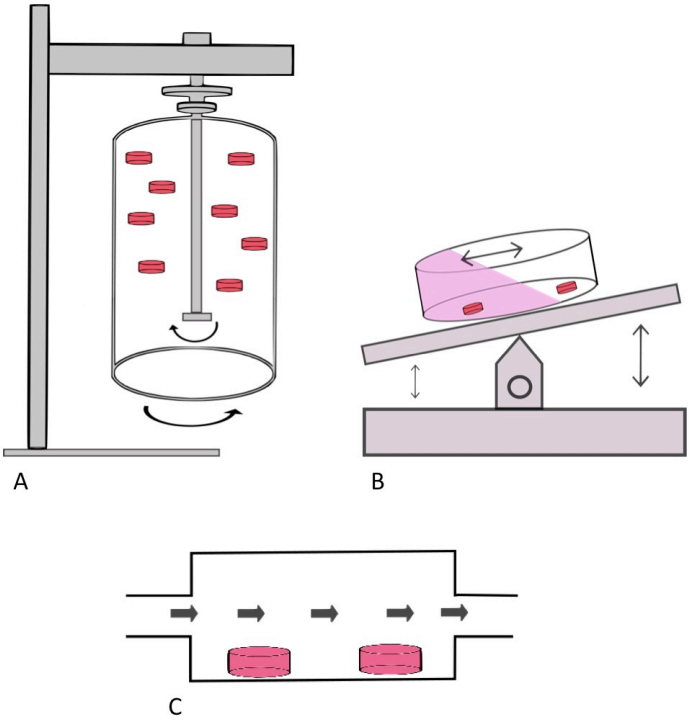

Figure 4. 1– Dynamic physiological culture techniques that have been utilised for ex vivo culture of primary human tissue. (A) Illustration of a rotational bioreactor, in which tissue is suspended in culture medium due to concurrent rotation of both inner rotating cylinder and outer vessel wall. (B) Illustration of a rocking bioreactor, rocking movement allows movement of media over cultured tissue. Media is redistributed through continuous movement. (C) An Illustration of the dynamic perfusion culture technique. Active inflow of media into the bioreactor is driven by a mechanical pump, which can be continuous or intermittent. Fresh media is continuously supplied to the cultured tissue, instead of redistributing the concurrent media as seen with the other two methods in A and B

We elected to utilise a commercially available perfusion plate to ensure reproducibility and the ability to upscale to a larger service, particularly in the context of a possible clinical trial. I first investigated the use of the ibidi perfusion slide (µ-Slide III 3D perfusion), however its design was better suited for studying

monolayer cell culture under perfusion. Several technical problems were encountered, including micro bubble entrapment and occlusion, cross communication between channels and tissue displacement. A description of each complication and the subsequent modifications trialled are recorded in the appendix. I subsequently trialled the Alvetex perfusion plate for the culture of patient derived cancer avatars. In comparison, the Alvetex perfusion plate possessed several advantages and was better suited for the ex vivo culture of avatars.

The Alvetex perfusion plate is comprised of 4 culturing wells (Figure 4.2). Each is interconnected to its adjacent neighbouring well (in a clockwise manner) via a short communicating channel which facilitates the dynamic flow of fluid throughout the circuit of the perfusion plate (Figure 4.2). The plate also possesses two distinct inflow and outflow channels. This serves as the site where tubing can be attached in order to connect the perfusion plate with a mechanical pump. The Alvetex plate differs from other perfusion devices as its total circulating fluid volume is significantly larger, thus it would be incorrect to label it as a microfluidic circuit (Astolfi et al., 2016). For systems with a low circulating fluid volume, it is sufficient to rely on passive outflow management (unsupported outflow through wide drainage driven by the force of the inflow). However, in the context of our perfusion plate such an approach is not possible and would place the system at risk of volume flooding if drainage was insufficient. Therefore we utilised an active outflow management technique whereby the perfusion plate (via the outflow channel) was connected to another mechanical pump to ensure fluid drainage and volume pull through. There are two reservoirs (both immediately before and after the perfusion circuit) on the

perfusion plate that can be used for fluid volume management, air bubble removal and serve as an area for drug loading (Figure 4.2).

I utilised two different mechanical pumps in order to establish the perfusion circuit (ColePalmer Masterflex Infusion/Withdrawal Pump). The media (+/- chemotherapy) for perfusion into the system is housed within a 60 ml syringe which is attached to the mechanical pump. The inflow pump is set on the push function and is connected to the perfusion plate via plastic tubing with an internal diameter of 2 mm, whereas, an empty 60 ml syringe is attached to the outflow pump which is set to the pull function (to actively remove fluid). In order to facilitate adequate drainage and to prevent volume overload, I used tubing with a larger diameter (3 mm) for the drainage channel and set the outflow pump to a speed that is 20 % greater than the inflow rate. A male connector elbow luer is utilised to connect tubing with different diameters. The tubing itself may serve as a source of potential contamination which may permit bacterial seeding into the perfusion plate. In order to prepare the tubing, I first measured, cut and assembled the inflow and outflow tubing within a sterile tissue culture hood. I subsequently manually perfuse 100ml of pure ethanol through the tubing three times in order to sterilise them. This is subsequently repeated with PBS in order to remove any excess ethanol. The final step consists of a further manual perfusion of 100 ml of our predefined culture media prior to constructing the circuit.

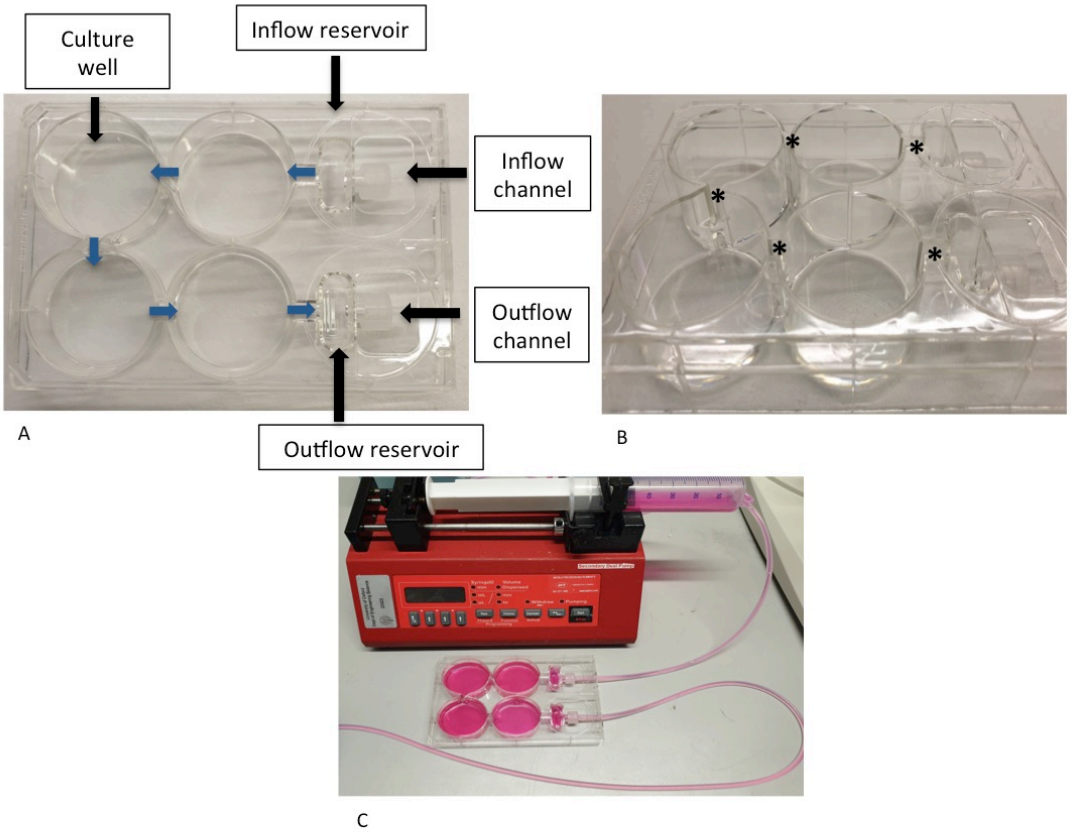

Figure 4. 2– Perfusion plate layout. (A) Photographic image of the perfusion plate. Key components of the plates have been identified and labelled. The blue arrows delineate the direction of perfused media flow through the circuit. (B) Communication channels between wells have been identified and labelled as *. (C) Photographic image of the perfusion plate attached to the mechanical inflow pump.

An additional important consideration is the nature of the culturing well, specifically where and whether a scaffold is utilised to house the patient derived avatar for ex vivo culture. Whilst it is possible to culture the avatar freely on the plastic base of the culturing well, caution is required with such an approach. Our initial experience illustrated that under high flow conditions, the avatars were frequently displaced and subjected to excess shear stress, which was detrimental to long-term successful culture rates. One could coat the floor of the well with a synthetic extra cellular matrix protein such as matrigel for additional stability, however its use can influence cell function and behaviour (DeQuach et al., 2010) and will significantly impair oxygen delivery to the avatar. Tissue oxygenation in the ex vivo context is a passive

process, where oxygen must diffuse passively into the tissue (Watson et al., 2019) . Failure to oxygenate the tissue slice will result in tissue necrosis and subsequent tissue loss. Several factors heavily influence oxygen permeation of tissue slices ex vivo, including the nature of the tissue, tissue thickness and the volume of media through which diffusion is required to take place (Freeman et al., 1984; Meijer et al., 2017). Within our current system, a minimum of 13 mls is required per well to allow flow through to the adjacent well via the communicating channel; as such this establishes a large volume and marked distance across which diffusion can occur. Emerging evidence within the literature illustrates the benefit of using a porous membrane for 3D tissue culture (Davies et al., 2015). We utilised the Alvetex strata membrane as a scaffold to house and culture our avatars on for the duration of ex vivo culture (Knight et al., 2011). The Alvetex membrane forms part (the base) of a hanging basket which can be subsequently placed into a culturing well. The basket elevates the sample from the base of the well, thereby reducing the media volume on top of the avatar and subsequent diffusion distance for oxygen permeation. The membranes were rendered hydrophilic prior to their use by incubating them in 70 % Ethanol for 2 minutes, in order to promote adherence.

The communicating channel between the culture wells is not sited at the bottom of the well. Rather, it is approximately 13mm in distance (on a vertical axis) from the bottom of the well. In light of this, I wanted to determine whether the perfused media mixed thoroughly throughout the well or whether the laminar streamlined flow resulted in minimal mixture. This was important to determine, especially in the context of downstream applications of perfusion experiments notably in the use of

drug delivery. In order to investigate this further, I firstly set up the perfusion plate and filled the full fluid circuit with water. The fluid circuit is defined as the continuous column of fluid from the inflow syringe, inflow tubing, to the perfusion plate and outflow tubing. I then filled the inflow reservoir with a blue dye prior to perfusing 60 mls of water into the circuit. I then observed for colour saturation within the culture wells. Over time, it was noted that each well in turn became saturated with the blue dye prior to returning to a clear, see through consistency as the entirety of the well volume was replaced by the perfused inflow of fresh water content (Figure 4.3). This illustrates the extent of fluid mixing within the wells. It also demonstrates that this approach permits a physiologically more representative technique of drug delivery, instead of the conventional approach of loading the maximal concentration of the drug immediately into the culture well, and that we are able to perfuse in the drug which accumulates within the well over time.

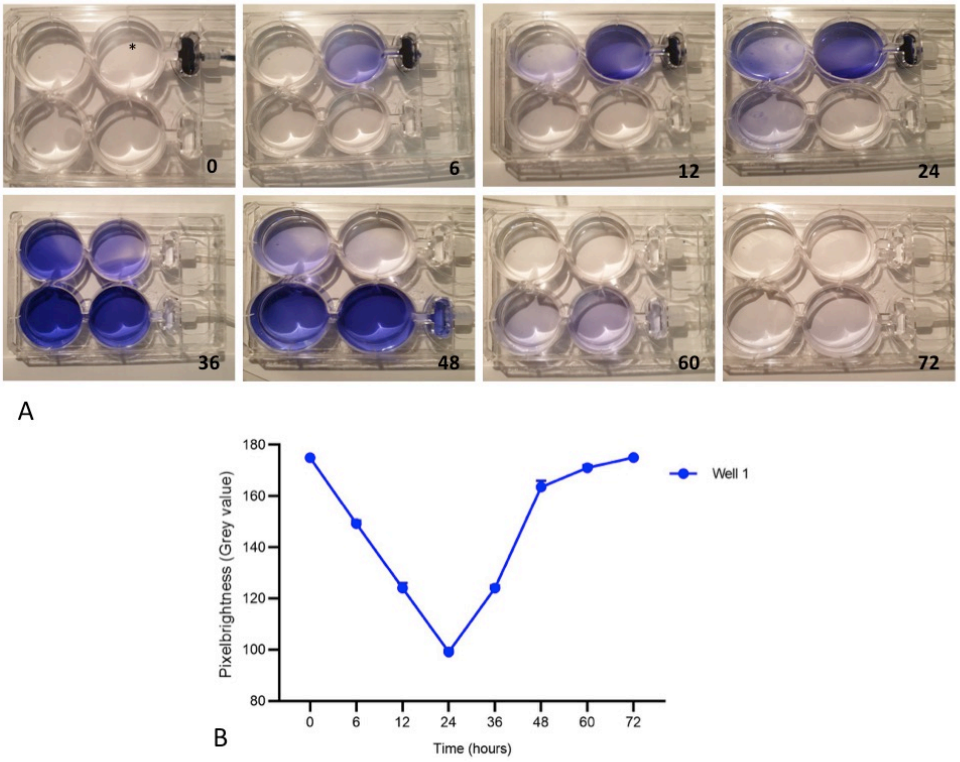

Figure 4. 3– Geospatial distribution of the perfusate. (A) Serial aerial images of the perfusion plate whilst a blue dye was perfused into the system in order to determine the extent of perfusate mixing within each culture well. Images taken at predefined time points (hours). The * denotes the reference culture well for quantification. (B) Quantification of the pixel brightness (Grey Value) as a proxy measure of perfusate mixing

4.2.2 Monolayer cell culture under perfusion conditions

In order to determine whether perfusion culture of patient derived cancer avatars improves the long-term rates of successful avatar culture ex vivo, I first investigated the impact of perfusion on cell culture. It has been previously described that replenishing the concentration of nutrients in static culture is dependent upon exchanging the entire volume of the culture media, which in turn creates both an acute and drastic change to the culture environment (Henry et al., 2008). I therefore wanted to determine whether perfusion culture eliminates the cyclical cellular metabolic stress that occurs with frequent media exchange.

4.2.2.1 Metabolic profiling of nutrient availability during static culture

To start, I wanted to understand the daily variation of nutrient availability whilst under static culture conditions. For this in vitro analysis I cultured a commercially available pancreatic cancer cell line: PSN1, under conventional static culture conditions. This cell line was selected as it originated from a patient with a poorly differentiated pancreatic tumour and represents a tumour with an aggressive disease phenotype, given its relatively short cellular doubling time of approximately 21 hours (Yamada et al., 1986). During a culture period of 7 days, 100 uL of media was extracted at predefined time points and a luminescence based assay was used to determine glucose concentration within the culture media. A full media exchange was performed on day 3 and 6 respectively. It was noted that during the full time course of the experiment a statistically significant reduction ($p=0.0002$) in glucose availability within the media occurred (Figure 4.4 A). Daily variation in glucose availability was noted which was perpetuated by cell proliferation rates and an increase in overall cell numbers. Replenishing the full culture media did not ensure daily consistency of glucose availability over the time course of the experiment.

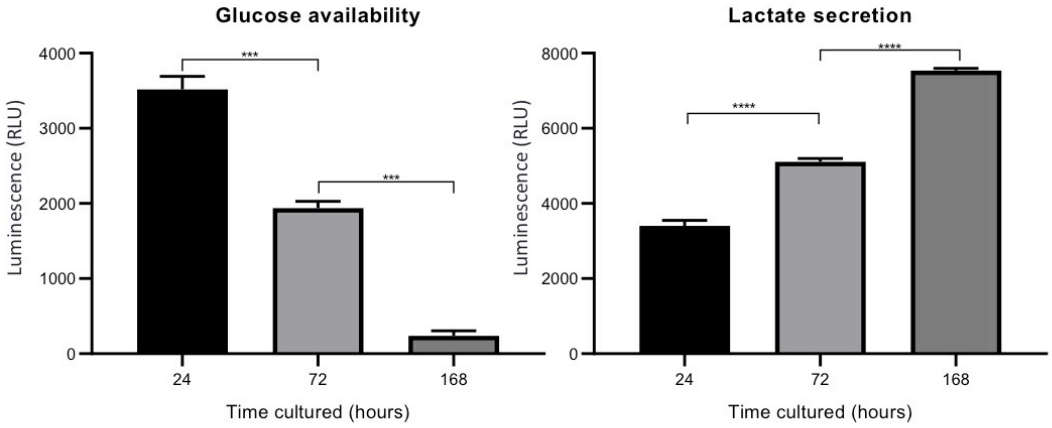

Figure 4. 4 – Metabolic profiling of nutrient availability during static culture. Human pancreatic cancer cell line (PSN1 cells) was cultured under conventional static culture conditions. Culture media (CM) was extracted at predefined time points and nutrient concentration was determined through a luminescence-based assay. (A) Glucose availability during static culture. (B) Lactate production rate during static culture. Data presented as mean ± SEM, statistical analysis performed by a one-way ANOVA with Tukey's *post hoc* adjustment (n=3). Data information: *** P <0.001, **** P < 0.0001

Glucose is considered as one of the key micronutrients that is essential for cellular metabolic processes (Palm et al., 2017). Given the trend of decreasing daily availability of glucose from within the culture media for cells under static culture conditions, I wanted to evaluate whether this negatively impacted on cellular metabolic processes. Media was extracted as previously described and the lactate production rate (lactate concentration within the culture medium) was measured. The opposite trend was noted; lactate concentration within the culture media significantly increased over time ($p<0.0001$) (Figure 4.4 B). Despite exchanging the media, a rapid reaccumulation of lactate was noted. Excess levels of lactate within the culture media (outside the physiological range), can adversely impact and

influence cellular proliferation and synthetic function (Duval et al., 1992; Freund et al., 2018).

The data from Figure 4.4 illustrates that static culture fails to maintain nutrient homeostasis, as there is marked variation in daily nutrient availability. Over the time course of 7 days, cells were exposed to increased conditions of glucose deprivation in addition to lactate excess. Such exposure may impact on cell function. Whilst in vivo, marked differences in nutrient availability can be detected with subsequent activation of compensatory mechanisms to restore homeostatic conditions, mechanisms such as shunting of blood to or from areas of nutrient excess or depletion. Such auto regulatory mechanisms are not possible in static culture as the cultured cells are entirely dependent on the culture media for their source of nutrients and metabolites. This effect could be further exacerbated in the context of avatar culture, given the multicellular composition of the avatar when compared to cellular monolayer culture. This deprivation in nutrient availability (combined with an accumulation of metabolic waste products), may serve as one of the mechanisms responsible for the rapid degradation of patient derived explants ex vivo and limited long-term successful culture rates (Powley et al., 2020). As such, the impact of perfusion culture on nutrient availability should be evaluated.

4.2.2.2 Physiological benefits associated with perfusion culture.

After establishing a perfusion culture platform, the previous experiment of profiling the daily availability of nutrients in the culture medium was repeated. However, this time cells were cultured either under static or perfusion culture conditions. The perfusion rate was set in order to ensure that there was a complete media volume exchange of the entire perfusion plate by the same time point as when the media was replenished in static culture (by 72 hours). This rate was calculated as 10 uL per minute. As illustrated in Figure 4.5 A, when compared to static culture, perfusion culture is able to maintain a significantly higher glucose concentration during the entire time course of the experiment over 7 days (at 24 hours $p=0.005$, at 72 hours $p = <0.0001$ and at 168 hours $p = <0.0001$). The data was normalised to the respective cell count. There is very little daily variation in glucose availability when cells are cultured under perfusion conditions. Additionally, perfusion culture was associated with a significantly lower lactate secretion rate (Figure 4.5 B). The data would suggest that perfusion culture permits a constant epistatic supply of nutrients, thus preventing cyclical episodes of nutrient depletion or excess. Given the variation in nutrient availability during static culture, I wanted to determine whether this impacted on cellular function. I therefore chose to study the effect of nutrient availability on the mammalian Target of Rapamycin (mTOR) pathway. mTOR is one of the key pathways that regulates cell survival (proliferation, growth and motility), metabolism, transcription and protein synthesis (Hay et al., 2004). It is acutely sensitive to the cellular environmental conditions (Laplante et al., 2012). Upstream to mTOR, it has multiple inputs that can activate the mTOR pathway, these include

but are not limited to growth factors, amino acid availability, energy, stress and oxygen levels (Laplante et al., 2012). After 7 days of culture, under static or perfusion conditions, PSN1 cells were harvested and a western blot was performed in order to assess the downstream mTOR products. Decreased protein expression of Cyclin D1 was observed with static culture and upon quantitative analysis a statistically significant difference was noted ($p < 0.0001$) (Figure 4.5 E). It was also observed that a statistically significant decrease in protein expression of phosphorylated p70S6 kinase (pS6) was also present in static culture ($p < 0.001$) (Figure 4.5 F). During conditions of cell stress or nutrient depletion, mTOR is inhibited in order to conserve the nutrient pool and reduce cellular energy expenditure (Saxton et al., 2017). Our data (Figure 4.5) would suggest that cells are less metabolically active in terms of proliferation capacity (via Cyclin D1) and protein synthesis (via pS6) when cultured under static conditions rather than perfusion culture. It was interesting to observe that mTOR activity was maintained across all four wells of the perfusion plate. No reduction in either protein levels was noted as the wells were progressively sited further away from the active inflow of the perfused media. From the results of this initial perfusion experiment, it would appear that perfusion culture is able to replicate in vivo physiology more efficiently than conventional static culture given the maintenance of nutrient delivery, suppression of lactate build up and maintaining cells in a metabolically active state.

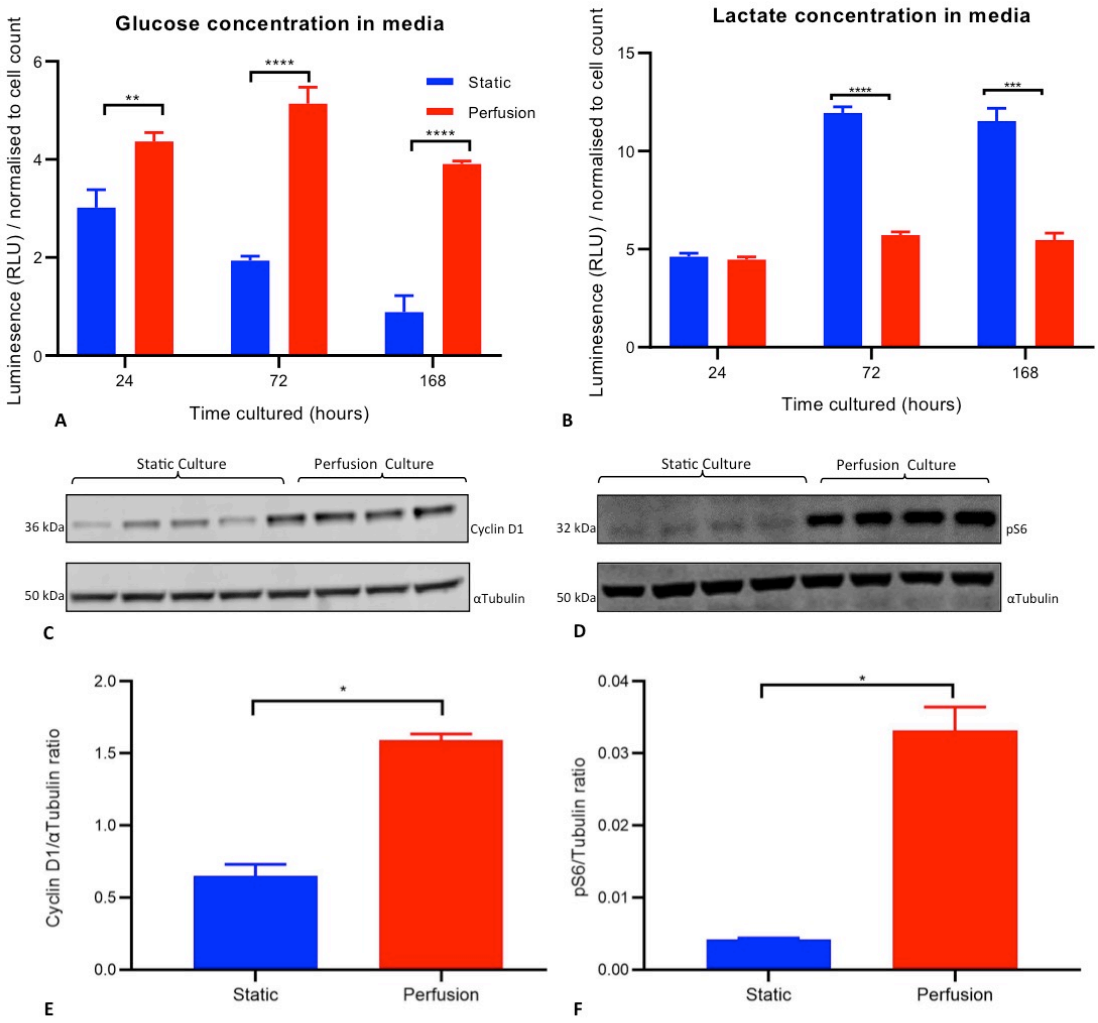

Figure 4. 5 - Physiological benefits associated with perfusion culture. Human pancreatic cancer cell line (PSN1 cells) was cultured under either conventional static culture condition or perfusion culture. Culture media (CM) was extracted at pre-defined time points and nutrient concentration was determined through a luminescence-based assay. (A) Glucose availability for cells during static and perfusion culture. (B) Lactate production rate by cells during static and perfusion culture. (C,D) After 7 days of culture, cells were harvested and western blot performed to determine the protein levels of downstream mTOR targets Cyclin D1 and pS6.(E,F) Protein levels were quantified by densitometry. Data presented as mean ± SEM, statistical analysis performed by Mann–Whitney U test, statistical analysis of protein quantification performed by unpaired Student T test (n=3). Data information: *p < 0.05; **p < 0.01; ***p < 0.001; **** p<0.0001

4.2.3 Perfusion culture of patient derived cancer avatars

In light of the results of the previous data regarding the effect of perfusion culture on monolayer cell culture, I was interested in determining whether perfusion culture of patient derived cancer avatars translated into successful long-term culture rates and whether the avatar viability was maintained ex vivo. Using the described avatar creation protocol in chapter 3, I created and subsequently cultured patient derived PDAC avatars under both static and perfusion conditions for 12 days ex vivo. An avatar was extracted from its culture chamber every 48 hours for histological assessment of viability and functionality.

One of the first human organs successfully cultured ex vivo using an organotypic tissue slice culture technique was the human brain (Verwer et al., 2002). As with any ex vivo primary tissue culture system, a strong emphasis is placed on developing a robust screening tool to assess for tissue viability in actual real time. Prompt identification of loss of viability or tissue compromise permits early intervention and alteration to the culture conditions or premature termination of the experiment. To assess the trend in the gross morphology of the PDAC avatars and to investigate whether the avatar surface area could be used as a proxy measure for tissue viability, I took serial macroscopic images of the avatars during ex vivo culture and quantified the surface area. Whilst the gross morphology remained constant, I noted that in the first 24 hours of ex vivo culture there was a significant reduction in the surface area of the avatars cultured under static culture conditions ($p=0.04$) (Figure 4. 6). This was subsequently followed by a gradual reduction in the surface areas of

the avatars from both culture conditions with no statistical difference between them. However, on both day 9 and 12 of ex vivo culture, a significant reduction in the surface area of the avatars cultured under static conditions was again noted (p=0.01 and p=0.01 respectively) (Figure 4.6). By day 12 of ex vivo culture, some avatar fragmentation was observed under static culture conditions, as illustrated in the macroscopic avatar image in Figure 4.6 on day 12.

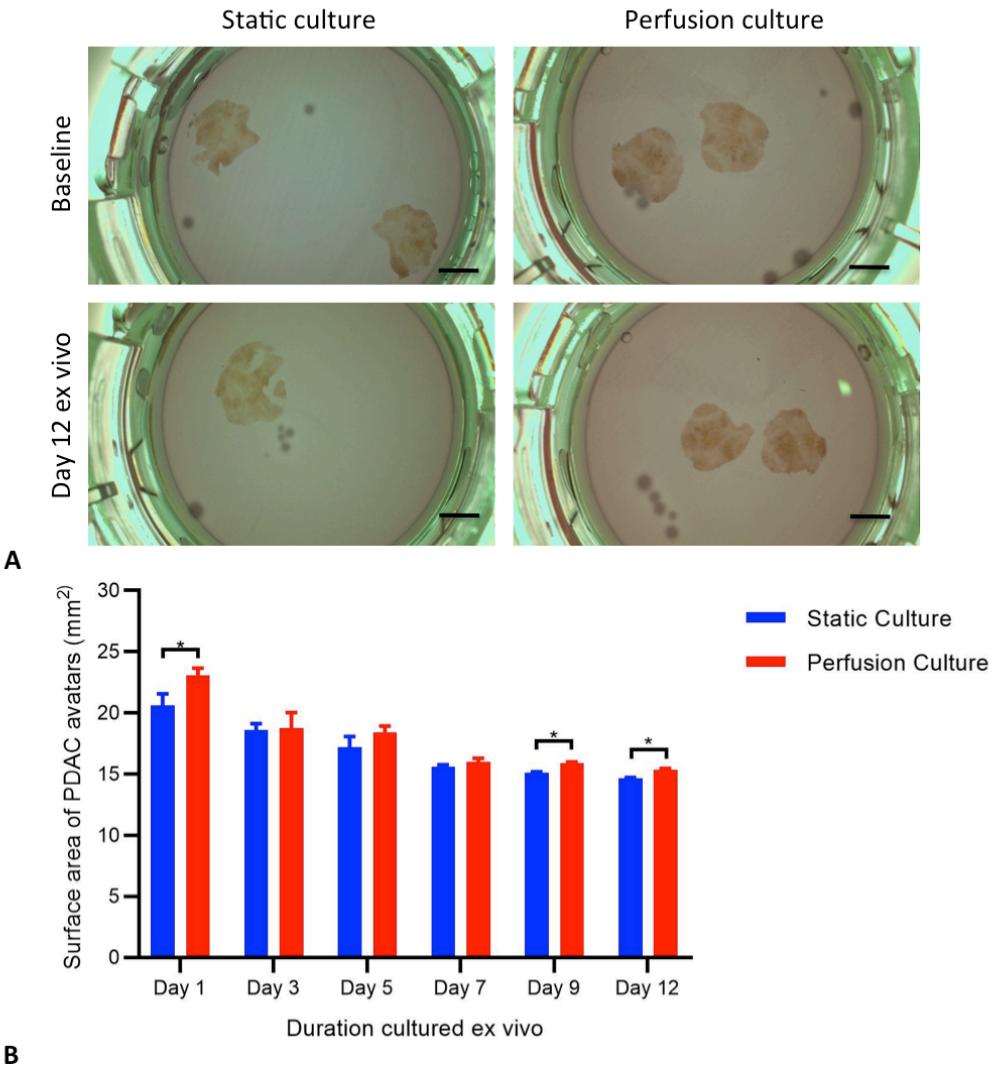

Figure 4. 6 – Macroscopic images of patient derived PDAC avatars and their surface area during ex vivo culture. (A) Gross image of PDAC avatars. Images taken at x1 magnification, scale bar 3mm. (B) Quantification of surface area during ex vivo culture. Data presented as mean ± SEM, statistical analysis performed by unpaired student t tests (n=3). Data information: *p < 0.05

Monitoring the avatar surface area may serve as a quick method for screening the general integrity of the avatars during ex vivo culture, however it remains as a crude measure of assessing tissue viability. It only provides a broad overview of the avatar on the macroscopic level. It provides no information or insight into the cellular morphology or native tissue architecture. Amongst the pre-existing published literature on primary human tissue slice culture, several studies have described the use of a viability scoring index as a way of assessing the viability/integrity of the cultured tissue (Erickson-DiRenzo et al., 2015; Gerlach et al., 2014; Naipal et al., 2016). Predefined parameters are selected and are subsequently scored across the cultured tissue (Naipal et al., 2016). Such an approach permits a directly quantifiable objective assessment of the tissue histology, instead of an overall subjective interpretation of the histological image (Naipal et al., 2016). To date, no universal viability scoring index has been proposed for patient derived cancer avatars. As such, I devised a method to numerically score avatar viability during ex vivo culture. The scoring index comprised a graded score, ranging from 1 (non viable) to 6 (good viability). The scoring index consisted of several parameters, including the presence and extent of necrosis, preservation of native tissue architecture, presence of tissue oedema, nuclear Hematoxylin staining and the incidence of nuclear abnormalities (nuclear pyknosis, karyolysis, karyorrhexis and apoptotic bodies) (Appendix A.3). Following ex vivo culture, avatars were extracted at specific time points and FFPE slides were created and subsequently stained with an H&E stain. A predefined, labelled matrix grid comprising annotated squares (500 by 500 um) was

superimposed over the digital image and sequential scoring of the grid was undertaken. Within the first 24 hours of ex vivo culture, a significant reduction from baseline was noted in the tissue viability score within both static and perfusion culture conditions. This was followed by a further gradual decrease in the tissue viability score, until day 12 ex vivo where a marked reduction in viability was observed in the avatars cultured under static conditions ($p < 0.001$), (Figure 4.7). The reduction in the viability score also correlated with the tactile feedback of handling the avatars whilst preparing them for formalin fixation; avatars from within static culture were much more prone to tissue fracture upon handling.

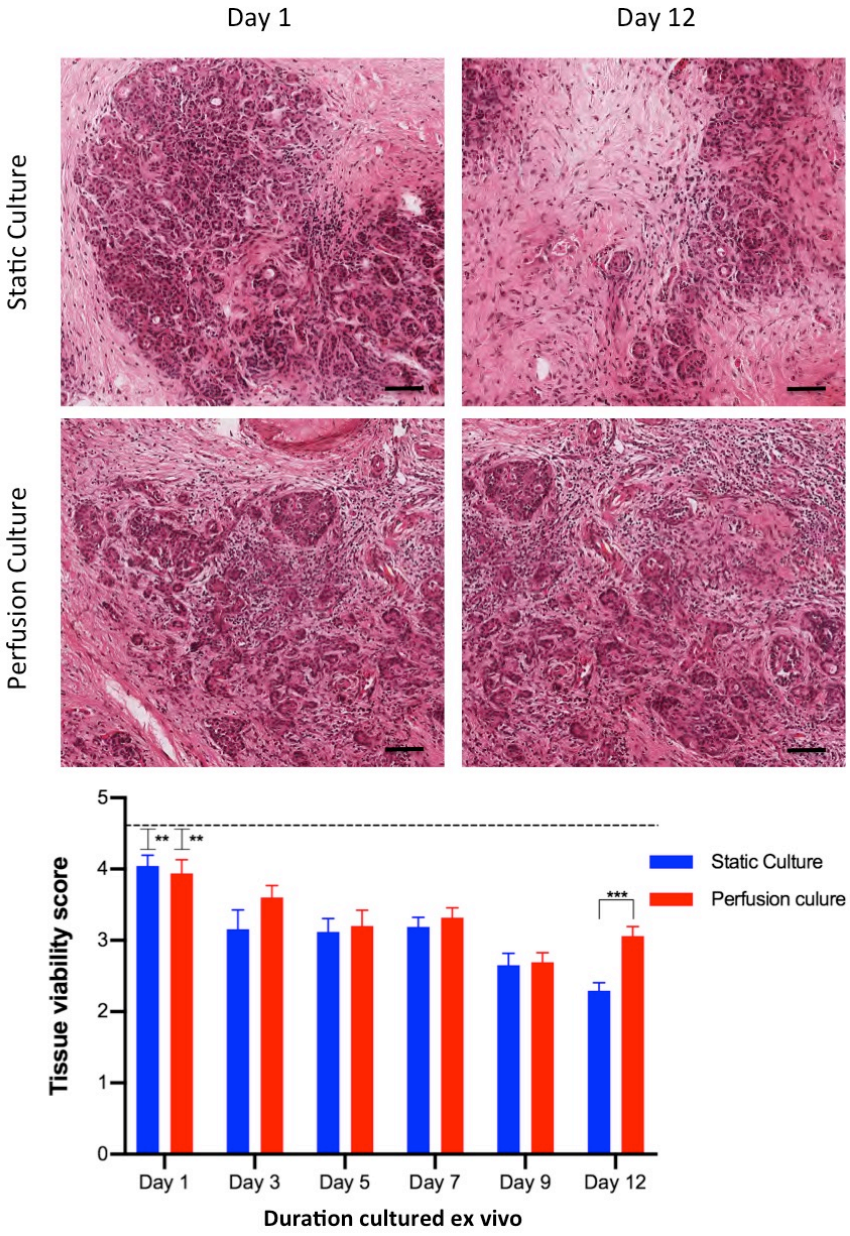

Figure 4. 7– Perfusion culture preserves microscopic viability of PDAC avatars during ex vivo culture. (A) Representative images of H&E-stained PDAC avatars after 12 days of ex vivo culture. Images displayed with scale bar 100um (n=2). (B) Quantification of tissue viability scores during ex vivo culture. Interrupted horizontal line on the x axis represents the baseline (Day 0) tissue viability score (4.62). Data presented as mean ± SEM, statistical analysis performed by Mann–Whitney U test (n=2). Data information: *p < 0.05; **p < 0.01; ***p < 0.001

4.2.3.1 Avatar proliferation index during ex vivo culture

It has been previously described that maintaining physiological culture conditions preserves both cellular and tissue function (Atkuri et al., 2007; Konduri et al., 2005). I consequently investigated the effect of perfusion culture on native cell function within the cultured avatars. Unopposed cellular proliferation serves as one of the cardinal features of cancer (Hanahan et al., 2011). I therefore wanted to determine whether the cancer avatars retained their proliferative capability ex vivo. At predefined time points, cancer avatars were extracted from either static or perfusion culture and following the creation of FFPE slides, IHC was performed. I stained initially for Ki-67 in order to identify proliferating cells. The proliferation index (proportion of Ki-67 positive cells) was calculated for each avatar. At the baseline time point, PDAC avatars were highly proliferative (proliferation index of 39.30 %). After 24 hours of ex vivo culture, irrespective of the culture condition a significant reduction in the proliferation index was noted from the baseline value ($p=0.01$ and $p=0.002$ respectively) (Figure 4.8). For the remaining time course, it was observed that there was a significant decrease in the proliferative index within the avatars cultured under static conditions when compared to perfusion culture (Figure 4.8). The proliferation index was maintained under perfusion culture. A marked reduction in the proliferation index was noted on day 5 ex vivo in avatars cultured under static conditions. The avatar proliferation index within perfusion culture was significantly higher on day 12 ex vivo. The data would suggest that avatars cultured under perfusion conditions sustained their proliferative capacity for a significantly longer

time period ex vivo when compared to static culture. This illustrates the benefits of utilising perfusion for avatar culture.

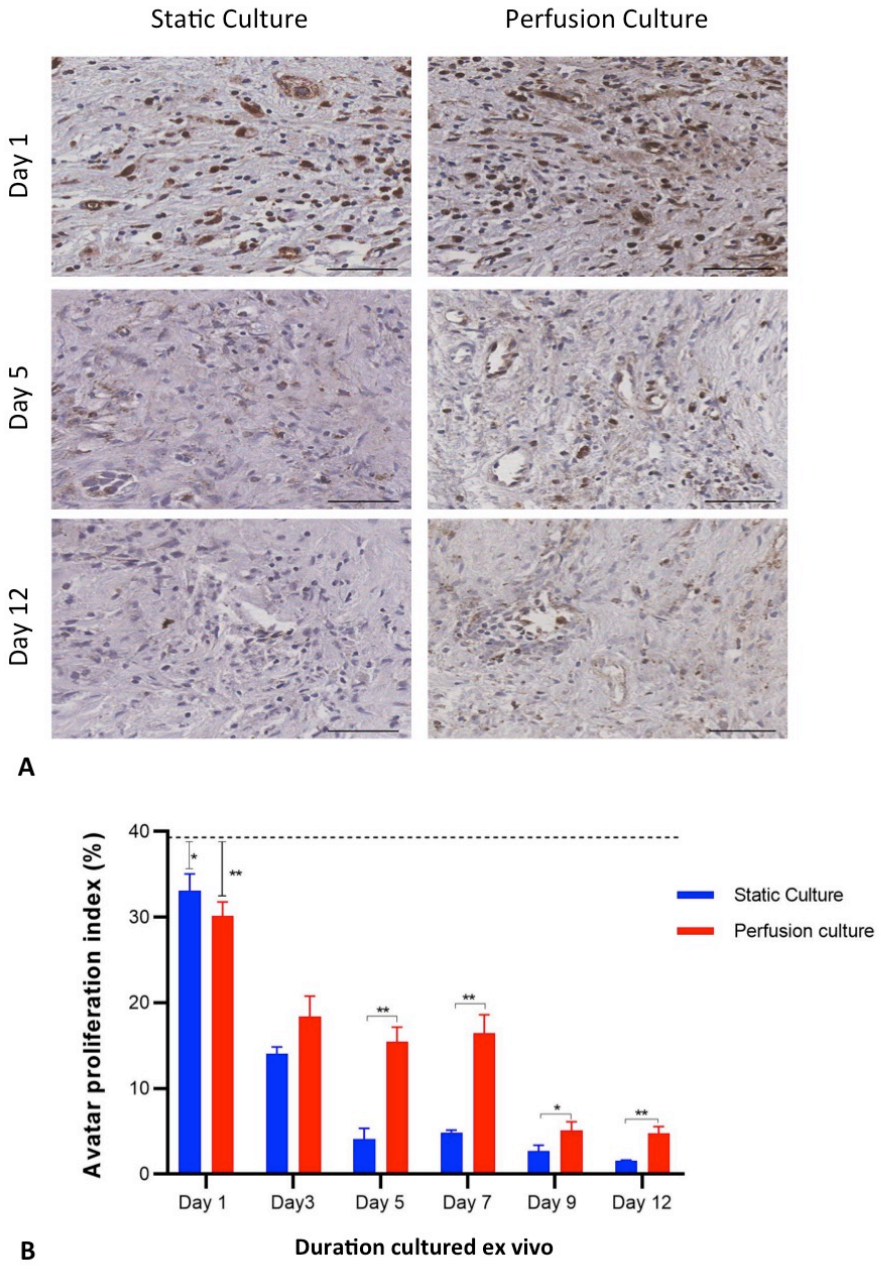

Figure 4. 8 - Proliferation index trend during ex vivo culture of PDAC avatars. (A) Representative images of immunohistochemical staining of PDAC avatars for Ki67 positivity during ex vivo culture. Proliferation index was calculated by the percentage of Ki67 positive cells across the tissue slices over time. Scale bar 50um (n=2). (B)

Quantification of the proliferation index during ex vivo culture. Interrupted horizontal line on the x axis represents the baseline (Day 0) proliferation index (39.30). Data presented as mean ± SEM, statistical analysis performed by Mann–Whitney U test. Data information: *p < 0.05; **p < 0.01; ***p < 0.001

4.2.3.2 Avatar cell death trends during ex vivo culture

Throughout the time course of ex vivo culture, the proliferation index under static culture conditions progressively decreased, however a striking loss of proliferative capacity was noted on day 5 ex vivo. In light of this finding, I wanted to investigate as to whether the proliferation index correlated with cellular apoptotic rates within the avatars. Programmed cell death is coordinated by the activation of the caspase cascade (Galluzzi et al., 2018). Activation of the initiator caspases may occur either through the intrinsic or extrinsic pathways (Galluzzi et al., 2018). Once initiated, the final component of the cascade is the activation of the executioner caspases from their inactive proenzyme state, following which scheduled apoptosis can occur (Galluzzi et al., 2016). I therefore performed IHC staining for Cleaved Caspase 3 to assess for apoptosis rates within the avatars. On day 5 ex vivo, a significantly higher apoptosis rate was observed in static culture when compared to perfusion culture (p=0.01), (Figure 4.9). The data illustrates that the reduction in proliferative index within static culture on day 5 correlates with a peak in apoptosis rates as per the activation and increase in Cleaved Caspase 3 staining observed.

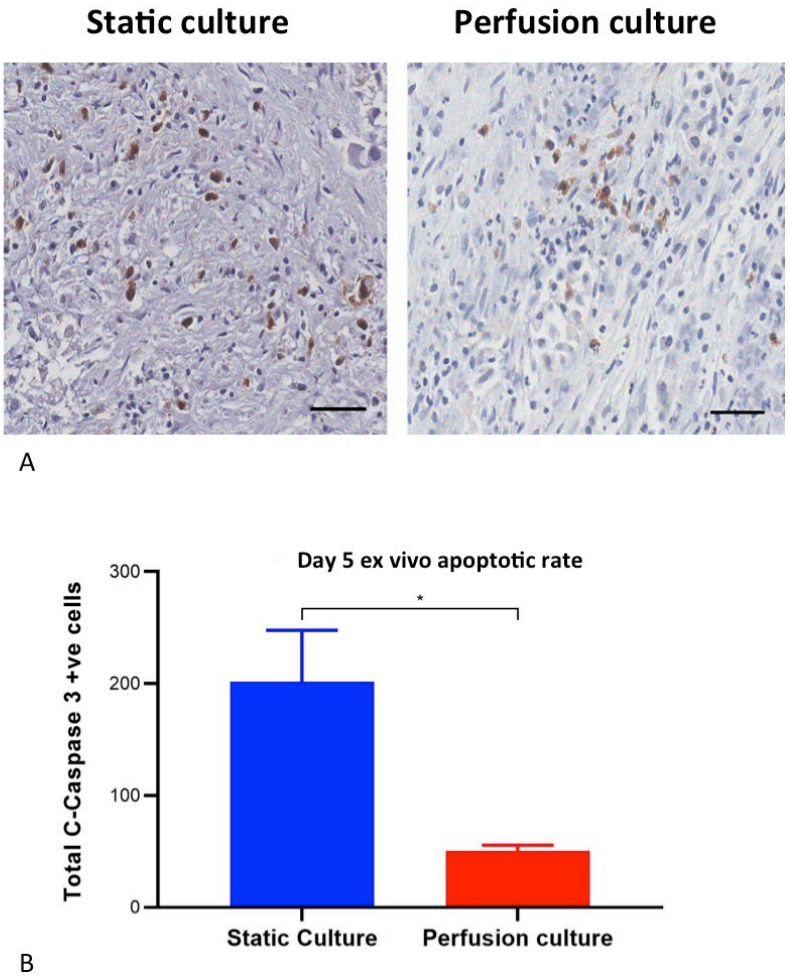

Figure 4. 9 - Apoptosis rates of PDAC avatars on day 5 of ex vivo culture. (A) Representative images of immunohistochemical staining of three different human derived PDAC avatars for Cleaved – Caspase 3 positivity on day 5 of ex vivo culture. All positive cells were counted per high power field across the avatar. Scale bar 50um(n=3). (B) Quantification of total Cleaved – Caspase 3 positive cells during day 5 of ex vivo culture. Data presented as mean ± SEM, statistical analysis performed by unpaired Student T test. Data information: *p < 0.05

Our previous analysis of the effect of culture conditions on monolayer cell culture illustrated that metabolic function via mTOR activity was maintained when perfusion culture was utilised (figure 4.10). Given this result, I wanted to determine whether the same advantage was observed (mTOR activity preservation) when avatars were cultured under perfusion conditions. Therefore, after ex vivo culture I performed IHC

staining of pS6 to determine the metabolic mTOR activity within the avatars. At the baseline time point, avatars displayed high metabolic activity and strong pS6 staining (Figure 4.10 A). A significant decrease in metabolic activity was observed in the first 24 hours of avatar ex vivo culture, with a large reduction in positive pS6 staining area within static culture conditions ($p=0.04$) (Figure 4.10). A further significant reduction in pS6 staining was observed at day 3 of ex vivo culture in static culture conditions ($p=0.0026$). On day 5 of ex vivo culture, the mTOR activity within both culture conditions had <1% positive pS6 staining of the avatar surface area.

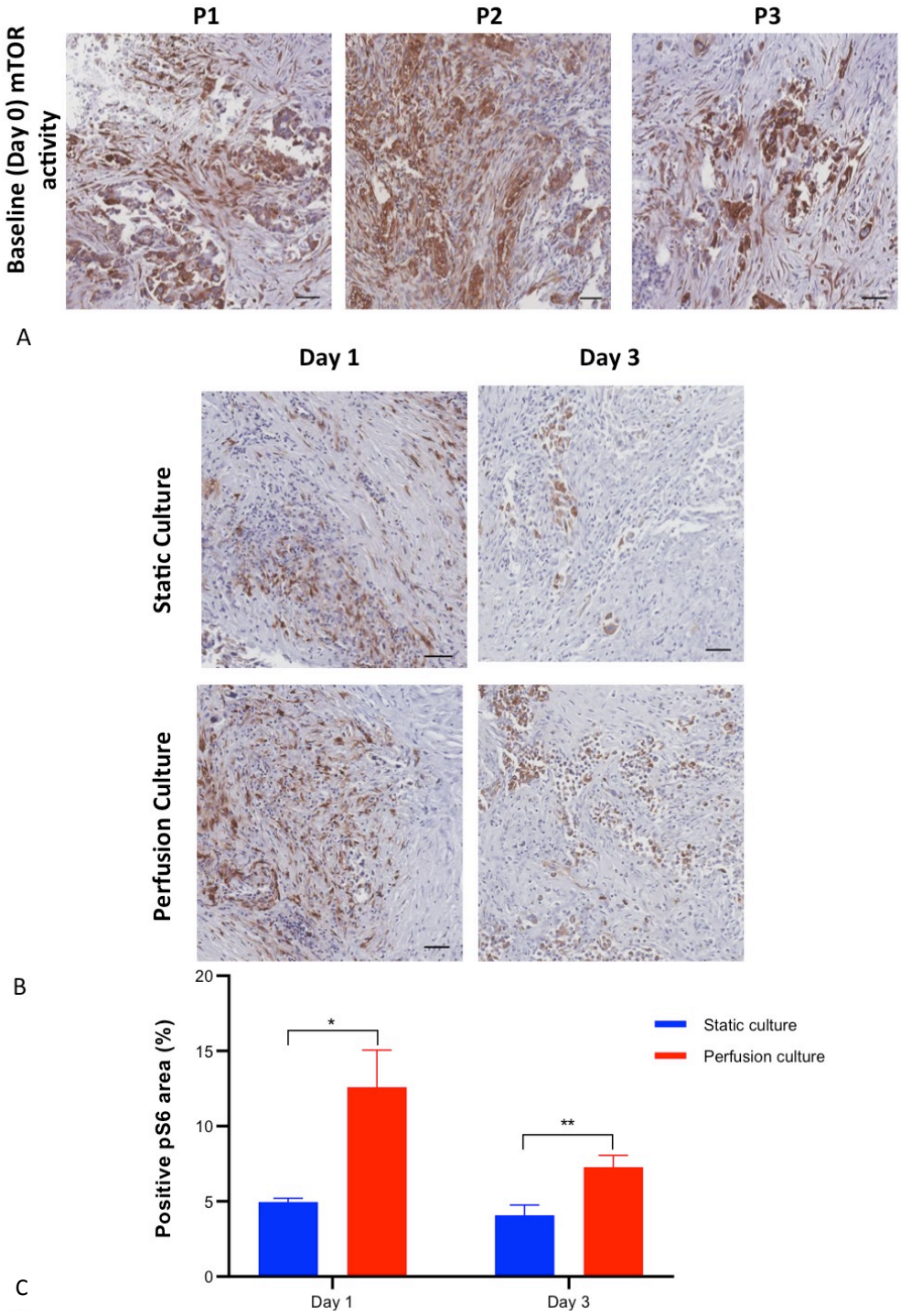

Figure 4. 10 - Metabolic activity of PDAC avatars during ex vivo culture. (A) Representative images of immunohistochemical staining of 3 different PDAC avatars for pS6 positivity at the baseline (Day 0) timepoint. (B) Representative images of immunohistochemical staining for PDAC avatars pS6 positivity during ex vivo culture. Scale bar 50um (n=3). (C) Quantification of the metabolic activity during ex vivo culture. The percentage pS6 positive area was calculated per high power field across the avatar using a set threshold. Data presented as mean ± SEM, statistical analysis performed by Mann–Whitney U test. Data information: *p < 0.05; **p < 0.01.

4.2.4 Spatial transcriptomic changes within the avatars during ex vivo culture

Whilst I had previously investigated the impact of perfusion on native biological processes within the avatars during culture, what remained unclear was whether the transcriptomic profiles of the avatars changed during ex vivo culture. A transcriptomic analysis would provide insight into specific cell function and metabolic pathways. It therefore could be used as an assessment tool to determine the effect of ex vivo culture on the avatars and also help determine the maximum duration of culture. Whilst bulk RNA extraction and subsequent sequencing could be performed, this would provide limited insight. Bulk RNA sequencing would provide an overview of the transcriptome of the avatar in its entirety. However, we would be unable to identify as to where or within which part of the tumour microenvironment these changes occurred. Through collaboration with the Medicines Discovery Catapult (Manchester, United Kingdom), we performed spatial transcriptomic analysis of the avatars following ex vivo culture. The GeoMx Digital Spatial Profiler (nanostring) was used as it allows for spatial sequencing based on pre-defined areas of interest. The GeoMx experiment was performed by Dr M Eyres (Medicines Discovery Catapult). During ex vivo culture, an avatar was extracted at pre defined time periods and corresponding FFPE slides were created. Each avatar was initially segmented into tumour and stromal regions. Segmentation was based upon areas of pan-cytokeratin staining, whereby areas of positive pan-cytokeratin stain were labelled as tumour regions and conversely negative areas of pan-cytokeratin staining were labelled as stroma regions (Figure 4.11).

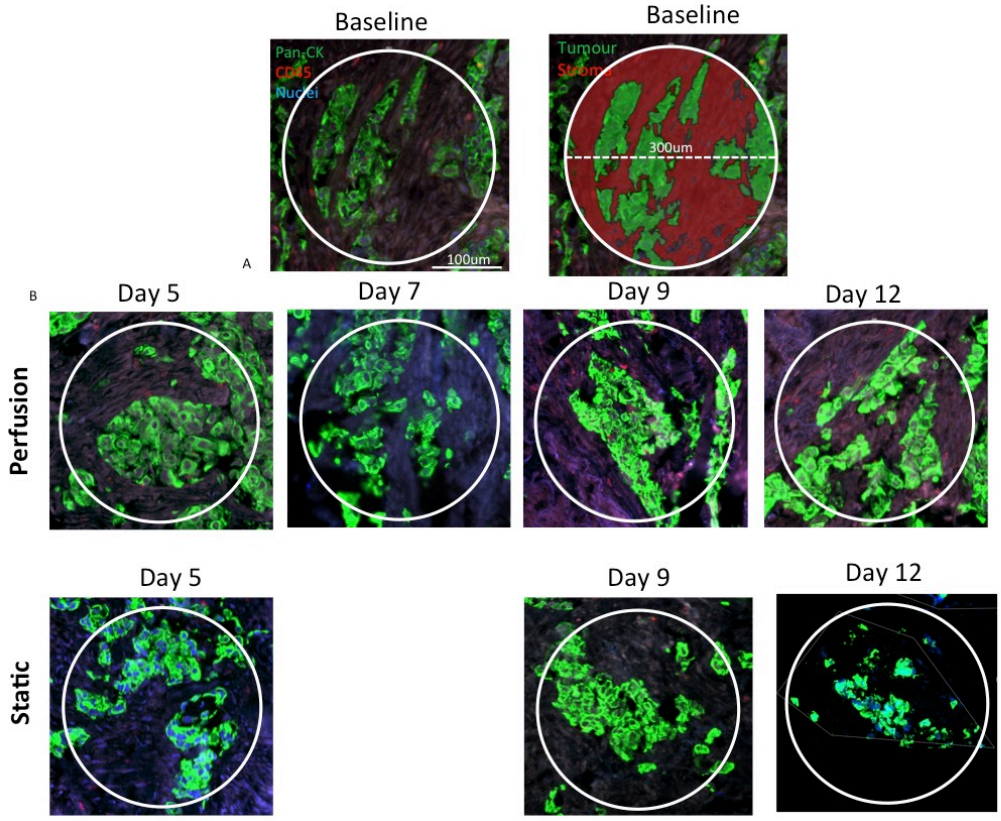

Figure 4. 11 - GeoMx segmentation of PDAC avatars. (A) Overview of the segmentation process of the PDAC avatars using the GeoMx platform. Machine based learning is utilised to identify tumour (Pan-CK positive) and stromal regions (Pan-CK negative). Digital images are subsequently segmented accordingly. Regions of interests are annotated and are subsequently sequenced. (B) Representative images of tumour regions within the avatars during ex vivo culture

After image segmentation, regions of interest were annotated. RNA sequencing was subsequently performed and the GeoMx platform allowed for normalisation and pooling of data as per the segmentation profile. After filtering out duplicated genes and those that were expressed in fewer than 5% of the ROIs, there were 2920 genes remaining in the dataset. This loss of available sequencing data appears to be mainly due to instability of RNA and the paucity of material and is a common problem when tumour tissue is used in the GeoMX workflow.

Subsequent analysis was performed using the R 'pheatmap' package by Dr F Willenbrock (O'Neill group). A comparison between the transcriptomic profile of the perfused and non-perfused avatars was performed. The data was subsequently filtered and processed further in order to look at the tumour and stroma as two separate regions. The transcriptomic profile of avatars that were cultured under perfusion conditions demonstrated some alteration in gene expression over time (Figure 4.12). However upon clustering analysis, there was no grouping of individual time points. The transcriptomic profile of avatars from different time points (day 5,7,9 or 12 ex vivo) was all intermixed and clustering failed to group them according to time. The data would suggest that the transcriptomic profile of these avatars remained similar during ex vivo perfusion culture and as a consequence the gene expression remained fairly constant between day 5 and 12 of ex vivo culture. A very different result was observed amongst the tumoural compartment of the avatars maintained in static culture. As per the respective heatmap (Figure 4.12 B), widespread gene expression changes are observed with greater levels of gene

upregulation. However, what is clear is that the transcriptomic profile allows for clear clustering which corresponds to duration cultured ex vivo. There is sequential clustering of avatars from day 5, 7 and 12 ex vivo. This illustrates persistent and progressive changes in gene expression over time. This finding was not present under perfusion conditions. Whilst under static culture conditions, there is significant alteration to the transcriptomic profiles present. Static culture fails to maintain homeostasis within the avatars and as such avatars from later time points are transcriptomically different to those from an earlier time point.

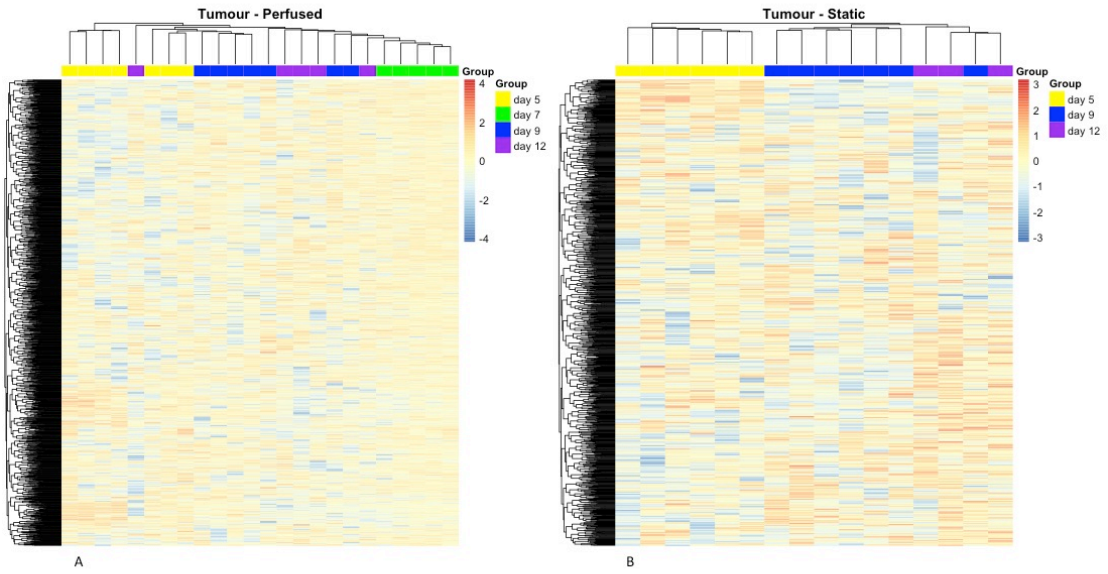

Figure 4. 12 - Spatial transcriptomic changes of the tumour compartment of PDAC avatars during ex vivo culture. Heatmaps of differentially expressed genes within the tumour compartment of the avatars over time. (A) Avatars cultured under perfusion conditions. (B) Avatars cultured under static conditions

We also reviewed the stromal compartment of the tumour microenvironment in order to determine whether its transcriptomic profile altered during the time course of ex vivo culture (Figure 4.13). Under perfusion culture conditions, no clear clustering was observed over time, whereas static culture was associated with more

pronounced changes in individual gene expression and a trend towards clustering over time. Data from both transcriptomic analyses further support the benefit of using perfusion culture to maintain avatars ex vivo. The use of perfusion culture maintains the transcriptomic profile of the avatars over serial days (day 5 to 12) and thereby provides further evidence for the role of perfusion culture.

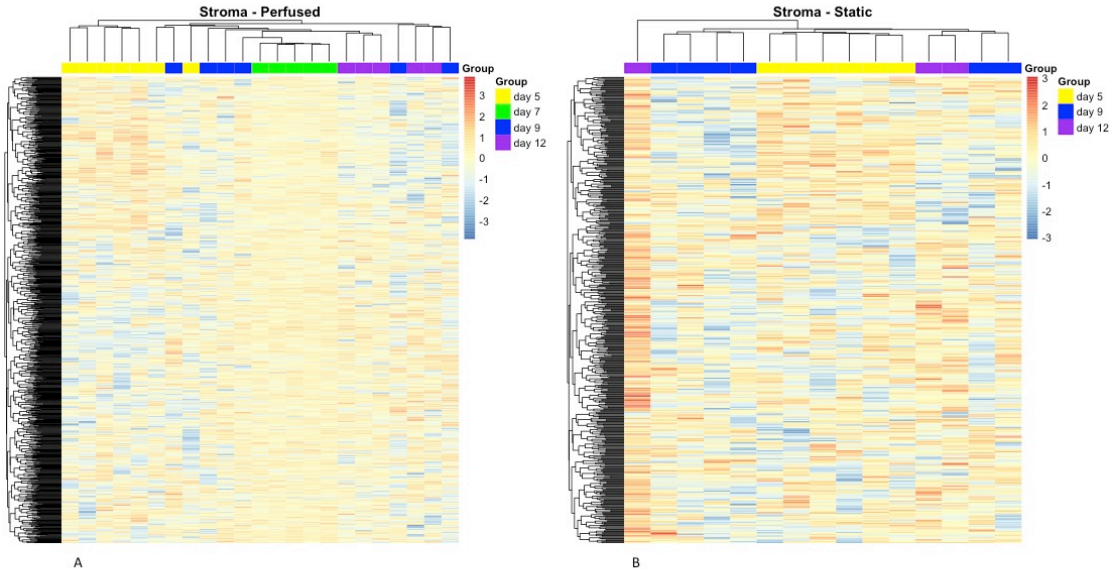

Figure 4. 13 - Spatial transcriptomic changes of the stromal compartment of PDAC avatars during ex vivo culture. Heatmaps of differentially expressed genes within the stromal compartment of the avatars over time. (A) Avatars cultured under perfusion conditions. (B) Avatars cultured under static conditions

In order to gain further information regarding the cellular composition of the avatars, single cell deconvolution of the sequencing data was performed by Dr F Willenbrock (O'Neill group). This method consists of using pre defined gene sets (described in Lin et al (2020)) that are uniquely expressed per specific cell type. The analysis subsequently uses these gene sets as the basis for quantifying the different cell types present amongst the samples. We wanted to determine whether perfusion culture had any specific effect on a particular cell type within the tumour

microenvironment. We first analysed the effect of the different culture methods on the epithelial tumour cells. As the current platform was being established with the intention of long-term culture of PDAC avatars, we wanted to ensure that we were able to maintain the tumour cells specifically during ex vivo culture. Whilst under perfusion conditions, an initial significant reduction in tumour cell count was observed between baseline and day 5 ($p<0.05$) (Figure 4.14). No further significant reduction in tumour cells were observed between day 5 and day 12 of ex vivo culture. This would suggest a degree of stability within the tumoural compartment with perfusion. However when we analysed the effect of conventional static culture, we observed a clear difference. Under static culture conditions, the avatars progressively lost epithelial tumour cells over the time course of ex vivo culture and a significant reduction was observed on day 9 and 12 of culture ($p <0.01$) (Figure 4.14).

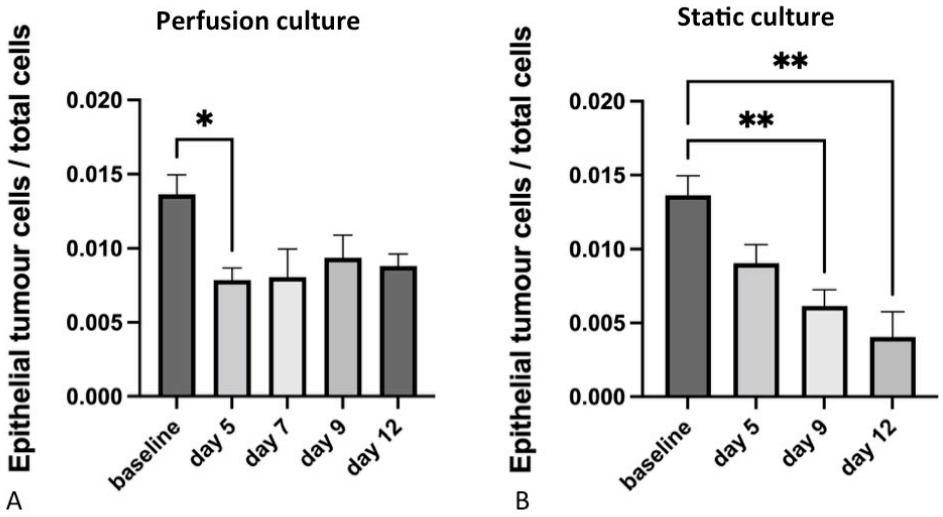

Figure 4. 14 - Quantification of epithelial tumour cells during ex vivo culture. Single cell deconvolution of the sequencing data was performed to monitor trends in epithelial tumour cell number over time during ex vivo culture. Both Perfusion (A) and static culture (B) conditions were examined. Data presented as mean ± SEM, statistical analysis performed by a one-way ANOVA with Tukey's *post hoc*

adjustment. Data information: *p < 0.05; **p < 0.01.

We subsequently investigated as to whether any other cell type was also affected by the culture condition. We assessed both the normal and activated fibroblasts within the tumour microenvironment of the avatars. Irrespective of the culture condition used, we observed a progressive loss of activated fibroblasts over time. There was a considerably lower percentage of normal fibroblasts and the difference in numbers observed over time therefore was not significantly different. The data from the deconvolution experiment highlights that within the current system design, epithelial tumour cells are maintained ex vivo however the activated fibroblast population is lost over time.

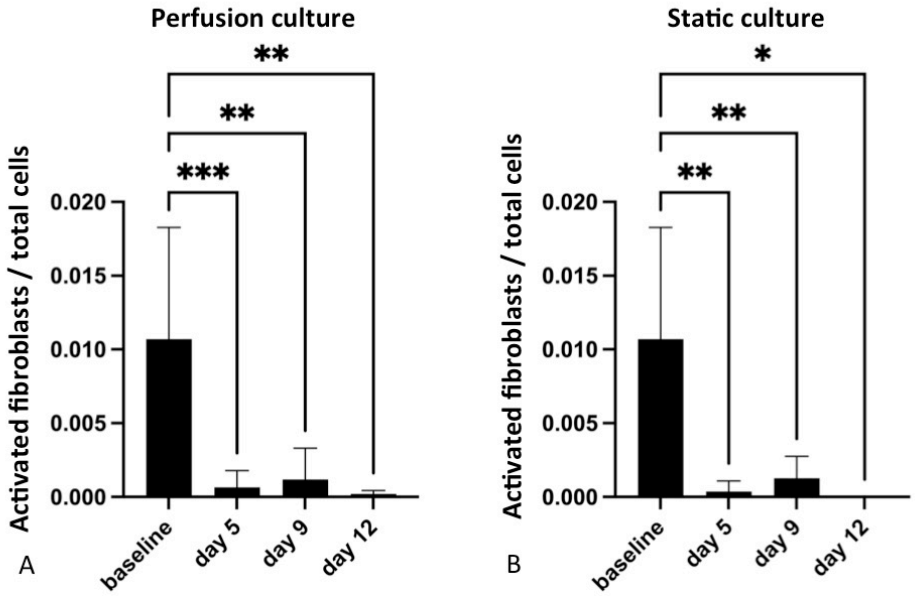

Figure 4. 15 - Quantification of activated fibroblasts during ex vivo culture. Single cell deconvolution of the sequencing data was performed to monitor trends in activated fibroblasts cell number over time during ex vivo culture. Both Perfusion (A) and static culture (B) conditions were examined. Data presented as mean ± SEM, statistical analysis performed by a one-way ANOVA with Tukey's *post hoc* adjustment. Data information: *p < 0.05; **p < 0.01; ***p < 0.001.

The deconvolution method described by Lin et al distinguishes 3 clusters of CAFs: CAF0, CAF1 and CAF2. Unfortunately, these do not correlate directly with the CAF states reported previously in the literature, namely myofibroblasts (myCAFs), inflammatory fibroblasts (iCAFs) and antigen-presenting fibroblasts (apCAFs) (Elyada et al). It was suggested that the CAFs in cluster 0 most closely resemble myCAFs whereas those in cluster 1 are more similar to normal, quiescent CAFs. The third cluster bears no resemblance to apCAFs. Since there is this discrepancy between the CAF classifications, I have chosen to use the descriptive terms of "activated fibroblasts" for the CAF0 cluster and "normal fibroblasts" for those in cluster 1. The uncertainty regarding this classification could not be resolved using other methods (DECODER, CIBERSORT, EPIC, ECOTYPER) because the number of genes in our dataset was too low for any of these to give meaningful information.

4.2.5 Mathematical modelling of shear stress exerted on to the avatars during perfusion culture

Through introducing perfusion culture within our experimental design, I wanted to determine whether the presence of perfusion resulted in excess shear stress upon the avatars. High levels of shear tension stress could adversely impact on the avatar and consequently reduce ex vivo culture duration. Firstly, through using the COMSOL Multiphysics software I constructed a representative 3D reconstruction of the culture well from the perfusion plate to scale. I subsequently used the laminar flow model in order to simulate media perfusion. Whilst creating the simulation

model, I had to determine the fluid properties. As the software did not include 'culture media' as a substance, I used water as a proxy measure for culture media. The model incorporated the perfusion flow rate, diameter of the inflow and outflow tubing, the volume of the well and the material of the perfusion plate as parameters within the simulation. Avatars placed in the centre of the well experienced low shear stress (denoted by the heat map result in Figure 4.11 B) whilst under perfusion conditions.

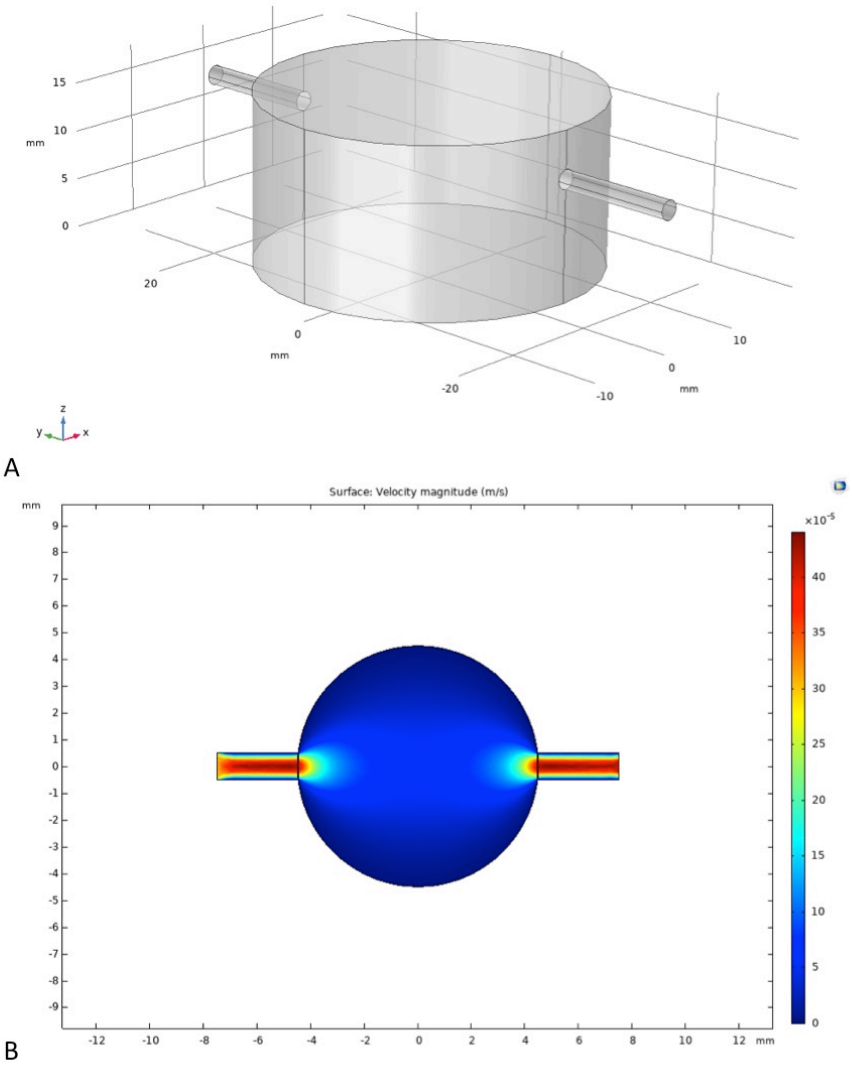

Figure 4. 16– Virtual simulation and mathematical modeling of shear stress experienced during perfusion culture. (A) A 3D reconstruction of a culture well from our perfusion plate. The culture well includes an inflow and outflow channel for perfusion of media. This model serves as the foundation for the simulation (B)

Velocity field simulation of the shear stress production within a culture well which is exerted on the avatar during perfusion culture. The heatmap describes the flow velocity. Higher flow velocity is denoted as a shift towards the red spectrum of colours. The height (z axis) of the image is taken at 13mm vertical distance from the base of the well. Within this simulation model, no avatar was placed in the well. From the results of the model, it would suggest that avatars that are placed centrally within the culture well experience low shear stress during perfusion culture.

4.3 Discussion

Within this chapter I investigated as to whether perfusion culture served as an alternative culturing technique and if it was able to recapitulate the in vivo physiological conditions of the tumour microenvironment. Our data illustrates the limitations of conventional static culture, notably the daily variation in nutrient availability and the dependency of the system for media exchange to replenish the concentrations of nutrients and metabolites (Figure 4.5). It would appear that cells under static culture are responsive to these marked changes within the culture environment and as a consequence can reduce metabolic activity through suppression of the mTOR pathway (Figure 4.5). However, whilst under perfusion conditions metabolite delivery remains constant and mTOR activity can be preserved. The benefits of perfusion culture were not just observed within monolayer cellular culture, we also noted a marked benefit when culturing avatars under perfusion conditions. Notably this was the ability to maintain proliferative capacity, reduce apoptosis rates and sustain metabolic function of the avatars during prolonged ex vivo culture (Figure 4.8, 4.9 and 10). As such we propose that perfusion culture should be utilised when establishing ex vivo models or culturing patient derived cancer avatars.

Despite our initial data illustrating the advantages of using perfusion over static culture, the exact mechanism that underpins the physiological benefit of perfusion culture has yet to be determined. Conceptually, one could argue that it is the constant delivery of nutrients to the cultured specimen (be that cells or tissue) instead of the conventional cyclical media exchange. An interesting observation by Garcia-Montero et al. in 2001 was that media exchange alone was sufficient to induce a stress response within cells (Garcia-Montero et al., 2001). After culturing 8 different cell lines (combination of normal and cancer cell lines) they noted that media exchange was associated with an increase in gene expression of stress induced genes and activation of the mitogen-activated protein kinase (MAPK) cascade (Garcia-Montero et al., 2001). Nakatani et al, also observed the activation of the MAPK cascade upon media exchange (Nakatani et al., 1998). Given that there is no acute environmental change or nutrient shock (either excess or depleted concentration) rather, a slow but constant renewal, this may serve the basis of the physiological advantage. However, another conceivable explanation is that perfusion culture may allow constant delivery of nutrients but it also permits continuous removal of cellular metabolic waste processes. As such, cells are not continually bathed in the noxious end products of both catabolic and anabolic processes. Several studies have published on the detrimental effect of metabolic waste products (notably ammonia and lactate) on cellular function and proliferation (Duval et al., 1992; Glacken et al., 1986; Lao et al., 1997). Excess lactate may cause acidification of the culture media (Ozturk et al., 1992). Nutrient deprivation may cause a flux in cell metabolism pathways, switching from conventional aerobic

metabolism pathways driven through the Kreb's cycle to lactate fermentation pathways with excess glycolysis, which in turn will perpetuate lactate production and accumulation. One could question within our current system, whether perfusion culture prevents cells from fluxing into a glycolysis driven metabolism trend or whether perfusion simply removes all waste products continuously and thus prevents the natural build up. It might be possible to differentiate between both through measuring cellular bioenergetics and measuring the lactate concentration within the perfusion plate and downstream in the outflow waste reservoir in order to see whether accumulation had occurred.

Several practical considerations should be considered when establishing a perfusion culture system. Our initial experience highlighted the need to have a tissue culture hood within close proximity to the culturing incubator. This facilitated easy transfer between the two for experimental analysis within a sterile environment (for example media extraction, imaging or tissue collection) without the need to suspend perfusion. One of the limitations of our concurrent perfusion culture set up is that our inflow perfusion pump is external to the incubator. The significance of this is that the culture media reservoir (housed within the inflow perfusion syringe) is kept at room temperature rather than at the conditions within the incubator (in terms of temperature and humidity). Such a limitation can be rectified through the use of a mechanical pump that can be housed within the incubator (one which can withstand the humidity of the incubator). Another important consideration for the perfusion system is the type of the perfusion inflow, specifically the nature of media delivery. Our system utilised a mechanical pump that delivered a continuous flow of media

into the perfusion circuit. An alternative technique that could be implemented would be the use of a peristaltic pump, where media can be perfused in intermittent, short bursts (Whitticar et al., 2016). No definitive evidence has been published regarding the superiority of either inflow delivery techniques. Conceptually, intermittent peristaltic inflow may resemble the normal human cardiac output. It would be interesting to directly compare both methods in order to assess whether there is a physiological benefit associated with either delivery system. This could serve as a reference point for future work.

One of the most challenging aspects of implementing perfusion culture within our experimental set up was determining the perfusion rate. An extensive body of literature exists on human physiology, in particular systemic blood flow distribution (Calzia E., 2005; Eckert R, 2002). However, this is predominantly based on healthy individuals (Cantor et al., 2017). A broad range of blood delivery rates is observed across organs; for example in a healthy, average 70 kg individual the renal blood flow is 1.2 L/min whereas the cerebral blood flow is only 0.75 L/min (Cantor et al., 2017). It is important to highlight that the weight of the organ does not dictate the flow rate, rather it is the underlying function as illustrated by the fact that the kidneys despite having a low combined weight (approximately 0.3 kg) receive 1.2 L/min of blood flow whereas the liver, a substantially larger organ (approximately 1.5 kg) receives only a fraction higher flow rate (1.4 L/min). Quantified measurements of blood flow to the digestive organs of the alimentary tract are limited and the literature, albeit historic in nature, is largely based on invasive measurement

techniques within animal models (Goodhead, 1969). However, recent advances in cross-sectional imaging and radiolabeled isotopes may provide a greater insight (Tsushima et al., 2011). Whilst determining the gross organ flow rate on a broad perspective is possible (arterial inflow into the organ), the difficulty remains in determining the flow rate of the intra-parenchymal capillary circulation. Another important factor to highlight within our system is that we are not culturing normal pancreatic tissue; rather we are culturing grossly abnormal tissue, pancreatic cancer. Neoangiogenesis serves as a crucial mechanism for tumour establishment and survival (Yadav et al., 2015). However, PDAC is a profoundly hypoxic tumour (Koong et al., 2000). The florid desmoplastic reaction and dense stroma associated with PDAC contributes to the hypoxic environment. High levels of interstitial and intratumoural pressure result in the collapse of the vasculature, which in turn impedes blood flow and oxygen delivery (Katsuta et al., 2019; Longo et al., 2016). A low micro-vascular density is observed (Katsuta et al., 2019). With the aforementioned factors, it is difficult to compute inter-tumoural blood flow. Our perfusion system incorporates a low flow rate in order to reduce shear stress across the avatar and to mimic the postulated flow rates within a capillary vascular bed. Further research efforts should be focussed on identifying the optimal perfusion flow rate for ex vivo culture of human derived PDAC avatars. Optimisation of the flow rate may translate into prolonged ex vivo culture duration and improved physiological conditions.

Establishing a robust analysis method in order to assess and quantify the overall health of the cultured avatars, serves equally as a crucial component of the

perfusion culture system. Whilst having a single test to confirm avatar health would be ideal, the reality is that several analyses are required in order to deduce this information. The viability scoring index is a simple method of assessing the global integrity of the avatar, however the robustness of the method can be improved through introducing a blinded assessor assessment of the avatar. The use of Ki67 has been widely described in primary tissue culture as a marker to assess proliferative capacity (Martin et al., 2019; W. Xu et al., 2012). However, Ki67 is not expressed when cells are in a quiescent state (Miller et al., 2018). What is needed is a test to assess for a unique function of the native tissue being cultured to determine whether this function is being preserved in the tissue ex vivo. Paish et al, cultured human liver tissue slices (obtained from a normal resection margin following a hepatectomy for colorectal liver metastases) and measured the albumin secretion rate. Albumin formation is a synthetic function of the native liver (Paish et al., 2019). Cheah et al, cultured cardiac muscle acquired from patient biopsies and measured electrical stimulation response ex vivo (Cheah et al., 2010). Perrard et al, cultured human testicular tissue ex vivo and measured spermatogenesis rates (Perrard et al., 2016). However, in the context of cancer avatar culture, there is no native tissue function per say to assess during ex vivo culture. One could possibly overcome such a limitation through assessing certain disease characteristics, such as exosome production (Nuzhat et al., 2017).

Within this chapter, I have discussed the establishment of a perfusion system and investigated the effects of perfusion culture on both monolayer cell culture and avatar culture ex vivo. The data suggests that there is a benefit to the use of

perfusion culture whereby avatar viability and functionality is preserved ex vivo. This evidence base serves as a foundation and as justification for the use of perfusion culture of avatars for future experiments. What is now needed is a detailed profile of the different cellular components within the avatars, specifically, the stability of each component of the tumour microenvironment during ex vivo culture. This will determine the optimal time interval for conducting a drug screen, during which the avatar cellular composition closely mimics that of the in vivo tumour. In this way a representative system could be created to deliver precision therapy for patients.

Chapter 5

Profiling the cellular composition of avatars during ex vivo culture

The work within the previous chapter illustrates the physiological benefit of utilising perfusion culture for ex vivo culture of cancer avatars; notably the maintenance of proliferative capacity, suppression of cell death rates and conservation of metabolic activity. Whilst the functional properties of the avatars have been examined during ex vivo culture, what has yet to be determined is whether the cellular composition of the avatar changes over time. Profiling the native cell populations within the avatars must be performed with both IHC and a multiplex immunofluorescence panel in order to monitor cell population trends under both static and perfusion culture conditions during the course of ex vivo culture.

5.1 Cellular diversity of PDAC tumours

Historically, it was considered that tumours were entirely composed of cancer cells alone. As a consequence, therapies focussed solely upon targeting a single cell type. However, advances in our understanding of cancer biology has illustrated that

tumours consist of a diverse cellular ecosystem of numerous different cell types (Weinberg, 2008). As such, when studying cancer evolution or investigating novel therapeutic targets it is essential that this cellular diversity is taken into context.

The tumour microenvironment (TME) comprises several distinct compartments. A pathognomonic feature of PDAC tumours is that the tumour cells form the minority of the tumour mass (Leppanen et al., 2019). Key constituents of the tumour include the stroma, fibroblasts (notably cancer associated fibroblasts CAFs) endothelial cells and components of the immune system (Lorusso et al., 2008). Our understanding as to how these different components contribute to disease progression, promote metastasis, manipulate the immune system and influence response to treatment continues to evolve. Pancreatic stellate cells represent a unique cluster of cells within the pancreas. These myofibroblast cells only occupy approximately 4% of the native gland cellularity (Bachem et al., 1998). In their quiescent state, they are responsible for Extra Cellular Matrix (ECM) turnover and recycling through their production and secretion of matrix metalloproteinases (MMPs) (Apte et al., 2012). However once activated, denoted by alpha-Smooth Muscle Actin (a-SMA) expression, a phenotypic switch is observed where their functional role now predominantly involves ECM production and deposition (Apte et al., 2012). Excessive deposition of ECM ultimately leads to fibrosis (Apte et al., 2012). The abundance of fibrosis within the stroma of PDAC contributes to the hypoxic environment and can impair drug delivery to the tumour through sequestering the drug in the stromal compartment (Olive et al., 2009). Not only does the stroma influence treatment response, but also through cytokine production it can induce an epithelial-

mesenchymal transition and promote a relative immunosuppressive environment (B. Jiang et al., 2020; Thind et al., 2017).

In light of the fact that the TME in PDAC clearly has a diverse functional role and can directly impact on therapeutic response, it is crucial that precision therapy models have a stromal compartment within them. As previously discussed, one of the biggest limitations of monolayer 2D cellular models for precision therapy is that they lack the cellular diversity of the tumour. There is no intact stromal compartment. PDX based models for precision therapy are a bridge towards a system that recapitulates the primary tumour, in terms of the cellularity of TME. However there are important limitations to note. Over time, the stroma is gradually replaced by murine based ECM and murine fibroblasts become dominant (G. J. Yoshida, 2020). In addition disparities exist between the immune system of two different species, an example of which is that murine IL-2 is significantly less effective at stimulating human T cells when compared to human IL-2. These differences, albeit subtle in nature, may significantly impact the validity of the drug screen findings. Our decision to use patient derived cancer avatars as a foundation for our model for precision therapy was in part due to the fact that this methodology would ensure that the diversity of the TME was preserved and was incorporated into every avatar. What was unknown and yet to be determined was the stability of each component within the TME of the avatars during ex vivo culture.

5.1.1 Aims

In the following chapter, I will profile the tumoural, stromal and immune cell composition within the avatars.

5.2 Results

5.2.1 Extra Cellular Matrix composition

Of the diverse cellular ecosystem that comprises PDAC tumours, the fibrotic stroma forms the bulk of the tumour mass (Weniger et al., 2018). The stroma is predominantly composed of Extra Cellular Matrix (ECM) proteins, notably collagen (Weniger et al., 2018). A total of 28 different collagen proteins have been identified, of which collagen I is present in abundance within PDAC ECM (Ricard-Blum, 2011; Whatcott et al., 2015). The functional role of the ECM has been heavily debated; the majority of the evidence would suggest that it fosters an aggressive disease phenotype by promoting tumour cell survival and metastasis, hinders drug delivery, serves as a nutritional reservoir for tumour cells and can have immune-modulatory effects (Kamphorst et al., 2015; Martinez-Bosch et al., 2018; Weniger et al., 2018). However, variable clinical benefits have been observed within clinical trials using stromal depletion agents. Notably in the context of hedgehog inhibition, there was a paradoxical increase in tumour growth and metastasis rate, thus highlighting a potential anti-tumoural regulatory role of the stroma (Madden, 2012). The stroma

remains an essential component of the tumour microenvironment and serves as an important target for drug development. As such we wanted to assess whether our patient derived avatar model would serve as a platform to study the stroma. Therefore we had to firstly determine the stability of the stromal compartment of our PDAC avatars during ex vivo culture.

In order to identify and quantify the ECM within the patient avatars, I performed IHC with a Masson's Trichrome Stain. Staining was performed at baseline and at pre-defined time points ex vivo in order to assess trends in the stability of the compartment. PDAC avatars displayed a florid collagenous ECM stroma at baseline (Figure 5.1 A). As previously reported within the literature, we observed evidence of both loose and/or dense stroma organisation within the avatars (L. M. Wang et al., 2016)**.** After staining, all slides were scanned in order to obtain a digital image for further analysis. In order to quantify the amount of collagen ECM present within the avatars, I utilised a colour deconvolution plugin on imagej to determine the collagen area positivity of the whole avatar surface area (% positive area). At baseline, marked collagen deposition was present 58.6%. On day 12 of ex vivo culture, collagen ECM remained abundant within avatars, with no significant reduction from baseline and no variation between culture conditions ($p>0.05$). The data suggests a degree of stability for the ECM component of the avatars during ex vivo culture.

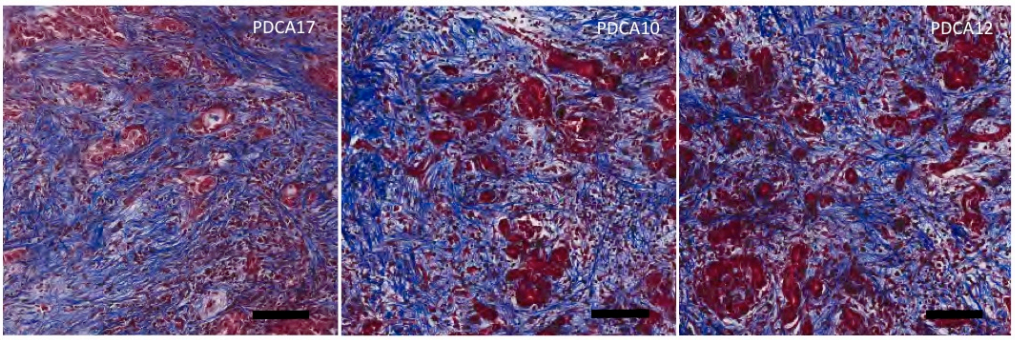

A

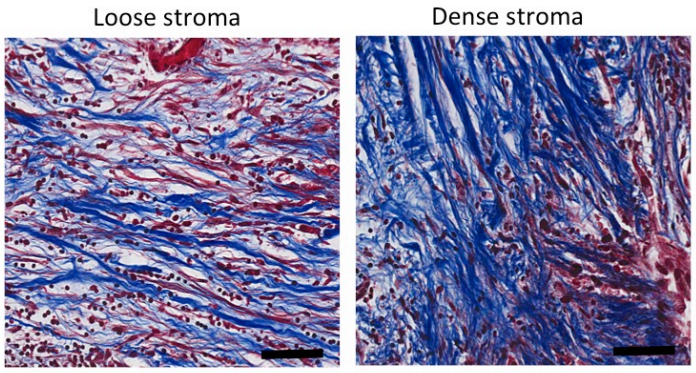

B

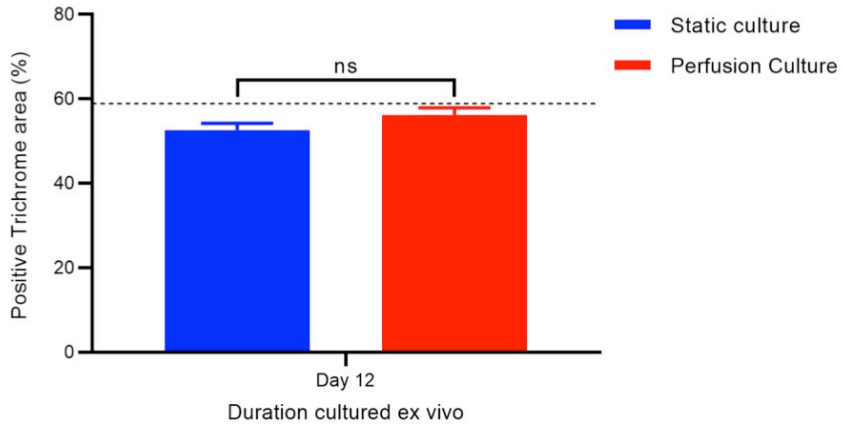

C

Figure 5. 1– Determining the stability of the Extra Cellular Matrix during ex vivo perfusion culture. (A) Representative images of Masson's Trichrome staining for collagen deposition within the Extra Cellular Matrix (ECM) of 3 different Human PDAC avatars. The blue staining denotes collagen deposition. Scale bar 100µm (n=3). (B) Representative images of the two different collagen deposition patterns observed within the PDAC avatars. (C) Quantification of the proportion of collagen in the ECM across avatars at baseline and following 12 days of ex vivo culture. The percentage positive area was calculated per high power field across the avatar. Interrupter horizontal line represents baseline value (58.6%). Data presented as mean ± SEM, statistical analysis performed by unpaired Student T test. Data

information: ns=no significance.

5.2.2 Tumoural compartment within the avatars

As the main focus of the avatar platform was to assess chemotherapeutic responsiveness, it was essential that we determined the stability of the tumour component of the avatars during ex vivo culture. An inability to maintain sufficient tumour cell volume within the avatars would render this approach to precision therapy null and void. IF staining of sequential avatars was performed in order to visualise the tumour compartment (stained with Pan Cytokeratin pCK) (Figure 5.2 A). The Indica Labs HALO® software was used to run an Artificial Intelligence (AI) algorithm through a Random Forest Classifier module in order to identify the separate sub components within the avatar. The training of the AI module allowed the identification of tumour, stroma and background glass of the slide. After running the taught AI module, the IF images were segmented into the separate compartments and a tumour mask was created (Figure 5.2 B). After obtaining the spatial information from the tumour mask, this data could be converted into numeric value and as such quantification of the tumour area was possible. Quantification of the tumour as a percentage of the full surface area (normalised to baseline) of the avatar across three different patient avatars during ex vivo culture was performed. On day 7 of ex vivo culture, no significant difference was noted between static and perfusion culture. However on day 12 ex vivo, a significant reduction in the positive tumour area (%) was observed amongst avatars

cultured under static culture conditions (p = 0.02) (Figure 5.2 C). As highlighted by the data, the tumour component of the avatars is preserved ex vivo whilst utilising perfusion culture. The current system maintains tumour cells within the avatar to day 12 ex vivo.

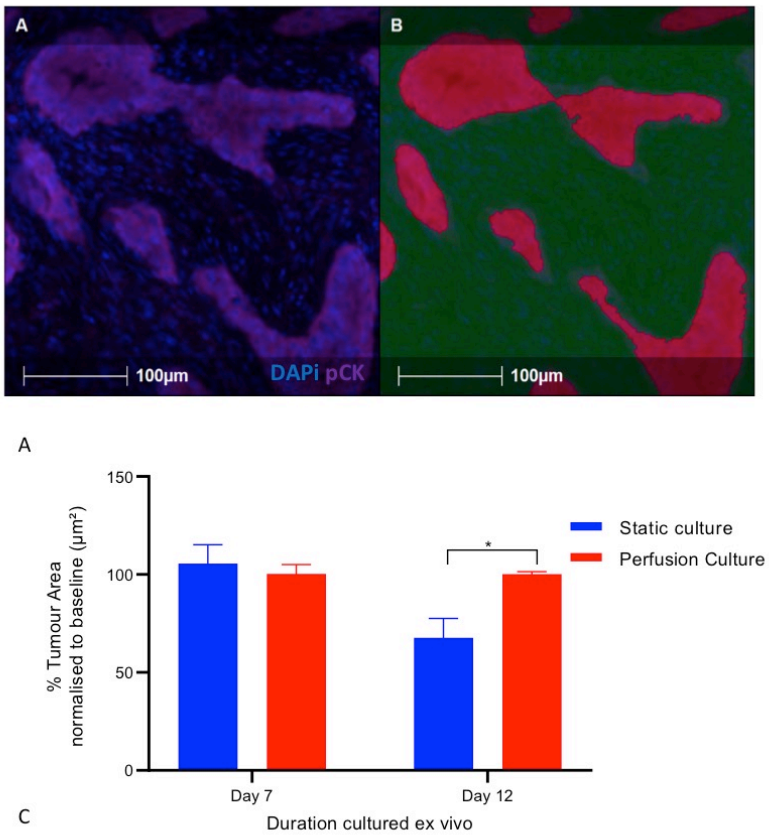

Figure 5. 2 – Profiling the stability of the tumour compartment during ex vivo culture. (A) The tumour compartment within the avatar was identified by staining for pan Cytokerratin (pCK). Representative IF image of the tumour compartment. (B) Machine based learning allows for the automated identification of the tumour compartment. A Random Forest Classifier algorithm was trained and subsequently run in order to identify the tumour compartment (defined as areas of positive pCK staining). The digital image is segmented and a tumour mask (red area) is overlaid over the original IF image (as in A). (C) Quantification of the tumour area as a percentage of the full surface area (normalised to baseline) of the avatar Data presented as mean ± SEM, statistical analysis performed by an unpaired Student T test (n=3). Data information: *p < 0.05

5.2.3 Immune infiltrate within avatars

Immuno-oncology mediates tumour cell killing through several different strategies, ranging from promoting intra-tumoural immune cell infiltration, improving neoantigen recognition and presentation, to alleviating inhibitory signals and preventing immune cell exhaustion (Marshall et al., 2018). Despite the significant impact in survival noted amongst some malignancies (notably melanoma) with immunotherapy, a lack of therapeutic effect has been observed within the cohort of patients with PDAC (Hamid et al., 2013). In 2017, the U.S. Food and Drug Administration issued licence for the use of pembrolizumab (a PD-1 immune checkpoint blocker) for PDAC (Boyiadzis et al., 2018). However, it is important to emphasise that this is only for a specific, small sub cohort of patients (advanced disease with high microsatellite instability). Additional T cell signalling pathways have also been targeted for PDAC, such as CTLA-4 checkpoint blockage, with variable results (Bengsch et al., 2017). Given the cellular diversity of the immune cell infiltrate, several other immuno-modulatory therapies have been trialled in PDAC. Myeloid-derived suppressor cells (MDSCs) are an immunosuppressive cell type that are present in abundance within the TME of PDAC. They have a pro-tumour effect and cause disease progression (Thyagarajan et al., 2019). Preliminary evidence from the scientific literature would suggest that targeting MDSCs serves as a therapeutic target (Steele et al., 2016). MDSCs upregulate C-X-C Motif Chemokine Receptor 2 (CXCR2) signalling within the TME. Inhibiting CXCR2 results in reducing PDAC metastasis rates (Steele et al., 2016). Within a KPC experiment, Steele (2016) demonstrated that selective inhibition of CXCR2 resulted in prolongation of tumour-

free survival. They also demonstrated that this inhibition improved the sensitivity to anti-PD1 therapy (Steele et al., 2016). Tumour associated macrophages (TAMs) serve as another important target for immuno-modulatory treatment. TAMs that are polarised to a M2 phenotype posses a pro-tumour effect. Treatment options include depleting TAMs within the TME or preventing additional recruitment (Poh et al., 2021). Recent focus has been drawn to developing strategies to reprogramme TAMs (from M2 to a M1 phenotype) through targeting CD40, CD11b and RIP1 (Poh et al., 2021). Regulatory T cells (Tregs) serve as another immune cell population that are responsible for an immunosuppressive effect within tumours. Selective targeting may allow for anti-tumour effect. Our current system was designed in order to evaluate the chemotherapeutic effects of treatment on the patient avatars (to mirror clinical practice with the use of systemic chemotherapy). However, with the ongoing advances with immunotherapy, it is perceivable that within the future this may be implemented into the armoury of treatment options for PDAC. As such, we wanted to evaluate the stability of the immune cell component within the patient avatars during ex vivo culture and determine whether the system could be used as a model to assess immunotherapy response.

5.2.3.1 Creation of a Mulitiplex Immunofluorescence Immune Panel

Due to the small tissue volume of the avatars and the subsequent low yield of FFPE slide creation for each avatar, it was felt that the IHC technique for immune cell identification was suboptimal. IHC would only allow for staining of a few cell markers

per FFPE slide. This subsequently would require the use of several FFPE slides to establish a picture of the immune cell infiltrate present within the avatars at each time point, thus rapidly depleting our tissue library. In order to overcome this issue, we opted to use IF staining, as this would allow for multiplexing of numerous stains per slide. We collaborated with the Oxford Translational Histopathology Laboratory, which subsequently performed a multiplex IF stain of the avatars following ex vivo culture. The immune panel used had been previously validated within a human context and provided a global overview of the immune cell infiltrate present. The panel consisted of 7 stain and covered cells from both within the lymphoid (CD4+ and CD8 + lymphocytes, regulatory t lymphocytes (Tregs) and B cells) and myeloid cell lineage (macrophages) (Figure 5.3). A tumour marker (pan-Cytokeratin) was also included in order to evaluate spatial relationships between the tumour cells and immune cell infiltrate.

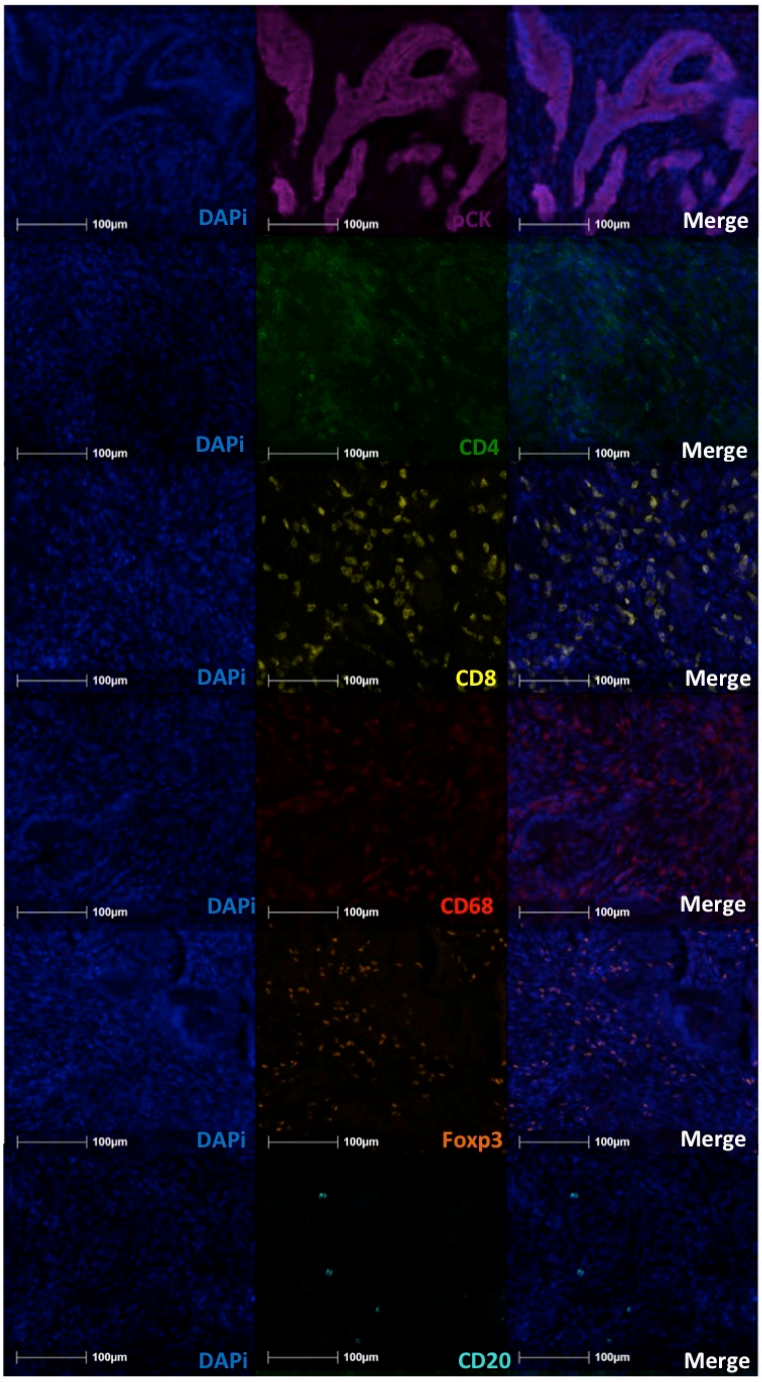

Figure 5. 3 – Creation of a Multiplex IF panel for immune profiling of patient derived cancer avatars during ex vivo culture. (A) Representative images of the 7 colour multiplex IF panel used to profile native immune infiltrate within the cancer avatars. The panel identifies immune cells from both the lymphoid (CD4+ and CD8 + lymphocytes, regulatory t lymphocytes and B cells) and myeloid cell lineage (macrophages). Tumour cells were identified by pCK staining and used for spatial reference.

The initial step was identifying individual cells of particular interest. This was achieved through using the Indica Labs predesigned algorithm - High Plex FL v3.2.1. In summary the algorithm is taught which features should be utilised to define the cell phenotype of interest (presence of nuclear, cytoplasmic and/or membranous expression against predefined thresholds) as highlighted in Figure 5.4. After training, the algorithm can then self run and analyse the entire slide. The raw image is segmented into a binary automated illustration depicting the cells present. Cells that meet the criteria of the specific phenotype are outlined in yellow (Figure 5.4 D). This automated cell image can be subsequently translated into a numeric value and therefore provide a numeric readout count of the cells present that are of the predefined phenotype.

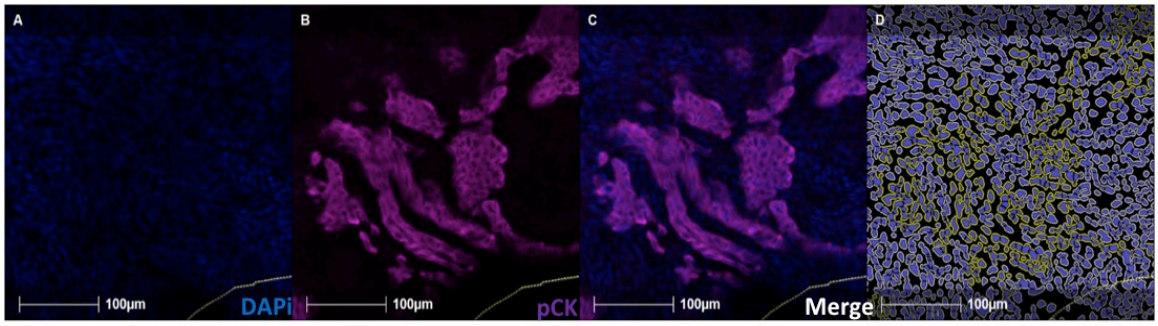

Figure 5. 4 – Machine based learning enables the identification of distinct cell phenotypes. (A,B,C) Overview of the machine based learning process. The algorithm is taught the defining characteristics of the cell phenotype of interest. Within this example the cell of interest is a tumour cell. The tumour cell phenotype is defined by positive nuclear DAPi staining combined with cytoplasmic pCK staining. (D) Once the algorithm has been optimised and thresholds set, automated detection of cells is performed. The image is subsequently segmented and individual cells are defined. Those cells that meet the predefined criteria of the phenotype of interest are successively identified by a yellow outline. It is then possible to convert the segmented image into a numeric value and produce a cell count.

5.2.3.2 Avatar immune infiltrate at baseline

The previously described method was used to phenotype specific immune infiltrate of interest. Across three different patient avatars, we observed significant variation with the native immune cell infiltration into the avatars at baseline. This time point is defined as the day of the resection i.e. day 0. Avatars were fixed in formalin within 3 hours of acquisition. The most abundant immune cell infiltrate within all three avatars were macrophages (CD68+). Two different phenotypes were observed with regard to lymphocyte infiltration: two avatars (PDCA10 and PDCA13) displayed low infiltrate numbers, whereas one avatar (PDCA12) had much higher numbers of infiltrating lymphocytes at baseline.

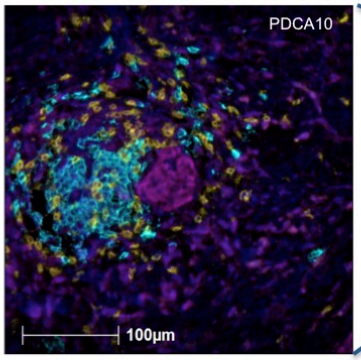

Cell phenotype	% Positive cells (all) (Baseline)
CD4 +	4.1
CD8 +	3.4
Tregs (CD4 + Foxp3 +)	0.2
Macrophages (CD68+)	15.8
B Cells (CD20 +)	0.9

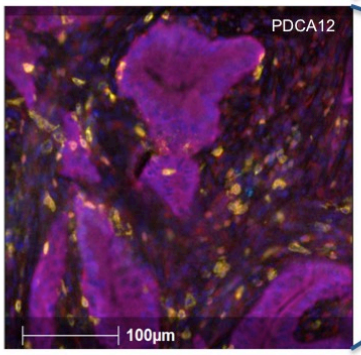

Cell phenotype	% Positive cells (all) (Baseline)
CD4 +	16.0
CD8 +	10.1
Tregs (CD4 + Foxp3 +)	3.2
Macrophages (CD68+)	44.7
B Cells (CD20 +)	2.4

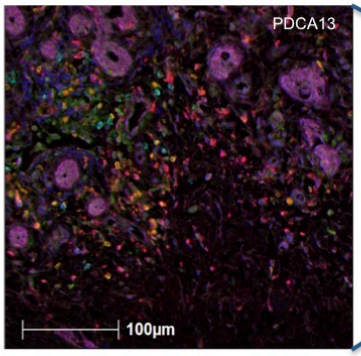

Cell phenotype	% Positive cells (all) (Baseline)
CD4 +	7.6
CD8 +	0.7
Tregs (CD4 + Foxp3 +)	2.8
Macrophages (CD68+)	18.7
B Cells (CD20 +)	3.0

Figure 5. 5- Immune profiling of patient derived pancreatic cancer avatars. Multiplex IF panel staining of native immune cell infiltrate present within patient derived cancer avatars at baseline (Day 0, within 3 hours of resection). Profiling of immune cells performed in three different patients (PDCA10, PDCA12 and PDCA13). Individual cell phenotype were defined and subsequently quantified. Cell count presented as % positive of all DAPi positive cells within avatar

5.2.3.3 Spatial analysis of immune infiltrate within the avatars

In order to establish a better understanding of the spatial relationship of the immune infiltrate within the avatars, a spatial analysis was performed using the pre automated nearest neighbour algorithm. The immune cell phenotypes were

predefined and the tumour cells were selected as the cells of reference. Therefore the algorithm would measure the distance from the cell phenotype of interest (immune cell) to the nearest cell of reference (tumour cell). The work through of the analysis is highlighted in Figure 5.6 A,B,C. Once the phenotypes are defined, the image is segmented into a binary two cell colour image (cell of interest and cell of reference) which serves as the basis for the measurement assessment (Figure 5.6 A,B,C). Across the three patient avatars at baseline, the macrophages (CD68+) were the immune cells that were within the closest distance to the tumour cells (19.8 – 30.3 um). This correlates with the previous data, Figure 5.5, given that the macrophages were the most abundant immune cell infiltrate within these tumours. An interesting observation was that the native B cells (CD20+) present in the avatars were either in close proximity to the tumour cells (as in PDCA13) or at a marked distance away (as in the case of PDCA10 and PDCA12) from the tumour cells. Emerging evidence within the literature would suggest that infiltrating B cells serve as a prognostic marker for long-term survival for patients with PDAC (Brunner et al., 2020). We also observed the same relationship with the native Tregs (CD4+ Foxp3+) within the avatars. Two patient avatars (PDCA12 and PDCA13) displayed very close proximity of the Tregs to the tumour cells, within 62 um. However the remaining avatar of PDCA10 had over a fourfold increase in the average distance between Tregs and tumour cells (253.8 um). Given this heterogeneity in immune cell infiltrate numbers and spatial relationship across avatars, this may serve as a possible explanation for the different survival outcomes observed, in particular the very small cohort of long-term survivors.

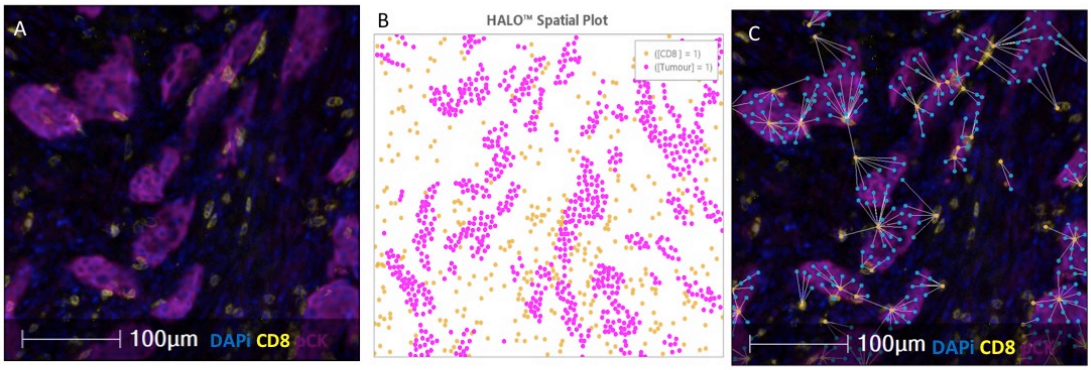

D

PDCA10

Cell phenotype	Average Distance to Tumour cell (um)
CD4 +	78.0
CD8 +	77.7
Tregs (CD4 + Foxp3 +)	253.8
Macrophages (CD68+)	30.3
B Cells (CD20 +)	294.5

PDCA12

Cell phenotype	Average Distance to Tumour cell (um)
CD4 +	37.9
CD8 +	31.8
Tregs (CD4 + Foxp3 +)	61.9
Macrophages (CD68+)	13.8
B Cells (CD20 +)	251.7

PDCA13

Cell phenotype	Average Distance to Tumour cell (um)
CD4 +	32.5
CD8 +	97.0
Tregs (CD4 + Foxp3 +)	53.1
Macrophages (CD68+)	19.8
B Cells (CD20 +)	60.1

Figure 5. 6- Evaluating the spatial relationship between immune cell phenotypes and the tumour cells within patient derived cancer avatars. (A, B, C) Overview of the machine based learning process for the nearest neighbour proximity analysis algorithm. A cell of reference was selected in addition to a cell of interest in order to calculate spatial proximity. The average distance between every cell of reference and its closest cell of interest is computed (A) Representative IF image of tumour cells stained with pCK (cell of reference) and C8+ lymphocytes (cell of interest) within this example. (B) Automated run of the machine based learning algorithm results in segmentation of the image into a binary 2 colour image spatial plot. The pink dots correspond to tumour cells and yellow to CD8+ lymphocytes. (C) Nearest neighbour distance measurements, presented as networks, superimposed over original IF

image. (D) Quantification of the spatial relationship between native immune infiltrate and tumour cells at baseline (Day 0) performed in three different patients (PDCA10, PDCA12 and PDCA13). Data presented as average distance to tumour cell (um).

Whilst the nearest neighbour algorithm provides useful information regarding the proximity of the immune cells to the tumour cells within the avatar, it does not provide specific spatial information such as the proportion of immune infiltrate that is intratumoural or peritumoural. Being able to identify and define the aforementioned parameters is crucial in the context of immunotherapy, especially where the drug mechanism is to promote immune infiltrate into the tumours. One could subsequently analyse avatars both pre and post treatment to determine whether a therapeutic effect is noted. We investigated as to whether it was possible to determine and measure this spatial relationship with our multiplex IF panel. The initial step was creating a predefined tumour mask that allowed segmentation of the image and identification of the tumour components across the avatar (as per the method described in Figure 5.2). Once the tumour mask was established, two annotation interfaces (50 um each) were created within each tumour mask (Figure 5.7). One interface layer was defined as the intratumoural area (identified per the yellow coloured zone (measurements -15 to 0 um of the interface)), whereas the remaining interface layer was defined as the peritumoural area (represented by the light blue coloured zone (measurements 0 to 15 um of the interface)). Through using the described method above, we were able to directly quantify the spatial relationship. Across the three patient avatars at baseline, we observed variation with the intratumoural immune cell infiltrate. PDCA12 avatar at baseline displayed the highest proportion of infiltrating CD4+ and CD8+ lymphocytes in the

intratumoural area (-15 to 0 um of the interface) when compared to PDCA10 and PDCA13. It was observed that PDCA13 avatar had the greatest proportion of intratumoural Tregs (CD4 + Foxp3 +) in comparison to PDCA10 and PDCA12. All three avatars shared one common finding, that the vast majority of the macrophages present were located in the peritumoural stroma regions. This may provide further insight into the immunosuppressive role of the stroma within PDAC. Despite B cells (CD20+) being the least frequent immune cell infiltrate, 2 avatars displayed a similar pattern with higher rates of B cells (CD20+) within the peritumoral stroma regions (PDCA10 and PDCA12), whereas the remaining avatar (PDCA13) had a much higher B cells (CD20+) presence within the tumour.

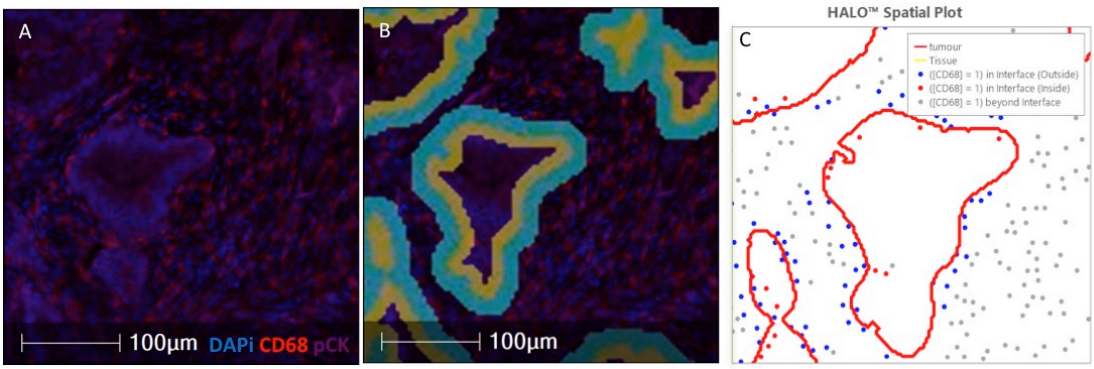

D

PDCA10

Cell phenotype	Immune cell count within Intratumoural annotation area (-15 to 0 um of interface)	Immune cell count within Peritumoural annotation area (0 to 15 um of interface)
CD4 +	425	550
CD8 +	106	380
Tregs (CD4 + Foxp3 +)	10	21
Macrophages (CD68+)	848	1656
B Cells (CD20 +)	12	46

PDCA12

Cell phenotype	Immune cell count within Intratumoural annotation area (-15 to 0 um of interface)	Immune cell count within Peritumoural annotation area (0 to 15 um of interface)
CD4 +	2280	2688
CD8 +	1021	1750
Tregs (CD4 + Foxp3 +)	420	534
Macrophages (CD68+)	2977	7698
B Cells (CD20 +)	257	278

PDCA13

Cell phenotype	Immune cell count within Intratumoural annotation area (-15 to 0 um of interface)	Immune cell count within Peritumoural annotation area (0 to 15 um of interface)
CD4 +	1031	267
CD8 +	30	39
Tregs (CD4 + Foxp3 +)	460	53
Macrophages (CD68+)	845	1841
B Cells (CD20 +)	347	12

Figure 5. 7 – Mapping immune cell infiltrate within pancreatic cancer avatars. (A, B, C) Overview of the machine based learning process for immune cell infiltration analysis. Within this example, CD68+ Macrophages were mapped in order to determine infiltration into the tumour compartment. (A) Representative IF image of tumour cells stained with pCK and CD68+ Macrophages. (B) A tumour mask is applied to the raw image. Two annotation interfaces (both measuring 50 um each) were created within each tumour mask. One interface layer was defined as the intratumoural area (identified per the yellow coloured zone) , whereas the remaining

interface layer was defined as the peritumoural stromal area (represented by the light blue coloured zone). (C) Automated run of the machine based learning algorithm for invasion analysis results in segmentation of the image into a three colour image spatial plot. The red cells correspond to CD68+ cells within the intratumoural annotation area, blue cells corresponds to CD68+ cells within the peritumoural annotation area and the grey cells are representative of cells outside of both annotated layer thresholds. (D) Quantification of the immune cell infiltrate within the intratumoural and peritumoural area at baseline (Day 0) performed in three different patients (PDCA10, PDCA12 and PDCA13). Data presented as total cell count within each annotated area.

5.2.3.4 Determining the stability of the immune infiltrate within avatars during ex vivo culture

Our initial analysis of the native immune cell infiltrate with our multiplex IF panel confirmed the presence of and our ability to detect immune cell subpopulations at baseline (day 0) within the avatars. The subsequent analysis that we needed to perform was to determine the stability of the immune component within the avatars during ex vivo culture, specifically whether we were maintaining the native immune populations during the time course of the experiment. In order to address this question, immune cell profiling was performed with the multiplex IF panel on avatars after 12 days of ex vivo culture. Avatars were cultured either under static or perfusions conditions in order to evaluate the effect of the culturing technique on the stability of the immune cell subpopulation within the avatars. Upon analysing the multiplex IF of the avatars on day 12 ex vivo, it was noted that the immune cell infiltrate remained detectable across all three patient avatars (Table 5.1). After quantification, it was clear that no individual cell phenotype was lost in its entirety from within the avatars on day 12 ex vivo. In addition there was no significant

outgrowth/over proliferation of one specific immune cell subtype following ex vivo culture. Through comparing the avatars on day 12 that were cultured in static or perfusion conditions, it would appear that the avatars that were maintained in perfusion culture were more representative of the baseline samples based upon the raw numeric values of the immune cell infiltrate present.

Cell phenotype	PDCA10		
	Baseline (% Positive cells/all)	D12 static (% Positive cells/all)	D12 perfusion (% Positive cells/all)
CD4 +	4.1	1.5	5.6
CD8 +	3.4	1.9	8.4
Tregs (CD4 + Foxp3 +)	0.2	0.8	0.9
Macrophages (CD68+)	15.8	17.0	18.4
B Cells (CD20 +)	0.9	0.38	1.0

Cell phenotype	PDCA12		
	Baseline (% Positive cells/all)	D12 static (% Positive cells/all)	D12 perfusion (% Positive cells/all)
CD4 +	16.0	9.8	13.1
CD8 +	10.1	3.0	9.1
Tregs (CD4 + Foxp3 +)	3.2	0.2	1.4
Macrophages (CD68+)	44.7	39.5	38.6
B Cells (CD20 +)	2.4	0.1	0.9

Cell phenotype	PDCA13		
	Baseline (% Positive cells/all)	D12 static (% Positive cells/all)	D12 perfusion (% Positive cells/all)
CD4 +	7.6	2.3	9.9
CD8 +	0.7	1.6	5.0
Tregs (CD4 + Foxp3 +)	2.8	0.72	2.0
Macrophages (CD68+)	18.7	11.7	12.7
B Cells (CD20 +)	3.0	0.6	0.6

Table 5. 1 - Determining the stability of the avatar immune component during ex vivo culture. A comparison of the total native immune cell infiltrate present within patient derived cancer avatars at baseline and at day 12 ex vivo following static or perfusion culture. Profiling of immune cells performed in three different patients

(PDCA10, PDCA12 and PDCA13). Individual cell phenotype were defined and subsequently quantified. Cell count presented as % positive of all DAPi positive cells within avatar

In order to determine whether one particular immune cell subtype was more sensitive to its culturing conditions compared to its counterparts, a formal comparison between the day 12 avatars immune infiltrate was performed (Figure 5.8). Immune infiltrate was normalised to the baseline values of each corresponding avatar and subsequently pooled. On day 12, a statistical reduction in the CD4+ cells present in static culture was noted ($p = 0.02$). A trend of a reduction in CD8+ cells in static culture was also observed, albeit not statistically significant ($p= 0.057$). No statistically significant difference was noted amongst the other immune cell phenotypes on day 12 of ex vivo culture.

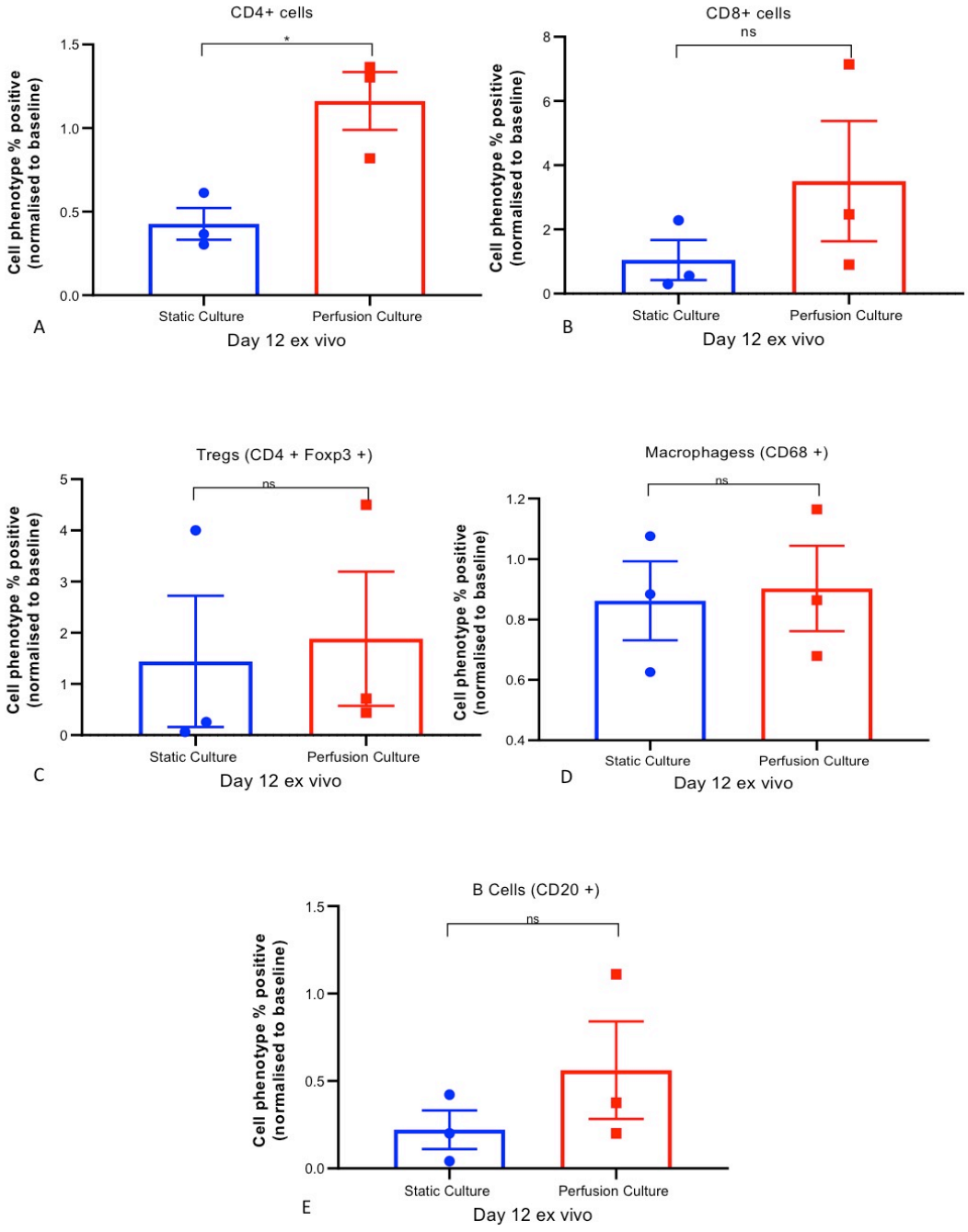

Figure 5. 8 – Stability of immune cell infiltrate during perfusion culture. (A) Quantification of CD4+ cells on day 12 ex vivo following perfusion or static culture. Data presented as % positive of cell phenotype normalised to baseline. (B) as in (A) Quantification of CD8+ cells. (C) As in (A) Quantification of Tregs cells. (D) As in (A) Quantification of CD68+ cells. (E) As in (A) Quantification of CD20+ cells. Statistical analysis performed by an unpaired Student T test (n=3). Data information: *p < 0.05, ns = non significant.

To evaluate whether the spatial relationship between the immune cell infiltrate and tumour cells change over the time course of ex vivo culture, the nearest neighbour algorithm was run on the day 12 avatars under perfusion conditions ex vivo (Table 5.2). Across the three patient avatars, it was noted that the CD4+ and CD8+ lymphocytes displayed a trend of migrating towards the tumour cells during the course of ex vivo culture. One patient avatar showed a migration of the B cells (CD20+) towards the tumour cells (PDCA10), whereas the opposite trend was noted amongst the remaining 2 avatars (PDCA12 and PDCA13). Very little variation was noted across the three avatars with regard to the movement of macrophages during ex vivo culture.

	PDCA10	
	Baseline	Day 12 Perfusion
Cell phenotype	Average Distance to Tumour cell (um)	Average Distance to Tumour cell (um)
CD4 +	78.0	75.6
CD8 +	77.7	50.1
Tregs (CD4 + Foxp3 +)	253.8	153.4
Macrophages (CD68+)	30.3	24.5
B Cells (CD20 +)	294.5	184.7

	PDCA12	
	Baseline	Day 12 Perfusion
Cell phenotype	Average Distance to Tumour cell (um)	Average Distance to Tumour cell (um)
CD4 +	37.9	18.2
CD8 +	31.8	29.2
Tregs (CD4 + Foxp3 +)	61.9	57
Macrophages (CD68+)	13.8	13.6
B Cells (CD20 +)	251.7	327

	PDCA13	
	Baseline	Day 12 Perfusion
Cell phenotype	Average Distance to Tumour cell (um)	Average Distance to Tumour cell (um)
CD4 +	32.5	20.1
CD8 +	97.0	38.0
Tregs (CD4 + Foxp3 +)	53.1	63.7
Macrophages (CD68+)	19.8	27.2
B Cells (CD20 +)	60.1	164.2

Table 5. 2- Monitoring the spatial relationship between immune cell phenotypes and the tumour cells during ex vivo perfusion culture. A comparison of the spatial relationship between native immune infiltrate and tumour cells at baseline (Day 0) and day 12 day of ex vivo culture performed in three different patients (PDCA10, PDCA12 and PDCA13). Data presented as average distance to tumour cell (um).

5.3 Discussion

Within this chapter, a comprehensive interrogation of the cellular composition of the avatars was performed using a variety of methods. Avatars were analysed at different time points ex vivo in order to determine the stability of each compartment. Perfusion culture may serve as a superior technique for culturing cancer avatars, especially given the statistically significant reduction in the tumour area that was noted with static culture technique following ex vivo culture. Our analysis illustrates that within our current system, on day 12 ex vivo, the cellular diversity of the avatars is preserved. There is no complete loss of any specific avatar cellular compartment. Immune infiltrate remains present and is quantifiable to day 12 ex vivo. Therefore a degree of stability is observed within the avatar cellular sub compartments through using our current method of ex vivo avatar culture. This provides further validation of our approach to avatar maintenance and their use for precision therapy. In addition, confidence is gained that when administering therapy (be that chemotherapy or immunotherapy) , it will be possible to assess and determine the effect of the treatment strategy not only on the tumour cells but rather on the diverse cellular composition of PDAC.

Our previous experience of maintaining the avatars ex vivo highlighted the detectable change in the integrity of the avatars on day 12 ex vivo following static culture. A higher tissue fragmentation rate and a reduction in avatar surface area were noted. I wanted to determine whether an underlying biological mechanism was driving this change in the mechanical strength of the avatars. One possible mechanism proposed is that of the loss of the ECM within the avatars which subsequently contributes to a structural weakness. However, upon quantifying the

amount of collagen within the avatars following ex vivo culture, there was no statistical difference in the proportion of collagen present between baseline and day 12 ex vivo irrespective of culture conditions (Figure 5.1). It should therefore be considered that the amount of ECM present is not responsible for structural integrity, rather it is the composition of the ECM. The stroma of PDAC is heterogenous in nature. Wang, et al (2016) illustrated that stromal density varied across patients with PDAC and concluded that three different stromal deposition patterns were observed: loose, moderate and dense stroma organisation (L. M. Wang et al., 2016). However the stroma organisation was not just a histological phenomenon, it directly correlated with survival rates and served as a prognostic measure (L. M. Wang et al., 2016). It is possible that the collagen deposition of the avatars alters during ex vivo culture, changing from a high density stroma (characterised by mature collagen fibres in numerous layers interlinked by keloid collagen bands) to a loose stroma organisation (smaller and finer collagen fibres). Another factor to consider is that the Masson's Trichrome stain stains all connective tissue. It does not preferentially stain one specific type of collagen over another. Therefore it may be possible that a specific type of collagen within the ECM of the avatars is lost during ex vivo culture and that the loss is masked as the total collagen content is stained. In addition, the ECM is composed of several other components (glycosaminoglycans , hyaluronic acid etc) which would not be stained routinely by the Masson's Trichrome stain. Therefore significant changes within these polysaccharides during ex vivo culture may not be identified upon staining and these may be responsible for the change in structural integrity (Frantz et al., 2010).

Profiling the avatars at baseline has provided an invaluable insight into the immune infiltrate present within PDAC. The immune infiltrate is diverse and there is significant heterogeneity across patient tumours. We noted that macrophages (CD68+) were the most abundant immune cell infiltrate within all three patient avatars. Our findings correlate with the wider literature regarding native immune cells within pancreatic tumours. An interesting paper published by Blando, et al (2019) compared the immune infiltrate present between PDAC and melanoma tumours (Blando et al., 2019). They also described that macrophages (CD68+) were the most frequent immune cell subtype present within PDAC (Blando et al., 2019). They noted a significant reduction in infiltrating CD3, CD4 and CD8 lymphocytes within pancreatic tumours when compared to melanoma tumours (Blando et al., 2019). We also observed relatively low numbers of CD4+ and CD8+ lymphocytes within our PDAC avatars. The authors subsequently performed a spatial analysis and concluded that the macrophages were statistically at much higher density within the stromal compartment when compared to the tumour. (Blando et al., 2019), The same phenomenon was observed within our avatars. The total amount of T cell infiltration into PDAC tumours has been correlated with survival (high infiltrate associated with prolonged survival) (Karamitopoulou, 2019). However, it would appear that another important factor for prognosis is not purely the amount of infiltrating lymphocytes present, rather their spatial positioning in relation to the tumour (Carstens et al., 2017; Masugi et al., 2019). Masugi , et al (2019) demonstrated that patients with a high CD8+ density within the tumoural compartment had a significantly greater survival outcome (Masugi et al., 2019). Within our avatars, we observed the majority of the infiltrating CD8+ cells within the

peritumoural stroma rather than within the tumour compartment. A similar trend with infiltrating CD4+ lymphocytes was noted, however one patient's avatar displayed the opposite trend with a high proportion of intratumoural CD4+ lymphocyte infiltrate when compared to the stroma. In light of the heterogeneity and the cellular diversity of immune infiltrate within the PDAC avatars, one could propose that different immunotherapy treatment strategies should be implemented for each patient instead of a standardised one treatment for all approach. For example in the context of a patient with a high intratumoural immune infiltrate , therapies should be tailored toward overcoming local check point immune blockage and preventing immune cell exhaustion.

The multiplex IF panel used in the analysis undoubtedly provided us with an excellent opportunity to interrogate the cellular composition of the avatars in detail. However there are some limitations to the panel that should be highlighted. The panel itself only comprises seven fluorophores, one of which is reserved for DAPi nuclear staining. As such only six cell phenotypes can be identified consecutively. Larger multiplex panels have been reported within the literature which subsequently allow cellular profiling on a broader spectrum (Tan et al., 2020). However, for our own specific research requirements, being able to obtain a global overview of the common immune infiltrates present within the tumours, we felt that the current panel was sufficient. It is likely that the panel would require further modifications if immune profiling was being performed with the intention of obtaining an in-depth understanding of a single immune cell phenotype. Emerging evidence within the field of immuno-oncology has illustrated that Tumour Associated Macrophages

(TAMs) play a key role with regard to creating an immunosuppressive microenvironment and metastatic dissemination of the disease (Yang et al., 2020). Under the influence of external stimuli (such as cytokines, exosomes, metabolic factors etc), TAMs can be polarised into a M1 or M2 phenotype, with the latter being associated with disease progression (Yang et al., 2020). With the current panel, we are only able to identify all macrophages present within the avatar. We are unable to differentiate and distinguish between the two polarised phenotypes. Through altering the panel and including markers such as CD80+ and CD206+ it would be possible to identify and quantify both phenotypes of TAMs within the avatars (Bertani et al., 2017; Yang et al., 2020). The difficult decision is determining how to alter the equilibrium between the breadth of the screen and being able to profile in greater depth into phenotype identification. Through using the current panel, we have been able to confirm the presence of 5 different immune cell populations present on day 12 of ex vivo culture within the avatars. However, what the panel does not provide is any information regarding the functional status of these immune cells. As such, it is not possible to determine whether these immune cells continue to function or if they display characteristics of an exhausted immune cell phenotype. Incorporating functional markers within the multiplex panel (such as TIGIT (T cell immunoreceptor with Ig and ITIM domains)) would allow a functional assessment on day 12 ex vivo.

Our initial analysis of how the spatial relationship between the immune infiltrate and tumour cells changed during the time course of ex vivo culture, suggested a migration of lymphocytes (CD8+ in particular) towards the tumour. This may

represent tumour engagement with subsequent infiltration of native immune cells. Changes to the absolute immune cell numbers present on day 12 ex vivo may be indicative of selective destruction/elimination of regulatory cells by engaged and activated lymphocytes. An important confounding factor to address when assessing spatial relationships of the immune cells during ex vivo culture is that of the possible effect of tissue slice variation. Whilst all avatars are derived from a single core biopsy of the patient's primary tumour, each individual avatar represent a different tissue slice from within the core biopsy. What is challenging to ascertain is how much heterogeneity exists between different tissue slices. This represents the main limitation of our current model for delivering precision therapy; the possibility of variation across all avatars. The avatars are consecutive tissue slices and are only 250 um thick which may reduce the heterogeneity. Care is therefore needed when interpreting changes in the spatial positioning of the immune cells during ex vivo culture. What is difficult to determine is whether the observed movement of immune infiltrate is representative of actual cell migration and invasion through the tissue or whether it is a perceived phenomenon secondary to tissue slice variability. What is needed to overcome this uncertainty is incorporating live cell imaging within the system. Being able to identify and track immune cell movement in real time would provide evidence that detectable spatial differences were due to active cell migration rather than spatial differences between tissue slices. Such an approach has previously been described in an in vivo murine lung cancer model that assessed the interaction between immune infiltrate and the tumour (Hanna et al., 2016). In addition, being able to fluorescently label specific immune cells would provide further clarity on cell migration patterns and tumour infiltration. Determining how

the current system could function with concurrent live cell imaging should serve as a foundation reference point for future work. This would be crucial, especially in the context of immunomodulatory therapy, where there is a clear need to be able to have spatial movement data on a single cell level within the avatars.

Within the previous chapters, the role of perfusion culture has been explored. Our current perfusion system model not only maintains the functionality within the avatars but also retains the native cell populations present during the time course of ex vivo culture. In light of this stability, patient derived avatars represent a unique opportunity to study the primary tumour in the ex vivo setting. What has yet to be determined is whether the platform can be altered in order to facilitate drug delivery and whether a therapeutic response to chemotherapy can be detected within the avatars.

Chapter 6

Evaluating patient derived pancreatic cancer avatars as a model for precision therapy

The work within the previous chapters illustrates that within our current avatar model and perfusion culture system we are able to maintain functionality of the avatars ex vivo. This data demonstrates that the cellular composition within each individual compartment of the avatar remains relatively stable during the time course of ex vivo culture. As such, we have avatars that retain the cellular diversity of the primary tumour. Therefore, when conducting a drug screen, it will be possible to determine the effect of the drug on the multiple components of the TME. Within this chapter it will be determined whether the perfusion system can be utilised for drug delivery and whether a therapeutic response of drug efficacy can be detected within the avatars. The avatar response will be correlated with patient outcomes in order to validate cancer avatars as a method for delivering precision therapy.

6.1 Systemic therapy for PDAC

Over the last two decades, the management of PDAC has evolved significantly. Where the biggest change has been observed is in our ability to deliver effective systemic therapy for our patients. Gemcitabine has been the foundation of systemic therapy since it was approved in 1997 (Thota et al., 2014). Approval was granted following the publication of a trial result where symptomatic patients with advanced disease were allocated to either Gemcitabine monotherapy or Fluorouracil (5-FU) (Burris et al., 1997). Despite the trial being initially structured to assess for symptomatic benefit (the primary outcome measures were pain control, weight gain and performance status), it actually highlighted a survival benefit (Burris et al., 1997). A further example of the significant impact of systemic therapy on survival was published in 2011. The same cohort of patients as selected by Burris et al in 1997 (advanced disease with metastases), were randomised by the PRODIGE group to receive either standard of care (Gemcitabine) or combination multi-agent chemotherapy (FOLFIRINOX) (Conroy et al., 2011). What was observed was a significant doubling of the median overall survival with combination therapy (11.1 months vs 6.8 months, $p < 0.001$) and the overall survival rate at 12 months (48.4% vs 20.6%) (Conroy et al., 2011). This survival benefit has now also been witnessed in a cohort of patients with resectable disease (Conroy et al., 2018). A significant rate of serious adverse side effects is observed with combination chemotherapy use.

The response rate to chemotherapy differs significantly between patients. An interesting study by He et al. 2018, assessed the relationship between treatment response (in the context of complete pathological response and Neo-Adjuvant

therapy) and overall survival rates (He et al., 2018). They noted that patients who had a complete pathological response to Neo-Adjuvant therapy had a significantly longer overall survival when compared to patients with no response (He et al., 2018). However, the most striking finding of the study was that when comparing outcomes of patients with a limited response to therapy, their overall survival trajectory closely mimicked that of patients with no response and no survival benefit was noted (He et al., 2018). This illustrates that the survival benefit only occurred when patients fully responded to their treatment (instead of a partial response), thus highlighting the importance of selecting the correct systemic therapy for each patient.

In light of the variation in response rates to systemic therapy, patients will have significantly different outcomes. The mechanisms that underpin this variation in treatment response are vast. They include intrinsic intracellular mechanisms (such as alteration in transport protein expression, epigenetic control over gene transcription and microRNA influence) and the effect of the TME (Swayden et al., 2018). Within current clinical practice, there is a predefined approach to systemic therapy in PDAC. This is based upon the patients' general level of fitness and co-morbidity profile (NICE, 2018). Such a generic approach to systemic therapy for PDAC fails to acknowledge the significant diversity across tumours and the variability in treatment response rates. The individual tumour biology is neglected and is not utilised for patient stratification for treatment. What is needed, is a paradigm shift in the manner in which we address PDAC, moving away from the preconceived idea that all PDACs are the same and as such should be treated as one disease, to acknowledging

the heterogeneity that exists and the fact that no two tumours are identical in nature. A hybrid approach where performance status is considered alongside tumour biology is necessary. Precision therapy enables the use of previously generated data on therapeutic responsiveness to be incorporated and utilised in the treatment algorithm when selecting systemic therapy for PDAC. Such an approach will impact on survival outcomes.

6.1.1 Aims

The aim of this chapter is to determine whether drug delivery is possible within our perfusion system. I also intend to correlate the responses observed within the patient derived cancer avatars following treatment with that of the clinical outcomes of the same patient from which the avatar was derived. Such an approach will determine whether both patient and avatar share the same chemotherapeutic susceptibility and thus validate the use of patient derived cancer avatars as a method to deliver personalised therapy for patients with pancreatic cancer.

6.2 Results

6.2.1 Drug delivery

In order to be able to conduct a drug screen within our system, we firstly had to determine a route for drug delivery. I initially thought of using the inflow reservoir as

a location for drug loading and subsequently have normal media perfused through the reservoir to carry the drug into the perfusion plate. However, I noted that the volume of the reservoir is much smaller than that of the culturing well and as such the preparation of the drug would need to be concentrated and in a minimal volume. After trialling different methods, it was felt that the most ergonomic approach was diluting the drug in the culture media and storing it within the inflow syringe. Such an approach is not constrained by volume and allows precise measurement of drug volume delivery. When treatment was scheduled to finish, I would subsequently disconnect the inflow syringe and tubing and replace it with a fresh syringe and inflow tubing containing media alone to allow the circulation and removal of the drug from the perfusion plate. We utilised Gemcitabine monotherapy for the treatment of the avatars ex vivo. The treatment strategy is illustrated in Figure 6.1. A Gemcitabine dose of 0.25 mM was used for treatment within these experiments. This dose was calculated based on the pre-existing literature on Gemcitabine treatment of PDAC tumours and also incorporating the total media volume of the well (Koay et al., 2014). A single treatment dose was used instead of serial dosing in order to demonstrate as proof of principle that ex vivo perfusion treatment of avatars was possible. The time points for analysis were selected based on the previous data generated in chapter 4. I had previously demonstrated that under static culture conditions a statistically significant reduction in cellular proliferation and an increase in cellular apoptosis rates occurred on day 5 of ex vivo culture. However, under perfusion culture a degree of stability in proliferation rates was observed between day 3 and day 7 of culture. I selected day 3 of ex vivo culture for the first time point for analysis, as this would have permitted sufficient time for

nuclear incorporation of Gemcitabine into the DNA with subsequent time for cellular replication in order to have a therapeutic effect. To determine whether there was a sustained response to therapy, I selected a further time point at which avatars were extracted and subsequently analysed for a response (day 6 of ex vivo culture).

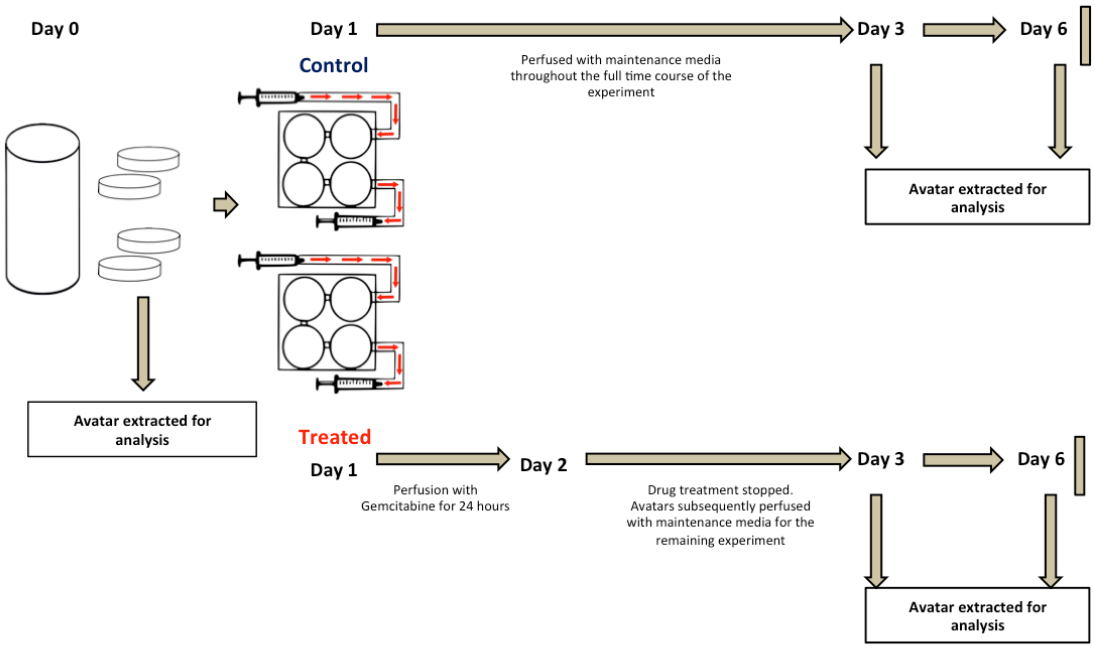

Figure 6. 1 - Illustration of ex vivo treatment of cancer avatars experiment design. Visual representation of the protocol for ex vivo treatment of cancer avatars. Day 0 is the day of surgical resection and subsequent tissue acquisition. Avatars are created within 3 hours following resection of the primary tumour. Some avatars are extracted immediately for baseline analysis (IHC and RNA extraction). The remaining avatars are either treated or serve as control. The treated avatars are subsequently treated with 24 hours of Gemcitabine perfusion ex vivo. After 24 hours, a new inflow circuit (comprised of media alone) is connected to the perfusion system and will deliver culturing media for the remainder of the experiment. The control group of avatars are perfused with media alone for the full time course of the experiment. Avatars are extracted on day 3 and day 6 for analysis to determine whether a therapeutic response is noted.

6.2.2 Ex vivo treatment of patient derived cancer avatars

The first patient derived cancer avatar that was treated with ex vivo chemotherapy (PDCA14) was obtained from a patient who underwent a Whipple procedure for a pT2 N2 (5/18) M0 R0 L1 V0 tumour. As per the experiment design, the avatars were treated ex vivo with Gemcitabine for 24 hours followed by continuous perfusion of media alone until the predefined experimental end point. Avatars were extracted at day 3 and day 6 for histological analysis of treatment response.

In order to gain a further insight into whether PDCA14 avatars were sensitive to Gemcitabine monotherapy, I performed IHC staining for Ki67 positive cells to assess the avatar proliferation index. The rationale for this approach is that Gemcitabine sensitive tumours will be vulnerable to the cytotoxic effect of the drug and as such cell replication rates will be directly affected. At the baseline time point, PDCA14 was noted to be a highly proliferative tumour (avatar proliferation index of 64.7%). However a significant reduction in the proliferation index was observed on day 3 ex vivo when comparing the treated and non treated avatars **(**$p< 0.001$) (Figure 6.2). This response was maintained and an even greater reduction in the proliferation index was noted on the final time point of the experiment, on day 6 ex vivo ($p< 0.0001$) (Figure 6.2).

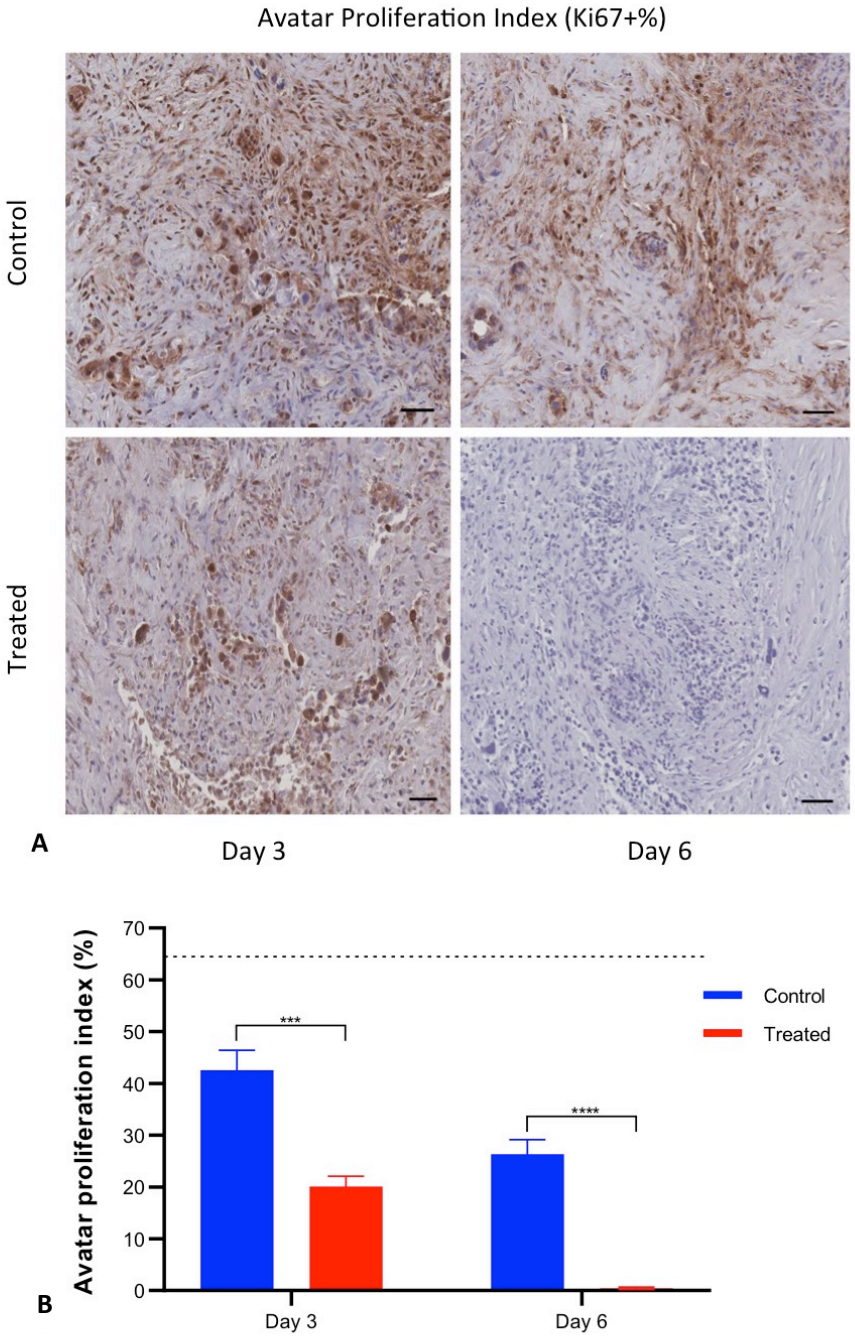

Figure 6. 2 – Proliferation index of PDAC avatars following ex vivo drug treatment. (A) Representative images of immunohistochemical staining of PDCA14's avatar for Ki67 positivity during ex vivo culture. Proliferation index was calculated by the percentage of Ki67 positive cells across the tissue slice. Scale bar 50 um . (B) Quantification of proliferation index during ex vivo drug treatment. Interrupted horizontal line on the x axis represents the baseline (Day 0) mean proliferation index (64.71%). Data presented as mean ± SEM, statistical analysis performed by unpaired Student T test. Data information: *** p< 0.001; **** p< 0.0001.

In light of the significant reduction in the proliferative index following drug treatment, I wanted to assess whether this correlated with trends in cell death. As such, I performed IHC staining to identify cells that were undergoing programmed cell death through apoptosis (defined by C-C3 positive staining). Whilst a gradual increase in C-C3 positive cells were observed in the untreated avatars, a significantly higher rate of C-C3 positive cells were noted in the treated avatars at both time points (Figure 6.3). The data correlated with the Ki67 trend, within the treated avatars the proliferation index decreased and a subsequent increase in cell death was observed.

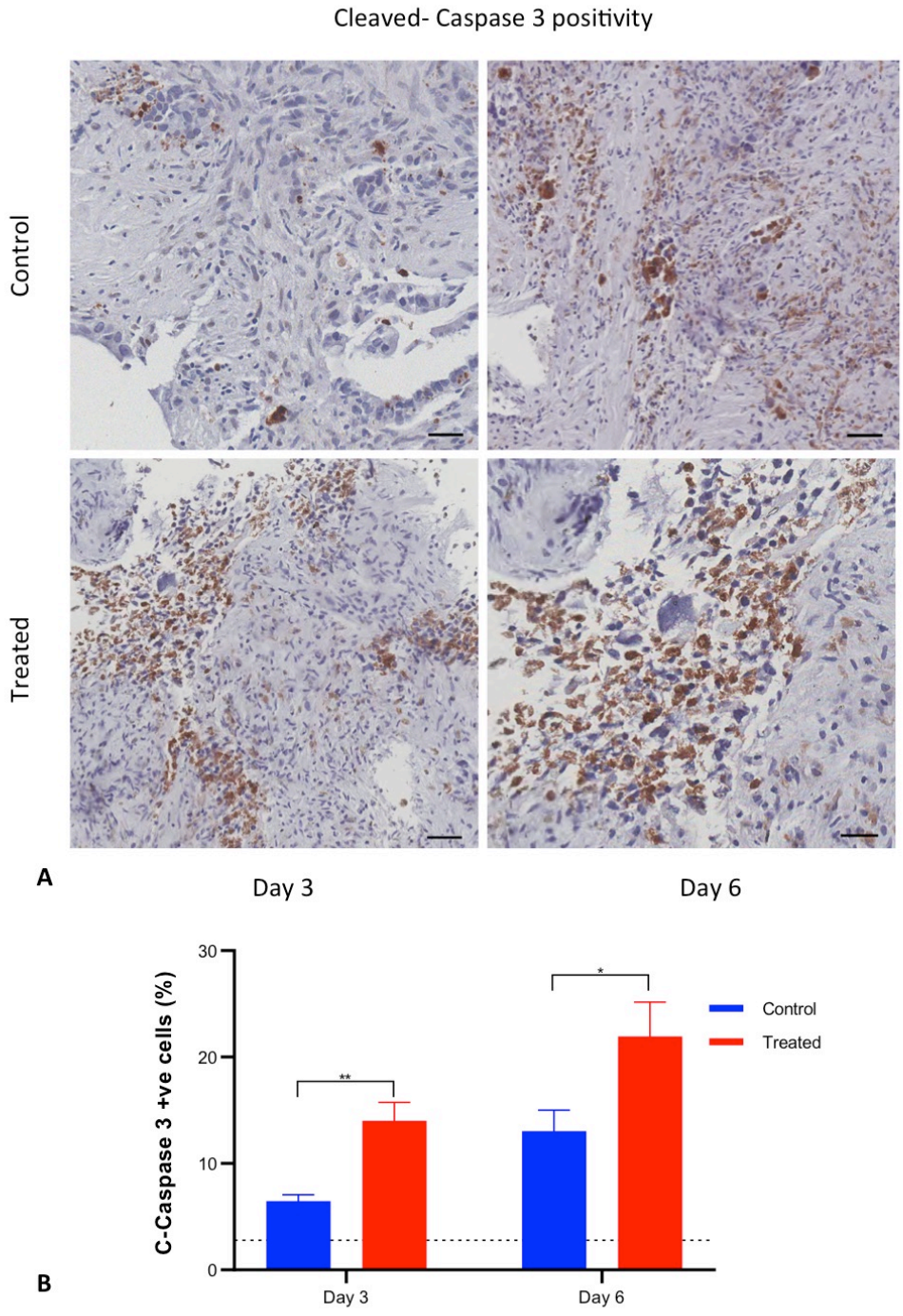

Figure 6. 3 – Apoptosis rates of PDAC avatars following ex vivo drug treatment. (A) Representative images of immunohistochemical staining of PDCA14's avatar for Cleaved-Caspase 3 positivity during ex vivo culture. Percentage of Cleaved-Caspase 3 positive cells across the tissue slice calculated. Scale bar 50 um. (B) Quantification of apoptosis rates during ex vivo drug treatment. Interrupted horizontal line on the x axis represents the baseline (Day 0) mean apoptosis rate (2.78%). Data presented as mean ± SEM, statistical analysis performed by unpaired Student T test. Data information: * p< 0.05; ** p< 0.01.

It was noted on the histological review of the H&E slides of PDCA14 that the treated avatars displayed a marked increase in nuclear abnormalities across the avatar. Given the mechanism of action for Gemcitabine (a nucleoside analogue which is incorporated into the cell DNA which subsequently inhibits DNA synthesis) I wanted to determine whether there was a detectable difference in DNA damage (by quantifying γ-H2AX positivity) within the treated and untreated avatars.

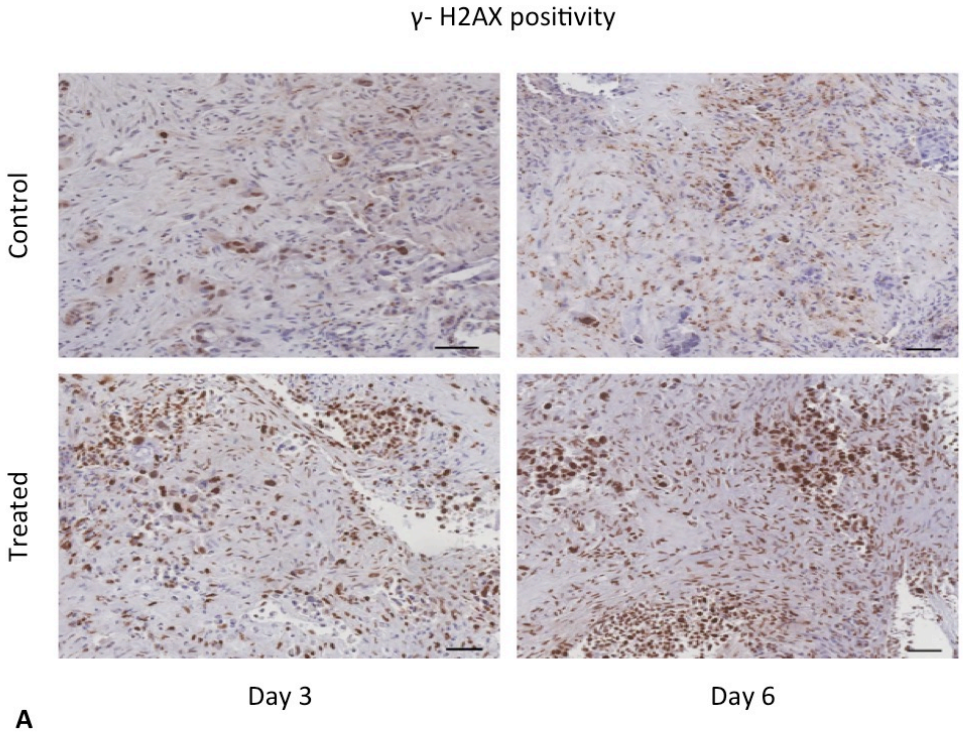

A

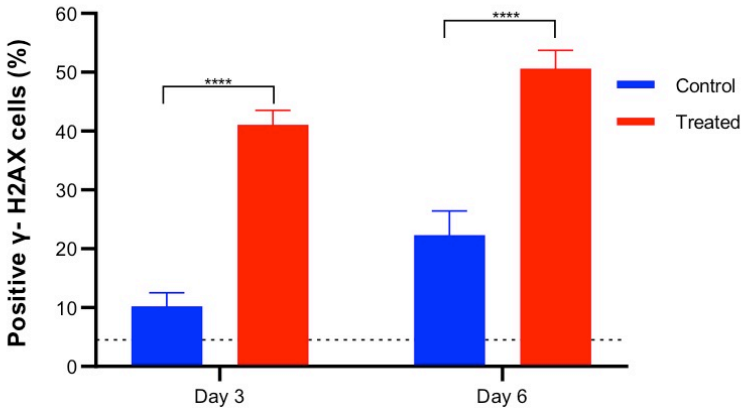

B

Figure 6. 4– γ- H2AX positivity rates of PDAC avatars following ex vivo drug treatment. (A) Representative images of immunohistochemical staining of PDCA14's avatar for γ- H2AX positivity during ex vivo culture. Percentage of γ- H2AX positive cells across the tissue slice calculated. Scale bar 50 um. (B) Quantification of γ- H2AX positivity during ex vivo drug treatment. Interrupted horizontal line on the x axis represents the baseline (Day 0) mean γ- H2AX positivity rate (4.51%). Data presented as mean ± SEM, statistical analysis performed by unpaired Student T test. Data information: **** p< 0.0001

It was noted at both time points that γ- H2AX positivity was significantly higher within the treated avatars compared to controls, thereby suggesting successful nuclear incorporation of the drug and a subsequent biological response witnessed.

Combining all three data sets (proliferation index, apoptosis rates and γ- H2AX activation), there is supporting evidence to suggest that drug delivery has been successful and a therapeutic response has been identified.

In light of the therapeutic response detected following the ex vivo treatment of the first cancer avatar (PDCA14), an important question yet to be addressed was how to determine and quantify the sensitivity to treatment between different patient avatars? A possibility that we needed to consider was whether this initial response observed (with PDCA14) was reflective of the tumour's sensitivity to Gemcitabine therapy or whether it was a generalised response of all avatars to ex vivo treatment. In order to evaluate this further we would need a larger sample size of treated avatars to enable us to gain confidence in assessing therapeutic response and to correlate findings.

6.2.3 Comparing therapeutic response between patient derived cancer avatars following ex vivo treatment

Prior to the first national lockdown in 2021, 2 further patients were recruited to the study. I was able to create patient derived cancer avatars from their resected tumours, which were subsequently treated with chemotherapy ex vivo. This resulted in us obtaining a cohort of 3 patients, all of which were treated with the same chemotherapeutic strategy (Gemcitabine) as per the treatment protocol previously described (Figure 6.1). It was interesting to note that the treatment response was not uniform across all avatars. A very different therapeutic response (changes in proliferation or apoptosis rates) was observed between patients. Within 2 patient avatars (PDCA16 and PDCA17) we observed no evidence upon IHC staining of a therapeutic response. In comparison to the respective control avatars, there was no statistical difference in the avatar proliferation index or apoptosis rates. This was strikingly different to the response observed following the treatment of PDCA14's avatars, where a marked reduction in the proliferative index was observed accompanied by an increase in cell death following treatment. It is possible that the therapeutic response witnessed is reflective of that tumour's sensitivity to treatment instead of a universal response to ex vivo treatment. To further validate the avatar response, what is required is a clinical correlation with the patients' survival

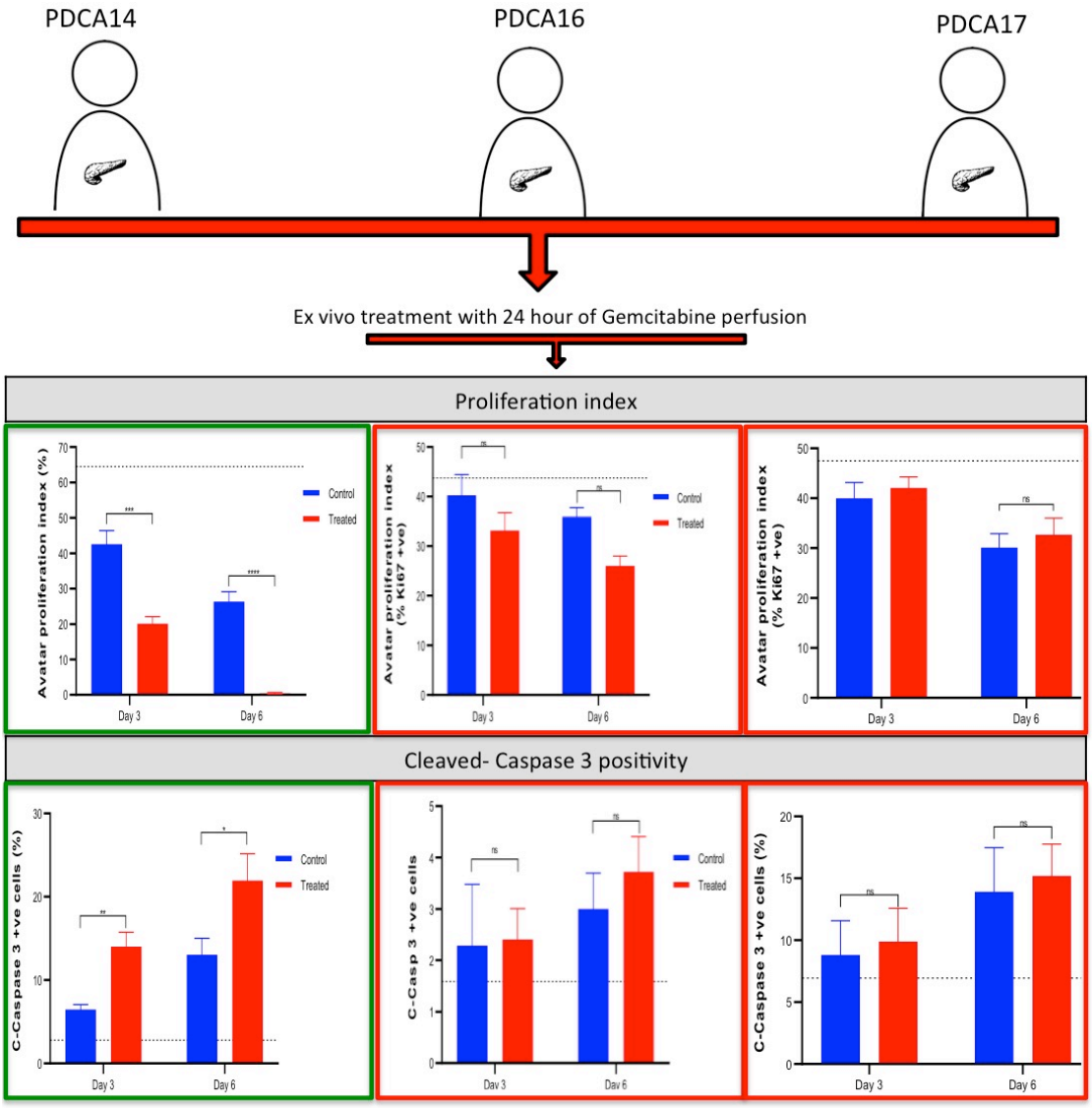

Figure 6. 5 - Profiling three different avatar responses to ex vivo Gemcitabine treatment. Three different patients' avatars were treated ex vivo with Gemcitabine therapy. All avatars were subsequently analysed with IHC staining for proliferation and apoptosis markers (Ki67 and CC3 respectively) to assess and compare therapeutic responses. A therapeutic response was defined as when a statistical difference in either proliferation or apoptosis rates was noted between the treated and control avatars. Of the three treated patient avatars, only one (PDCA14) was suggestive of a response to Gemcitabine treatment.

6.2.4 Molecular profiling pancreatic avatars into transcriptomic subtypes

In light of the variable therapeutic response observed to Gemcitabine treatment, I was interested to determine whether this was due to different transcriptomic subtypes of the PDAC avatars. Emerging evidence would suggest that different subtypes have specific sensitivities to different chemotherapeutic treatment regimes (Torres et al., 2018). My intention was to perform RNA-sequencing on the avatars (at baseline) to determine the subtypes. However, obtaining sufficient RNA yield from the avatars proved difficult (in light of the small tissue volume). A variety of extraction methods were performed in an attempt to increase the RNA yield (Table 6.1) . Nonetheless we were unable to obtain a sufficient amount of RNA (quality) for formal sequencing.

Table 6. 1– RNA extraction methods trialled

Method trialled	RNA Concentration (ng/ ul)	260/280 ratio	260/230 ratio
1) Enzymatic dissociation	2.6	1.69	1.48
2) Manual homogenisation followed by enzymatic dissociation	5.3	1.57	0.52
3) Manual homogenisation followed by QIAshredder column and enzymatic dissociation	12.9	1.76	0.90

I therefore decided to perform a qPCR gene expression analysis on specific genes (from each subtype) in an attempt to try and gain a further insight into the possible subtypes of tumours present. I looked at GATA6 and KRT81 expression within the avatars (Figure 6.6). Opposite trends were noted in the gene expression profile between PDCA14 and PDCA16 and PDCA17.The data suggests that PDCA14 is a basal tumour whereas PDCA16 and PDCA17 are classical tumours with respect to their

GATA6 and KRT81 expression. In keeping with the literature, basal tumours are reported to have a greater sensitivity to Gemcitabine therapy (as observed within our drug treated avatar cohort). Further validation is required with subtype identification with formal RNA sequencing.

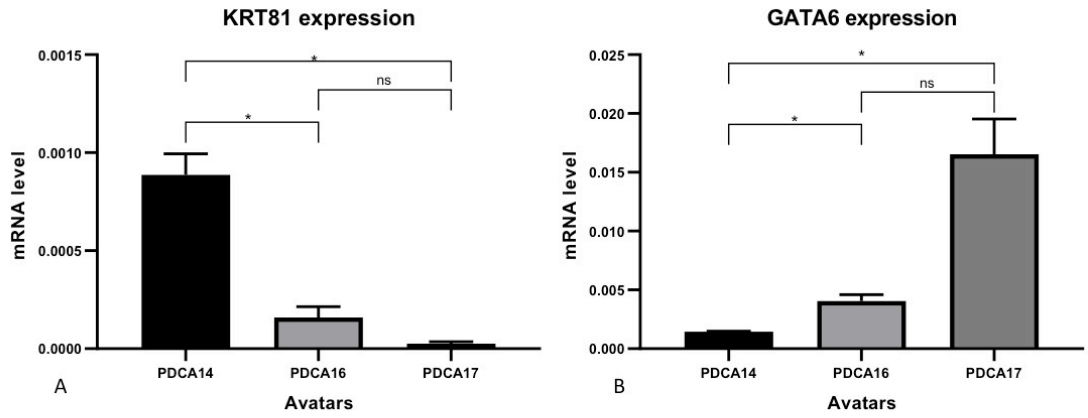

Figure 6. 6 – Determining whether tumour subtypes correlate with Gemcitabine response . (A) qPCR performed to determine KRT81 expression in the avatars at baseline. (B) qPCR performed to determine GATA6 expression in the avatars at baseline. Data presented as mean ± SEM, statistical analysis performed by unpaired Student T test. Data information: * p< 0.05, ns non significance

6.2.5 Correlating the avatar and patient response to chemotherapy

At the time of submitting this thesis, survival outcome data was obtained for all patients. A minimum of 18 month follow up was recorded. Data regarding adjuvant treatment, recurrence rates, site of recurrence and mortality was collected.

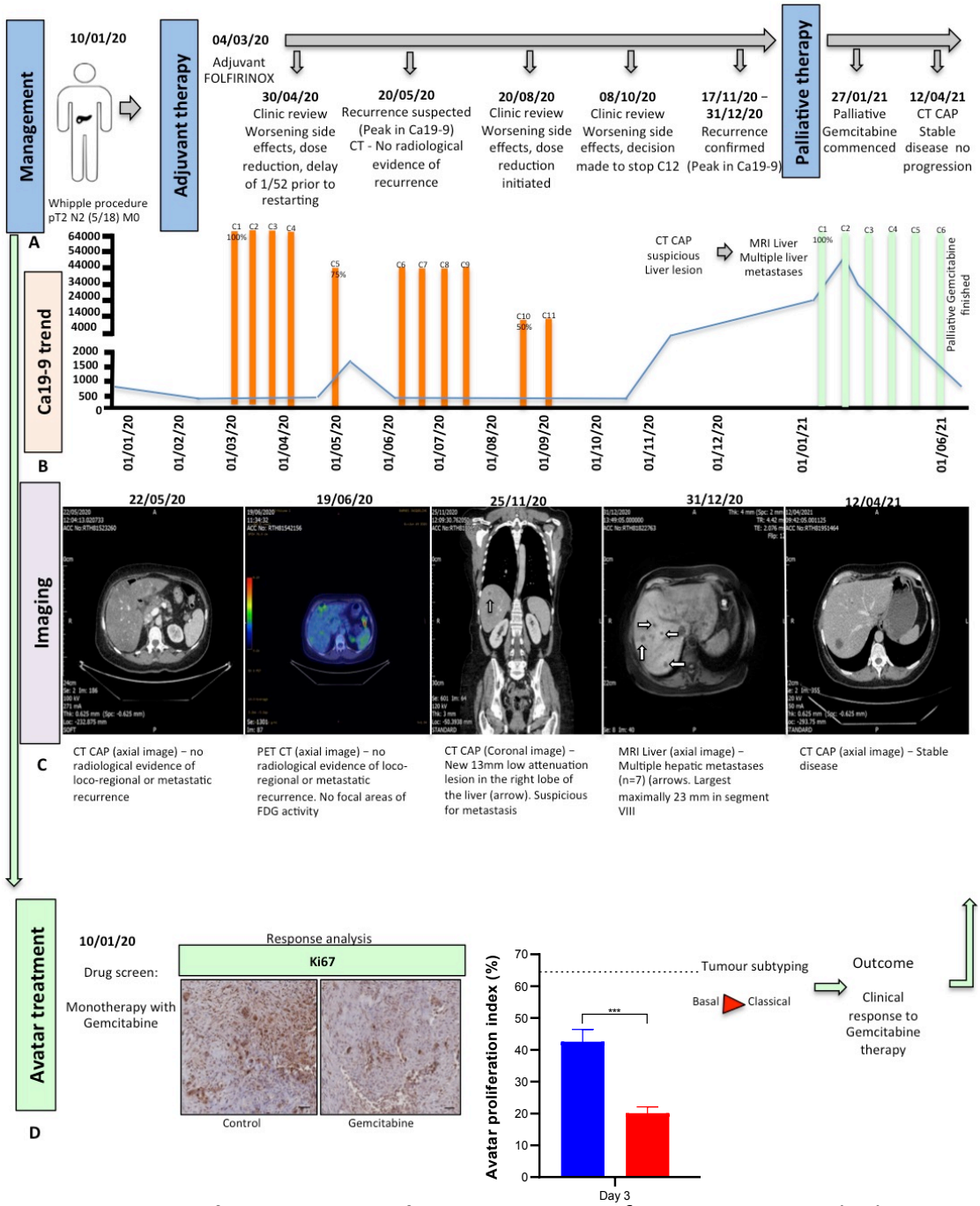

Figure 6. 7 – Correlating avatar and patient response for PDCA14. Visual schematic of PDCA14's clinical journey from diagnosis. (A) Clinical information presented regarding the patient's management, follow up and outcome. (B) Patient's tumour marker trends over time presented as a line graph. Orange bars correspond to FOLFIRINOX treatment cycles; green bars correspond to Gemcitabine treatment cycles. The height of the bar is representative of the dose, a full dose is recorded as 100%. A dose reduction is represented by a reduction in the height of the bar. (C) Cross-sectional imaging performed during follow up. (D) The patient's response is subsequently compared with that of their corresponding avatar. The avatar

displayed sensitivity to Gemcitabine monotherapy as a statistically significant reduction in proliferation was noted, combined with a marked increase in apoptosis rates.

Patient response

PDCA14 was derived from a patient who underwent a Whipple pancreaticoduodenectomy for a moderately differentiated pT2 N2 (5/18) M0 L1 V0 R0 pancreatic cancer in January 2020. Their initial Ca19-9 at diagnosis was 879 U/ml, which dropped to 285 U/ml in the immediate postoperative period. No complications occurred and the patient was discharged home after a brief length of stay of 6 days. Within two months of the surgery, the patient was reviewed in the Oncology clinic. In light of the pathological findings (nodal disease) it was felt that the patient would benefit from adjuvant therapy. As the patient had a good performance status and minimal co-morbidities, it was suggested that they would be a candidate for the FOLFIRINOX regime. After completing 4 cycles of FOLFIRINOX by April 2020, the patient had started to develop some side effects to therapy (peripheral paraesthesia) and following a clinic review the decision was made to reduce the dose of therapy to 75% and to postpone the next cycle. This was then unfortunately accompanied by an insidious peak in the Ca19-9 tumour marker (1857 U/ml). This raised the concern for possible disease recurrence and as such cross-sectional imaging was urgently arranged to investigate. However there was no radiological evidence of disease recurrence either loco-regionally or metastatic on either the CT CAP in May or the PET CT in June 2020. As such the patient continued with their FOLFIRINOX regime for another 5 cycles. In August 2020 the patient had

completed 9 cycles of the FOLFIRINOX regime, however the side effects had progressed further and another dose reduction (50%) in FOLFIRINOX was implemented. In October 2020, the decision was made to prematurely end the adjuvant therapy in light of the marked side effects to the treatment. Unfortunately in November 2020 (10 months post surgery) a significant rise in the patient's Ca19-9 was observed (5693 U/ml). Cross-sectional imaging was again organised and a new liver lesion (13 mm low attenuation lesion) was noted in the right lobe of the liver on the CT CAP. The lesion was further characterised with an MRI, which confirmed the presence of multiple liver metastases. An exponential rise in the Ca19-9 was observed (40,592 U/ml). The patient commenced palliative Gemcitabine therapy in January 2021 (12 months post op). The patient has subsequently completed all 6 cycles of palliative Gemcitabine therapy. A drastic reduction in the Ca19-9 was noted (27,752 to 10,999 to 4,178 to <1000 U / ml currently). In addition, we have 8 months of stable metastatic disease. There has been no radiological evidence of disease progression within the liver (no increase in metastases size or in number) and no evidence of any other recurrence either loco-regionally or within the thorax. At the time of submission, the patient is currently under surveillance follow up and is due a further CAP to assess the disease burden.

Avatar response

Immediately after the patient's surgery in January 2020, I created numerous patient derived cancer avatars and conducted a drug screen using Gemcitabine monotherapy. At both time points we observed a significant reduction in the proliferative index of the treated cancer avatars in comparison to the controls. We

also observed a significant increase in cellular apoptosis rates in the treated avatars. In an attempt to identify the tumour subtype, a selected gene panel qPCR was performed. On the basis of this panel, it would appear that the avatars for PDCA14 were likely to be of the Basal tumour phenotype. In light of the response observed in the avatar following ex vivo drug therapy, we labelled PDCA14 as a likely Gemcitabine sensitive tumour.

Patient and avatar comparison

In comparing the avatar response and that of the patient's clinical outcome, it is apparent that the FOLFIRINOX regime may have initially secured systemic control over the disease. However, over time the therapeutic effect was lost and tumour outgrowth and metastases occurred. This may have been partially due to dose reduction, treatment delay and premature termination of adjuvant therapy. What is interesting is comparing the tumour behaviour after the administration of palliative Gemcitabine. Not only was a striking reduction in the Ca19-9 tumour marker noted, but also we have 8 months of stable metastatic disease with no radiological evidence of progression. This is very different to the tumour behaviour prior to Gemcitabine therapy, where the disease burden had significantly increased in the time interval between the CT and MRI at the end of 2020. As there has been no increase in the metastatic burden since completing palliative therapy, this could suggest sensitivity of the tumour to Gemcitabine. As noted in the avatar treatment, Gemcitabine induced a marked change in the proliferation index of the avatars and an increased cell death rate was observed in comparison to the controls.

The following 2 patients illustrate the effect of the Covid-19 pandemic on our treatment strategy for patients with PDAC.

Patient - PDCA16

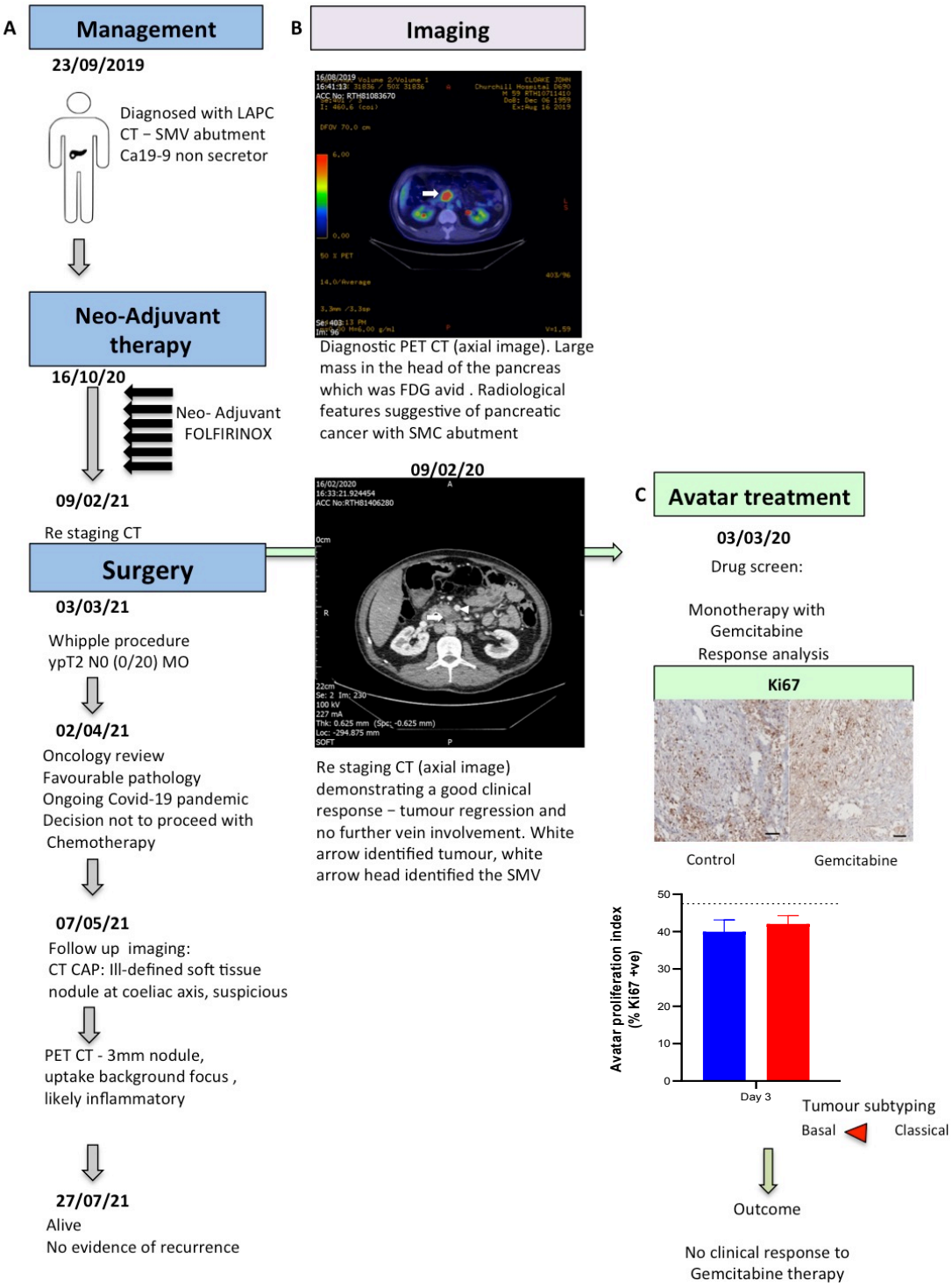

Figure 6. 8 – Correlating avatar and patient response for PDCA16. (A)Visual schematic of PDCA16's clinical journey from diagnosis. Each black arrow corresponds to a completed FOLFIRINOX treatment cycle. (B) Cross-sectional imaging performed during follow up. (C) The patient's response is subsequently compared with that of their corresponding avatar. No measurable therapeutic response was detected in

the avatar following Gemcitabine monotherapy. There was no statistical difference in the proliferation or apoptosis rates in the treated avatars when compared to the controls.

Patient response

PDCA16 was derived from the tumour of a 41 year old patient who initially presented with epigastric pain with subsequent jaundice. The initial CT identified the tumour as a locally advanced PDAC in light of the >180 degree SMV involvement. The patient was a Ca19-9 non secretor. After a review in the Oncology clinic, it was felt that the patient would be a candidate for Neo-Adjuvant Chemotherapy and as such FOLFIRINOX was commenced in October 2019. After completing 6 cycles of Neo-Adjuvant therapy, the patient was re-staged and there was evidence of radiological treatment response (Figure 6.8). In light of the tumour response and the patient's performance status, it was felt that an exploratory laparotomy should be performed with the intention of proceeding to a Whipple procedure if no evidence of metastatic disease was noted intra operatively. As such a Whipple pancreaticoduodenectomy was performed for a moderately differentiated ypT2 N0 (0/20) MO L0 V0 R0 pancreatic tumour in March 2020. The patient was discharged from hospital on postoperative day 7.

The patient was reviewed in the Oncology clinic within 6 weeks, where adjuvant therapy was discussed. In light of the ongoing global Covid-19 pandemic, the patient opted not to pursue adjuvant therapy due to the possible risk of immunosuppression and subsequent infection with Covid-19. This is not reflective of the routine

management of PDAC following resection and it also illustrates the difficult decisions that were required during this challenging time period. The patient was placed under active observation with regular follow up. It was noted on the first follow up imaging (approximately 2 months post operatively) that there was a new, ill defined 1.25 cm soft tissue mass at the coeliac plexus. Whilst the radiological features were not typical for a recurrence, there was a need to determine whether this soft tissue mass was a loco-regional recurrence. The soft tissue mass was re-evaluated with a PET CT. The mass was not PET FDG avid and no further increase in size was noted. The radiological appearances were more in keeping with inflammatory postoperative changes rather than disease recurrence. The patient underwent further follow up cross-sectional imaging, however the radiological appearance has remained the same. At the time of submitting this thesis, the patient is still alive 17 months post operatively with no evidence of disease recurrence.

Avatar response

Patient derived cancer avatars were immediately created following surgical resection of the patient's tumour in March 2020. A monotherapy drug screen with Gemcitabine was performed. We observed no evidence of a therapeutic response to Gemcitabine therapy at either time points. There were no detectable differences in proliferation or apoptosis rates following treatment. Profiling the avatars gene expression with qPCR was suggestive of a Classical tumour phenotype. PDCA16 was labelled as a likely Gemcitabine resistant tumour as we did not observe a statistically significant change in cellular proliferation rates, cell death or γ- H2AX activation following drug administration in comparison to the control.

Patient and avatar comparison

In comparing the avatar response to that of the patient's clinical outcome, this case highlights the impact of the Covid-19 pandemic on patient management and on this research project. Whilst it would have been informative to assess the tumour biology whilst on adjuvant therapy, clearly the risk of chemotherapy induced immunosuppression in the context of the pandemic, placed the patient at significant risk. An initial significant response to FOLFIRINOX therapy was noted with the down staging of the primary tumour, which ultimately permitted resection. Given the fact that the patient is still alive 17 months following resection with no recurrence (despite not receiving adjuvant therapy) it is likely that this patient had favourable tumour biology. Classical tumours possess a more favourable prognosis and are responsive to FOLFIRINOX therapy. At the time of submitting this thesis, there was no evidence of a recurrence. It would be interesting to continue to collect survival data on this patient in order to measure the disease-free progression time interval and to evaluate if a recurrence occurs, where does it manifest in addition to its response to adjuvant therapy.

Patient - PDCA17

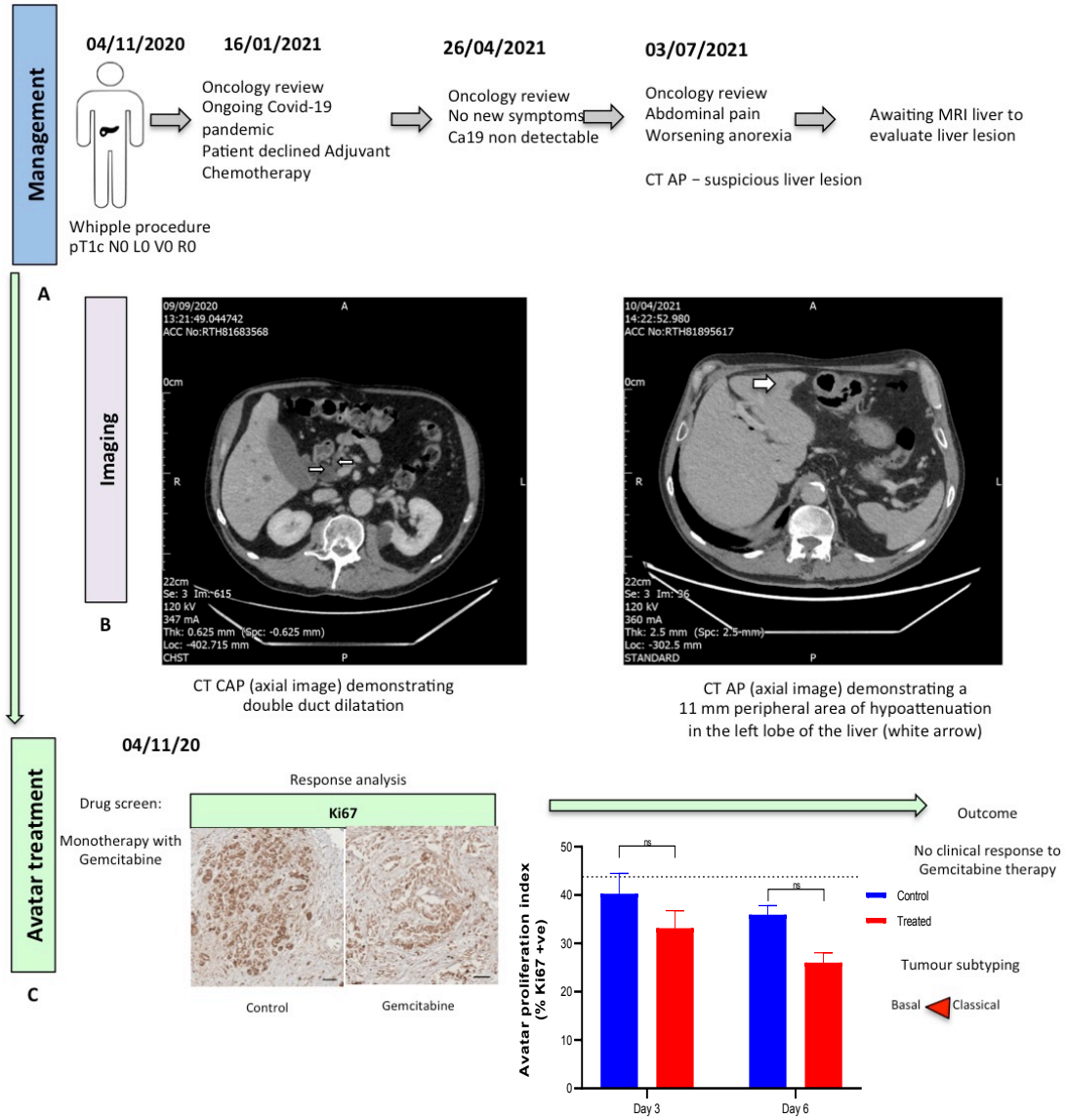

Figure 6. 9 – Correlating avatar and patient response for PDCA17. (A) Visual schematic of PDCA17's clinical journey from diagnosis. (B) Cross-sectional imaging performed during follow up. (C) The patient's response is subsequently compared with that of their corresponding avatar. There was no statistical difference in the proliferation or apoptosis rates in the treated avatars when compared to the controls following Gemcitabine monotherapy treatment.

Patient response

PDCA17 was derived from the tumour of a 66 year old patient who presented with epigastric pain. The initial CT demonstrated a small head of pancreas tumour which

had no vascular involvement. As the tumour was resectable at diagnosis, the patient proceeded straight to resection with no Neo-Adjuvant therapy. The patient underwent a Whipple procedure for a pT1c N0 L0 V0 R0 tumour in November 2020.There was no intraoperative complications and the postoperative period was uneventful. The patient was discharged home on postoperative day 10. The patient was seen virtually in the oncology clinic 2 months following their surgery. A lengthy discussion regarding the risk and benefits of adjuvant therapy in the context of the ongoing Covid-19 pandemic was undertaken. The patient opted to decline adjuvant therapy in light of the pandemic; as such the patient was placed under close surveillance for follow up. Eight months following their surgery, the patient presented to the oncology clinic with new symptoms (non specific abdominal pain and anorexia), a CT AP was organised which demonstrated a small liver lesion in the left hemi liver. The radiological features were not conventional for a metastasis but in light of the clinical history further investigation was warranted. At the time of submitting this thesis the patient was awaiting a liver MRI in order to characterise the lesion in greater detail.

Avatar response

Multiple patient avatars were created immediately after surgical resection of the primary tumour and placed in culture. Ex vivo treatment with Gemcitabine therapy was performed as per the previously described protocol (Figure 6.9). Upon histological analysis of the avatars (following treatment and in comparison to the controls), there were no identifiable features suggestive of a therapeutic response. There was no statistical difference between the proliferation index or cell death rate

within the avatars following the administration of Gemcitabine therapy. We concluded that PDCA17's avatars could be Gemcitabine resistant tumours as no objective response (a statistical reduction in proliferation rates) to treatment was observed.

Patient and avatar comparison

As PDCA17 declined adjuvant therapy, we are unable to directly compare avatar and patient outcomes. However there is a suggestion that a recurrence may have occurred early (within 8 months of resection) pending further investigation. If confirmed to be a recurrence, this will directly impact on long-term survival. Upon analysing the avatar's response to Gemcitabine, there was no objective response to therapy. What is needed in this case is a greater follow up period in order to further understand the biology of this patient's tumour.

6.3 Discussion

Within this chapter, I have demonstrated that our current perfusion system can be utilised to deliver chemotherapy to the avatars during ex vivo culture. A therapeutic response was observed upon IHC staining for proliferation and apoptosis markers within the avatars following treatment. Given that these changes occurred post treatment, it is suggestive of successful drug delivery. As variation was noted in the therapeutic responses across avatars, this could be reflective of individual tumour sensitivity to the specific treatment strategy instead of a universal avatar response

to ex vivo treatment in general. Through recruiting additional patients to the study, we will be able to secure a larger portfolio of treated avatars, amongst which it may be possible to start quantifying the extent of the treatment response between patients and to use this metric for the purpose of patient stratification for therapy.

The systemic therapy trialled within our experimental design was Gemcitabine monotherapy. Our rationale for using Gemcitabine is that it remains as one of the key chemotherapeutic treatment strategies that is used for PDAC management within current clinical practice. It is utilised both in the setting of metastatic disease and for 'curative' intent, however it is normally reserved for patients of a select demographic (older with limited performance status) (NICE, 2018). Whilst it would have been interesting to be able to assess the effect of FOLFIRINOX on the patient avatars, there were several practical barriers. Firstly, the use of ex vivo chemotherapy perfusion treatment of patient avatars has not been described within the literature, and as such, as a proof of principle we selected the chemotherapy regime with the simplest dosing protocol in order to establish and validate our methodology. Secondly, the FOLFIRINOX regime contains 4 different drugs: folinic acid, fluorouracil, irinotecan and oxaliplatin, and comprises a complex dosing regime (Conroy et al., 2018). As such we felt that it would be difficult to deliver such a protocol ex vivo as a first attempt, however it serves as a target for future experiments. Thirdly, it was felt that if we were able to identify the most effective therapeutic regime with the smallest side effect profile then this would allow maximum benefit and minimal risk for patients. Identifying patients who would benefit the most from Gemcitabine therapy would result in preventing patients from

receiving FOLFIRINOX, where they would not gain any survival advantage but would experience the adverse side effects of this potent chemotherapy regime.

Creating a method that closely replicates in vivo drug delivery remains challenging. The current universal technique for dosing cells is delivering the drug (in a set volume) directly on to the cells in culture (M. Yoshida et al., 1975). Such an approach results in an acute delivery of the maximum drug load to the cells. The same method is also utilised in the context of tissue slice culture. Naipal et al, 2016 assessed the effect of 5-FU, Doxorubicin and Cyclophosphamide on breast cancer tissue slices by loading the drugs directly on to the tissue slice prior to assessing for a therapeutic response (Naipal et al., 2016). Such an approach to therapeutic dosing does not replicate the in vivo physiology of drug delivery. Our method of perfusion delivery of chemotherapy to the avatars ensures a slow but constant delivery of the drug to the avatars over time. We feel that this technique is more physiologically representative, as the in vivo tumour would receive the drug in the same manner albeit through the native tumour vasculature (rather than an acute and direct maximal dosing of the drug). There remains a need to validate the pharmacokinetic and pharmacodynamic effects of perfusion delivery of drugs within our current system. Conceptually, perfusion drug delivery has several theoretical advantages and may mimic in vivo drug pharmacokinetics, notably drug clearance through active outflow from the perfusion plate with simultaneous drug removal.

The optimal dosing strategy for avatar treatment has yet to be determined. It is well documented in the clinical literature that Gemcitabine uptake within the tumour is

highly variable between patients (Koay et al., 2014). Some solid tumours (notably PDAC) have altered mass transport properties in comparison to normal tissue which hinders drug delivery (Pascal et al., 2013). An interesting study performed by Koay et al., 2014 , looked at real time quantification of Gemcitabine dosing in patients with resectable PDAC. The clinical trial was structured so that patients received an intraoperative infusion of Gemcitabine prior to surgical resection of the tumour. During the operation blood was taken at predefined time points to measure serum levels of Gemcitabine in addition to tumour samples being taken from pathology to determine the proportion of Gemcitabine incorporation into the tumour DNA (Koay et al., 2014). When assessing the patients' serum, Gemcitabine was detectable in the serum of all patients however the concentration varied. During the operation, a linear response was noted with an increase in serum Gemcitabine concentration over time. However upon analysing the tumour, significant variation in the detectable amount of Gemcitabine that had been incorporated into the tumour was noted (Koay et al., 2014), with some patients displaying subnormal levels comparable to adjacent normal pancreatic tissue (Koay et al., 2014). Within our avatar system, further work is needed to validate the dosing strategy, especially in the context of multi drug combination therapies. One approach that could be utilised would be prior to using a new systemic treatment, performing a high-performance liquid chromatography (HPLC) on control avatars in order to determine the average drug uptake. Such information could subsequently be used to tailor future therapeutic doses.

Whilst comparing the avatar response to the clinical response of the corresponding patient, there are several important discussion points to highlight. In the case of PDCA14, despite the patient being commenced on adjuvant FOLFIRINOX, they still succumbed to metastatic disease recurrence within 11 months of their curative resection. It appears that the initial adjuvant treatment strategy with FOLFIRINOX was able to sustain a degree of systemic control over the disease in light of the supressed CA19-9 level, however this was not permanent. Tumour outgrowth and escape eventually occurred. The mechanisms driving this are unclear although it is likely multifactorial in origin (effect of reduced dosing, prolonging dosing interval and premature termination of therapy combined with tumour evolution). It also highlights that it is likely that it is the residual cancer stem cell niche that is responsible for recurrence (Liu et al., 2015). Proliferating tumour cells are susceptible to the cytotoxic effect of systemic chemotherapy, whereas the dormant, non cyclical stem cells are not (Yu et al., 2012). Whilst the patient was off systemic therapy, disease outbreak occurred. Another possible use for our avatar system would be to evaluate when to alter systemic therapy. This is reflected in the case of PDCA16's avatar. This tumour was initially locally advanced, however it was successfully downstaged following a good response to FOLFIRINOX. The patient declined adjuvant therapy and at the time of submission of this thesis, had no detectable recurrence. If the patient's disease recurs, the decision would be whether they should restart their Neo-Adjuvant regime or commence a different therapy for palliation. Based on the data generated from the avatar, no therapeutic response was noted with Gemcitabine. As such, an argument that could be made is that palliative Gemcitabine should not be commenced and that the Neo-Adjuvant

regime (FOLFIRINOX) should be recommenced in light of the previous response however further validation is required

Our initial experience of ex vivo treatment of avatars shows promise as a possible model to deliver precision therapy. No uniform response was observed across all avatars and a correlation was noted between the response of both avatars and patients to systemic treatment. One must acknowledge the current limitations with the model, notably the small sample size (n=3). The Covid pandemic drastically impacted our ability to recruit further patients to the study. Further validation is certainly needed with a larger patient cohort in order to build additional confidence and evidence that the avatars provide an insight into the patient's response. However, the foundations of the model have been laid, a protocol created and the technology/technique is ready for use. The data illustrates that patients who share a common cancer diagnosis, actually have distinct and individual tumour behaviours. As such a generalised treatment approach is inappropriate. Treatment should be specific for each individual patient.

Chapter 7

Identifying a biomarker for localised disease

Treatment failure in PDAC management constitutes either a loco-regional or metastatic recurrence (Groot et al., 2018). The true incidence of either recurrence pattern has yet to be clearly defined as the majority of the published literature is based on small, single centre, retrospective case series. A published review of the ESPAC 4 trial patient cohort provided an invaluable insight into the recurrence patterns of PDAC (Jones et al., 2019). ESPAC 4 was a multicentre randomised, adjuvant therapy trial where patients with resectable PDAC were randomised to either Gemcitabine monotherapy or Gemcitabine and Capecitabine combination therapy (Jones et al., 2019). Of the 730 included patients, 65.6% suffered from a disease recurrence during follow up (Jones et al., 2019). A local recurrence was the most frequent recurrence pattern (49.7% of all recurrences), closely followed by distant metastatic recurrence in 40.3% (Jones et al., 2019). Only 10% of patients recurred with both local and metastatic disease (Jones et al., 2019). The time to disease recurrence varied between sites, however distant sites recurred quicker when compared to loco-regional recurrence (Jones et al., 2019).

Early recurrence of PDAC following surgery is a well-described pathological phenomenon (Fischer et al., 2012). Groot et al, 2018 reviewed a single (large

volume) centre's experience of 692 patients who underwent pancreatectomy for PDAC (Groot et al., 2018). They noted that liver only recurrence occurred quickly during follow up, strikingly at a median of 6.9 months post operatively (Groot et al., 2018). Given the speed of these recurrences, it is highly likely that these patients had micro-metastatic disease at their initial diagnosis that was not detectable on routine cross-sectional imaging techniques. It is therefore probable that cancer cell systemic seeding is an early event during the tumorigenesis of PDAC. Rhim, et al 2012 demonstrated that early PanIN lesions with concurrent KRAS mutation can undergo epithelial-to-mesenchymal transition, whereby allowing migration from the native pancreatic parenchyma and permitting entry into systemic circulation (Rhim et al., 2012). These circulating pancreatic cells were profiled and they displayed stem cell-like properties and a mesenchymal phenotype (Rhim et al., 2012). From our own experience of creating and maintaining pancreatic cancer avatars, we observed patients who succumbed to early disease recurrence, notably in the case of PDCA14 where bilobar liver metastases developed within 11 months of surgery despite the patient receiving adjuvant FOLFIRINOX therapy. It is clear that these patients who suffer from early disease recurrence have tumours with intrinsic bad tumour biology, which manifests as an aggressive disease phenotype. As such, there is an argument that we should identify these individuals with unfavourable tumour biology and use this as a basis for risk stratification for management.

Within the previous chapters of this thesis, we have approached precision therapy from the perspective of identifying the optimal treatment regime for each individual patient. However, an alternative interpretation of precision therapy could be, rather

than focussing on what treatment to give, determining the timing of when to give treatment. This is especially true in the context of high-risk patients with an aggressive disease phenotype (those patients whose disease recur quickly post operatively). For this unique patient cohort, the conventional treatment algorithm (surgery followed by adjuvant therapy) may be incorrect. In light of their high risk of disease relapse, they may benefit from upfront systemic treatment prior to surgery. This would have two main advantages; firstly it would allow early systemic control over the disease and secondly it would provide both an opportunity to study the biology of the patient's tumour and improve the patient selection process for surgery. For patients who show disease progression whilst on systemic therapy, this is clearly indicative of highly unfavourable tumour biology and as such resection should not be pursued. To date, the evidence base for Neo-Adjuvant therapy for PDAC is predominantly centred on patients with locally advanced or borderline resectable tumours (Michelakos et al., 2019; Oba et al., 2020). Its role in resectable tumours has yet to be determined. Conflicting data has been published on its use in this specific patient cohort (Oba et al., 2020). Concerns predominantly revolve around the fact that pursuing systemic treatment will delay definitive surgery and may allow the tumour to grow/metastases thus precluding the patient from resection (Oba et al., 2020). In addition Neo-Adjuvant therapy would normally require the patient to have biliary decompression and as such exposes them to the risks associated with endoscopic drainage (Oba et al., 2020).

It is possible that the benefit of Neo-Adjuvant therapy in resectable PDAC has yet to be noted in light of the heterogeneity of the patient cohort. The ability to be able to

risk stratify patients on the foundation of timing to recurrence may identify which patients should complete systemic therapy prior to resection. As such, precision therapy may be delivered from the perspective of identifying which patients should receive an alternative treatment strategy.

7.1 Aims

The aim of this chapter is to investigate as to whether it is possible to detect a novel biomarker to identify which patients are at highest risk of early disease relapse.

7.2 Results

7.2.1 TCGA analysis

In order to identify potential biomarkers which are predictive of early disease recurrence, PDAC sequencing data was required in addition to a large sample size of patients (for sufficient statistical power). I subsequently used the publically available pancreatic cancer dataset (PAAD) from The Cancer Genome Atlas (TCGA). The RNA sequencing data and corresponding clinical data were downloaded and utilised as the foundation for the exploratory biomarker discovery analysis.

The initial dataset comprised 185 patients (Figure 7.1). However, upon reviewing the data it transpired that this was a highly heterogeneous patient cohort and as a

consequence data filtering was required. I initially excluded all patients who were non PDAC pathology on the final histology report (this was predominantly patients with neuroendocrine tumours or rarer forms of pancreatic cancer such as acinar cell or adenosquamous tumours). I subsequently excluded any patient who had sequencing performed from non primary tumour sites (e.g biopsied liver metastases or peritoneal disease). This was in order for us to be able to assess the biology of the primary tumour. Finally, I made the decision to exclude all patients with a R1 or R2 resection margin status. My rationale for this was that the analysis was looking at patients with disease that recurred quickly following resection. In the context of a positive resection margin I felt that it would be difficult to conclude whether the metastasis had occurred secondary to systemic tumour cell seeding or from the residual positive margin. Excluding the patients with a positive margin subsequently created a smaller but homogenous patient cohort. This resulted in a final cohort of 95 patients. The cohort was divided into 2 groups; “early recurrence” and “no early recurrence”. A 12-month time point post operatively was used as a reference point to define a local recurrence.

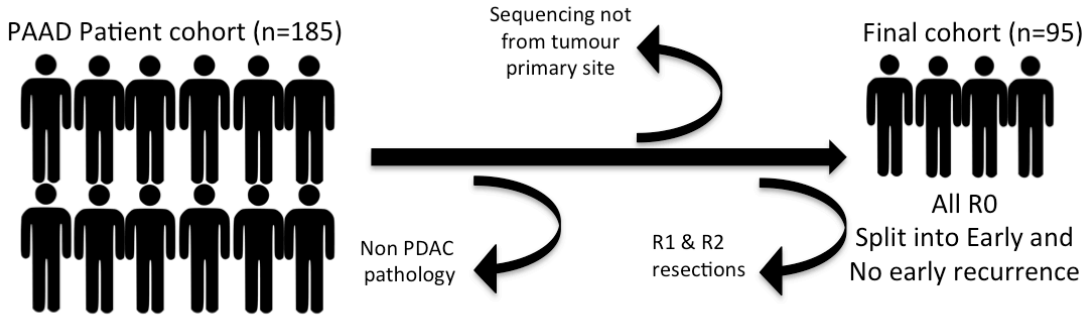

Figure 7. 1 – Overview of patient selection process from the TCGA dataset. The initial patient cohort was highly heterogeneous and was not uniform in nature. Filtering and exclusion of cases was performed based on the criteria highlighted in the figure. The final patient cohort was smaller in sample size. However this patient

population was much more consistent and homogenous.

7.2.1.1 Impact of early recurrence on overall survival

Firstly, in order to determine whether early disease recurrence has a clinically meaningful impact on patient survival I performed a survival analysis on the cohort. Early disease recurrence was associated with a significantly worse overall survival (Figure 7.2).

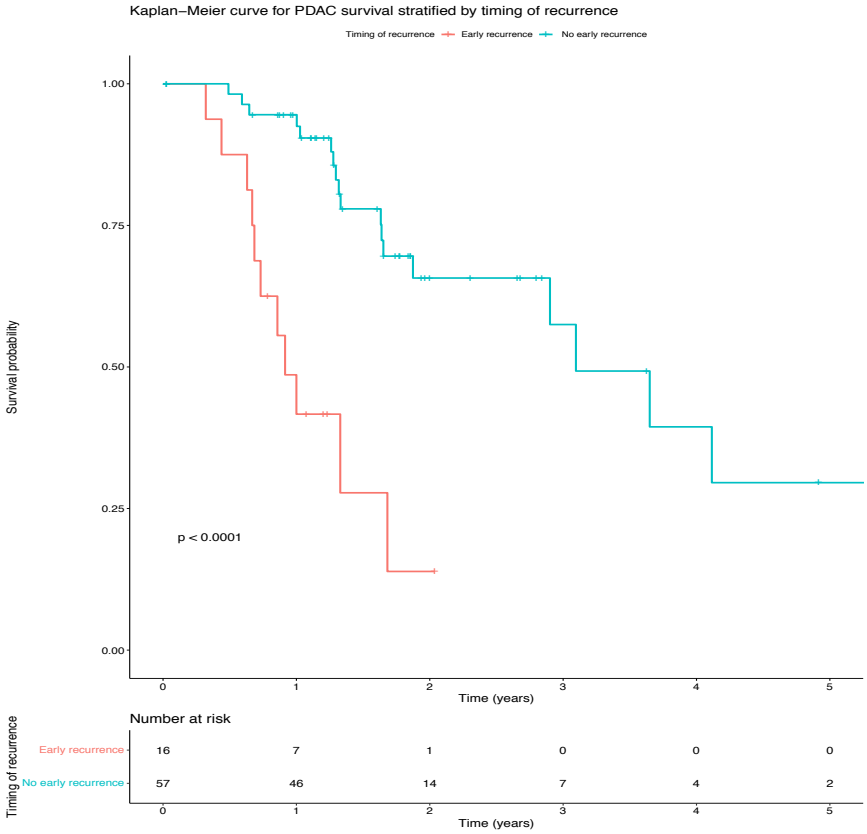

Figure 7. 2– Impact of early recurrence on overall survival. Kaplan-Meier survival curve of overall survival trends of PDAC patients stratified by timing of recurrence. The patient cohort with an early recurrence (<12 months) following resection had a statistically significant reduced overall survival (p< 0.0001).

7.2.1.2 Demographics of patients with an early recurrence

In light of the significant impact on survival, I wanted to determine whether it was possible to identify this sub-cohort of patients. Firstly I investigated as to whether there was any difference within the patient demographics or the histopathological features of these tumours. There was no statistical difference between the demographics of either cohort or the aetiological risk factors of PDAC (Table 7.1). Interestingly, there was also no statistical difference in the gross histopathological features between these tumours, thus ruling out the hypothesis that these patients had an early recurrence due to larger or more advanced (as per staging) tumours. As there was no difference in gross histopathological features, this may be suggestive that there are fundamental differences within the intrinsic tumour biology between these 2 patient cohorts.

Table 7. 1 –Demographics of the TCGA patient cohort

Demographics	Early recurrence (n=16)	No early recurrence (n=79)	P value
Age (mean)	66	64	0.5[%]
Female Male	5 11	38 41	0.33[&]
Past medical history History of Chronic Pancreatitis: Yes No	 14 1	 54 8	 0.6[$]
History of Diabetes: Yes No	 11 4	 46 19	 1[&]
Smoking pack year history (Mean)	14.4	24.1	0.3[%]

Histopathology			
T stage:			
T1	2	3	0.4[$]
T2	2	10	
T3	12	64	
T4	0	1	
N stage:			
N0	5	25	1[&]
N1	11	54	
Stage:			
Stage Ia	1	3	0.9[$]
Stage Ib	1	5	
Stage IIa	3	14	
Stage IIb	11	53	
Stage III	0	1	
Stage IV	0	2	

Statistical test performed: $ Fisher's exact test, % Student T-test, & Chi squared test

7.2.2 Differential gene expression of tumours with an early recurrence

To assess the differences in the transcriptomic profile of tumours that recurred early in comparison to those that did not, the RNA sequencing data (RNA seq) of the tumours of the respective cohorts were analysed. The edgeR package was used in R to assess the raw data and to generate a list of differentially expressed (DE) genes between both patient populations (Robinson et al., 2010) . Through visual exploration of the sequencing data, it was apparent that a statistically significant difference in the gene expression profile of a number of genes was present between the two patient cohorts defined by the timing of their disease relapse (Figure 7.3). Table 7.2 highlights the main 20 DE genes ordered by their false discovery rate.

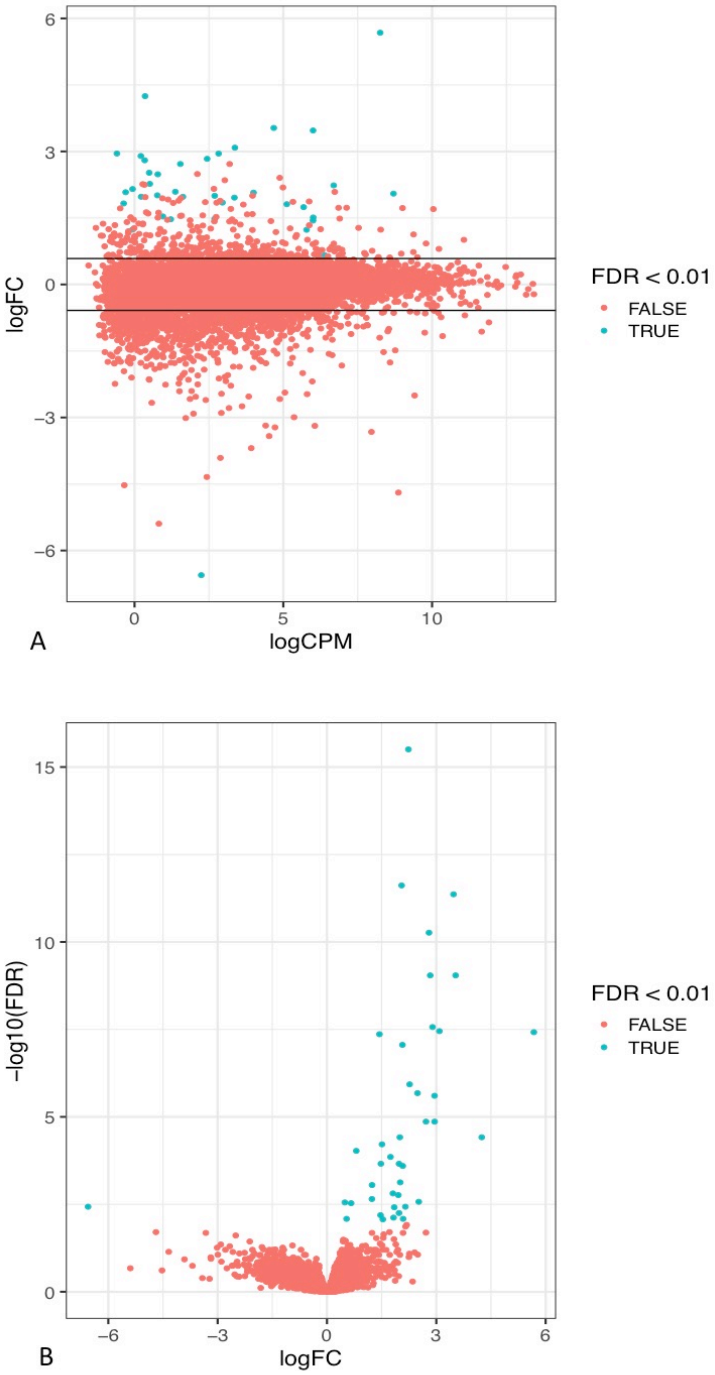

Figure 7. 3 – Identification of DE genes in patients with an early disease recurrence using edgeR. (A) Smear plot (MA plot) illustrating the relationship between gene expression (logCPM) and the logFC of DE genes. An absolute fold change of 1.5 is represented by the horizontal threshold lines. (B) Volcano plot illustrating the logFC of the DE genes against the negative log10FDR in order to present the most significant results.

Table 7. 2- Top 20 DE genes between patient with and without an early recurrence following resection for PDAC

Genes	logFC	logCPM	LR	P Value	FDR
PGAP3	2.234863421	6.692849271	85.43104973	2.40E-20	3.12E-16
ERBB2	2.048574468	8.702957168	66.3790854	3.72E-16	2.42E-12
C20orf56	3.472741222	5.999955935	64.42943056	1.00E-15	4.34E-12
GRIP2	2.800221839	0.34221273	58.88971646	1.67E-14	5.43E-11
HEPACAM2	3.52979217	4.680186101	52.9183579	3.48E-13	9.04E-10
REP15	2.833085067	2.439755412	52.56329868	4.17E-13	9.04E-10
BPI	2.897046925	0.212890127	45.59065609	1.46E-11	2.71E-08
CD177	3.085022682	3.372787741	44.8040761	2.18E-11	3.54E-08
MUC2	5.677339448	8.25616174	44.43688388	2.63E-11	3.80E-08
C17orf37	1.44088583	5.997701124	43.96865629	3.34E-11	4.34E-08
HES6	2.070971354	3.999807969	42.41237216	7.39E-11	8.75E-08
KLHL32	2.268442251	0.512018374	37.16812282	1.08E-09	1.18E-06
PKD1L2	2.484755825	0.781779596	35.88371452	2.09E-09	2.10E-06
CDX1	2.951638627	2.825814057	35.40002688	2.68E-09	2.50E-06
CCL24	2.716997309	1.53944708	31.92261059	1.60E-08	1.37E-05
MYADML2	2.953404861	-0.592385685	31.82951301	1.68E-08	1.37E-05
KLK12	4.246698942	0.35431791	29.66490429	5.14E-08	3.83E-05
APCDD1L	1.999333334	2.693405844	29.60405642	5.30E-08	3.83E-05
GRB7	1.510253759	6.005227248	28.60095229	8.89E-08	6.09E-05
MCM7	0.804754718	6.798879106	27.66823142	1.44E-07	9.37E-05
HSD11B2	1.743807374	5.683524172	26.80139663	2.25E-07	0.00013973

Table of the top 20 DE genes between patient with and without an early recurrence following curative resection for PDAC. Genes are ordered as per a decreasing FDR rate. (logFC = log fold change; logCPM = log counts per million; FDR = False Discovery rate) .

7.2.3 Alteration in signalling pathways associated with early recurrence

Identification of individual DE genes is a useful starting point for the analysis of the underlying biology of the tumours in patients who develop an early disease recurrence. However, instead of trying to understand and interpret individual gene results, it is important to consider these results in a wider biological context. Gene set enrichment analysis allows genes that share a common functionality to be grouped together within a specific pathway. Such an approach (through a pathway enrichment analysis) provides a unique opportunity to obtain a global view of how individual genes may act in synergy to change the behaviour of a tumour. To understand the aggressive disease phenotype present in the tumours that recurred early, I performed a pathway enrichment analysis on the predefined hallmarks of cancer pathways using a false discovery rate (FDR) of 0.1. Of the 50 hallmarks of cancer pathways analysed, 18 were significantly enriched at the 0.1 FDR cut off value (Figure 7.4).

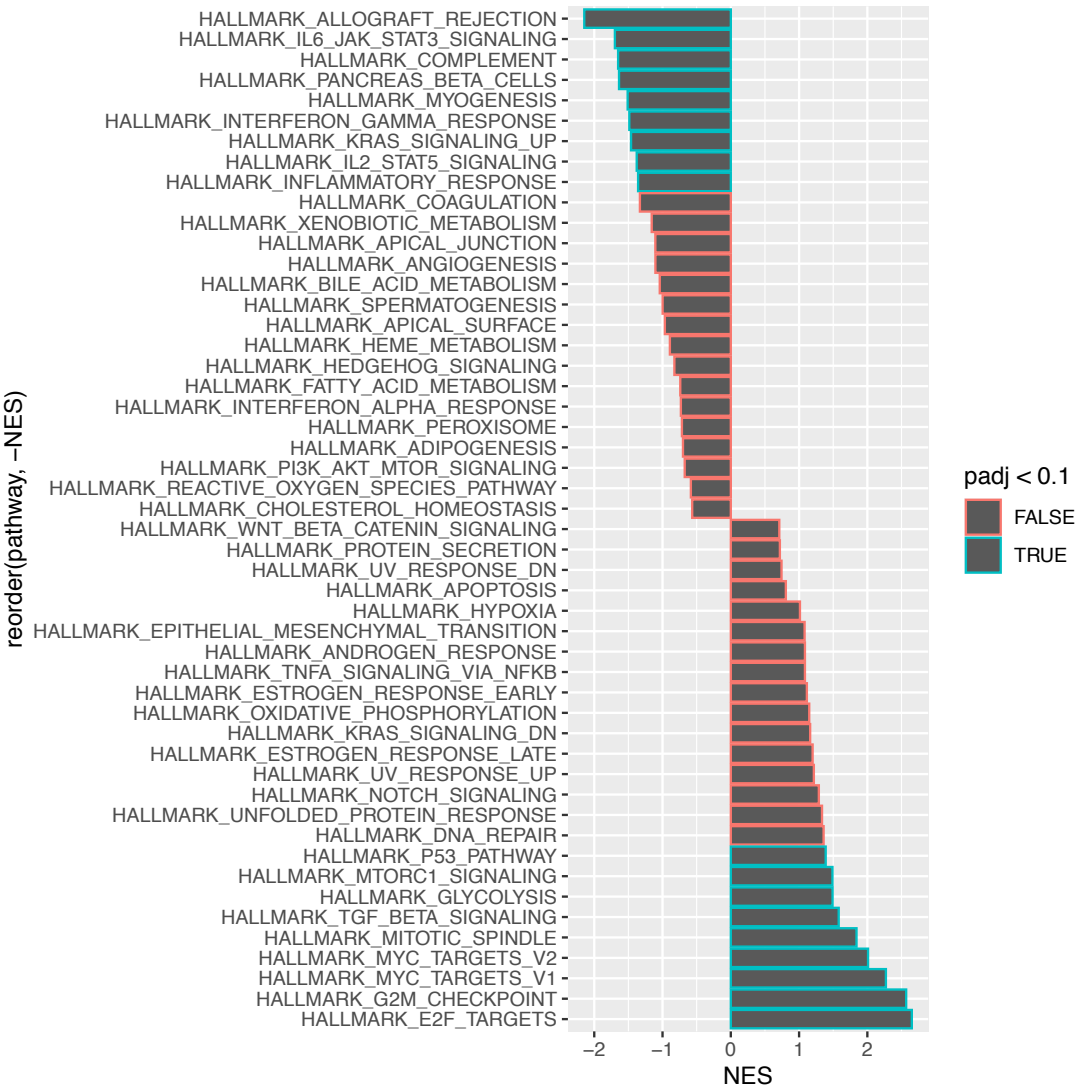

Figure 7. 4– Pathway enrichment analysis of the normalised enrichment scores (NES) of the 50 hallmark cancer pathways presented in a stacked bar chart ordered by FDR. A total of 18 different cancer pathways were enriched within tumours that recurred within 12 months of resection. FDR – False Discovery Rate

An interesting observation was that the most significantly downregulated pathway was “HALLMARK_ALLOGRAFT_REJECTION”. This pathway includes numerous genes that are routinely upregulated during transplant graft rejection (Liberzon et al., 2015). Graft rejection is an immune mediated mechanism whereby the recipient’s immune system identifies the donor’s specific antigens as foreign and therefore pathogenic in nature, thus activating a T lymphocyte mediated immune response

against the graft. This mechanism induces a pro-inflammatory and hypersensitive immune state. Therefore, this selective downregulation of the pathway would consequently imply that there was a generalised immune suppressive function within these tumours that recur early. In order to evaluate whether a specific immune pathway was involved, I subsequently performed a further gene set enrichment analysis, however this time using the Kyoto Encyclopaedia of Genes and Genomes (KEGG) pathways database. The KEGG database is a comprehensive archive of several different pathways that is not solely restricted to hallmarks of cancer related pathways. It includes a diverse number of pathways ranging from normal biological processes to disease specific pathways. It was noted that 34 different KEGG pathways were significantly downregulated within tumours that recurred within 12 months of resection (Figure 7.5). These included several independent immune function pathways such as T cell receptor signalling, B cell receptor signalling, chemokine signalling, toll like receptor signalling and natural killer cell mediated cytotoxicity (Figure 7.5). In light of the numerous downregulated independent immune pathways, it would suggest that these tumours promote an immune suppressive environment and may therefore utilise immune escape as a mechanism to avoid detection after systemic dissemination and subsequently relapse early.

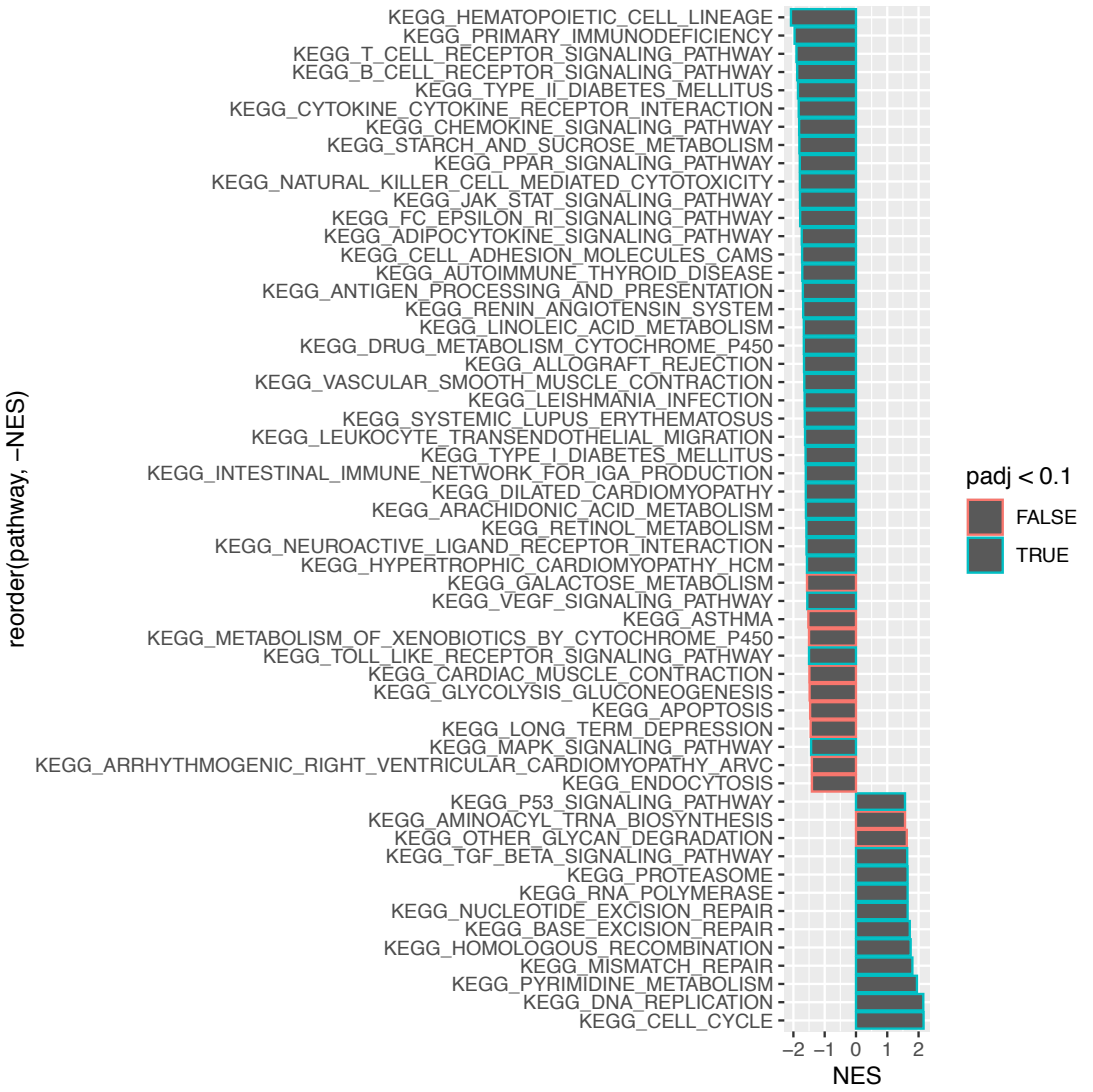

Figure 7. 5– KEGG pathways enrichment analysis. The normalised enrichment scores (NES) of each pathway is presented within a stacked bar chart that is ordered by the false discovery rate. A total of 34 different KEGG pathways were significantly downregulated and 11 pathways significantly upregulated.

7.2.4 Identification of biomarkers for early recurrence

No universal method has been accepted as a gold standard technique for identifying biomarkers during exploratory analyses of sequencing data. The previous analysis through the edgeR software package identified DE genes within the patient cohort

who developed an early disease recurrence. In order to improve the statistical accuracy of the biomarker search, I performed another DE gene analysis through an alternative software package DESeq2. After the identification of the DE gene list within DESeq2, I subsequently compared the DE gene list from both software packages and determined the correlation between the logFC of genes within both edgeR and DESeq2. A positive correlation was noted (Figure 7.6).

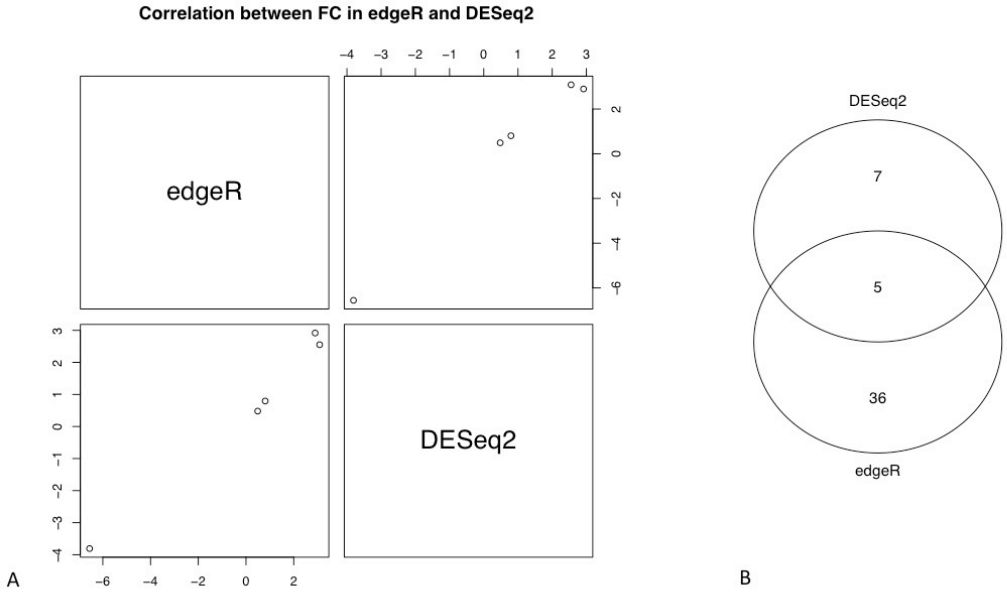

Figure 7. 6 – Comparative analysis of DE genes between DESeq2 and edgeR (A) Visual correlation between the logFC of DE genes in both the DESeq2 and edgeR packages. Linear positive correlation noted between both. (B) Venn diagram illustrating the overlap of genes identified by DESeq2 and edgeR respectively as DE using a cut off of a false discovery rate of 0.01

Through performing a matching algorithm, genes that were recorded as DE within both software packages were identified. A total of 5 different genes had been identified as DE by both edgeR and DESeq2 software packages. These genes included BPI, C6orf58, CD177, MCM7 and NUDT15 (Figure 7.6) . These 5 genes are therefore potential biomarkers of clinical interest. In light of the fact that they had been

identified as DE genes by two separate analyses by two independent software packages, this increases the validity and statistical robustness of the exploratory sequencing analysis results.

7.2.4.1 Determining the accuracy of biomarkers at identifying early recurrence

In order to further evaluate these potential biomarkers for detecting early recurrence, I performed repeated receiver operating characteristic (ROC) curve analysis to determine their respective sensitivity and diagnostic ability. The area under the curve (AUC) was calculated for each ROC curve in order to assess the model's performance (Figure 7.7). All 5 of the identified targets had an AUC value >50% (Figure 7.7). However within the field of biomarker discovery, the wider research literature suggests that only biomarkers with a AUC values >80% should be selected as higher AUC scores are reflective of a superior model with greater diagnostic ability and clinical relevance (Cook, 2010). Consequently, only 1 of the previously described biomarkers met the threshold: NUDT15.

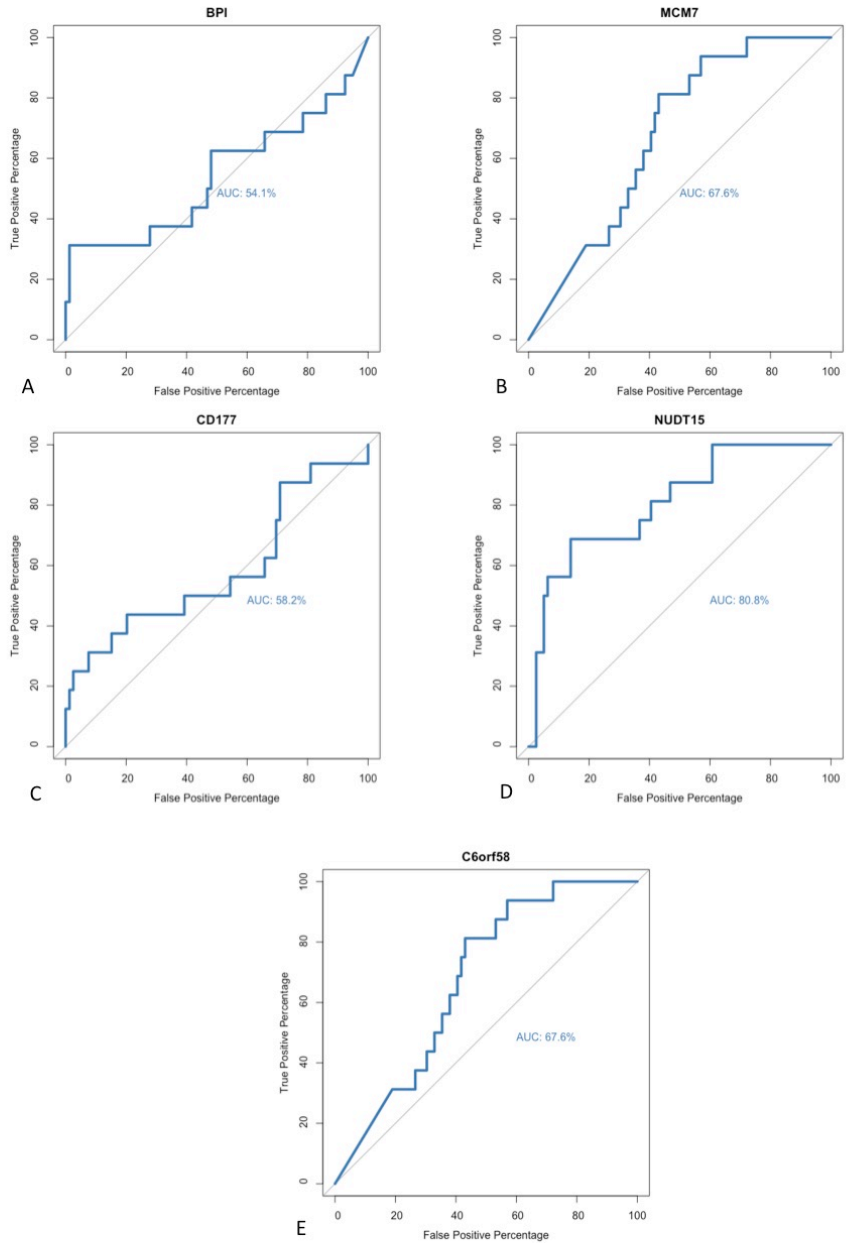

Figure 7. 7 - Receiver operating characteristic curve analysis to determine biomarker sensitivity. ROC curves and area under the curve (AUC) calculated for (A) BPI, (B) MCM7, (C) CD177, (D) NUDT15, (E) C6orf58

Nudix hydrolase 15 also referred to as NUDT15 is an enzyme from the Nudix hydrolases superfamily (Carreras-Puigvert et al., 2017). The enzymatic function of this family is to hydrolyse nucleoside diphosphates into nucleoside monophosphate (Carreras-Puigvert et al., 2017). The activity of the enzymes is induced by oxidative

damage or pathological transversion events during DNA replication. Its role within cancer development or metastatic dissemination has yet to be determined. The enzyme has been thoroughly investigated in the context of therapeutic drug toxicity (predominantly with the thiopurine class of drugs of purine antimetabolites) (Moriyama et al., 2017) . Mutations in the NUDT15 gene are associated with inadequate metabolism of thiopurines and may cause myelotoxicity (Moriyama et al., 2017). In light of the high diagnostic ability (as per the AUC score of 80.8%) and its capacity to identify patients at risk of early disease relapse, I wanted to assess whether the protein expression was sufficient in order for it to be utilised as a biomarker. This may have clinical implications, especially in the context of peri-operative biopsy (through EUS) where patients could be risk stratified for early relapse at the point of their diagnosis.

I therefore evaluated recurrence patterns within our cohort of patient avatars. Of the 13 PDCA, 3 (23%) developed early disease recurrence within 12 months of their surgery. Distant metastases were the most common site of recurrence (Liver or Lung) (table 7.3).

Table 7. 3– Survival outcomes of recruited patients

Patient	Date of surgery	Adjuvant therapy	Recurrence	Site of Recurrence	Date of Recurrence	Time to Recurrence (days)	Early Recurrence	Current status
1	29/07/19	Yes	Yes	Aortocaval nodes	19/11/20	479	No	Alive
2	14/08/19	Yes	No	n/a	n/a	n/a	n/a	Alive
3	27/08/19	No	No	n/a	n/a	n/a	n/a	Dead (13/05/20)
4	29/08/19	Yes	Yes	Lung and Bone	01/06/20	277	Yes	Dead (27/12/20)
5	02/10/19	Yes	Yes	Liver metastases , Portal and SMA nodes	15/08/20	318	Yes	Dead (23/09/20)
6	17/10/19	No	No	n/a	n/a	n/a	n/a	Dead

								(5/5/21)
7	28/10/19	Yes	No	n/a	n/a	n/a	n/a	Alive
8	07/11/19	No	Yes	Lung, pleural and mediastinal nodes	29/06/21	600	No	Dead (30/07/21)
9	27/11/19	Yes	No	n/a	n/a	n/a	n/a	Alive
10	10/01/20	Yes	Yes	Liver	25/11/20	320	Yes	Alive
11	17/02/20	No	No	n/a	n/a	n/a	n/a	Alive
12	03/03/20	No	No	n/a	n/a	n/a	n/a	Alive
13	06/05/21	Yes	No	n/a	n/a	n/a	n/a	Alive

Having identified some patients with early disease recurrence, I wanted to determine whether NUDT15 protein expression was detectable within the avatars. The inability to detect it on a protein level could preclude its use as a biomarker. I subsequently performed IHC staining for NUDT15 on the avatars at the baseline time point (day 0 – day of surgery). NUDT15 was detectable on a protein level within the avatars. As we had a cohort of 3 patients with an early disease recurrence, I wanted to compare their protein expression with that of the cohort of no early recurrence. A statistically higher NUDT15 positive staining area was noted within the avatars with an early recurrence (Figure 7.8).

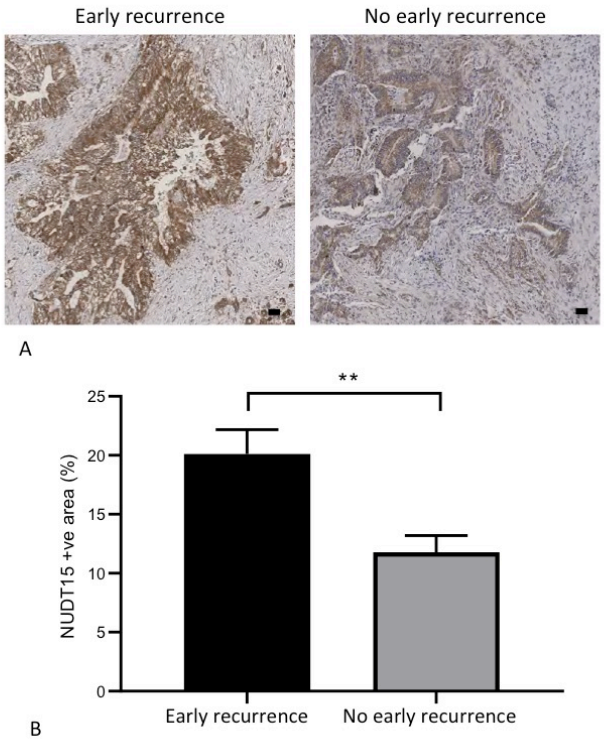

Figure 7. 8 – NUDT15 expression within avatars. (A) Representative IHC staining of NUDT15 expression within avatars of patients who developed an early disease recurrence. Scale bar 50 um. (B) Quantification of NUDT15 expression within avatars. Data presented as mean ± SEM, statistical analysis performed by unpaired Student-T test. Data information: **p < 0.01

A possible limitation of the previous analysis of the TCGA data is that it is looking at a specific patient cohort. This unique cohort (R0 status) is not representative of the general PDAC patient population and as such the validity of the biomarker could be questioned. In addition, by excluding PDAC subtypes that are of an aggressive phenotype (e.g. adenosquamous) this may underpower the analysis (as these tumours should recur quickly). Therefore in order to investigate the use of NUDT15 as a biomarker for all patients, I subsequently re-analysed the TCGA dataset (Figure 7.9). During this analysis, I did not exclude patients with variations in PDAC pathology or based on their margin status. Only 4 patients were excluded as they

were noted to have a colloid tumour type of PDAC (which is biologically distinct to PDAC). As a consequence 163 patients were analysed (Figure 7.9 A). Differential gene expression analysis was performed. Upon visual exploration of the results, it was clear that a statistically significant difference in the gene expression profile was noted between the two patient cohorts (early vs no early recurrence) (Figure 7.9 B). The differential gene expression analysis was subsequently performed in 2 independent sequencing processing software packages. A positive correlation was noted between the identified genes in both packages (Figure 7.9 C). A further paired matching algorithm was performed in order to identity the differentially expressed genes that had been identified in both packages simultaneously (Figure 7.9 C). As previously described in the chapter, NUDT5 was identified as a gene that was differentially expressed in relation to timing of recurrence. This finding validates the earlier work in the chapter regarding biomarkers for disease relapse. Further confirmation is required in a larger cohort of patients in addition to determining whether it is possible to obtain sufficient tissue yield from a EUS biopsy to be able to stain for NUDT15.

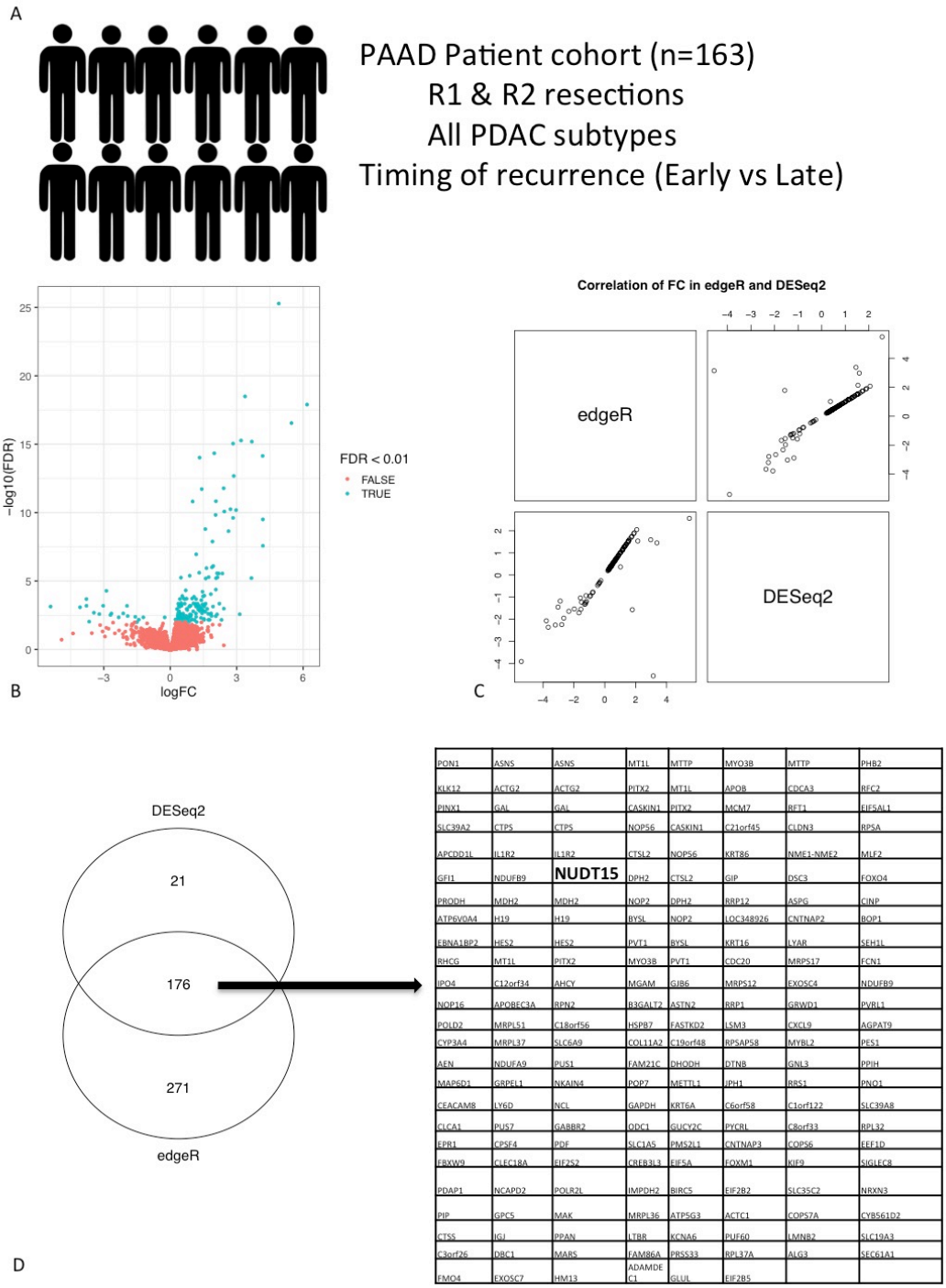

PON1	ASNS	ASNS	MT1L	MTTP	MYO3B	MTTP	PHB2
KLK12	ACTG2	ACTG2	PITX2	MT1L	APOB	CDCA3	REC2
PINX1	GAL	GAL	CASKIN1	PITX2	MCM7	RFT1	EIF5AL1
SLC39A2	CTPS	CTPS	NOP56	CASKIN1	C21orf45	CLDN3	RPSA
APCDD1L	IL1R2	IL1R2	CTSL2	NOP56	KRT86	NME1-NME2	MLF2
GFI1	NDUFB9	**NUDT15**	DPH2	CTSL2	GIP	DSC3	FOXO4
PRODH	MDH2	MDH2	NOP2	DPH2	RRP12	ASPG	CINP
ATP6V0A4	H19	H19	BYSL	NOP2	LOC348926	CNTNAP2	BOP1
EBNA1BP2	HES2	HES2	PVT1	BYSL	KRT16	LYAR	SEH1L
RHCG	MT1L	PITX2	MYO3B	PVT1	CDC20	MRPS17	FCN1
IPO4	C12orf34	AHCY	MGAM	GJB6	MRPS12	EXOSC4	NDUFB9
NOP16	APOBEC3A	RPN2	B3GALT2	ASTN2	RRP1	GRWD1	PVRL1
POLD2	MRPL51	C18orf56	HSPB7	FASTKD2	LSM3	CXCL9	AGPAT9
CYP3A4	MRPL37	SLC6A9	COL11A2	C19orf48	RPSAP58	MYBL2	PES1
AEN	NDUFA9	PUS1	FAM21C	DHODH	DTNB	GNL3	PPIH
MAP6D1	GRPEL1	NKAIN4	POP7	METTL1	JPH1	RRS1	PNO1
CEACAM8	LY6D	NCL	GAPDH	KRT6A	C6orf58	C1orf122	SLC39A8
CLCA1	PUS7	GABBR2	ODC1	GUCY2C	PYCRL	C8orf33	RPL32
EPR1	CPSF4	PDF	SLC1A5	PMS2L1	CNTNAP3	COPS6	EEF1D
FBXW9	CLEC18A	EIF2S2	CREB3L3	EIF5A	FOXM1	KIF9	SIGLEC8
PDAP1	NCAPD2	POLR2L	IMPDH2	BIRC5	EIF2B2	SLC35C2	NRXN3
PIP	GPC5	MAK	MRPL36	ATP5G3	ACTC1	COPS7A	CYB561D2
CTSS	IGJ	PPAN	LTBR	KCNA6	PUF60	LMNB2	SLC19A3
C3orf26	DBC1	MARS	FAM86A	PRSS33	RPL37A	ALG3	SEC61A1
FMO4	EXOSC7	HM13	ADAMDEC1	GLUL	EIF2B5		

Figure 7. 9 – Evaluating NUDT15 as a biomarker. (A) An overview of the TCGA patient cohort analysed. (B). Volcano plot illustrating the differentially expressed genes between the two patient cohorts. (C) Correlation between the logFC of differentially expressed genes in both the DESeq2 and edgeR packages. Linear positive correlation noted between both. (B) Venn diagram illustrating the overlap of genes identified by DESeq2 and edgeR respectively as differentially expressed. Both programes identified NUDT15 as differentially expressewd with regards to timing of disease relapse

7.3 Discussion

My intention within this chapter is to consider whether it is possible to risk stratify patients based on biomarkers that were predictive of early disease recurrence. Being able to identify this high-risk patient cohort would have significant clinical impact. These patients may benefit from early systemic therapy prior to resection in order to treat the micro-metastatic disease. As observed within our own experience of patient avatar maintenance, early recurrence was present in 23% of all patients. As highlighted by the survival analysis (Figure 7.2) this group of patients have a very poor survival. Developing biomarkers specific for risk of relapse would therefore allow early identification of this patient cohort.

The field of biomarker discovery has significantly evolved over the last decade. The 'multiomic' approach allows the incorporation and integration of multiple types of sequencing data. It is important to highlight that there is no universal approach for transcriptomic analysis and in the context of DE gene evaluation, several different software programmes and statistical packages exist that can be used for this work through. There is no standardised approach for this type of bioinformatics analysis. A published review in 2017 compared 9 different software packages for differential gene expression analysis and concluded that there was not one optimal package (Costa-Silva et al., 2017). The authors did highlight that the DESeq2 package was associated with a very high true positive rate (84%) (Costa-Silva et al., 2017). A similar review by Rapaport, et al 2013 that reviewed 7 software packages concluded the same result with a slight advantage reported with the edgeR package (Rapaport

et al., 2013). The fundamental difference between these packages is their inbuilt method of data normalisation. Within the analysis I performed for biomarker discovery, I utilised two different packages to conduct a DE analysis. I subsequently pooled the results and only selected the genes that had been identified with a statistically different gene expression profile by both packages. Such an approach increases the statistical accuracy of the analysis and our confidence in the results as these genes had been identified by two separate analyses.

In order to validate the findings of the exploratory analysis, a literature search on the identified genes was undertaken. Interestingly, it was noted that three of the identified genes (C6orf58, CD177, and MCM7) had been previously identified as prognostic factors for survival in PDAC. Wang et al, 2018 investigated the impact of tumoural infiltration of neutrophils with CD177 expression and demonstrated that high levels of infiltration were associated with a significant reduction in overall survival ($p= 0.01$) (Y. Wang et al., 2018). Liao et al, 2018 performed RNA sequencing of early stage PDAC patients and assessed the relationship between MCM gene expression and overall survival (Liao et al., 2018). A total of 6 MCM genes were studied and higher expression was noted within the tumours when compared to adjacent healthy tissue (Liao et al., 2018). Whilst differences were noted in survival trends when patients were stratified by individual MCM gene expression, the most significant impact on survival was in the context of high MCM4 gene expression (Liao et al., 2018). Wu et al, 2011 performed a Cox regression analysis in order to identify a gene signature associated with long term survival of PDAC (Wu et al., 2011). They identified 12 genes of interest, one of which was C6orf58. However due

to the paucity of literature on the gene at the time of publication, they were unable to describe in detail the function of the gene (Wu et al., 2011). We can therefore be confident with the output of the exploratory analysis as 3 of the 5 identified genes have been preciously described in the context of PDAC. This serves as an internal validation of the results.

Biomarker discovery for PDAC has been a very active field over the last decade. Most efforts revolve around developing biomarkers for early disease detection. The principal argument is that by diagnosing patients early, a greater proportion would be amenable to curative surgery. In addition, our current and only licenced diagnostic biomarker (CA19-9), is not without its limitations, notably its false positivity rate and poor predictive value in asymptomatic patients (Ballehaninna et al., 2012). With the recent acknowledgment of the molecular sub classes of PDAC, research initiatives are now focussing on developing biomarkers that allow quick identification of PDAC sub classes (Orth et al., 2019). This ability would allow early risk stratification of patients at the time of their diagnosis. Obtaining this information would also dictate future treatment strategies. A good example of this is the current phase 2 trial PASS-01 which is actively recruiting patients with metastatic PDAC (ClinicalTrials.gov, 2020). This randomised clinical trial will evaluate two different chemotherapy regimes in the context of molecular profiling and biomarker validation (ClinicalTrials.gov, 2020), notably using GATA6 to discriminate between basal and classical tumours. This is a clear example of harnessing the tumour biology to dictate therapy. Our approach with our biomarker discovery was to focus on identifying a sub population of patients who were at risk of early recurrence.

NUDT15 was associated with the best ROC and AUC value, and as such was further evaluated with IHC staining for protein level expression. Within our small cohort, a statistical difference was noted in expression level between cohorts of early and no early recurrence.

The identified biomarkers display a possible benefit of being able to identify patients at highest risk of early relapse. This unique patient cohort would require an alternative treatment strategy either through altering the timing of systemic therapy or modifying the chemotherapeutic treatment regime. However, further validation in a larger prospective patient cohort is required to confirm the validity of the identified biomarkers for their ability to be able to identify patients at greater risk of early recurrence. What is clear is that we must acknowledge PDAC as a diverse cohort of tumours and that there is a clear need to develop alternative stratification strategies for prognostic measures. These variables must be based on intrinsic tumour biology in order to guide therapy or to inform survival probability.

Chapter 8

Discussion

Within this study, we presented our proposed system for precision medicine that can be utilised to deliver personalised therapy for patients with PDAC, using real time quantitative feedback of therapeutic responses. The information generated from the drug screen can be used to inform future treatment strategies, both in terms of first and second line therapies. Whilst other groups have described the use of organotypic tissue slice culture of PDAC, the novelty within our system lies within the incorporation of perfusion culture technology (Lim et al., 2018). Such an approach has yet to be described within the literature. In our published systematic review of physiological culture techniques, perfusion culture has yet to be combined with pancreatic tissue for ex vivo culture (Hughes et al., 2021). The physiological benefit of using perfusion culture within our system translated into a greater time period of successful ex vivo culture. Maintaining nutritional delivery and the removal of metabolic waste products was achieved. We noted the preservation of functional activity within the avatars (proliferation rates and mTOR activity). At day 12 ex vivo, we observed that the cellular diversity of the primary tumour had been preserved and a full compliment of immune cells (both from lymphoid and myeloid lineage) remained present. The avatars' response to therapy mimicked that of the

patient's response and as such they provide a window of insight into how patients will respond to adjuvant therapy.

8.1 Key advantages of using avatars for precision therapy

Our model for delivering precision therapy has several advantages over the previously described techniques:

1) Speed of avatar creation

Our system allows a rapid turnaround time for avatar creation following the acquisition of the tumour sample. After gaining familiarity with the protocol and relevant equipment, avatars were routinely created within 3 hours of receiving the tissue. To put this into perspective, avatars could be created and subsequently placed in ex vivo perfusion culture prior to the patient leaving theatre and going into recovery. In light of this quick process, therapeutic drug testing of the avatars could be commenced whilst the patient remained on the operating table. This is strikingly different to PDX based models for precision therapy. Kamili et al, 2020 published their experience of creating PDX's from patients with neuroblastoma (Kamili et al., 2020). Neuroblastoma represents an aggressive paediatric malignancy, where high risk disease is associated with high relapse rates and a 5 year survival rate of less than 50 % (Pinto et al., 2015). Within the study reported by Kamili et al, 2020, only 44% of PDXs were successfully established at the patient's diagnosis (Kamili et al.,

2020). Within our model, every core biopsy acquired was successfully transformed into avatars (100% success rate). However of greater significance was the time period required for engraftment and maturation of their PDX models. Successful engraftment was defined as a tumour with a tumour volume of 1000 mm^3. On average the time to successful engraftment was 107 days (range 33–210 days). In 5 patients, there was no evidence of successful engraftment by 12 months. In light of the aggressive nature of these patients' disease, systemic therapy is indicated. However if reliant on the PDX model then a significant delay prior to commencing therapy would occur. Our model allows for rapid avatar creation within a clinically meaningful time frame.

2) Preservation of the cellular diversity of the primary tumour

Whilst patient derived organoids represent a 3D model that encompasses a multicellular entity and includes information on cell-cell interaction, it provides no insight into the presence and function of additional cell types within the TME. Huang et al, 2020 published their report on establishing organoids from resected PDAC samples, however the characterisation of their organoids purely consisted of defining tumoural phenotype and their gene expression profile (W. Huang et al., 2020). Tsai et al, 2018 also produced patient derived PDAC organoids and in an attempt to re-establish the TME, co-cultured the organoids with isolated Cancer Associated Fibroblasts (CAFs) or T lymphocytes (Tsai et al., 2018). Whilst this increases the complexity of their model and allows for some representation of the original TME, it is important to highlight that they have only provided/incorporated 2

elements from the extremely diverse original TME (Tsai et al., 2018). They also demonstrated that the sensitivity of the organoids to Gemcitabine treatment was altered in the coculture model with CAFs (with an increase in levels of therapeutic resistance observed) (Tsai et al., 2018). This clearly highlights the marked effects that the TME has on PDAC responsiveness to therapy and the need to have it present within precision therapy models. One could question the validity of a drug screen performed in a model where there is no TME present. Within the co-culture model of Tsai et al, 2018 it would be interesting to assess whether further Gemcitabine resistance is noted as the variety of the TME is re-established (Tsai et al., 2018). Within our avatar model we have demonstrated that the diversity of the TME is preserved (with a stromal element, ECM and immune component) and maintained during ex vivo culture. An advantage of our model is that the original TME of the tumour is not perturbed. In contrast to the organoid creation protocol, the original tissue is dissociated (through manual and enzymatic processing) into isolated individual components prior to being cultured and an attempt to scale back to the original tissue is undertaken (Maenhoudt et al., 2021). However, within the avatars there is minimal modification to the tissue following the acquisition of the patients' tumour. The avatars are in essence miniature versions of the original tumour and therefore we believe our model allows for a better representation of the tumour and TME for ex vivo study.

3) Financial cost

As with any precision therapy model, understanding the cost of establishing and maintaining the system is important. This is especially true in the context of being able to use the technology as a therapeutic adjunct and as a standard of care for all patients. In light of the increased incidence in PDAC diagnosis globally, there must be an equilibrium between the costing and therapeutic benefit of the system. The appeal of using PDX models for precision therapy is the ability to be able to work with 3D, multicellular tumours that provide a good representation of the primary tumour. However there is a significant financial burden associated with the PDX model. Not only is there a cost for each individual mouse for tumour implantation, but there are ongoing costs following the creation of the PDX model including fees associated with housing, maintenance and aftercare. In addition there is a requirement for frequent daily monitoring of the PDXs which is both time and labour intensive. The appeal of using patient derived cell lines or organoids is the relatively inexpensive cost of creation and maintenance. However the clear compromise is the relatively simple representation of the primary tumour. Patient derived cancer avatars are an inexpensive model for precision therapy, especially when compared to PDX models. By far the biggest cost of the system is the initial acquisition of the mechanical pumps, however the creation and maintenance of the avatars are of minimal cost. Automated programming of the mechanical pumps permits continuous perfusion and as such there is minimal daily labour requirement for maintenance. Therefore the avatar system benefits from inexpensive costing without losing the complexity of the model and the diverse and multicellular representation of the primary tumour.

8.2 Incorporating patient derived cancer avatars into clinical practice

Our current proposed model for precision therapy can be implemented within clinical practice. However this is specifically in the context of adjuvant therapy (acquisition of tumour following surgery, avatar creation followed by a drug screen to determine adjuvant therapy). There are two other practical scenarios that could benefit from this model; Neo-Adjuvant therapy and in patients with metastatic disease.

8.2.1 Neo-Adjuvant therapy dictated by cancer avatar response.

To date Neo-Adjuvant therapy in PDAC is reserved for patients with borderline resectable tumours or LAPC. Currently there is insufficient evidence to advocate the routine use of Neo-Adjuvant therapy for all patients with resectable disease. However in the future, it is conceivable that Neo-Adjuvant therapy could become a standard of care for resectable disease. The PREOPANC trial from the Dutch Pancreatic Cancer Research Group was an RCT evaluating preoperative chemoradiotherapy against upfront surgery in resectable and borderline PDAC (Versteijne et al., 2020). Despite the trial failing to show a difference in their primary outcome measure (overall survival by intention to treat analysis), their secondary outcome measures suggested an advantage to Neo-Adjuvant therapy (Versteijne et al., 2020). This included higher rates of R0 resection, lower incidence of pathological

lymph node involvement and lymphovascular invasion, in addition to an improved disease-free survival rate (Versteijne et al., 2020). One of the main criticisms of the trial was their use of Gemcitabine based chemoradiotherapy as Neo-Adjuvant therapy. This is not a regime that is truly representative of current clinical practice, especially in the modern era of multimodal chemotherapy regimes (notably FOLFIRINOX). This provided the rationale for creating PREOPANC2 trial, where FOLFIRINOX would be evaluated as Neo-Adjuvant therapy (Janssen et al., 2021). In the context of Neo-Adjuvant therapy for borderline resectable tumours or LAPC, the aim of treatment is to downstage the tumour for it to become resectable. Within this setting, it is essential that patients have a good response to therapy in order for them to become surgical candidates. It is therefore conceivable that precision therapy would be extremely important within this context, as one could increase the probability of successful downstaging of the tumour with selected therapies that had a previously detectable therapeutic response within the avatars. Our model could be utilised within this setting. However some modifications to the technique would be required. As we would not have access to the resected specimen, tissue acquisition would be achieved through EUS biopsy. The tissue yield from a biopsy is considerably less. However, recent advances in endoscopic technology have resulted in the development of novel biopsy tools that can obtain a much larger tissue volume biopsy (Bang et al., 2018). As such we could use our current system and technology as a foundation, prior to adapting the technique in order to create avatars on a much smaller scale.

8.2.2 Determining the standard of care for patients with metastatic disease

Unfortunately, the majority of our patients are diagnosed with metastatic, thus incurable disease. For this large cohort of patients, palliative chemotherapy remains as the only treatment option. However, utilising our avatar approach within this setting may also provide a therapeutic benefit. Patients with metastatic disease are often recruited into RCTs and frequently the inclusion criteria mandate a histological diagnosis prior to enrolment. Therefore percutaneous biopsies of metastatic disease burden could form the foundation of tissue acquisition within this patient cohort. Creating avatars in this setting would permit an assessment of palliative chemotherapy treatment regimes. As such the optimal treatment strategy with the lowest side effect profile could be implemented in order to ensure that patients gained a survival benefit with no detrimental impact to their quality of life. In addition, further treatment strategies, as second line therapies, could be identified for use in the context of disease relapse.

8.3 Critical analysis of patient derived cancer avatars as a model for precision therapy.

Patient derived avatar creation serves as an appealing model for precision therapy, however there are some limitations within our current system that merit discussion. Our ability to create numerous avatars is directionally proportional to the size of the core biopsy. With experience and familiarity with the system, on average a minimum of 10 avatars per biopsy was created. The overall yield is smaller when compared to other techniques of precision therapy and as such only a narrow drug screen can be performed. An important consideration is the use and allocation of each avatar within the experimental design. To evaluate specific changes in the avatars over the time course of ex vivo culture, one avatar was extracted at each time point for analysis. However for future experiments, it may be prudent to reduce the number of time points analysed. The advantage of this approach would be that it conserves avatars and would allow pooling of multiple avatars at the same time point. Not only would this allow technical replicates for each time point, but of greater importance it would increase the tissue yield for analysis. This is particularly true with regard to RNA extraction. Due to the small dimension of each avatar (tissue bulk), we encountered a very poor RNA extraction yield, which directly limited our ability to sequence the avatars. Despite trialling different extraction and purification methods, our RNA yield was insufficient for formal sequencing. For future experiments, I would propose pooling of multiple avatars at the same time points in order to be able to perform bulk RNA extraction in an attempt to increase the RNA yield for formal sequencing.

Another important consideration is defining the maximum time period for ex vivo culture. Other groups have reported a much shorter time period for ex vivo culture

of their PDAC explants (6 days) (X. Jiang et al., 2017). This time interval should be dictated by the intended purpose of the experiment. In the context of a drug screen, ex vivo culture should be brief so that therapeutic testing can be commenced and rapidly fed back to the clinic. Within our current system, avatars were cultured to day 12 ex vivo. Whilst we demonstrated that the native cell populations within the avatars remained relatively constant, we did observe decreasing functional properties within the avatars (proliferation rates and mTOR activity). As such, if the experimental aim is to maintain avatars for a prolonged period ex vivo, further modifications to the culture conditions, media composition and perfusion settings would be required.

The main limitation of the avatar model for precision therapy is the heterogeneity between individual tissue slices. Whilst all avatars are created from the same core biopsy, from the same location within the primary tumour, it is likely that not all avatars are identical in nature. Whilst this does not impact our ability to assess function within the avatars or the effect of the drug screen on the tumour, it is important in the context of determining the presence of individual cell types, notably immune infiltrate present. Variation in native immune cell infiltrates or their spatial location between tissue slices could be construed as an effect of an immunotherapy drug modulation or active migration of immune cells ex vivo. What is needed in this context is the ability for live cell tracking, whereby a single avatar can be used for the entire time course of the experiment and under direct visualisation immune cells can be counted and mapped. As such, any changes in overall number or location is due to the experimental conditions instead of tissue slice heterogeneity and variation. In

order to increase the representation of the primary tumour, it would be possible to take several core biopsies from different locations and subsequently turn these into individual avatars for co culture. However PDAC tumours are relatively small, larger tumours are less likely to be resectable and undertaking biopsies from the primary cannot compromise the pathological margins of the tumour. Whilst the stroma within PDAC tumours is heterogenous in nature, there is little spatial heterogeneity of the mutational burden of the primary tumour. When assessing how representative the avatars are of the original tumour, this model overcomes the limitations associated with organoid creation and provides a unique opportunity to study the tumour at a level of detail that was not previously achievable.

8.4 Impact of the Covid-19 pandemic

The global pandemic has significantly impacted on this research project. Our elective pancreatic cancer service drastically decreased during this time and as a direct consequence I was unable to secure any further fresh human tumour. In the 12 months preceding the submission of this thesis, only 2 tumours were secured and subsequently turned into avatars. The lack of tissue acquisition meant that I was unable to complete some previously designed experiments. These included being able to culture additional avatars ex vivo for further validation and for technical replicates. My ambition was to perform a drug screen with a range of chemotherapies (including FOLFIRINOX) however this was not possible. I decided to treat the avatars with the same regime (Gemcitabine) so that a cross comparison

between avatars could be performed. Due to the scarcity of the tissue, I had to prioritise experiments and subsequent analysis. Under normal circumstances (pre-pandemic), I would have been able to utilise several avatars for optimisation purposes of the system. This would have included defining the optimal media composition for culture, whether a bolus of one dose of antimicrobials was required instead of a continuous supplementation (in an attempt to create a more physiological culture media), investigating the heterogeneity between individual avatars and the best settings for perfusion culture. As only three avatars were treated with ex vivo chemotherapy, this provided a limited opportunity to compare the avatars and patients' response. Clearly having more avatars treated would allow a more comprehensive comparison with the clinical outcomes of the patient and provide further validation of the ability of the avatars to predict a response. The Covid-19 pandemic directly impacted on the management of patients with PDAC as demonstrated within this thesis (Chapter 6). Of the three treated avatars ex vivo, only one patient completed adjuvant therapy. Both remaining patients decided not to receive adjuvant therapy. Whilst this is clearly understandable in the midst of a global pandemic (in light of the risk of chemotherapy induced immunosuppression) this is clearly not representative of conventional clinical practice. Both of these patients were fit and well with a good performance status and subsequently would have been candidates for adjuvant therapy. It is known that not all patients following surgical resection of PDAC will receive adjuvant therapy. This ranges from 20-50% depending on the case series (Lambert et al., 2019). The reasons for this are either due to a failure to recover after surgery, age, or frailty (Lambert et al., 2019). It is uncommon for patients to refuse adjuvant therapy out of personal choice in light of

the survival benefit that is associated with adjuvant therapy. During the national lockdown, access to the laboratory was prohibited. I utilised this time to learn bioinformatics skills and constructed another research question regarding precision therapy (Chapter 7). Despite the restrictions of the pandemic, we believe we have been able to demonstrate as proof of principal the clinical application of our system alongside our novel approach of culturing avatars ex vivo under perfusion culture conditions.

8.5 Future work

With the foundations established within this research project to date, there are several additional experimental ideas that could be pursued in the future. Initially, we need to gain a greater experience of treating avatars ex vivo with chemotherapy, not only to increase our sample study size but also to establish a larger repertoire of treated avatars. This would validate their ability of being able to mimic the patient's therapeutic response and provide us with an invaluable resource which we could investigate as to whether it is possible to distinguish any specific characteristics, features or cell types that are predictive of treatment response or failure. Incorporating additional treatment strategies in the ex vivo setting is prudent. This would include multimodal regimes such as FOLFIRINOX or Gemcitabine and Nab-paclitaxel. What would be required is determining how this would be delivered, especially with regard to the dosing regime. Further work should focus on identifying how best to deliver multi agent treatment, whether this would need

individual bolus perfusions of each drug, an infusion all at once or incorporating multiple inflow channels into the perfusion plate to allow concurrent but individual drug delivery. Drawing from clinical practice, another consideration would be as to whether repeated episodes of treatment would be required, in order to replicate the cyclical nature of chemotherapy treatment that patients receive within the clinic.

Being able to formally sequence the avatars would be another extremely useful interrogative ability and should be a focus for future work. In addition, sequencing the avatars both pre and post treatment should be performed, especially once the clinical data had been collected as it would be possible to compare the transcriptomic profile of responders and non responders. Not only would this potentially provide further insight into drug resistance mechanisms but it could be also utilised to investigate further biomarkers either for treatment response or recurrence patterns. These biomarkers could be assessed for at the initial diagnostic biopsy and could subsequently dictate the future treatment algorithm (in terms of timing of systemic therapy and which regime to use). Our initial experience with sequencing the avatars was hindered by the small RNA extraction yield. This is partly due to the dense desmoplastic ECM present within the tumours (and relatively small epithelial component) but predominantly due to the avatar size and subsequent small tissue volume. Pooling multiple avatars for bulk RNA extraction would serve as one possible solution. However such an approach utilises much of our limited resources (in terms of total avatar numbers) and as such may prevent certain experiments from being conducted or reduce the number of time points for analysis following ex vivo culture.

Whilst the system we have presented has been established on the concept of delivering and assessing therapeutic response to chemotherapy treatment, further modifications to its structure may allow it to be utilised to evaluate the effect of immunomodulatory drugs. Immuno-oncology is a rapidly evolving field and immunotherapy has become a standard of care for several cancers. To date, there is no established platform to evaluate the effect of immunomodulation within PDAC tumours within the clinical setting of precision therapy. Currently predicting a response to programmed cell-death receptor (PD-1) and its corresponding ligand (PD-L1) is based upon IHC staining for the previously named inhibitory checkpoint pathway (Cottrell et al., 2018). However there are numerous limitations to this approach ranging from spatial heterogeneity of expression within the tumour to determining the threshold for positivity in addition to antibody performance and sensitivity (Cottrell et al., 2018). This approach also depends on the analysis of stained and fixed tissue (FFPE slides) and as such there is no functional assessment of the immune cells present. As previously discussed, being able to introduce live cell imaging within our system would provide a unique opportunity to obtain functional information of immune cells post immunotherapy treatment in real time. This may identify and provide further insight into the deregulated immune pathways in PDAC that contribute to a relative immunosuppressive state. Another argument as to why the system should be further adapted in order to assess the effect of immunotherapy is the fact that we are unable to modify the composition of the ECM within the avatars. Previous attempts at ECM remodelling within clinical trials have

been unsuccessful. However, this is not true for the immune component within the avatars. Immunomodulation within our system would be possible (through pharmacological manipulation) and should serve as a future research focus. The initial research emphasis should be placed on overcoming the current limitation of the system for immunotherapy evaluation, notably that there is no intact immune system ex vivo. One of the current limitations is that only the immune cell infiltrate present in the tumour at the time of surgical resection will be incorporated within the avatars. There is an inability to recruit additional immune cell infiltrate from secondary lymphoid structures within our current system. One possible option for overcoming this limitation would be to co-culture the avatars with isolated immune cells (peripheral blood mononuclear cells (PBMCs)) obtained from the same patient. PBMCs could be isolated from the patient's whole blood, which is easily accessible pre operatively, and could be perfused into the perfusion plate during ex vivo culture. Dijkstra et al, 2018 published their experience of coculturing patient tumour organoids with peripheral blood lymphocytes from the corresponding patient (Dijkstra et al., 2018). They demonstrated that coculture allowed enrichment of tumour-reactive T cells and that their system allows an assessment of T cell killing of tumour organoids (Dijkstra et al., 2018). Perfusing in PBMCs within our system would allow for an assessment to see whether it would be possible to recruit additional immune cells from within the media and to determine whether immune cell infiltration into the avatar would be possible. This would overcome the current limitations of the system (a finite number of immune cells present within the avatars).

8.6 Conclusion

Within this thesis we present our experience of creating, maintaining and treating cancer avatars and propose that it should be considered as a method for delivering precision therapy for patients with PDAC. Our established avatar protocol allows consistent avatar formation and maximises the creation yield from each core biopsy. Through incorporating perfusion technology within our ex vivo culture system, we are able to recapitulate the physiological conditions of the tumour in vivo and maintain native biological function within the avatars for a prolonged period of time ex vivo. The use of perfusion permits a physiologically representative technique of drug delivery, especially when compared to the conventional method (direct dosing). Our initial experience with ex vivo treatment of cancer avatars with systemic chemotherapy is promising, with a range of therapeutic responses being detected. In addition, upon correlation with the patient's response to therapy a general concordance between patient and avatar response was observed. We envisage that this platform could be incorporated into current clinical practice and delivered in a clinically relevant time frame. The use of cancer avatars will allow us to transition away from the traditional, rigid and binary approach to the systemic treatment of PDAC. We must acknowledge that there should not be a standardised chemotherapy treatment regime for all patients. Treatment should be dictated by the individual biology of the patient's tumour. Age and performance status should

be used as additional adjuncts only, to risk stratify patients for specific treatment regimes. The use of precision therapy recognises the significant heterogeneity between patients and the diversity across all PDAC tumours. Such an approach may finally allow a paradigm shift in survival rates for this lethal disease.

A Appendix

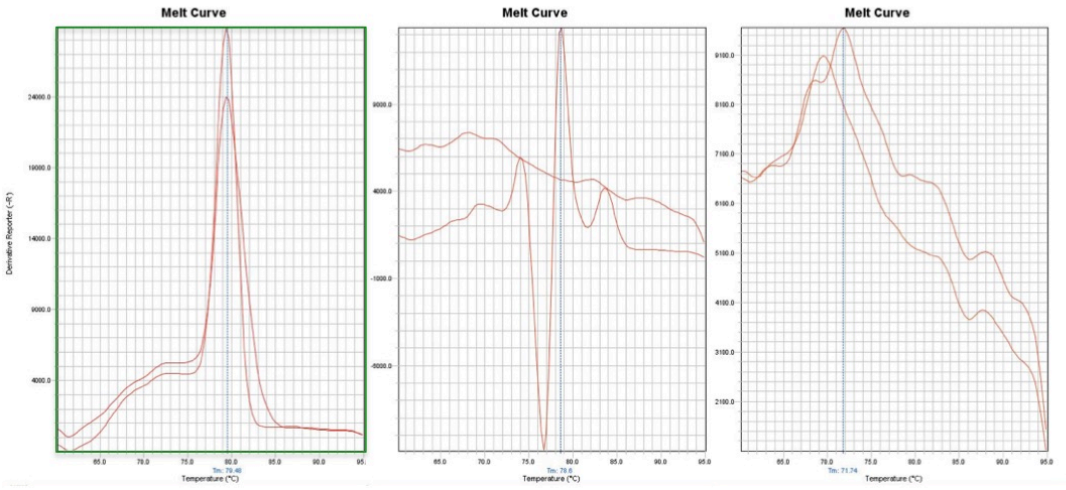

Figure A. 1– Selection process for qPCR primers. Each purchased primer was screened by assessing the melt and dilution curves

Problem		Intervention	Outcome
No access to media		Introduction of a 3 way tap to inflow and outflow	Resolved
Bubble formation		Media, tubing and slide equilibration in incubator for 24 hours prior to set up	Incidence of 'large' bubbles reduced, ongoing very small bubble formation (possibly due to externalised pump or cell metabolism)
Cross communication between channels		Single use of central lane and application of a hydrophobic pen to lid	Problem resolved but wasteful
Displacement of tissue and occlusion of outflow Displacement of Organoids	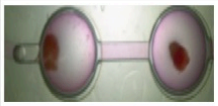	Coating of well in 10,20 and 50% Matrigel	Reduction in total displacement rates, minor migration persists. Outflow occlusion by Matrigel in 2 cases. Peripheral displacement of organoids
Unresolved issues: Difficulty with the 'set up' of the system Size and volume of well impacts on the amount of tissue that can be placed in the Ibidi perfusion slide Access to tissue post experiment			
Conclusion: With modification and appropriate optimization, the ibidi perfusion slide may serve as a suitable system to evaluate the effect of perfusion in monolayer 2D cell culture however caution is required in its application with tissue culture			

Figure A. 2 - Modifications performed on the µ-Slide III 3D Perfusion (Ibidi) to optimise for avatar culture

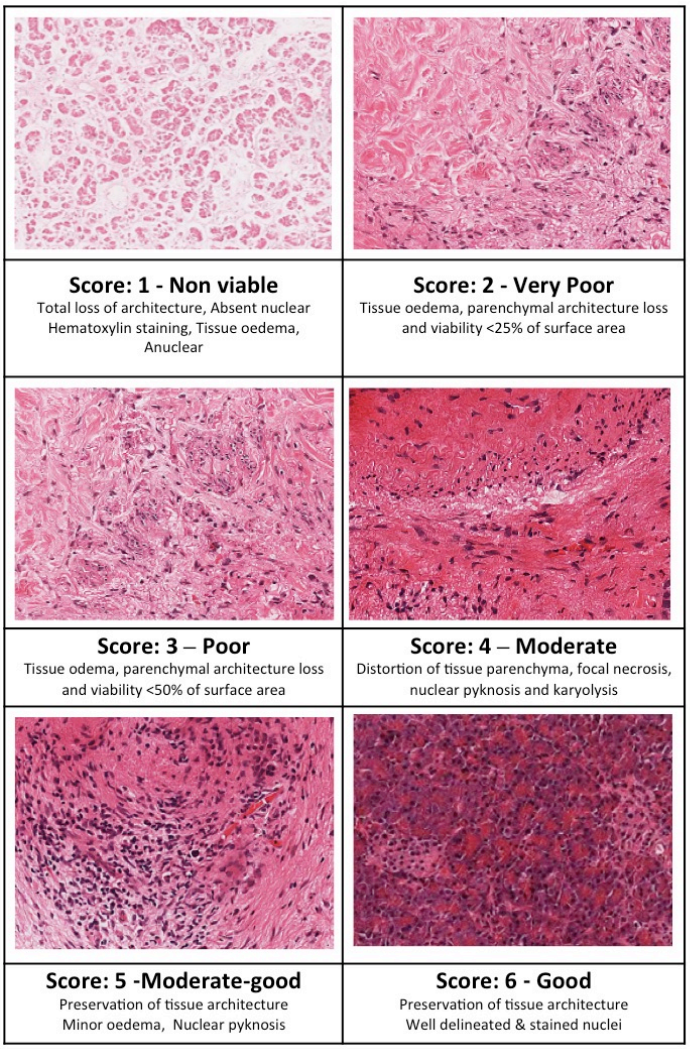

Figure A. 3- Representative H&E images of the tissue viability scoring criteria

Bibliography

Adham, M., Mirza, D. F., Chapuis, F., Mayer, A. D., Bramhall, S. R., Coldham, C., Baulieux, J., & Buckels, J. (2006). Results of vascular resections during pancreatectomy from two European centres: an analysis of survival and disease-free survival explicative factors. *HPB (Oxford), 8*(6), 465-473. doi:10.1080/13651820600839944

Aguirre, A. J., Nowak, J. A., Camarda, N. D., Moffitt, R. A., Ghazani, A. A., Hazar-Rethinam, M., Raghavan, S., Kim, J., Brais, L. K., Ragon, D., Welch, M. W., Reilly, E., McCabe, D., Marini, L., Anderka, K., Helvie, K., Oliver, N., Babic, A., Da Silva, A., Nadres, B., Van Seventer, E. E., Shahzade, H. A., St Pierre, J. P., Burke, K. P., Clancy, T., Cleary, J. M., Doyle, L. A., Jajoo, K., McCleary, N. J., Meyerhardt, J. A., Murphy, J. E., Ng, K., Patel, A. K., Perez, K., Rosenthal, M. H., Rubinson, D. A., Ryou, M., Shapiro, G. I., Sicinska, E., Silverman, S. G., Nagy, R. J., Lanman, R. B., Knoerzer, D., Welsch, D. J., Yurgelun, M. B., Fuchs, C. S., Garraway, L. A., Getz, G., Hornick, J. L., Johnson, B. E., Kulke, M. H., Mayer, R. J., Miller, J. W., Shyn, P. B., Tuveson, D. A., Wagle, N., Yeh, J. J., Hahn, W. C., Corcoran, R. B., Carter, S. L., & Wolpin, B. M. (2018). Real-time Genomic Characterization of Advanced Pancreatic Cancer to Enable Precision Medicine. *Cancer Discov, 8*(9), 1096-1111. doi:10.1158/2159-8290.CD-18-0275

Akram, K. M., Yates, L. L., Mongey, R., Rothery, S., Gaboriau, D. C. A., Sanderson, J., Hind, M., Griffiths, M., & Dean, C. H. (2019). Live imaging of alveologenesis in precision-cut lung slices reveals dynamic epithelial cell behaviour. *Nat Commun, 10*(1), 1178. doi:10.1038/s41467-019-09067-3

Andersson, R., Aho, U., Nilsson, B. I., Peters, G. J., Pastor-Anglada, M., Rasch, W., & Sandvold, M. L. (2009). Gemcitabine chemoresistance in pancreatic cancer: molecular mechanisms and potential solutions. *Scand J Gastroenterol, 44*(7), 782-786. doi:10.1080/00365520902745039

Annaratone, L., Marchio, C., Russo, R., Ciardo, L., Rondon-Lagos, S. M., Goia, M., Scalzo, M. S., Bolla, S., Castellano, I., Verdun di Cantogno, L., Bussolati, G., & Sapino, A. (2013). A collection of primary tissue cultures of tumors from vacuum packed and cooled surgical specimens: a feasibility study. *PLoS One, 8*(9), e75193. doi:10.1371/journal.pone.0075193

Apte, M. V., Pirola, R. C., & Wilson, J. S. (2012). Pancreatic stellate cells: a starring role in normal and diseased pancreas. *Front Physiol, 3*, 344. doi:10.3389/fphys.2012.00344

Are, C., Dhir, M., & Ravipati, L. (2011). History of pancreaticoduodenectomy: early misconceptions, initial milestones and the pioneers. *HPB (Oxford), 13*(6), 377-384. doi:10.1111/j.1477-2574.2011.00305.x

Assifi, M. M., Lu, X., Eibl, G., Reber, H. A., Li, G., & Hines, O. J. (2011). Neoadjuvant therapy in pancreatic adenocarcinoma: a meta-analysis of phase II trials. *Surgery, 150*(3), 466-473. doi:10.1016/j.surg.2011.07.006

Astolfi, M., Peant, B., Lateef, M. A., Rousset, N., Kendall-Dupont, J., Carmona, E., Monet, F., Saad, F., Provencher, D., Mes-Masson, A. M., & Gervais, T. (2016). Micro-dissected tumor tissues on chip: an ex vivo method for drug testing and personalized therapy. *Lab Chip, 16*(2), 312-325. doi:10.1039/c5lc01108f

Atkuri, K. R., Herzenberg, L. A., Niemi, A. K., Cowan, T., & Herzenberg, L. A. (2007). Importance of culturing primary lymphocytes at physiological oxygen levels. *Proc Natl Acad Sci U S A, 104*(11), 4547-4552. doi:10.1073/pnas.0611732104

Atlas, S. J., & Deyo, R. A. (2001). Evaluating and managing acute low back pain in the primary care setting. *J Gen Intern Med, 16*(2), 120-131. doi:10.1111/j.1525-1497.2001.91141.x

Bachem, M. G., Schneider, E., Gross, H., Weidenbach, H., Schmid, R. M., Menke, A., Siech, M., Beger, H., Grunert, A., & Adler, G. (1998). Identification, culture, and characterization of pancreatic stellate cells in rats and humans. *Gastroenterology, 115*(2), 421-432. doi:10.1016/s0016-5085(98)70209-4

Bailey, P., Chang, D. K., Nones, K., Johns, A. L., Patch, A. M., Gingras, M. C., Miller, D. K., Christ, A. N., Bruxner, T. J., Quinn, M. C., Nourse, C., Murtaugh, L. C., Harliwong, I., Idrisoglu, S., Manning, S., Nourbakhsh, E., Wani, S., Fink, L., Holmes, O., Chin, V., Anderson, M. J., Kazakoff, S., Leonard, C., Newell, F., Waddell, N., Wood, S., Xu, Q., Wilson, P. J., Cloonan, N., Kassahn, K. S., Taylor, D., Quek, K., Robertson, A., Pantano, L., Mincarelli, L., Sanchez, L. N., Evers, L., Wu, J., Pinese, M., Cowley, M. J., Jones, M. D., Colvin, E. K., Nagrial, A. M., Humphrey, E. S., Chantrill, L. A., Mawson, A., Humphris, J., Chou, A., Pajic, M., Scarlett, C. J., Pinho, A. V., Giry-Laterriere, M., Rooman, I., Samra, J. S., Kench, J. G., Lovell, J. A., Merrett, N. D., Toon, C. W., Epari, K., Nguyen, N. Q., Barbour, A., Zeps, N., Moran-Jones, K., Jamieson, N. B., Graham, J. S., Duthie, F., Oien, K., Hair, J., Grutzmann, R., Maitra, A., Iacobuzio-Donahue, C. A., Wolfgang, C. L., Morgan, R. A., Lawlor, R. T., Corbo, V., Bassi, C., Rusev, B., Capelli, P., Salvia, R., Tortora, G., Mukhopadhyay, D., Petersen, G. M., Australian Pancreatic Cancer Genome, I., Munzy, D. M., Fisher, W. E., Karim, S. A., Eshleman, J. R., Hruban, R. H., Pilarsky, C., Morton, J. P., Sansom, O. J., Scarpa, A., Musgrove, E. A., Bailey, U. M., Hofmann, O., Sutherland, R. L., Wheeler, D. A., Gill, A. J., Gibbs, R. A., Pearson, J. V., Waddell, N., Biankin, A. V., & Grimmond, S. M. (2016). Genomic analyses identify molecular subtypes of pancreatic cancer. *Nature, 531*(7592), 47-52. doi:10.1038/nature16965

Balcom, J. H. t., Rattner, D. W., Warshaw, A. L., Chang, Y., & Fernandez-del Castillo, C. (2001). Ten-year experience with 733 pancreatic resections: changing indications, older patients, and decreasing length of hospitalization. *Arch Surg, 136*(4), 391-398. doi:10.1001/archsurg.136.4.391

Ballehaninna, U. K., & Chamberlain, R. S. (2012). The clinical utility of serum CA 19-9 in the diagnosis, prognosis and management of pancreatic adenocarcinoma: An evidence based appraisal. *J Gastrointest Oncol, 3*(2), 105-119. doi:10.3978/j.issn.2078-6891.2011.021

Bang, J. Y., Hebert-Magee, S., Navaneethan, U., Hasan, M. K., Hawes, R., & Varadarajulu, S. (2018). EUS-guided fine needle biopsy of pancreatic masses can yield true histology. *Gut, 67*(12), 2081-2084. doi:10.1136/gutjnl-2017-315154

Bengsch F, Knoblock DM, Liu A, McAllister F, Beatty GL. CTLA-4/CD80 pathway regulates T cell infiltration into pancreatic cancer. *Cancer Immunol Immunother*. 2017;66(12):1609-1617. doi:10.1007/s00262-017-2053-4

Bardeesy, N., & DePinho, R. A. (2002). Pancreatic cancer biology and genetics. *Nat Rev Cancer, 2*(12), 897-909. doi:10.1038/nrc949

Basturk, O., Hong, S. M., Wood, L. D., Adsay, N. V., Albores-Saavedra, J., Biankin, A. V., Brosens, L. A., Fukushima, N., Goggins, M., Hruban, R. H., Kato, Y., Klimstra, D. S., Kloppel, G., Krasinskas, A., Longnecker, D. S., Matthaei, H., Offerhaus, G. J., Shimizu, M., Takaori, K., Terris, B., Yachida, S., Esposito, I., Furukawa, T., & Baltimore Consensus, M. (2015). A Revised Classification System and Recommendations From the Baltimore Consensus Meeting for Neoplastic Precursor Lesions in the Pancreas. *Am J Surg Pathol, 39*(12), 1730-1741. doi:10.1097/PAS.0000000000000533

Bertani, F. R., Mozetic, P., Fioramonti, M., Iuliani, M., Ribelli, G., Pantano, F., Santini, D., Tonini, G., Trombetta, M., Businaro, L., Selci, S., & Rainer, A. (2017). Classification of M1/M2-polarized human macrophages by label-free hyperspectral reflectance confocal microscopy and multivariate analysis. *Sci Rep, 7*(1), 8965. doi:10.1038/s41598-017-08121-8

Bertotti, A., Migliardi, G., Galimi, F., Sassi, F., Torti, D., Isella, C., Cora, D., Di Nicolantonio, F., Buscarino, M., Petti, C., Ribero, D., Russolillo, N., Muratore, A., Massucco, P., Pisacane, A., Molinaro, L., Valtorta, E., Sartore-Bianchi, A., Risio, M., Capussotti, L., Gambacorta, M., Siena, S., Medico, E., Sapino, A., Marsoni, S., Comoglio, P. M., Bardelli, A., & Trusolino, L. (2011). A molecularly annotated platform of patient-derived xenografts ("xenopatients") identifies HER2 as an effective therapeutic target in cetuximab-resistant colorectal cancer. *Cancer Discov, 1*(6), 508-523. doi:10.1158/2159-8290.CD-11-0109

Bickford, R. G., & Winton, F. R. (1937). The influence of temperature on the isolated kidney of the dog. *J Physiol, 89*(2), 198-219. doi:10.1113/jphysiol.1937.sp003473

Blando, J., Sharma, A., Higa, M. G., Zhao, H., Vence, L., Yadav, S. S., Kim, J., Sepulveda, A. M., Sharp, M., Maitra, A., Wargo, J., Tetzlaff, M., Broaddus, R., Katz, M. H. G., Varadhachary, G. R., Overman, M., Wang, H., Yee, C., Bernatchez, C., Iacobuzio-Donahue, C., Basu, S., Allison, J. P., & Sharma, P. (2019). Comparison of immune infiltrates in melanoma and pancreatic cancer highlights VISTA as a potential target in pancreatic cancer. *Proc Natl Acad Sci U S A, 116*(5), 1692-1697. doi:10.1073/pnas.1811067116

Boulay, B. R., & Parepally, M. (2014). Managing malignant biliary obstruction in pancreas cancer: choosing the appropriate strategy. *World J Gastroenterol, 20*(28), 9345-9353. doi:10.3748/wjg.v20.i28.9345

Boyiadzis, M. M., Kirkwood, J. M., Marshall, J. L., Pritchard, C. C., Azad, N. S., & Gulley, J. L. (2018). Significance and implications of FDA approval of pembrolizumab for biomarker-defined disease. *J Immunother Cancer, 6*(1), 35. doi:10.1186/s40425-018-0342-x

Brar, G., Blais, E. M., Joseph Bender, R., Brody, J. R., Sohal, D., Madhavan, S., Picozzi, V. J., Hendifar, A. E., Chung, V. M., Halverson, D., Mikhail, S., Matrisian, L. M., Rahib, L., Petricoin, E., & Pishvaian, M. J. (2019). Multi-omic molecular comparison of primary versus metastatic pancreatic tumours. *Br J Cancer, 121*(3), 264-270. doi:10.1038/s41416-019-0507-5

Bray, F., Ferlay, J., Soerjomataram, I., Siegel, R. L., Torre, L. A., & Jemal, A. (2018). Global cancer statistics 2018: GLOBOCAN estimates of incidence and mortality worldwide for 36 cancers in 185 countries. *CA Cancer J Clin, 68*(6), 394-424. doi:10.3322/caac.21492

Bronckaers, A., Balzarini, J., & Liekens, S. (2008). The cytostatic activity of pyrimidine nucleosides is strongly modulated by Mycoplasma hyorhinis infection: Implications for cancer therapy. *Biochem Pharmacol, 76*(2), 188-197. doi:10.1016/j.bcp.2008.04.019

Brunner, M., Maier, K., Rummele, P., Jacobsen, A., Merkel, S., Benard, A., Krautz, C., Kersting, S., Grutzmann, R., & Weber, G. F. (2020). Upregulation of CD20 Positive B-Cells and B-Cell Aggregates in the Tumor Infiltration Zone is Associated with Better Survival of Patients with Pancreatic Ductal Adenocarcinoma. *Int J Mol Sci, 21*(5). doi:10.3390/ijms21051779

Bryant, K. L., Mancias, J. D., Kimmelman, A. C., & Der, C. J. (2014). KRAS: feeding pancreatic cancer proliferation. *Trends Biochem Sci, 39*(2), 91-100. doi:10.1016/j.tibs.2013.12.004

Buras, R. R., Shabahang, M., Davoodi, F., Schumaker, L. M., Cullen, K. J., Byers, S., Nauta, R. J., & Evans, S. R. (1995). The effect of extracellular calcium on colonocytes: evidence for differential responsiveness based upon degree of cell differentiation. *Cell Prolif, 28*(4), 245-262. doi:10.1111/j.1365-2184.1995.tb00067.x

Burris, H. A., 3rd, Moore, M. J., Andersen, J., Green, M. R., Rothenberg, M. L., Modiano, M. R., Cripps, M. C., Portenoy, R. K., Storniolo, A. M., Tarassoff, P., Nelson, R., Dorr, F. A., Stephens, C. D., & Von Hoff, D. D. (1997). Improvements in survival and clinical benefit with gemcitabine as first-line therapy for patients with advanced pancreas cancer: a randomized trial. *J Clin Oncol, 15*(6), 2403-2413. doi:10.1200/JCO.1997.15.6.2403

Calzia E., I. Z., Radermacher P. (2005). *Determinants of Blood Flow and Organ Perfusion* (Vol. 42). Berlin, Heidelberg: Springer.

Cantor, J. R., Abu-Remaileh, M., Kanarek, N., Freinkman, E., Gao, X., Louissaint, A., Jr., Lewis, C. A., & Sabatini, D. M. (2017). Physiologic Medium Rewires Cellular Metabolism and Reveals Uric Acid as an Endogenous Inhibitor of UMP Synthase. *Cell, 169*(2), 258-272 e217. doi:10.1016/j.cell.2017.03.023

Carreras-Puigvert, J., Zitnik, M., Jemth, A. S., Carter, M., Unterlass, J. E., Hallstrom, B., Loseva, O., Karem, Z., Calderon-Montano, J. M., Lindskog, C., Edqvist, P. H., Matuszewski, D. J., Ait Blal, H., Berntsson, R. P. A., Haggblad, M., Martens, U., Studham, M., Lundgren, B., Wahlby, C., Sonnhammer, E. L. L., Lundberg, E., Stenmark, P., Zupan, B., & Helleday, T. (2017). A comprehensive structural, biochemical and biological profiling of the human NUDIX hydrolase family. *Nat Commun, 8*(1), 1541. doi:10.1038/s41467-017-01642-w

Carstens, J. L., Correa de Sampaio, P., Yang, D., Barua, S., Wang, H., Rao, A., Allison, J. P., LeBleu, V. S., & Kalluri, R. (2017). Spatial computation of intratumoral

T cells correlates with survival of patients with pancreatic cancer. *Nat Commun, 8*, 15095. doi:10.1038/ncomms15095

Catenacci, D. V., Junttila, M. R., Karrison, T., Bahary, N., Horiba, M. N., Nattam, S. R., Marsh, R., Wallace, J., Kozloff, M., Rajdev, L., Cohen, D., Wade, J., Sleckman, B., Lenz, H. J., Stiff, P., Kumar, P., Xu, P., Henderson, L., Takebe, N., Salgia, R., Wang, X., Stadler, W. M., de Sauvage, F. J., & Kindler, H. L. (2015). Randomized Phase Ib/II Study of Gemcitabine Plus Placebo or Vismodegib, a Hedgehog Pathway Inhibitor, in Patients With Metastatic Pancreatic Cancer. *J Clin Oncol, 33*(36), 4284-4292. doi:10.1200/JCO.2015.62.8719

Chakraborty, S., & Singh, S. (2013). Surgical resection improves survival in pancreatic cancer patients without vascular invasion- a population based study. *Ann Gastroenterol, 26*(4), 346-352.

Cheah, L. T., Dou, Y. H., Seymour, A. M., Dyer, C. E., Haswell, S. J., Wadhawan, J. D., & Greenman, J. (2010). Microfluidic perfusion system for maintaining viable heart tissue with real-time electrochemical monitoring of reactive oxygen species. *Lab Chip, 10*(20), 2720-2726. doi:10.1039/c004910g

Chen, Y., Yu, Q., & Xu, C.-B. A convenient method for quantifying collagen fibers in atherosclerotic lesions by ImageJ software. *Int J Clin Exp Med, 10*(10), 14904-14910.

Choi HJ, N. T., Song H, Chang CH, Kim GM. (2020). Fabrication of Microfluidic Cell Culture Platform for Real-time Monitoring of Lidocaine Concentration. *Int. J. Precis. Eng. Manuf, 21*, 2399–2405

ClinicalTrials.gov. (2020). Pancreatic Adenocarcinoma Signature Stratification for Treatment (PASS-01).

Collisson, E. A., Sadanandam, A., Olson, P., Gibb, W. J., Truitt, M., Gu, S., Cooc, J., Weinkle, J., Kim, G. E., Jakkula, L., Feiler, H. S., Ko, A. H., Olshen, A. B., Danenberg, K. L., Tempero, M. A., Spellman, P. T., Hanahan, D., & Gray, J. W. (2011). Subtypes of pancreatic ductal adenocarcinoma and their differing responses to therapy. *Nat Med, 17*(4), 500-503. doi:10.1038/nm.2344

Conroy, T., Desseigne, F., Ychou, M., Bouche, O., Guimbaud, R., Becouarn, Y., Adenis, A., Raoul, J. L., Gourgou-Bourgade, S., de la Fouchardiere, C., Bennouna, J., Bachet, J. B., Khemissa-Akouz, F., Pere-Verge, D., Delbaldo, C., Assenat, E., Chauffert, B., Michel, P., Montoto-Grillot, C., Ducreux, M., Groupe Tumeurs Digestives of, U., & Intergroup, P. (2011). FOLFIRINOX versus gemcitabine for metastatic pancreatic cancer. *N Engl J Med, 364*(19), 1817-1825. doi:10.1056/NEJMoa1011923

Conroy, T., Hammel, P., Hebbar, M., Ben Abdelghani, M., Wei, A. C., Raoul, J. L., Chone, L., Francois, E., Artru, P., Biagi, J. J., Lecomte, T., Assenat, E., Faroux, R., Ychou, M., Volet, J., Sauvanet, A., Breysacher, G., Di Fiore, F., Cripps, C., Kavan, P., Texereau, P., Bouhier-Leporrier, K., Khemissa-Akouz, F., Legoux, J. L., Juzyna, B., Gourgou, S., O'Callaghan, C. J., Jouffroy-Zeller, C., Rat, P., Malka, D., Castan, F., Bachet, J. B., Canadian Cancer Trials, G., & the Unicancer, G. I. P. G. (2018). FOLFIRINOX or Gemcitabine as Adjuvant Therapy for Pancreatic Cancer. *N Engl J Med, 379*(25), 2395-2406. doi:10.1056/NEJMoa1809775

Cook, N. R. (2010). Methods for evaluating novel biomarkers - a new paradigm. *Int J Clin Pract, 64*(13), 1723-1727. doi:10.1111/j.1742-1241.2010.02469.x

Costa-Silva, J., Domingues, D., & Lopes, F. M. (2017). RNA-Seq differential expression analysis: An extended review and a software tool. *PLoS One, 12*(12), e0190152. doi:10.1371/journal.pone.0190152

Cottrell, T. R., & Taube, J. M. (2018). PD-L1 and Emerging Biomarkers in Immune Checkpoint Blockade Therapy. *Cancer J, 24*(1), 41-46. doi:10.1097/PPO.0000000000000301

Damanakis, A. I., Ostertag, L., Waldschmidt, D., Kutting, F., Quaas, A., Plum, P., Bruns, C. J., Gebauer, F., & Popp, F. (2019). Proposal for a definition of "Oligometastatic disease in pancreatic cancer". *BMC Cancer, 19*(1), 1261. doi:10.1186/s12885-019-6448-9

Datta, P., Dey, M., Ataie, Z. *et al.* 3D bioprinting for reconstituting the cancer microenvironment. *npj Precis. Onc.* **4**, 18 (2020). https://doi.org/10.1038/s41698-020-0121-2

Davies, E. J., Dong, M., Gutekunst, M., Narhi, K., van Zoggel, H. J., Blom, S., Nagaraj, A., Metsalu, T., Oswald, E., Erkens-Schulze, S., Delgado San Martin, J. A., Turkki, R., Wedge, S. R., af Hallstrom, T. M., Schueler, J., van Weerden, W. M., Verschuren, E. W., Barry, S. T., van der Kuip, H., & Hickman, J. A. (2015). Capturing complex tumour biology in vitro: histological and molecular characterisation of precision cut slices. *Sci Rep, 5*, 17187. doi:10.1038/srep17187

Demir, I. E., Jager, C., Schlitter, A. M., Konukiewitz, B., Stecher, L., Schorn, S., Tieftrunk, E., Scheufele, F., Calavrezos, L., Schirren, R., Esposito, I., Weichert, W., Friess, H., & Ceyhan, G. O. (2018). R0 Versus R1 Resection Matters after Pancreaticoduodenectomy, and Less after Distal or Total Pancreatectomy for Pancreatic Cancer. *Ann Surg, 268*(6), 1058-1068. doi:10.1097/SLA.0000000000002345

DeQuach, J. A., Mezzano, V., Miglani, A., Lange, S., Keller, G. M., Sheikh, F., & Christman, K. L. (2010). Simple and high yielding method for preparing tissue specific extracellular matrix coatings for cell culture. *PLoS One, 5*(9), e13039. doi:10.1371/journal.pone.0013039

Deyo, R. A., Rainville, J., & Kent, D. L. (1992). What can the history and physical examination tell us about low back pain? *JAMA, 268*(6), 760-765.

di Magliano, M. P., & Logsdon, C. D. (2013). Roles for KRAS in pancreatic tumor development and progression. *Gastroenterology, 144*(6), 1220-1229. doi:10.1053/j.gastro.2013.01.071

Dijkstra, K. K., Cattaneo, C. M., Weeber, F., Chalabi, M., van de Haar, J., Fanchi, L. F., Slagter, M., van der Velden, D. L., Kaing, S., Kelderman, S., van Rooij, N., van Leerdam, M. E., Depla, A., Smit, E. F., Hartemink, K. J., de Groot, R., Wolkers, M. C., Sachs, N., Snaebjornsson, P., Monkhorst, K., Haanen, J., Clevers, H., Schumacher, T. N., & Voest, E. E. (2018). Generation of Tumor-Reactive T Cells by Co-culture of Peripheral Blood Lymphocytes and Tumor Organoids. *Cell, 174*(6), 1586-1598 e1512. doi:10.1016/j.cell.2018.07.009

Dreyer, S. B., Jamieson, N. B., Cooke, S. L., Valle, J. W., McKay, C. J., Biankin, A. V., & Chang, D. K. (2020). PRECISION-Panc: the Next Generation Therapeutic Development Platform for Pancreatic Cancer. *Clin Oncol (R Coll Radiol), 32*(1), 1-4. doi:10.1016/j.clon.2019.07.011

Driehuis, E., Kretzschmar, K., & Clevers, H. (2020). Establishment of patient-derived cancer organoids for drug-screening applications. *Nat Protoc, 15*(10), 3380-3409. doi:10.1038/s41596-020-0379-4

Duval, D., Demangel, C., Miossec, S., & Geahel, I. (1992). Role of metabolic waste products in the control of cell proliferation and antibody production by mouse hybridoma cells. *Hybridoma, 11*(3), 311-322. doi:10.1089/hyb.1992.11.311

Eckert R, R. D., Burggren W, French K. (2002). *Circulation*. New York: WH Freeman & Co.

Erickson-DiRenzo, E., Sivasankar, M. P., & Thibeault, S. L. (2015). Utility of cell viability assays for use with ex vivo vocal fold epithelial tissue. *Laryngoscope, 125*(5), E180-185. doi:10.1002/lary.25100

Fatehullah, A., Tan, S. H., & Barker, N. (2016). Organoids as an in vitro model of human development and disease. *Nat Cell Biol, 18*(3), 246-254. doi:10.1038/ncb3312

Feig, C., Gopinathan, A., Neesse, A., Chan, D. S., Cook, N., & Tuveson, D. A. (2012). The pancreas cancer microenvironment. *Clin Cancer Res, 18*(16), 4266-4276. doi:10.1158/1078-0432.CCR-11-3114

Fischer, R., Breidert, M., Keck, T., Makowiec, F., Lohrmann, C., & Harder, J. (2012). Early recurrence of pancreatic cancer after resection and during adjuvant chemotherapy. *Saudi J Gastroenterol, 18*(2), 118-121. doi:10.4103/1319-3767.93815

Frantz, C., Stewart, K. M., & Weaver, V. M. (2010). The extracellular matrix at a glance. *J Cell Sci, 123*(Pt 24), 4195-4200. doi:10.1242/jcs.023820

Freeman, B. A., & O'Neil, J. J. (1984). Tissue slices in the study of lung metabolism and toxicology. *Environ Health Perspect, 56*, 51-60. doi:10.1289/ehp.845651

Freund, N. W., & Croughan, M. S. (2018). A Simple Method to Reduce both Lactic Acid and Ammonium Production in Industrial Animal Cell Culture. *Int J Mol Sci, 19*(2). doi:10.3390/ijms19020385

Froeling, F. E. M., Casolino, R., Pea, A., Biankin, A. V., & Chang, D. K. (2021). Molecular Subtyping and Precision Medicine for Pancreatic Cancer. *J Clin Med, 10*(1). doi:10.3390/jcm10010149

Gajria, D., & Chandarlapaty, S. (2011). HER2-amplified breast cancer: mechanisms of trastuzumab resistance and novel targeted therapies. *Expert Rev Anticancer Ther, 11*(2), 263-275. doi:10.1586/era.10.226

Galluzzi, L., Lopez-Soto, A., Kumar, S., & Kroemer, G. (2016). Caspases Connect Cell-Death Signaling to Organismal Homeostasis. *Immunity, 44*(2), 221-231. doi:10.1016/j.immuni.2016.01.020

Galluzzi, L., Vitale, I., Aaronson, S. A., Abrams, J. M., Adam, D., Agostinis, P., Alnemri, E. S., Altucci, L., Amelio, I., Andrews, D. W., Annicchiarico-Petruzzelli, M., Antonov, A. V., Arama, E., Baehrecke, E. H., Barlev, N. A., Bazan, N. G., Bernassola, F., Bertrand, M. J. M., Bianchi, K., Blagosklonny, M. V., Blomgren, K., Borner, C., Boya, P., Brenner, C., Campanella, M., Candi, E., Carmona-Gutierrez, D., Cecconi, F., Chan, F. K., Chandel, N. S., Cheng, E. H., Chipuk, J. E., Cidlowski, J. A., Ciechanover, A., Cohen, G. M., Conrad, M., Cubillos-Ruiz, J. R., Czabotar, P. E., D'Angiolella, V., Dawson, T. M., Dawson, V. L., De Laurenzi, V., De Maria, R., Debatin, K. M., DeBerardinis, R. J., Deshmukh, M., Di Daniele, N., Di Virgilio, F., Dixit, V. M., Dixon, S. J., Duckett, C. S., Dynlacht, B. D., El-Deiry, W. S., Elrod, J. W., Fimia, G. M., Fulda, S., Garcia-Saez, A. J., Garg, A. D., Garrido, C., Gavathiotis, E., Golstein, P., Gottlieb, E., Green, D. R., Greene, L. A., Gronemeyer, H., Gross, A.,

Hajnoczky, G., Hardwick, J. M., Harris, I. S., Hengartner, M. O., Hetz, C., Ichijo, H., Jaattela, M., Joseph, B., Jost, P. J., Juin, P. P., Kaiser, W. J., Karin, M., Kaufmann, T., Kepp, O., Kimchi, A., Kitsis, R. N., Klionsky, D. J., Knight, R. A., Kumar, S., Lee, S. W., Lemasters, J. J., Levine, B., Linkermann, A., Lipton, S. A., Lockshin, R. A., Lopez-Otin, C., Lowe, S. W., Luedde, T., Lugli, E., MacFarlane, M., Madeo, F., Malewicz, M., Malorni, W., Manic, G., Marine, J. C., Martin, S. J., Martinou, J. C., Medema, J. P., Mehlen, P., Meier, P., Melino, S., Miao, E. A., Molkentin, J. D., Moll, U. M., Munoz-Pinedo, C., Nagata, S., Nunez, G., Oberst, A., Oren, M., Overholtzer, M., Pagano, M., Panaretakis, T., Pasparakis, M., Penninger, J. M., Pereira, D. M., Pervaiz, S., Peter, M. E., Piacentini, M., Pinton, P., Prehn, J. H. M., Puthalakath, H., Rabinovich, G. A., Rehm, M., Rizzuto, R., Rodrigues, C. M. P., Rubinsztein, D. C., Rudel, T., Ryan, K. M., Sayan, E., Scorrano, L., Shao, F., Shi, Y., Silke, J., Simon, H. U., Sistigu, A., Stockwell, B. R., Strasser, A., Szabadkai, G., Tait, S. W. G., Tang, D., Tavernarakis, N., Thorburn, A., Tsujimoto, Y., Turk, B., Vanden Berghe, T., Vandenabeele, P., Vander Heiden, M. G., Villunger, A., Virgin, H. W., Vousden, K. H., Vucic, D., Wagner, E. F., Walczak, H., Wallach, D., Wang, Y., Wells, J. A., Wood, W., Yuan, J., Zakeri, Z., Zhivotovsky, B., Zitvogel, L., Melino, G., & Kroemer, G. (2018). Molecular mechanisms of cell death: recommendations of the Nomenclature Committee on Cell Death 2018. *Cell Death Differ, 25*(3), 486-541. doi:10.1038/s41418-017-0012-4

Galuppini, F., Dal Pozzo, C. A., Deckert, J., Loupakis, F., Fassan, M., & Baffa, R. (2019). Tumor mutation burden: from comprehensive mutational screening to the clinic. *Cancer Cell Int, 19*, 209. doi:10.1186/s12935-019-0929-4

Garcia-Montero, A., Vasseur, S., Mallo, G. V., Soubeyran, P., Dagorn, J. C., & Iovanna, J. L. (2001). Expression of the stress-induced p8 mRNA is transiently activated after culture medium change. *Eur J Cell Biol, 80*(11), 720-725. doi:10.1078/0171-9335-00209

Geller, L. T., Barzily-Rokni, M., Danino, T., Jonas, O. H., Shental, N., Nejman, D., Gavert, N., Zwang, Y., Cooper, Z. A., Shee, K., Thaiss, C. A., Reuben, A., Livny, J., Avraham, R., Frederick, D. T., Ligorio, M., Chatman, K., Johnston, S. E., Mosher, C. M., Brandis, A., Fuks, G., Gurbatri, C., Gopalakrishnan, V., Kim, M., Hurd, M. W., Katz, M., Fleming, J., Maitra, A., Smith, D. A., Skalak, M., Bu, J., Michaud, M., Trauger, S. A., Barshack, I., Golan, T., Sandbank, J., Flaherty, K. T., Mandinova, A., Garrett, W. S., Thayer, S. P., Ferrone, C. R., Huttenhower, C., Bhatia, S. N., Gevers, D., Wargo, J. A., Golub, T. R., & Straussman, R. (2017). Potential role of intratumor bacteria in mediating tumor resistance to the chemotherapeutic drug gemcitabine. *Science, 357*(6356), 1156-1160. doi:10.1126/science.aah5043

Georgakopoulos, N., Prior, N., Angres, B., Mastrogiovanni, G., Cagan, A., Harrison, D., Hindley, C. J., Arnes-Benito, R., Liau, S. S., Curd, A., Ivory, N., Simons, B. D., Martincorena, I., Wurst, H., Saeb-Parsy, K., & Huch, M. (2020). Long-term expansion, genomic stability and in vivo safety of adult human pancreas organoids. *BMC Dev Biol, 20*(1), 4. doi:10.1186/s12861-020-0209-5

Gerlach, M. M., Merz, F., Wichmann, G., Kubick, C., Wittekind, C., Lordick, F., Dietz, A., & Bechmann, I. (2014). Slice cultures from head and neck squamous cell carcinoma: a novel test system for drug susceptibility and

mechanisms of resistance. *Br J Cancer, 110*(2), 479-488. doi:10.1038/bjc.2013.700
Gillen, S., Schuster, T., Meyer Zum Buschenfelde, C., Friess, H., & Kleeff, J. (2010). Preoperative/neoadjuvant therapy in pancreatic cancer: a systematic review and meta-analysis of response and resection percentages. *PLoS Med, 7*(4), e1000267. doi:10.1371/journal.pmed.1000267
Glacken, M. W., Fleischaker, R. J., & Sinskey, A. J. (1986). Reduction of waste product excretion via nutrient control: Possible strategies for maximizing product and cell yields on serum in cultures of mammalian cells. *Biotechnol Bioeng, 28*(9), 1376-1389. doi:10.1002/bit.260280912
Go, K. L., Delitto, D., Judge, S. M., Gerber, M. H., George, T. J., Jr., Behrns, K. E., Hughes, S. J., Judge, A. R., & Trevino, J. G. (2017). Orthotopic Patient-Derived Pancreatic Cancer Xenografts Engraft Into the Pancreatic Parenchyma, Metastasize, and Induce Muscle Wasting to Recapitulate the Human Disease. *Pancreas, 46*(6), 813-819. doi:10.1097/MPA.0000000000000843
Goodhead, B. (1969). Blood flow in different areas of the gastrointestinal tract in the anesthetized dog. *Can J Physiol Pharmacol, 47*(9), 787-790. doi:10.1139/y69-132
Goonetilleke, K. S., & Siriwardena, A. K. (2007). Systematic review of carbohydrate antigen (CA 19-9) as a biochemical marker in the diagnosis of pancreatic cancer. *Eur J Surg Oncol, 33*(3), 266-270. doi:10.1016/j.ejso.2006.10.004
Greenhalf, W., Ghaneh, P., Neoptolemos, J. P., Palmer, D. H., Cox, T. F., Lamb, R. F., Garner, E., Campbell, F., Mackey, J. R., Costello, E., Moore, M. J., Valle, J. W., McDonald, A. C., Carter, R., Tebbutt, N. C., Goldstein, D., Shannon, J., Dervenis, C., Glimelius, B., Deakin, M., Charnley, R. M., Lacaine, F., Scarfe, A. G., Middleton, M. R., Anthoney, A., Halloran, C. M., Mayerle, J., Olah, A., Jackson, R., Rawcliffe, C. L., Scarpa, A., Bassi, C., Buchler, M. W., & European Study Group for Pancreatic, C. (2014). Pancreatic cancer hENT1 expression and survival from gemcitabine in patients from the ESPAC-3 trial. *J Natl Cancer Inst, 106*(1), djt347. doi:10.1093/jnci/djt347
Groot, V. P., Rezaee, N., Wu, W., Cameron, J. L., Fishman, E. K., Hruban, R. H., Weiss, M. J., Zheng, L., Wolfgang, C. L., & He, J. (2018). Patterns, Timing, and Predictors of Recurrence Following Pancreatectomy for Pancreatic Ductal Adenocarcinoma. *Ann Surg, 267*(5), 936-945. doi:10.1097/SLA.0000000000002234
Gudapati, H., Dey, M. & Ozbolat, I. A comprehensive review on droplet-based bioprinting: past, present and future. *Biomaterials* **102**, 20–42 (2016).
Gutierrez, C., & Schiff, R. (2011). HER2: biology, detection, and clinical implications. *Arch Pathol Lab Med, 135*(1), 55-62. doi:10.1043/2010-0454-RAR.110.5858/2010-0454-RAR.1
Hackert, T., Niesen, W., Hinz, U., Tjaden, C., Strobel, O., Ulrich, A., Michalski, C. W., & Buchler, M. W. (2017). Radical surgery of oligometastatic pancreatic cancer. *Eur J Surg Oncol, 43*(2), 358-363. doi:10.1016/j.ejso.2016.10.023
Haeno, H., Gonen, M., Davis, M. B., Herman, J. M., Iacobuzio-Donahue, C. A., & Michor, F. (2012). Computational modeling of pancreatic cancer reveals kinetics of metastasis suggesting optimum treatment strategies. *Cell, 148*(1-2), 362-375. doi:10.1016/j.cell.2011.11.060

Hamid, O., Robert, C., Daud, A., Hodi, F. S., Hwu, W. J., Kefford, R., Wolchok, J. D., Hersey, P., Joseph, R. W., Weber, J. S., Dronca, R., Gangadhar, T. C., Patnaik, A., Zarour, H., Joshua, A. M., Gergich, K., Elassaiss-Schaap, J., Algazi, A., Mateus, C., Boasberg, P., Tumeh, P. C., Chmielowski, B., Ebbinghaus, S. W., Li, X. N., Kang, S. P., & Ribas, A. (2013). Safety and tumor responses with lambrolizumab (anti-PD-1) in melanoma. *N Engl J Med, 369*(2), 134-144. doi:10.1056/NEJMoa1305133

Hanahan, D., & Weinberg, R. A. (2011). Hallmarks of cancer: the next generation. *Cell, 144*(5), 646-674. doi:10.1016/j.cell.2011.02.013

Hanna, R. N., Chodaczek, G., & Hedrick, C. C. (2016). In vivo Imaging of Tumor and Immune Cell Interactions in the Lung. *Bio Protoc, 6*(20). doi:10.21769/BioProtoc.1973

Hay, N., & Sonenberg, N. (2004). Upstream and downstream of mTOR. *Genes Dev, 18*(16), 1926-1945. doi:10.1101/gad.1212704

He, J., Blair, A. B., Groot, V. P., Javed, A. A., Burkhart, R. A., Gemenetzis, G., Hruban, R. H., Waters, K. M., Poling, J., Zheng, L., Laheru, D., Herman, J. M., Makary, M. A., Weiss, M. J., Cameron, J. L., & Wolfgang, C. L. (2018). Is a Pathological Complete Response Following Neoadjuvant Chemoradiation Associated With Prolonged Survival in Patients With Pancreatic Cancer? *Ann Surg, 268*(1), 1-8. doi:10.1097/SLA.0000000000002672

He, J., Page, A. J., Weiss, M., Wolfgang, C. L., Herman, J. M., & Pawlik, T. M. (2014). Management of borderline and locally advanced pancreatic cancer: where do we stand? *World J Gastroenterol, 20*(9), 2255-2266. doi:10.3748/wjg.v20.i9.2255

Heinrich, S., Besselink, M., Moehler, M., van Laethem, J. L., Ducreux, M., Grimminger, P., Mittler, J., Lang, H., Lutz, M. P., Lesurtel, M., Scientific, Research Committee of the, E. A., & the, E. p. w. g. (2019). Opinions and use of neoadjuvant therapy for resectable, borderline resectable, and locally advanced pancreatic cancer: international survey and case-vignette study. *BMC Cancer, 19*(1), 675. doi:10.1186/s12885-019-5889-5

Henry, O., Kwok, E., & Piret, J. M. (2008). Simpler noninstrumented batch and semicontinuous cultures provide mammalian cell kinetic data comparable to continuous and perfusion cultures. *Biotechnol Prog, 24*(4), 921-931. doi:10.1002/btpr.17

Hidalgo, M., Cascinu, S., Kleeff, J., Labianca, R., Lohr, J. M., Neoptolemos, J., Real, F. X., Van Laethem, J. L., & Heinemann, V. (2015). Addressing the challenges of pancreatic cancer: future directions for improving outcomes. *Pancreatology, 15*(1), 8-18. doi:10.1016/j.pan.2014.10.001

Hirooka, Y.; Kasuya, H.; Ishikawa, T.; Kawashima, H.; Ohno, E.; Villalobos, I.B.; Naoe, Y.; Ichinose, T.; Koyama, N.; Tanaka, M.; et al. A Phase I clinical trial of EUS-guided intratumoral injection of the oncolytic virus, HF10 for unresectable locally advanced pancreatic cancer. BMC Cancer 2018, 18, 1–9.

Holliday, D. L., Moss, M. A., Pollock, S., Lane, S., Shaaban, A. M., Millican-Slater, R., Nash, C., Hanby, A. M., & Speirs, V. (2013). The practicalities of using tissue slices as preclinical organotypic breast cancer models. *J Clin Pathol, 66*(3), 253-255. doi:10.1136/jclinpath-2012-201147

Hruban, R. H., Adsay, N. V., Albores-Saavedra, J., Compton, C., Garrett, E. S., Goodman, S. N., Kern, S. E., Klimstra, D. S., Kloppel, G., Longnecker, D. S.,

Luttges, J., & Offerhaus, G. J. (2001). Pancreatic intraepithelial neoplasia: a new nomenclature and classification system for pancreatic duct lesions. *Am J Surg Pathol, 25*(5), 579-586. doi:10.1097/00000478-200105000-00003

Hruban, R. H., Maitra, A., Kern, S. E., & Goggins, M. (2007). Precursors to pancreatic cancer. *Gastroenterol Clin North Am, 36*(4), 831-849, vi. doi:10.1016/j.gtc.2007.08.012

Huang, H., & Brekken, R. A. (2019). The Next Wave of Stroma-Targeting Therapy in Pancreatic Cancer. *Cancer Res, 79*(2), 328-330. doi:10.1158/0008-5472.CAN-18-3751

Huang, L., Jansen, L., Balavarca, Y., Babaei, M., van der Geest, L., Lemmens, V., Van Eycken, L., De Schutter, H., Johannesen, T. B., Primic-Zakelj, M., Zadnik, V., Besselink, M. G., Schrotz-King, P., & Brenner, H. (2018). Stratified survival of resected and overall pancreatic cancer patients in Europe and the USA in the early twenty-first century: a large, international population-based study. *BMC Med, 16*(1), 125. doi:10.1186/s12916-018-1120-9

Huang, W., Navarro-Serer, B., Jeong, Y. J., Chianchiano, P., Xia, L., Luchini, C., Veronese, N., Dowiak, C., Ng, T., Trujillo, M. A., Huang, B., Pfluger, M. J., Macgregor-Das, A. M., Lionheart, G., Jones, D., Fujikura, K., Nguyen-Ngoc, K. V., Neumann, N. M., Groot, V. P., Hasanain, A., van Oosten, A. F., Fischer, S. E., Gallinger, S., Singhi, A. D., Zureikat, A. H., Brand, R. E., Gaida, M. M., Heinrich, S., Burkhart, R. A., He, J., Wolfgang, C. L., Goggins, M. G., Thompson, E. D., Roberts, N. J., Ewald, A. J., & Wood, L. D. (2020). Pattern of Invasion in Human Pancreatic Cancer Organoids Is Associated with Loss of SMAD4 and Clinical Outcome. *Cancer Res, 80*(13), 2804-2817. doi:10.1158/0008-5472.CAN-19-1523

Hughes, D. L., Hughes, A., Soonawalla, Z., Mukherjee, S., & O'Neill, E. (2021). Dynamic Physiological Culture of Ex Vivo Human Tissue: A Systematic Review. *Cancers (Basel), 13*(12). doi:10.3390/cancers13122870

Ierano, C., Nankervis, J. M., James, R., Rajkhowa, A., Peel, T., & Thursky, K. (2017). Surgical antimicrobial prophylaxis. *Aust Prescr, 40*(6), 225-229. doi:10.18773/austprescr.2017.073

Iwanicki-Caron, I., Basile, P., Toure, E., Antonietti, M., Lecleire, S., Di Fiore, A., Oden-Gangloff, A., Blanchard, F., Lemoine, F., Di Fiore, F., Sabourin, J. C., & Michel, P. (2013). Usefulness of circulating tumor cell detection in pancreatic adenocarcinoma diagnosis. *Am J Gastroenterol, 108*(1), 152-155. doi:10.1038/ajg.2012.367

Janssen, Q. P., van Dam, J. L., Bonsing, B. A., Bos, H., Bosscha, K. P., Coene, P., van Eijck, C. H. J., de Hingh, I., Karsten, T. M., van der Kolk, M. B., Patijn, G. A., Liem, M. S. L., van Santvoort, H. C., Loosveld, O. J. L., de Vos-Geelen, J., Zonderhuis, B. M., Homs, M. Y. V., van Tienhoven, G., Besselink, M. G., Wilmink, J. W., Groot Koerkamp, B., & Dutch Pancreatic Cancer, G. (2021). Total neoadjuvant FOLFIRINOX versus neoadjuvant gemcitabine-based chemoradiotherapy and adjuvant gemcitabine for resectable and borderline resectable pancreatic cancer (PREOPANC-2 trial): study protocol for a nationwide multicenter randomized controlled trial. *BMC Cancer, 21*(1), 300. doi:10.1186/s12885-021-08031-z

Jiang, B., Zhou, L., Lu, J., Wang, Y., Liu, C., You, L., & Guo, J. (2020). Stroma-Targeting Therapy in Pancreatic Cancer: One Coin With Two Sides? *Front Oncol, 10*, 576399. doi:10.3389/fonc.2020.576399

Jiang, S. M., Wu, J. H., & Jia, L. (2012). Intervention of mirtazapine on gemcitabine-induced mild cachexia in nude mice with pancreatic carcinoma xenografts. *World J Gastroenterol, 18*(22), 2867-2871. doi:10.3748/wjg.v18.i22.2867

Jiang, X., Seo, Y. D., Chang, J. H., Coveler, A., Nigjeh, E. N., Pan, S., Jalikis, F., Yeung, R. S., Crispe, I. N., & Pillarisetty, V. G. (2017). Long-lived pancreatic ductal adenocarcinoma slice cultures enable precise study of the immune microenvironment. *Oncoimmunology, 6*(7), e1333210. doi:10.1080/2162402X.2017.1333210

Jochmans, I., Brat, A., Davies, L., Hofker, H. S., van de Leemkolk, F. E. M., Leuvenink, H. G. D., Knight, S. R., Pirenne, J., Ploeg, R. J., Collaboration, C. T., & Consortium for Organ Preservation in, E. (2020). Oxygenated versus standard cold perfusion preservation in kidney transplantation (COMPARE): a randomised, double-blind, paired, phase 3 trial. *Lancet, 396*(10263), 1653-1662. doi:10.1016/S0140-6736(20)32411-9

Jones, R. P., Psarelli, E. E., Jackson, R., Ghaneh, P., Halloran, C. M., Palmer, D. H., Campbell, F., Valle, J. W., Faluyi, O., O'Reilly, D. A., Cunningham, D., Wadsley, J., Darby, S., Meyer, T., Gillmore, R., Anthoney, A., Lind, P., Glimelius, B., Falk, S., Izbicki, J. R., Middleton, G. W., Cummins, S., Ross, P. J., Wasan, H., McDonald, A., Crosby, T., Ting, Y., Patel, K., Sherriff, D., Soomal, R., Borg, D., Sothi, S., Hammel, P., Lerch, M. M., Mayerle, J., Tjaden, C., Strobel, O., Hackert, T., Buchler, M. W., Neoptolemos, J. P., & European Study Group for Pancreatic, C. (2019). Patterns of Recurrence After Resection of Pancreatic Ductal Adenocarcinoma: A Secondary Analysis of the ESPAC-4 Randomized Adjuvant Chemotherapy Trial. *JAMA Surg, 154*(11), 1038-1048. doi:10.1001/jamasurg.2019.3337

Jonker, D. J., O'Callaghan, C. J., Karapetis, C. S., Zalcberg, J. R., Tu, D., Au, H. J., Berry, S. R., Krahn, M., Price, T., Simes, R. J., Tebbutt, N. C., van Hazel, G., Wierzbicki, R., Langer, C., & Moore, M. J. (2007). Cetuximab for the treatment of colorectal cancer. *N Engl J Med, 357*(20), 2040-2048. doi:10.1056/NEJMoa071834

Jung, J., Seol, H. S., & Chang, S. (2018). The Generation and Application of Patient-Derived Xenograft Model for Cancer Research. *Cancer Res Treat, 50*(1), 1-10. doi:10.4143/crt.2017.307

Kamili, A., Gifford, A. J., Li, N., Mayoh, C., Chow, S. O., Failes, T. W., Eden, G. L., Cadiz, R., Xie, J., Lukeis, R. E., Norris, M. D., Haber, M., McCowage, G. B., Arndt, G. M., Trahair, T. N., & Fletcher, J. I. (2020). Accelerating development of high-risk neuroblastoma patient-derived xenograft models for preclinical testing and personalised therapy. *Br J Cancer, 122*(5), 680-691. doi:10.1038/s41416-019-0682-4

Kamphorst, J. J., Nofal, M., Commisso, C., Hackett, S. R., Lu, W., Grabocka, E., Vander Heiden, M. G., Miller, G., Drebin, J. A., Bar-Sagi, D., Thompson, C. B., & Rabinowitz, J. D. (2015). Human pancreatic cancer tumors are nutrient poor and tumor cells actively scavenge extracellular protein. *Cancer Res, 75*(3), 544-553. doi:10.1158/0008-5472.CAN-14-2211

Karamitopoulou, E. (2019). Tumour microenvironment of pancreatic cancer: immune landscape is dictated by molecular and histopathological features. *Br J Cancer, 121*(1), 5-14. doi:10.1038/s41416-019-0479-5

Katsuta, E., Qi, Q., Peng, X., Hochwald, S. N., Yan, L., & Takabe, K. (2019). Pancreatic adenocarcinomas with mature blood vessels have better overall survival. *Sci Rep, 9*(1), 1310. doi:10.1038/s41598-018-37909-5

Kaur, S., Kaur, I., Rawal, P., Tripathi, D. M., & Vasudevan, A. (2021). Non-matrigel scaffolds for organoid cultures. *Cancer Lett, 504*, 58-66. doi:10.1016/j.canlet.2021.01.025

Kim, E. J., Sahai, V., Abel, E. V., Griffith, K. A., Greenson, J. K., Takebe, N., Khan, G. N., Blau, J. L., Craig, R., Balis, U. G., Zalupski, M. M., & Simeone, D. M. (2014). Pilot clinical trial of hedgehog pathway inhibitor GDC-0449 (vismodegib) in combination with gemcitabine in patients with metastatic pancreatic adenocarcinoma. *Clin Cancer Res, 20*(23), 5937-5945. doi:10.1158/1078-0432.CCR-14-1269

Kim, J., Koo, B. K., & Knoblich, J. A. (2020). Human organoids: model systems for human biology and medicine. *Nat Rev Mol Cell Biol, 21*(10), 571-584. doi:10.1038/s41580-020-0259-3

Kim, S. Y., Lee, J. Y., Kim, D. H., Joo, H., Yun, M. R., Jung, D., Yun, J., Heo, S. G., Ahn, B., Park, C. W., Pyo, K. H., Chun, Y. J., Hong, M. H., Kim, H. R., & Cho, B. C. (2019). Patient-Derived Cells to Guide Targeted Therapy for Advanced Lung Adenocarcinoma. *Sci Rep, 9*(1), 19909. doi:10.1038/s41598-019-56356-4

Klein, A. P. (2019). Pancreatic cancer: a growing burden. *Lancet Gastroenterol Hepatol, 4*(12), 895-896. doi:10.1016/S2468-1253(19)30323-1

Klein, F., Puhl, G., Guckelberger, O., Pelzer, U., Pullankavumkal, J. R., Guel, S., Neuhaus, P., & Bahra, M. (2012). The impact of simultaneous liver resection for occult liver metastases of pancreatic adenocarcinoma. *Gastroenterol Res Pract, 2012*, 939350. doi:10.1155/2012/939350

Klinkenbijl, J. H., Jeekel, J., Sahmoud, T., van Pel, R., Couvreur, M. L., Veenhof, C. H., Arnaud, J. P., Gonzalez, D. G., de Wit, L. T., Hennipman, A., & Wils, J. (1999). Adjuvant radiotherapy and 5-fluorouracil after curative resection of cancer of the pancreas and periampullary region: phase III trial of the EORTC gastrointestinal tract cancer cooperative group. *Ann Surg, 230*(6), 776-782; discussion 782-774. doi:10.1097/00000658-199912000-00006

Knight, E., Murray, B., Carnachan, R., & Przyborski, S. (2011). Alvetex(R): polystyrene scaffold technology for routine three dimensional cell culture. *Methods Mol Biol, 695*, 323-340. doi:10.1007/978-1-60761-984-0_20

Koay, E. J., Truty, M. J., Cristini, V., Thomas, R. M., Chen, R., Chatterjee, D., Kang, Y., Bhosale, P. R., Tamm, E. P., Crane, C. H., Javle, M., Katz, M. H., Gottumukkala, V. N., Rozner, M. A., Shen, H., Lee, J. E., Wang, H., Chen, Y., Plunkett, W., Abbruzzese, J. L., Wolff, R. A., Varadhachary, G. R., Ferrari, M., & Fleming, J. B. (2014). Transport properties of pancreatic cancer describe gemcitabine delivery and response. *J Clin Invest, 124*(4), 1525-1536. doi:10.1172/JCI73455

Kodack, D. P., Farago, A. F., Dastur, A., Held, M. A., Dardaei, L., Friboulet, L., von Flotow, F., Damon, L. J., Lee, D., Parks, M., Dicecca, R., Greenberg, M., Kattermann, K. E., Riley, A. K., Fintelmann, F. J., Rizzo, C., Piotrowska, Z., Shaw, A. T., Gainor, J. F., Sequist, L. V., Niederst, M. J., Engelman, J. A., &

Benes, C. H. (2017). Primary Patient-Derived Cancer Cells and Their Potential for Personalized Cancer Patient Care. *Cell Rep, 21*(11), 3298-3309. doi:10.1016/j.celrep.2017.11.051

Kokkinos, J., Sharbeen, G., Haghighi, K.S. *et al.* Ex vivo culture of intact human patient derived pancreatic tumour tissue. *Sci Rep* **11**, 1944 (2021). https://doi.org/10.1038/s41598-021-81299-0

Konduri, S., Xing, Y., Warnock, J. N., He, Z., & Yoganathan, A. P. (2005). Normal physiological conditions maintain the biological characteristics of porcine aortic heart valves: an ex vivo organ culture study. *Ann Biomed Eng, 33*(9), 1158-1166. doi:10.1007/s10439-005-5506-4

Konig, J., Hartel, M., Nies, A. T., Martignoni, M. E., Guo, J., Buchler, M. W., Friess, H., & Keppler, D. (2005). Expression and localization of human multidrug resistance protein (ABCC) family members in pancreatic carcinoma. *Int J Cancer, 115*(3), 359-367. doi:10.1002/ijc.20831

Koong, A. C., Mehta, V. K., Le, Q. T., Fisher, G. A., Terris, D. J., Brown, J. M., Bastidas, A. J., & Vierra, M. (2000). Pancreatic tumors show high levels of hypoxia. *Int J Radiat Oncol Biol Phys, 48*(4), 919-922. doi:10.1016/s0360-3016(00)00803-8

Kromrey, M. L., Bulow, R., Hubner, J., Paperlein, C., Lerch, M. M., Ittermann, T., Volzke, H., Mayerle, J., & Kuhn, J. P. (2018). Prospective study on the incidence, prevalence and 5-year pancreatic-related mortality of pancreatic cysts in a population-based study. *Gut, 67*(1), 138-145. doi:10.1136/gutjnl-2016-313127

La Torre, M., Nigri, G., Ferrari, L., Cosenza, G., Ravaioli, M., & Ramacciato, G. (2012). Hospital volume, margin status, and long-term survival after pancreaticoduodenectomy for pancreatic adenocarcinoma. *Am Surg, 78*(2), 225-229.

Lambert, A., Schwarz, L., Borbath, I., Henry, A., Van Laethem, J. L., Malka, D., Ducreux, M., & Conroy, T. (2019). An update on treatment options for pancreatic adenocarcinoma. *Ther Adv Med Oncol, 11*, 1758835919875568. doi:10.1177/1758835919875568

Langer EM, Allen-Petersen BL, King SM, Kendsersky ND, Turnidge MA, Kuziel GM, Riggers R, Samatham R, Amery TS, Jacques SL, Sheppard BC, Korkola JE, Muschler JL, Thibault G, Chang YH, Gray JW, Presnell SC, Nguyen DG, Sears RC. Modeling Tumor Phenotypes In Vitro with Three-Dimensional Bioprinting. Cell Rep. 2019 Jan 15;26(3):608-623.e6. doi: 10.1016/j.celrep.2018.12.090. PMID: 30650355; PMCID: PMC6366459.

Lao, M. S., & Toth, D. (1997). Effects of ammonium and lactate on growth and metabolism of a recombinant Chinese hamster ovary cell culture. *Biotechnol Prog, 13*(5), 688-691. doi:10.1021/bp9602360

Laplante, M., & Sabatini, D. M. (2012). mTOR signaling in growth control and disease. *Cell, 149*(2), 274-293. doi:10.1016/j.cell.2012.03.017

Lee, P. J., Podugu, A., Wu, D., Lee, A. C., Stevens, T., & Windsor, J. A. (2018). Preoperative biliary drainage in resectable pancreatic cancer: a systematic review and network meta-analysis. *HPB (Oxford), 20*(6), 477-486. doi:10.1016/j.hpb.2017.12.007

Leppanen, J., Lindholm, V., Isohookana, J., Haapasaari, K. M., Karihtala, P., Lehenkari, P. P., Saarnio, J., Kauppila, J. H., Karttunen, T. J., Helminen, O., & Huhta, H. (2019). Tenascin C, Fibronectin, and Tumor-Stroma Ratio in

Pancreatic Ductal Adenocarcinoma. *Pancreas, 48*(1), 43-48. doi:10.1097/MPA.0000000000001195
Li, X. X., Liu, Y. M., Li, Y. J., Xie, N., Yan, Y. F., Chi, Y. L., Zhou, L., Xie, S. Y., & Wang, P. Y. (2016). High glucose concentration induces endothelial cell proliferation by regulating cyclin-D2-related miR-98. *J Cell Mol Med, 20*(6), 1159-1169. doi:10.1111/jcmm.12765
Liang, C., Shi, S., Meng, Q., Liang, D., Ji, S., Zhang, B., Qin, Y., Xu, J., Ni, Q., & Yu, X. (2017). Complex roles of the stroma in the intrinsic resistance to gemcitabine in pancreatic cancer: where we are and where we are going. *Exp Mol Med, 49*(12), e406. doi:10.1038/emm.2017.255
Liao, X., Han, C., Wang, X., Huang, K., Yu, T., Yang, C., Huang, R., Liu, Z., Han, Q., & Peng, T. (2018). Prognostic value of minichromosome maintenance mRNA expression in early-stage pancreatic ductal adenocarcinoma patients after pancreaticoduodenectomy. *Cancer Manag Res, 10*, 3255-3271. doi:10.2147/CMAR.S171293
Liberzon, A., Birger, C., Thorvaldsdottir, H., Ghandi, M., Mesirov, J. P., & Tamayo, P. (2015). The Molecular Signatures Database (MSigDB) hallmark gene set collection. *Cell Syst, 1*(6), 417-425. doi:10.1016/j.cels.2015.12.004
Lim, C. Y., Chang, J. H., Lee, W. S., Lee, K. M., Yoon, Y. C., Kim, J., & Park, I. Y. (2018). Organotypic slice cultures of pancreatic ductal adenocarcinoma preserve the tumor microenvironment and provide a platform for drug response. *Pancreatology, 18*(8), 913-927. doi:10.1016/j.pan.2018.09.009
Lin W, Noel P, Borazanci EH, Lee J, Amini A, Han IW, Heo JS, Jameson GS, Fraser C, Steinbach M, Woo Y, Fong Y, Cridebring D, Von Hoff DD, Park JO, Han H. Single-cell transcriptome analysis of tumor and stromal compartments of pancreatic ductal adenocarcinoma primary tumors and metastatic lesions. Genome Med. 2020 Sep 29;12(1):80. doi: 10.1186/s13073-020-00776-9.

Liu, H., Lv, L., & Yang, K. (2015). Chemotherapy targeting cancer stem cells. *Am J Cancer Res, 5*(3), 880-893.
Long, J., Zhang, Y., Yu, X., Yang, J., LeBrun, D. G., Chen, C., Yao, Q., & Li, M. (2011). Overcoming drug resistance in pancreatic cancer. *Expert Opin Ther Targets, 15*(7), 817-828. doi:10.1517/14728222.2011.566216
Longo, V., Brunetti, O., Gnoni, A., Cascinu, S., Gasparini, G., Lorusso, V., Ribatti, D., & Silvestris, N. (2016). Angiogenesis in pancreatic ductal adenocarcinoma: A controversial issue. *Oncotarget, 7*(36), 58649-58658. doi:10.18632/oncotarget.10765
Lorusso, G., & Ruegg, C. (2008). The tumor microenvironment and its contribution to tumor evolution toward metastasis. *Histochem Cell Biol, 130*(6), 1091-1103. doi:10.1007/s00418-008-0530-8
Love, M. I., Huber, W., & Anders, S. (2014). Moderated estimation of fold change and dispersion for RNA-seq data with DESeq2. *Genome Biol, 15*(12), 550. doi:10.1186/s13059-014-0550-8
Luchini, C., Capelli, P., & Scarpa, A. (2016). Pancreatic Ductal Adenocarcinoma and Its Variants. *Surg Pathol Clin, 9*(4), 547-560. doi:10.1016/j.path.2016.05.003
Lyratzopoulos, G., Saunders, C. L., Abel, G. A., McPhail, S., Neal, R. D., Wardle, J., & Rubin, G. P. (2015). The relative length of the patient and the primary care

interval in patients with 28 common and rarer cancers. *Br J Cancer, 112 Suppl 1*, S35-40. doi:10.1038/bjc.2015.40
Madden, J. (2012). Infinity reports update from Phase 2 study of Saridegib plus Gemcitabine in patients with metastatic pancreatic cancer. *Infin. Pharm*.
Maenhoudt, N., & Vankelecom, H. (2021). Protocol for establishing organoids from human ovarian cancer biopsies. *STAR Protoc, 2*(2), 100429. doi:10.1016/j.xpro.2021.100429
Marshall, H. T., & Djamgoz, M. B. A. (2018). Immuno-Oncology: Emerging Targets and Combination Therapies. *Front Oncol, 8*, 315. doi:10.3389/fonc.2018.00315
Martin, S. Z., Wagner, D. C., Horner, N., Horst, D., Lang, H., Tagscherer, K. E., & Roth, W. (2019). Ex vivo tissue slice culture system to measure drug-response rates of hepatic metastatic colorectal cancer. *BMC Cancer, 19*(1), 1030. doi:10.1186/s12885-019-6270-4
Martinez-Bosch, N., Vinaixa, J., & Navarro, P. (2018). Immune Evasion in Pancreatic Cancer: From Mechanisms to Therapy. *Cancers (Basel), 10*(1). doi:10.3390/cancers10010006
Masugi, Y., Abe, T., Ueno, A., Fujii-Nishimura, Y., Ojima, H., Endo, Y., Fujita, Y., Kitago, M., Shinoda, M., Kitagawa, Y., & Sakamoto, M. (2019). Characterization of spatial distribution of tumor-infiltrating CD8(+) T cells refines their prognostic utility for pancreatic cancer survival. *Mod Pathol, 32*(10), 1495-1507. doi:10.1038/s41379-019-0291-z
McGuigan, A., Kelly, P., Turkington, R. C., Jones, C., Coleman, H. G., & McCain, R. S. (2018). Pancreatic cancer: A review of clinical diagnosis, epidemiology, treatment and outcomes. *World J Gastroenterol, 24*(43), 4846-4861. doi:10.3748/wjg.v24.i43.4846
McKee, T. J., & Komarova, S. V. (2017). Is it time to reinvent basic cell culture medium? *Am J Physiol Cell Physiol, 312*(5), C624-C626. doi:10.1152/ajpcell.00336.2016
Meijer, T. G., Naipal, K. A., Jager, A., & van Gent, D. C. (2017). Ex vivo tumor culture systems for functional drug testing and therapy response prediction. *Future Sci OA, 3*(2), FSO190. doi:10.4155/fsoa-2017-0003
Melo, S. A., Luecke, L. B., Kahlert, C., Fernandez, A. F., Gammon, S. T., Kaye, J., LeBleu, V. S., Mittendorf, E. A., Weitz, J., Rahbari, N., Reissfelder, C., Pilarsky, C., Fraga, M. F., Piwnica-Worms, D., & Kalluri, R. (2015). Glypican-1 identifies cancer exosomes and detects early pancreatic cancer. *Nature, 523*(7559), 177-182. doi:10.1038/nature14581
Michelakos, T., Pergolini, I., Castillo, C. F., Honselmann, K. C., Cai, L., Deshpande, V., Wo, J. Y., Ryan, D. P., Allen, J. N., Blaszkowsky, L. S., Clark, J. W., Murphy, J. E., Nipp, R. D., Parikh, A., Qadan, M., Warshaw, A. L., Hong, T. S., Lillemoe, K. D., & Ferrone, C. R. (2019). Predictors of Resectability and Survival in Patients With Borderline and Locally Advanced Pancreatic Cancer who Underwent Neoadjuvant Treatment With FOLFIRINOX. *Ann Surg, 269*(4), 733-740. doi:10.1097/SLA.0000000000002600
Miller, I., Min, M., Yang, C., Tian, C., Gookin, S., Carter, D., & Spencer, S. L. (2018). Ki67 is a Graded Rather than a Binary Marker of Proliferation versus Quiescence. *Cell Rep, 24*(5), 1105-1112 e1105. doi:10.1016/j.celrep.2018.06.110

Misra, S., Moro, C.F., Del Chiaro, M. *et al. Ex vivo* organotypic culture system of precision-cut slices of human pancreatic ductal adenocarcinoma. *Sci Rep* **9**, 2133 (2019). https://doi.org/10.1038/s41598-019-38603-w

Moffitt, R. A., Marayati, R., Flate, E. L., Volmar, K. E., Loeza, S. G., Hoadley, K. A., Rashid, N. U., Williams, L. A., Eaton, S. C., Chung, A. H., Smyla, J. K., Anderson, J. M., Kim, H. J., Bentrem, D. J., Talamonti, M. S., Iacobuzio-Donahue, C. A., Hollingsworth, M. A., & Yeh, J. J. (2015). Virtual microdissection identifies distinct tumor- and stroma-specific subtypes of pancreatic ductal adenocarcinoma. *Nat Genet, 47*(10), 1168-1178. doi:10.1038/ng.3398

Mollberg, N., Rahbari, N. N., Koch, M., Hartwig, W., Hoeger, Y., Buchler, M. W., & Weitz, J. (2011). Arterial resection during pancreatectomy for pancreatic cancer: a systematic review and meta-analysis. *Ann Surg, 254*(6), 882-893. doi:10.1097/SLA.0b013e31823ac299

Mollenhauer, J., Roether, I., & Kern, H. F. (1987). Distribution of extracellular matrix proteins in pancreatic ductal adenocarcinoma and its influence on tumor cell proliferation in vitro. *Pancreas, 2*(1), 14-24. doi:10.1097/00006676-198701000-00003

Moriyama, T., Yang, Y. L., Nishii, R., Ariffin, H., Liu, C., Lin, T. N., Yang, W., Lin, D. T., Yu, C. H., Kham, S., Pui, C. H., Evans, W. E., Jeha, S., Relling, M. V., Yeoh, A. E., & Yang, J. J. (2017). Novel variants in NUDT15 and thiopurine intolerance in children with acute lymphoblastic leukemia from diverse ancestry. *Blood, 130*(10), 1209-1212. doi:10.1182/blood-2017-05-782383

Motoi, F., Kosuge, T., Ueno, H., Yamaue, H., Satoi, S., Sho, M., Honda, G., Matsumoto, I., Wada, K., Furuse, J., Matsuyama, Y., Unno, M., Study Group of Preoperative Therapy for Pancreatic, C., & Japanese Study Group of Adjuvant Therapy for Pancreatic, c. (2019). Randomized phase II/III trial of neoadjuvant chemotherapy with gemcitabine and S-1 versus upfront surgery for resectable pancreatic cancer (Prep-02/JSAP05). *Jpn J Clin Oncol, 49*(2), 190-194. doi:10.1093/jjco/hyy190

Mozar, A., Haren, N., Chasseraud, M., Louvet, L., Maziere, C., Wattel, A., Mentaverri, R., Morliere, P., Kamel, S., Brazier, M., Maziere, J. C., & Massy, Z. A. (2008). High extracellular inorganic phosphate concentration inhibits RANK-RANKL signaling in osteoclast-like cells. *J Cell Physiol, 215*(1), 47-54. doi:10.1002/jcp.21283

Nagaraj, A. S., Bao, J., Hemmes, A., Machado, M., Narhi, K., & Verschuren, E. W. (2018). Establishment and Analysis of Tumor Slice Explants As a Prerequisite for Diagnostic Testing. *J Vis Exp*(141). doi:10.3791/58569

Naipal, K. A., Verkaik, N. S., Sanchez, H., van Deurzen, C. H., den Bakker, M. A., Hoeijmakers, J. H., Kanaar, R., Vreeswijk, M. P., Jager, A., & van Gent, D. C. (2016). Tumor slice culture system to assess drug response of primary breast cancer. *BMC Cancer, 16*, 78. doi:10.1186/s12885-016-2119-2

Nakatani, K., Nakahata, N., Hamada, Y., Tsurufuji, S., & Ohizumi, Y. (1998). Medium change amplifies mitogen-activated protein kinase-mediated prostaglandin E2 synthesis in Swiss 3T3 fibroblasts. *Eur J Pharmacol, 356*(1), 91-100. doi:10.1016/s0014-2999(98)00523-8

Nasralla, D., Coussios, C. C., Mergental, H., Akhtar, M. Z., Butler, A. J., Ceresa, C. D. L., Chiocchia, V., Dutton, S. J., Garcia-Valdecasas, J. C., Heaton, N., Imber, C., Jassem, W., Jochmans, I., Karani, J., Knight, S. R., Kocabayoglu, P., Malago,

M., Mirza, D., Morris, P. J., Pallan, A., Paul, A., Pavel, M., Perera, M., Pirenne, J., Ravikumar, R., Russell, L., Upponi, S., Watson, C. J. E., Weissenbacher, A., Ploeg, R. J., Friend, P. J., & Consortium for Organ Preservation in, E. (2018). A randomized trial of normothermic preservation in liver transplantation. *Nature, 557*(7703), 50-56. doi:10.1038/s41586-018-0047-9

NCCN. (2019). *National comprehensive cancer network practice guidelines in oncology for pancreatic adenocarcinoma*.

NCI, U. S. (2018). Pancreatic cancer: statistics 2018. Retrieved from https://www.cancer.net/cancer-types/pancreatic-cancer/statistics

Neesse, A., Algul, H., Tuveson, D. A., & Gress, T. M. (2015). Stromal biology and therapy in pancreatic cancer: a changing paradigm. *Gut, 64*(9), 1476-1484. doi:10.1136/gutjnl-2015-309304

Neoptolemos, J. P., Palmer, D. H., Ghaneh, P., Psarelli, E. E., Valle, J. W., Halloran, C. M., Faluyi, O., O'Reilly, D. A., Cunningham, D., Wadsley, J., Darby, S., Meyer, T., Gillmore, R., Anthoney, A., Lind, P., Glimelius, B., Falk, S., Izbicki, J. R., Middleton, G. W., Cummins, S., Ross, P. J., Wasan, H., McDonald, A., Crosby, T., Ma, Y. T., Patel, K., Sherriff, D., Soomal, R., Borg, D., Sothi, S., Hammel, P., Hackert, T., Jackson, R., Buchler, M. W., & European Study Group for Pancreatic, C. (2017). Comparison of adjuvant gemcitabine and capecitabine with gemcitabine monotherapy in patients with resected pancreatic cancer (ESPAC-4): a multicentre, open-label, randomised, phase 3 trial. *Lancet, 389*(10073), 1011-1024. doi:10.1016/S0140-6736(16)32409-6

Neoptolemos, J. P., Stocken, D. D., Bassi, C., Ghaneh, P., Cunningham, D., Goldstein, D., Padbury, R., Moore, M. J., Gallinger, S., Mariette, C., Wente, M. N., Izbicki, J. R., Friess, H., Lerch, M. M., Dervenis, C., Olah, A., Butturini, G., Doi, R., Lind, P. A., Smith, D., Valle, J. W., Palmer, D. H., Buckels, J. A., Thompson, J., McKay, C. J., Rawcliffe, C. L., Buchler, M. W., & European Study Group for Pancreatic, C. (2010). Adjuvant chemotherapy with fluorouracil plus folinic acid vs gemcitabine following pancreatic cancer resection: a randomized controlled trial. *JAMA, 304*(10), 1073-1081. doi:10.1001/jama.2010.1275

Neoptolemos, J. P., Stocken, D. D., Friess, H., Bassi, C., Dunn, J. A., Hickey, H., Beger, H., Fernandez-Cruz, L., Dervenis, C., Lacaine, F., Falconi, M., Pederzoli, P., Pap, A., Spooner, D., Kerr, D. J., Buchler, M. W., & European Study Group for Pancreatic, C. (2004). A randomized trial of chemoradiotherapy and chemotherapy after resection of pancreatic cancer. *N Engl J Med, 350*(12), 1200-1210. doi:10.1056/NEJMoa032295

NICE. (2018). *Pancreatic cancer in adults: diagnosis and management. NICE guideline [NG85]Published date: 07 February 2018*. Retrieved from https://www.nice.org.uk/guidance/ng85.

NICE. (2019). Ex-situ machine perfusion for extracorporeal preservation of livers for transplantation. Interventional procedures guidance [IPG636].

Nuzhat, Z., Kinhal, V., Sharma, S., Rice, G. E., Joshi, V., & Salomon, C. (2017). Tumour-derived exosomes as a signature of pancreatic cancer - liquid biopsies as indicators of tumour progression. *Oncotarget, 8*(10), 17279-17291. doi:10.18632/oncotarget.13973

Oba, A., Ho, F., Bao, Q. R., Al-Musawi, M. H., Schulick, R. D., & Del Chiaro, M. (2020). Neoadjuvant Treatment in Pancreatic Cancer. *Front Oncol, 10*, 245. doi:10.3389/fonc.2020.00245

Oberg, K. (2018). Management of functional neuroendocrine tumors of the pancreas. *Gland Surg, 7*(1), 20-27. doi:10.21037/gs.2017.10.08

Oettle, H., Post, S., Neuhaus, P., Gellert, K., Langrehr, J., Ridwelski, K., Schramm, H., Fahlke, J., Zuelke, C., Burkart, C., Gutberlet, K., Kettner, E., Schmalenberg, H., Weigang-Koehler, K., Bechstein, W. O., Niedergethmann, M., Schmidt-Wolf, I., Roll, L., Doerken, B., & Riess, H. (2007). Adjuvant chemotherapy with gemcitabine vs observation in patients undergoing curative-intent resection of pancreatic cancer: a randomized controlled trial. *JAMA, 297*(3), 267-277. doi:10.1001/jama.297.3.267

Okada, S., Vaeteewoottacharn, K., & Kariya, R. (2019). Application of Highly Immunocompromised Mice for the Establishment of Patient-Derived Xenograft (PDX) Models. *Cells, 8*(8). doi:10.3390/cells8080889

Olivares, O., Mayers, J. R., Gouirand, V., Torrence, M. E., Gicquel, T., Borge, L., Lac, S., Roques, J., Lavaut, M. N., Berthezene, P., Rubis, M., Secq, V., Garcia, S., Moutardier, V., Lombardo, D., Iovanna, J. L., Tomasini, R., Guillaumond, F., Vander Heiden, M. G., & Vasseur, S. (2017). Collagen-derived proline promotes pancreatic ductal adenocarcinoma cell survival under nutrient limited conditions. *Nat Commun, 8*, 16031. doi:10.1038/ncomms16031

Olive, K. P., Jacobetz, M. A., Davidson, C. J., Gopinathan, A., McIntyre, D., Honess, D., Madhu, B., Goldgraben, M. A., Caldwell, M. E., Allard, D., Frese, K. K., Denicola, G., Feig, C., Combs, C., Winter, S. P., Ireland-Zecchini, H., Reichelt, S., Howat, W. J., Chang, A., Dhara, M., Wang, L., Ruckert, F., Grutzmann, R., Pilarsky, C., Izeradjene, K., Hingorani, S. R., Huang, P., Davies, S. E., Plunkett, W., Egorin, M., Hruban, R. H., Whitebread, N., McGovern, K., Adams, J., Iacobuzio-Donahue, C., Griffiths, J., & Tuveson, D. A. (2009). Inhibition of Hedgehog signaling enhances delivery of chemotherapy in a mouse model of pancreatic cancer. *Science, 324*(5933), 1457-1461. doi:10.1126/science.1171362

Orth, M., Metzger, P., Gerum, S., Mayerle, J., Schneider, G., Belka, C., Schnurr, M., & Lauber, K. (2019). Pancreatic ductal adenocarcinoma: biological hallmarks, current status, and future perspectives of combined modality treatment approaches. *Radiat Oncol, 14*(1), 141. doi:10.1186/s13014-019-1345-6

Ozbolat, I. T. & Hospodiuk, M. Current advances and future perspectives in extrusion-based bioprinting. *Biomaterials* **76**, 321–343 (2016).

Ozturk, S. S., Riley, M. R., & Palsson, B. O. (1992). Effects of ammonia and lactate on hybridoma growth, metabolism, and antibody production. *Biotechnol Bioeng, 39*(4), 418-431. doi:10.1002/bit.260390408

Pabla, B., Bissonnette, M., & Konda, V. J. (2015). Colon cancer and the epidermal growth factor receptor: Current treatment paradigms, the importance of diet, and the role of chemoprevention. *World J Clin Oncol, 6*(5), 133-141. doi:10.5306/wjco.v6.i5.133

Paish, H. L., Reed, L. H., Brown, H., Bryan, M. C., Govaere, O., Leslie, J., Barksby, B. S., Garcia Macia, M., Watson, A., Xu, X., Zaki, M. Y. W., Greaves, L., Whitehall, J., French, J., White, S. A., Manas, D. M., Robinson, S. M., Spoletini, G., Griffiths, C., Mann, D. A., Borthwick, L. A., Drinnan, M. J., Mann, J., & Oakley,

F. (2019). A Bioreactor Technology for Modeling Fibrosis in Human and Rodent Precision-Cut Liver Slices. *Hepatology, 70*(4), 1377-1391. doi:10.1002/hep.30651
Palm, W., & Thompson, C. B. (2017). Nutrient acquisition strategies of mammalian cells. *Nature, 546*(7657), 234-242. doi:10.1038/nature22379
Pannala, R., Basu, A., Petersen, G. M., & Chari, S. T. (2009). New-onset diabetes: a potential clue to the early diagnosis of pancreatic cancer. *Lancet Oncol, 10*(1), 88-95. doi:10.1016/S1470-2045(08)70337-1
Paoli, C., & Carrer, A. (2020). Organotypic Culture of Acinar Cells for the Study of Pancreatic Cancer Initiation. *Cancers (Basel), 12*(9). doi:10.3390/cancers12092606
Parente, A., Osei-Bordom, D. C., Ronca, V., Perera, M., & Mirza, D. (2020). Organ Restoration With Normothermic Machine Perfusion and Immune Reaction. *Front Immunol, 11*, 565616. doi:10.3389/fimmu.2020.565616
Park, H. M., Park, S. J., Han, S. S., & Kim, S. H. (2019). Surgery for elderly patients with resectable pancreatic cancer, a comparison with non-surgical treatments: a retrospective study outcomes of resectable pancreatic cancer. *BMC Cancer, 19*(1), 1090. doi:10.1186/s12885-019-6255-3
Pascal, J., Bearer, E. L., Wang, Z., Koay, E. J., Curley, S. A., & Cristini, V. (2013). Mechanistic patient-specific predictive correlation of tumor drug response with microenvironment and perfusion measurements. *Proc Natl Acad Sci U S A, 110*(35), 14266-14271. doi:10.1073/pnas.1300619110
Pavlacky, J., & Polak, J. (2020). Technical Feasibility and Physiological Relevance of Hypoxic Cell Culture Models. *Front Endocrinol (Lausanne), 11*, 57. doi:10.3389/fendo.2020.00057
Pavlou, S., Lindsay, J., Ingram, R., Xu, H., & Chen, M. (2018). Sustained high glucose exposure sensitizes macrophage responses to cytokine stimuli but reduces their phagocytic activity. *BMC Immunol, 19*(1), 24. doi:10.1186/s12865-018-0261-0
Peixoto, R. D., Speers, C., McGahan, C. E., Renouf, D. J., Schaeffer, D. F., & Kennecke, H. F. (2015). Prognostic factors and sites of metastasis in unresectable locally advanced pancreatic cancer. *Cancer Med, 4*(8), 1171-1177. doi:10.1002/cam4.459
Perrard, M. H., Sereni, N., Schluth-Bolard, C., Blondet, A., SG, D. E., Plotton, I., Morel-Journel, N., Lejeune, H., David, L., & Durand, P. (2016). Complete Human and Rat Ex Vivo Spermatogenesis from Fresh or Frozen Testicular Tissue. *Biol Reprod, 95*(4), 89. doi:10.1095/biolreprod.116.142802
Phillips, P. (2012). Pancreatic stellate cells and fibrosis. In P. J. Grippo & H. G. Munshi (Eds.), *Pancreatic Cancer and Tumor Microenvironment*. Trivandrum (India).
Pinto, N. R., Applebaum, M. A., Volchenboum, S. L., Matthay, K. K., London, W. B., Ambros, P. F., Nakagawara, A., Berthold, F., Schleiermacher, G., Park, J. R., Valteau-Couanet, D., Pearson, A. D., & Cohn, S. L. (2015). Advances in Risk Classification and Treatment Strategies for Neuroblastoma. *J Clin Oncol, 33*(27), 3008-3017. doi:10.1200/JCO.2014.59.4648
Pishvaian, M. J., Bender, R. J., Halverson, D., Rahib, L., Hendifar, A. E., Mikhail, S., Chung, V., Picozzi, V. J., Sohal, D., Blais, E. M., Mason, K., Lyons, E. E., Matrisian, L. M., Brody, J. R., Madhavan, S., & Petricoin, E. F., 3rd. (2018). Molecular Profiling of Patients with Pancreatic Cancer: Initial Results

from the Know Your Tumor Initiative. *Clin Cancer Res, 24*(20), 5018-5027. doi:10.1158/1078-0432.CCR-18-0531
Poh AR, Ernst M. Tumor-Associated Macrophages in Pancreatic Ductal Adenocarcinoma: Therapeutic Opportunities and Clinical Challenges. Cancers (Basel). 2021 Jun 8;13(12):2860. doi: 10.3390/cancers13122860. PMID: 34201127; PMCID: PMC8226457.
Pompili, L., Porru, M., Caruso, C., Biroccio, A., & Leonetti, C. (2016). Patient-derived xenografts: a relevant preclinical model for drug development. *J Exp Clin Cancer Res, 35*(1), 189. doi:10.1186/s13046-016-0462-4
Poplin E, Wasan H, Rolfe L, Raponi M, Ikdahl T, Bondarenko I, Davidenko I, Bondar V, Garin A, Boeck S, Ormanns S, Heinemann V, Bassi C, Evans TR, Andersson R, Hahn H, Picozzi V, Dicker A, Mann E, Voong C, Kaur P, Isaacson J, Allen A. Randomized, multicenter, phase II study of CO-101 versus gemcitabine in patients with metastatic pancreatic ductal adenocarcinoma: including a prospective evaluation of the role of hENT1 in gemcitabine or CO-101 sensitivity. J Clin Oncol. 2013 Dec 10;31(35):4453-61. doi: 10.1200/JCO.2013.51.0826. Epub 2013 Nov 12. PMID: 24220555.
Porta, M., Fabregat, X., Malats, N., Guarner, L., Carrato, A., de Miguel, A., Ruiz, L., Jariod, M., Costafreda, S., Coll, S., Alguacil, J., Corominas, J. M., Sola, R., Salas, A., & Real, F. X. (2005). Exocrine pancreatic cancer: symptoms at presentation and their relation to tumour site and stage. *Clin Transl Oncol, 7*(5), 189-197. doi:10.1007/BF02712816
Powley, I. R., Patel, M., Miles, G., Pringle, H., Howells, L., Thomas, A., Kettleborough, C., Bryans, J., Hammonds, T., MacFarlane, M., & Pritchard, C. (2020). Patient-derived explants (PDEs) as a powerful preclinical platform for anti-cancer drug and biomarker discovery. *Br J Cancer, 122*(6), 735-744. doi:10.1038/s41416-019-0672-6
Quintas-Cardama, A., & Cortes, J. (2009). Molecular biology of bcr-abl1-positive chronic myeloid leukemia. *Blood, 113*(8), 1619-1630. doi:10.1182/blood-2008-03-144790
R Core Team (2014). R: A language and environment for statistical computing. R Foundation for Statistical. Computing, Vienna, Austria. Retrieved from http://www.R-project.org/
Rapaport, F., Khanin, R., Liang, Y., Pirun, M., Krek, A., Zumbo, P., Mason, C. E., Socci, N. D., & Betel, D. (2013). Comprehensive evaluation of differential gene expression analysis methods for RNA-seq data. *Genome Biol, 14*(9), R95. doi:10.1186/gb-2013-14-9-r95
Rasheed, Z. A., Matsui, W., & Maitra, A. (2012). Pathology of pancreatic stroma in PDAC. In P. J. Grippo & H. G. Munshi (Eds.), *Pancreatic Cancer and Tumor Microenvironment*. Trivandrum (India).
Rawla, P., Sunkara, T., & Gaduputi, V. (2019). Epidemiology of Pancreatic Cancer: Global Trends, Etiology and Risk Factors. *World J Oncol, 10*(1), 10-27. doi:10.14740/wjon1166
RCPath. (2019). Dataset for histopathological reporting of carcinomas of the pancreas, ampulla of Vater and common bile duct.
Rhim, A. D., Mirek, E. T., Aiello, N. M., Maitra, A., Bailey, J. M., McAllister, F., Reichert, M., Beatty, G. L., Rustgi, A. K., Vonderheide, R. H., Leach, S. D., &

Stanger, B. Z. (2012). EMT and dissemination precede pancreatic tumor formation. *Cell, 148*(1-2), 349-361. doi:10.1016/j.cell.2011.11.025

Rhim AD, Oberstein PE, Thomas DH, Mirek ET, Palermo CF, Sastra SA, Dekleva EN, Saunders T, Becerra CP, Tattersall IW, Westphalen CB, Kitajewski J, Fernandez-Barrena MG, Fernandez-Zapico ME, Iacobuzio-Donahue C, Olive KP, Stanger BZ. Stromal elements act to restrain, rather than support, pancreatic ductal adenocarcinoma. Cancer Cell. 2014 Jun 16;25(6):735-47. doi: 10.1016/j.ccr.2014.04.021. Epub 2014 May 22. PMID: 24856585; PMCID: PMC4096698.

Ricard-Blum, S. (2011). The collagen family. *Cold Spring Harb Perspect Biol, 3*(1), a004978. doi:10.1101/cshperspect.a004978

Riva, G., Pea, A., Pilati, C., Fiadone, G., Lawlor, R. T., Scarpa, A., & Luchini, C. (2018). Histo-molecular oncogenesis of pancreatic cancer: From precancerous lesions to invasive ductal adenocarcinoma. *World J Gastrointest Oncol, 10*(10), 317-327. doi:10.4251/wjgo.v10.i10.317

Robert C, Ribas A, Wolchok JD, Hodi FS, Hamid O, Kefford R, Weber JS, Joshua AM, Hwu WJ, Gangadhar TC, Patnaik A, Dronca R, Zarour H, Joseph RW, Boasberg P, Chmielowski B, Mateus C, Postow MA, Gergich K, Elassaiss-Schaap J, Li XN, Iannone R, Ebbinghaus SW, Kang SP, Daud A. Anti-programmed-death-receptor-1 treatment with pembrolizumab in ipilimumab-refractory advanced melanoma: a randomised dose-comparison cohort of a phase 1 trial. Lancet. 2014 Sep 20;384(9948):1109-17. doi: 10.1016/S0140-6736(14)60958-2. Epub 2014 Jul 15. PMID: 25034862.

Robin, X., Turck, N., Hainard, A., Tiberti, N., Lisacek, F., Sanchez, J. C., & Muller, M. (2011). pROC: an open-source package for R and S+ to analyze and compare ROC curves. *BMC Bioinformatics, 12*, 77. doi:10.1186/1471-2105-12-77

Robinson, M. D., McCarthy, D. J., & Smyth, G. K. (2010). edgeR: a Bioconductor package for differential expression analysis of digital gene expression data. *Bioinformatics, 26*(1), 139-140. doi:10.1093/bioinformatics/btp616

Romero-Calvo, I., Weber, C. R., Ray, M., Brown, M., Kirby, K., Nandi, R. K., Long, T. M., Sparrow, S. M., Ugolkov, A., Qiang, W., Zhang, Y., Brunetti, T., Kindler, H., Segal, J. P., Rzhetsky, A., Mazar, A. P., Buschmann, M. M., Weichselbaum, R., Roggin, K., & White, K. P. (2019). Human Organoids Share Structural and Genetic Features with Primary Pancreatic Adenocarcinoma Tumors. *Mol Cancer Res, 17*(1), 70-83. doi:10.1158/1541-7786.MCR-18-0531

Ruan, H. Q., Liao, G. L., Peng, P., Liu, S. Q., Wu, C. L., Qin, J. F., Liang, Z. H., Tang, G. D., Qin, M. B., & Huang, J. A. (2019). Microbial Profiles and Risk Factors of Preexisting Biliary Infection in Patients with Therapeutic Endoscopy. *Gastroenterol Res Pract, 2019*, 1527328. doi:10.1155/2019/1527328

Ryu, A. H., Eckalbar, W. L., Kreimer, A., Yosef, N., & Ahituv, N. (2017). Use antibiotics in cell culture with caution: genome-wide identification of antibiotic-induced changes in gene expression and regulation. *Sci Rep, 7*(1), 7533. doi:10.1038/s41598-017-07757-w

Saad, A. M., Turk, T., Al-Husseini, M. J., & Abdel-Rahman, O. (2018). Trends in pancreatic adenocarcinoma incidence and mortality in the United States in the last four decades; a SEER-based study. *BMC Cancer, 18*(1), 688. doi:10.1186/s12885-018-4610-4

Saxton, R. A., & Sabatini, D. M. (2017). mTOR Signaling in Growth, Metabolism, and Disease. *Cell, 168*(6), 960-976. doi:10.1016/j.cell.2017.02.004

Scara, S., Bottoni, P., & Scatena, R. (2015). CA 19-9: Biochemical and Clinical Aspects. *Adv Exp Med Biol, 867*, 247-260. doi:10.1007/978-94-017-7215-0_15

Schneider, C. A., Rasband, W. S., & Eliceiri, K. W. (2012). NIH Image to ImageJ: 25 years of image analysis. *Nat Methods, 9*(7), 671-675. doi:10.1038/nmeth.2089

Sebastiani, V., Ricci, F., Rubio-Viqueira, B., Kulesza, P., Yeo, C. J., Hidalgo, M., Klein, A., Laheru, D., & Iacobuzio-Donahue, C. A. (2006). Immunohistochemical and genetic evaluation of deoxycytidine kinase in pancreatic cancer: relationship to molecular mechanisms of gemcitabine resistance and survival. *Clin Cancer Res, 12*(8), 2492-2497. doi:10.1158/1078-0432.CCR-05-2655

Sergushichev, A. (2016). An algorithm for fast preranked gene set enrichment analysis using cumulative statistic calculation. *bioRxiv 060012*. doi:doi:10.1101/060012.

Seufferlein, T., & Ettrich, T. J. (2019). Treatment of pancreatic cancer-neoadjuvant treatment in resectable pancreatic cancer (PDAC). *Transl Gastroenterol Hepatol, 4*, 21. doi:10.21037/tgh.2019.03.05

Sheikh, R., Walsh, N., Clynes, M., O'Connor, R., & McDermott, R. (2010). Challenges of drug resistance in the management of pancreatic cancer. *Expert Rev Anticancer Ther, 10*(10), 1647-1661. doi:10.1586/era.10.148

Steele CW, Karim SA, Leach JDG, Bailey P, Upstill-Goddard R, Rishi L, Foth M, Bryson S, McDaid K, Wilson Z, Eberlein C, Candido JB, Clarke M, Nixon C, Connelly J, Jamieson N, Carter CR, Balkwill F, Chang DK, Evans TRJ, Strathdee D, Biankin AV, Nibbs RJB, Barry ST, Sansom OJ, Morton JP. CXCR2 Inhibition Profoundly Suppresses Metastases and Augments Immunotherapy in Pancreatic Ductal Adenocarcinoma. Cancer Cell. 2016 Jun 13;29(6):832-845. doi: 10.1016/j.ccell.2016.04.014. Epub 2016 Jun 2. PMID: 27265504; PMCID: PMC4912354.

Strobel, O., Hank, T., Hinz, U., Bergmann, F., Schneider, L., Springfeld, C., Jager, D., Schirmacher, P., Hackert, T., & Buchler, M. W. (2017). Pancreatic Cancer Surgery: The New R-status Counts. *Ann Surg, 265*(3), 565-573. doi:10.1097/SLA.0000000000001731

Sugihara, K., Yamaguchi, Y., Usui, S., Nashimoto, Y., Hanada, S., Kiyokawa, E., Uemura, A., Yokokawa, R., Nishiyama, K., & Miura, T. (2020). A new perfusion culture method with a self-organized capillary network. *PLoS One, 15*(10), e0240552. doi:10.1371/journal.pone.0240552

Swayden, M., Iovanna, J., & Soubeyran, P. (2018). Pancreatic cancer chemo-resistance is driven by tumor phenotype rather than tumor genotype. *Heliyon, 4*(12), e01055. doi:10.1016/j.heliyon.2018.e01055

Takahashi, H., Ohigashi, H., Ishikawa, O., Eguchi, H., Gotoh, K., Yamada, T., Nakaizumi, A., Uehara, H., Tomita, Y., Nishiyama, K., & Yano, M. (2010). Serum CA19-9 alterations during preoperative gemcitabine-based chemoradiation therapy for resectable invasive ductal carcinoma of the pancreas as an indicator for therapeutic selection and survival. *Ann Surg, 251*(3), 461-469. doi:10.1097/SLA.0b013e3181cc90a3

Tan, W. C. C., Nerurkar, S. N., Cai, H. Y., Ng, H. H. M., Wu, D., Wee, Y. T. F., Lim, J. C. T., Yeong, J., & Lim, T. K. H. (2020). Overview of multiplex immunohistochemistry/immunofluorescence techniques in the era of cancer immunotherapy. *Cancer Commun (Lond), 40*(4), 135-153. doi:10.1002/cac2.12023

Tempero, M. A., Malafa, M. P., Al-Hawary, M., Asbun, H., Bain, A., Behrman, S. W., Benson, A. B., 3rd, Binder, E., Cardin, D. B., Cha, C., Chiorean, E. G., Chung, V., Czito, B., Dillhoff, M., Dotan, E., Ferrone, C. R., Hardacre, J., Hawkins, W. G., Herman, J., Ko, A. H., Komanduri, S., Koong, A., LoConte, N., Lowy, A. M., Moravek, C., Nakakura, E. K., O'Reilly, E. M., Obando, J., Reddy, S., Scaife, C., Thayer, S., Weekes, C. D., Wolff, R. A., Wolpin, B. M., Burns, J., & Darlow, S. (2017). Pancreatic Adenocarcinoma, Version 2.2017, NCCN Clinical Practice Guidelines in Oncology. *J Natl Compr Canc Netw, 15*(8), 1028-1061. doi:10.6004/jnccn.2017.0131

Terrell, J. A., Jones, C. G., Kabandana, G. K. M., & Chen, C. (2020). From cells-on-a-chip to organs-on-a-chip: scaffolding materials for 3D cell culture in microfluidics. *J Mater Chem B, 8*(31), 6667-6685. doi:10.1039/d0tb00718h

Therneau, T. M. (2021). A Package for Survival Analysis in R.

Thind, K., Padrnos, L. J., Ramanathan, R. K., & Borad, M. J. (2017). Immunotherapy in pancreatic cancer treatment: a new frontier. *Therap Adv Gastroenterol, 10*(1), 168-194. doi:10.1177/1756283X16667909

Thota, R., Pauff, J. M., & Berlin, J. D. (2014). Treatment of metastatic pancreatic adenocarcinoma: a review. *Oncology (Williston Park), 28*(1), 70-74.

Thyagarajan A, Alshehri MSA, Miller KLR, Sherwin CM, Travers JB, Sahu RP. Myeloid-Derived Suppressor Cells and Pancreatic Cancer: Implications in Novel Therapeutic Approaches. Cancers (Basel). 2019 Oct 24;11(11):1627. doi: 10.3390/cancers11111627. PMID: 31652904; PMCID: PMC6893814.

Timmer, F.E.F.; Geboers, B.; Nieuwenhuizen, S.; Dijkstra, M.; Schouten, E.A.C.; Puijk, R.S.; de Vries, J.J.J.; van den Tol, M.P.; Bruynzeel, A.M.E.; Streppel, M.M.; et al. Pancreatic Cancer and Immunotherapy: A Clinical Overview. Cancers 2021, 13, 4138. https://doi.org/10.3390/ cancers13164138

Tiriac, H., Belleau, P., Engle, D. D., Plenker, D., Deschenes, A., Somerville, T. D. D., Froeling, F. E. M., Burkhart, R. A., Denroche, R. E., Jang, G. H., Miyabayashi, K., Young, C. M., Patel, H., Ma, M., LaComb, J. F., Palmaira, R. L. D., Javed, A. A., Huynh, J. C., Johnson, M., Arora, K., Robine, N., Shah, M., Sanghvi, R., Goetz, A. B., Lowder, C. Y., Martello, L., Driehuis, E., LeComte, N., Askan, G., Iacobuzio-Donahue, C. A., Clevers, H., Wood, L. D., Hruban, R. H., Thompson, E., Aguirre, A. J., Wolpin, B. M., Sasson, A., Kim, J., Wu, M., Bucobo, J. C., Allen, P., Sejpal, D. V., Nealon, W., Sullivan, J. D., Winter, J. M., Gimotty, P. A., Grem, J. L., DiMaio, D. J., Buscaglia, J. M., Grandgenett, P. M., Brody, J. R., Hollingsworth, M. A., O'Kane, G. M., Notta, F., Kim, E., Crawford, J. M., Devoe, C., Ocean, A., Wolfgang, C. L., Yu, K. H., Li, E., Vakoc, C. R., Hubert, B., Fischer, S. E., Wilson, J. M., Moffitt, R., Knox, J., Krasnitz, A., Gallinger, S., & Tuveson, D. A. (2018). Organoid Profiling Identifies Common Responders to Chemotherapy in Pancreatic Cancer. *Cancer Discov, 8*(9), 1112-1129. doi:10.1158/2159-8290.CD-18-0349

Topp, M. D., Hartley, L., Cook, M., Heong, V., Boehm, E., McShane, L., Pyman, J., McNally, O., Ananda, S., Harrell, M., Etemadmoghadam, D., Galletta, L., Alsop, K., Mitchell, G., Fox, S. B., Kerr, J. B., Hutt, K. J., Kaufmann, S. H., Australian Ovarian Cancer, S., Swisher, E. M., Bowtell, D. D., Wakefield, M. J., & Scott, C. L. (2014). Molecular correlates of platinum response in human high-grade serous ovarian cancer patient-derived xenografts. *Mol Oncol, 8*(3), 656-668. doi:10.1016/j.molonc.2014.01.008

Torres, C., & Grippo, P. J. (2018). Pancreatic cancer subtypes: a roadmap for precision medicine. *Ann Med, 50*(4), 277-287. doi:10.1080/07853890.2018.1453168

Tsai, S., McOlash, L., Palen, K., Johnson, B., Duris, C., Yang, Q., Dwinell, M. B., Hunt, B., Evans, D. B., Gershan, J., & James, M. A. (2018). Development of primary human pancreatic cancer organoids, matched stromal and immune cells and 3D tumor microenvironment models. *BMC Cancer, 18*(1), 335. doi:10.1186/s12885-018-4238-4

Tseng, J. F., Raut, C. P., Lee, J. E., Pisters, P. W., Vauthey, J. N., Abdalla, E. K., Gomez, H. F., Sun, C. C., Crane, C. H., Wolff, R. A., & Evans, D. B. (2004). Pancreaticoduodenectomy with vascular resection: margin status and survival duration. *J Gastrointest Surg, 8*(8), 935-949; discussion 949-950. doi:10.1016/j.gassur.2004.09.046

Tsushima, Y., Miyazaki, M., Taketomi-Takahashi, A., & Endo, K. (2011). Feasibility of measuring human pancreatic perfusion in vivo using imaging techniques. *Pancreas, 40*(5), 747-752. doi:10.1097/MPA.0b013e318215ac22

Urbischek, M., Rannikmae, H., Foets, T., Ravn, K., Hyvonen, M., & de la Roche, M. (2019). Organoid culture media formulated with growth factors of defined cellular activity. *Sci Rep, 9*(1), 6193. doi:10.1038/s41598-019-42604-0

Valle, J. W., Palmer, D., Jackson, R., Cox, T., Neoptolemos, J. P., Ghaneh, P., Rawcliffe, C. L., Bassi, C., Stocken, D. D., Cunningham, D., O'Reilly, D., Goldstein, D., Robinson, B. A., Karapetis, C., Scarfe, A., Lacaine, F., Sand, J., Izbicki, J. R., Mayerle, J., Dervenis, C., Olah, A., Butturini, G., Lind, P. A., Middleton, M. R., Anthoney, A., Sumpter, K., Carter, R., & Buchler, M. W. (2014). Optimal duration and timing of adjuvant chemotherapy after definitive surgery for ductal adenocarcinoma of the pancreas: ongoing lessons from the ESPAC-3 study. *J Clin Oncol, 32*(6), 504-512. doi:10.1200/JCO.2013.50.7657

Vande Voorde, J., Ackermann, T., Pfetzer, N., Sumpton, D., Mackay, G., Kalna, G., Nixon, C., Blyth, K., Gottlieb, E., & Tardito, S. (2019). Improving the metabolic fidelity of cancer models with a physiological cell culture medium. *Sci Adv, 5*(1), eaau7314. doi:10.1126/sciadv.aau7314

Varadhachary, G. R., Tamm, E. P., Abbruzzese, J. L., Xiong, H. Q., Crane, C. H., Wang, H., Lee, J. E., Pisters, P. W., Evans, D. B., & Wolff, R. A. (2006). Borderline resectable pancreatic cancer: definitions, management, and role of preoperative therapy. *Ann Surg Oncol, 13*(8), 1035-1046. doi:10.1245/ASO.2006.08.011

Vauthey, J. N., & Dixon, E. (2009). AHPBA/SSO/SSAT Consensus Conference on Resectable and Borderline Resectable Pancreatic Cancer: rationale and

overview of the conference. *Ann Surg Oncol, 16*(7), 1725-1726. doi:10.1245/s10434-009-0409-5

Velasco, V., Shariati, S. A., & Esfandyarpour, R. (2020). Microtechnology-based methods for organoid models. *Microsyst Nanoeng, 6*(76). doi:https://doi.org/10.1038/s41378-020-00185-3

Versteijne, E., Suker, M., Groothuis, K., Akkermans-Vogelaar, J. M., Besselink, M. G., Bonsing, B. A., Buijsen, J., Busch, O. R., Creemers, G. M., van Dam, R. M., Eskens, F., Festen, S., de Groot, J. W. B., Groot Koerkamp, B., de Hingh, I. H., Homs, M. Y. V., van Hooft, J. E., Kerver, E. D., Luelmo, S. A. C., Neelis, K. J., Nuyttens, J., Paardekooper, G., Patijn, G. A., van der Sangen, M. J. C., de Vos-Geelen, J., Wilmink, J. W., Zwinderman, A. H., Punt, C. J., van Eijck, C. H., van Tienhoven, G., & Dutch Pancreatic Cancer, G. (2020). Preoperative Chemoradiotherapy Versus Immediate Surgery for Resectable and Borderline Resectable Pancreatic Cancer: Results of the Dutch Randomized Phase III PREOPANC Trial. *J Clin Oncol, 38*(16), 1763-1773. doi:10.1200/JCO.19.02274

Versteijne E, van Dam JL, Suker M, Janssen QP, Groothuis K, Akkermans-Vogelaar JM, Besselink MG, Bonsing BA, Buijsen J, Busch OR, Creemers GM, van Dam RM, Eskens FALM, Festen S, de Groot JWB, Groot Koerkamp B, de Hingh IH, Homs MYV, van Hooft JE, Kerver ED, Luelmo SAC, Neelis KJ, Nuyttens J, Paardekooper GMRM, Patijn GA, van der Sangen MJC, de Vos-Geelen J, Wilmink JW, Zwinderman AH, Punt CJ, van Tienhoven G, van Eijck CHJ; Dutch Pancreatic Cancer Group. Neoadjuvant Chemoradiotherapy Versus Upfront Surgery for Resectable and Borderline Resectable Pancreatic Cancer: Long-Term Results of the Dutch Randomized PREOPANC Trial. J Clin Oncol. 2022 Apr 10;40(11):1220-1230. doi: 10.1200/JCO.21.02233. Epub 2022 Jan 27. PMID: 35084987.

Verwer, R. W., Dubelaar, E. J., Hermens, W. T., & Swaab, D. F. (2002). Tissue cultures from adult human postmortem subcortical brain areas. *J Cell Mol Med, 6*(3), 429-432. doi:10.1111/j.1582-4934.2002.tb00522.x

Vestergaard, E. M., Hein, H. O., Meyer, H., Grunnet, N., Jorgensen, J., Wolf, H., & Orntoft, T. F. (1999). Reference values and biological variation for tumor marker CA 19-9 in serum for different Lewis and secretor genotypes and evaluation of secretor and Lewis genotyping in a Caucasian population. *Clin Chem, 45*(1), 54-61.

Vogenberg, F. R., Isaacson Barash, C., & Pursel, M. (2010). Personalized medicine: part 1: evolution and development into theranostics. *P T, 35*(10), 560-576.

Voss, N., Izbicki, J. R., & Nentwich, M. F. (2019). Oligometastases in pancreatic cancer (Synchronous resections of hepatic oligometastatic pancreatic cancer: Disputing a principle in a time of safe pancreatic operations in a retrospective multicenter analysis). *Ann Gastroenterol Surg, 3*(4), 373-377. doi:10.1002/ags3.12255

Wang, L. M., Silva, M. A., D'Costa, Z., Bockelmann, R., Soonawalla, Z., Liu, S., O'Neill, E., Mukherjee, S., McKenna, W. G., Muschel, R., & Fokas, E. (2016). The prognostic role of desmoplastic stroma in pancreatic ductal adenocarcinoma. *Oncotarget, 7*(4), 4183-4194. doi:10.18632/oncotarget.6770

Wang, Y., Fang, T., Huang, L., Wang, H., Zhang, L., Wang, Z., & Cui, Y. (2018). Neutrophils infiltrating pancreatic ductal adenocarcinoma indicate higher malignancy and worse prognosis. *Biochem Biophys Res Commun, 501*(1), 313-319. doi:10.1016/j.bbrc.2018.05.024

Watson, S. A., Terracciano, C. M., & Perbellini, F. (2019). Myocardial Slices: an Intermediate Complexity Platform for Translational Cardiovascular Research. *Cardiovasc Drugs Ther, 33*(2), 239-244. doi:10.1007/s10557-019-06853-5

Weinberg, R. A. (2008). Coevolution in the tumor microenvironment. *Nat Genet, 40*(5), 494-495. doi:10.1038/ng0508-494

Weniger, M., Honselmann, K. C., & Liss, A. S. (2018). The Extracellular Matrix and Pancreatic Cancer: A Complex Relationship. *Cancers (Basel), 10*(9). doi:10.3390/cancers10090316

Whatcott, C. J., Diep, C. H., Jiang, P., Watanabe, A., LoBello, J., Sima, C., Hostetter, G., Shepard, H. M., Von Hoff, D. D., & Han, H. (2015). Desmoplasia in Primary Tumors and Metastatic Lesions of Pancreatic Cancer. *Clin Cancer Res, 21*(15), 3561-3568. doi:10.1158/1078-0432.CCR-14-1051

Whitticar, N. B., Strahler, E. W., Rajan, P., Kaya, S., & Nunemaker, C. S. (2016). An Automated Perifusion System for Modifying Cell Culture Conditions over Time. *Biol Proced Online, 18*, 19. doi:10.1186/s12575-016-0049-7

Wickham, H., François, R., Henry, L., & Müller, K. (2021). dplyr: A Grammar of Data Manipulation. R package version 1.0.7.

Willis, C., Fiander, M., Tran, D., Korytowsky, B., Thomas, J. M., Calderon, F., Zyczynski, T. M., Brixner, D., & Stenehjem, D. D. (2019). Tumor mutational burden in lung cancer: a systematic literature review. *Oncotarget, 10*(61), 6604-6622. doi:10.18632/oncotarget.27287

Wu, T. T., Gong, H., & Clarke, E. M. (2011). A transcriptome analysis by lasso penalized Cox regression for pancreatic cancer survival. *J Bioinform Comput Biol, 9 Suppl 1*, 63-73. doi:10.1142/s0219720011005744

Xie, D., & Xie, K. (2015). Pancreatic cancer stromal biology and therapy. *Genes Dis, 2*(2), 133-143. doi:10.1016/j.gendis.2015.01.002

Xu, C., Li, X., Liu, P., Li, M., & Luo, F. (2019). Patient-derived xenograft mouse models: A high fidelity tool for individualized medicine. *Oncol Lett, 17*(1), 3-10. doi:10.3892/ol.2018.9583

Xu, W., Jong Hong, S., Jia, S., Zhao, Y., Galiano, R. D., & Mustoe, T. A. (2012). Application of a partial-thickness human ex vivo skin culture model in cutaneous wound healing study. *Lab Invest, 92*(4), 584-599. doi:10.1038/labinvest.2011.184

Yadav, L., Puri, N., Rastogi, V., Satpute, P., & Sharma, V. (2015). Tumour Angiogenesis and Angiogenic Inhibitors: A Review. *J Clin Diagn Res, 9*(6), XE01-XE05. doi:10.7860/JCDR/2015/12016.6135

Yamada, H., Sakamoto, H., Taira, M., Nishimura, S., Shimosato, Y., Terada, M., & Sugimura, T. (1986). Amplifications of both c-Ki-ras with a point mutation and c-myc in a primary pancreatic cancer and its metastatic tumors in lymph nodes. *Jpn J Cancer Res, 77*(4), 370-375.

Yang, S., Liu, Q., & Liao, Q. (2020). Tumor-Associated Macrophages in Pancreatic Ductal Adenocarcinoma: Origin, Polarization, Function, and Reprogramming. *Front Cell Dev Biol, 8*, 607209. doi:10.3389/fcell.2020.607209

Yoon JH, Jung YJ, Moon SH. Immunotherapy for pancreatic cancer. World J Clin Cases. 2021 May 6;9(13):2969-2982. doi: 10.12998/wjcc.v9.i13.2969. PMID: 33969083; PMCID: PMC8080736.

Yarchoan, M., Hopkins, A., & Jaffee, E. M. (2017). Tumor Mutational Burden and Response Rate to PD-1 Inhibition. *N Engl J Med, 377*(25), 2500-2501. doi:10.1056/NEJMc1713444

Yoshida, G. J. (2020). Applications of patient-derived tumor xenograft models and tumor organoids. *J Hematol Oncol, 13*(1), 4. doi:10.1186/s13045-019-0829-z

Yoshida, M., Hoshi, A., Kuretani, K., Kanai, T., & Ichino, M. (1975). Action of 5-fluorocyclocytidine on cultured L-5178Y cells. *Gan, 66*(5), 561-564.

Young, K., Iyer, R., Morganstein, D., Chau, I., Cunningham, D., & Starling, N. (2015). Pancreatic neuroendocrine tumors: a review. *Future Oncol, 11*(5), 853-864. doi:10.2217/fon.14.285

Yu, Z., Pestell, T. G., Lisanti, M. P., & Pestell, R. G. (2012). Cancer stem cells. *Int J Biochem Cell Biol, 44*(12), 2144-2151. doi:10.1016/j.biocel.2012.08.022

Zhang, L.; Wang, W.; Wang, R.; Zhang, N.; Shang, H.; Bi, Y.; Chen, D.; Zhang, C.; Li, L.; Yin, J.; et al. Reshaping the Immune Microenvironment by Oncolytic Herpes Simplex Virus in Murine Pancreatic Ductal Adenocarcinoma. Mol. Ther. 2020, 29, 744–761.